NATURE AND DISPOSITION OF THE GARNET-BIOTITE BOUNDARY AT BALQUHIDDER, PERTHSHIRE, SCOTLAND

by

SHERIF M.A. FAWZY, B.Sc., M.Sc.

A thesis submitted for the degree of Doctor of Philosophy

at

THE UNIVERSITY OF GLASGOW

Department of Geology and Applied Geology

NOVEMBER 1989

ProQuest LLC.
789 East Eisenhower Parkway
P.O. Box 1346
Ann Arbor, MI 48106 – 1346

To my wife,

ENAS

and

my son

AHMED

CONTENTS

		Page
	Contents	i
	List of Figures	v
	List of Tables	ix
	Acknowledgements	xiii
	Abstract	xiv
	Declaration	xvi
CHAPTER 1	GEOLOGICAL SETTING, ROCK UNITS AND STRUCTURAL FRAMEWORK.	
1.1	Isograd: their distribution and disposition	1
1.2	Geological setting and rock units	6
1.3	Rock chemistry	10
1.4	Structural framework	14
1.5	Comparison with structures in nearby areas	20
1.6	Scope of present investigation	23
1.7	Use of abbreviations	25
CHAPTER 2	SEQUENCE OF MINERAL GROWTHS	
2.1	Introduction	26
2.2	Methods of textural investigation	26
2.2.1	Porphyroblast *vs* matrix relations	27
2.2.2	Internal (si) *vs* external (Sc) fabrics	28
2.3	Growth of muscovite and chlorite	30
2.3.1	Introduction	30
2.3.2	Pre-S_2 growth	30
2.3.3	S_2-growths	31
2.3.4	S_2-deformation and later growths	31
2.4	Growth of garnet	32
2.4.1	D2 growth	32
2.4.1.1	Textural types - description	33

		Page
2.4.1.2	Textural types - interpretation	34
2.4.1.3	Matrix-grain coarsening	35
2.4.1.4	Tectonic environment	36
2.4.2	Post-D_2 – pre-D_4 growth	37
2.4.3	Grain size variation of garnet	38
2.5	Growth of biotite	43
2.6	Growth of albite	44
2.7	Growth of quartz	45
2.8	Growth of epidote	45
2.9	Growth of tourmaline	46
2.10	Growth of hornblende	46
2.11	Summary	47
CHAPTER 3	MINERAL CHEMISTRY	
3.1	Introduction	49
3.2	Chlorite chemistry	50
3.2.1	Analytical data	50
3.2.2	Data amplification	51
3.2.3	Discussion	53
3.3	Muscovite chemistry	65
3.3.1	Analytical data	65
3.3.2	Discussion	66
3.4	The co-existing phengite and chlorite	77
3.5	Compositional variations of garnets	90
3.5.1	Introduction	90
3.5.2	Compositional zonation in garnets	9O
3.5.3	Compositional variation of the syn-D_2 garnets	101

			Page
		3.5.3.1 G_{2A} garnet porphyroblasts	101
		3.5.3.2 G_{2B} garnet porphyroblasts	102
		3.5.3.3 G_{2C} garnet porphyroblasts	102
		3.5.3.4 D_2 garnets in the hornblende schists	111
	3.5.4	Compositional variation of the G2-4 garnet porphyroblasts	111
	3.5.5	Garnet-forming reaction (s)	111
	3.5.6	Discussion	118
3.6		Biotite chemistry	122
	3.6.1	Analytical data	122
	3.6.2	Possible biotite-forming reaction (s)	123
	3.6.3	Discussion	130
3.7		Compositional variation of albite	130
	3.7.1	Analytical data	130
	3.7.2	Discussion	131
3.8		Chemical composition of hornblende from the garnet-hornblende schists	138
CHAPTER 4		THE PHYSICAL CONDITIONS OF GARNET GROWTH	
4.1		Introduction	140
4.2		Geothermometry	141
4.3		Effect of octahedral substitution in garnet and biotite	145
4.4		Temperature of retrogression	146
4.5		Geobarometry146	
4.6		Summary	148
CHAPTER 5		SYNTHESIS AND DISCUSSION	
5.1		Garnet distribution and development	159

Page

5.2 Conditions of metamorphism 161

5.2.1 M_1 161

5.2.2 M_2 161

5.2.3 Post-M_2 – pre-M_4 (including M_3) 161

5.2.4 M_4 162

5.2.5 $M_{post\text{-}4}$ (Prograde) 162

5.2.6 $M_{post\text{-}4}$ (Retrograde) 163

5.3 Balquhidder in the Scottish Caledonides 163

CHAPTER 6 CONCLUSIONS 168

REFERENCES 171

LIST OF FIGURES
(Abbreviated titles)

		Page
FIGURE 1.1:	Metamorphic zones in the Scottish Caledonides	2
FIGURE 1.2:	Outline geological map of the Balquhidder district	4
FIGURE 1.3:	Map showing the Balquhidder area in the context of major structures in the SW Highlands	5
FIGURE 1.4:	Sample locality map	7
FIGURE 1.5:	Niggli plots and compositional fields of rocks for the Balquhidder district	15
FIGURE 1.6:	Structural features and relationships	21
FIGURE 1.7:	Structural features and relationships	22
FIGURE 3.1:	Plot of $Mg/(Mg+Fe^{2+})$ of the matrix chlorite (m) *vs* modal % of biotite	54
FIGURE 3.2:	Plot of Na-content in phengite *vs* Na_2O in the bulk rock	67
FIGURE 3.3:	Plot of K-content in phengite *vs* K_2O in the bulk rock	68
FIGURE 3.4:	Plot of K_{Dmg} *vs* X_{mg}^{ph}	79
FIGURE 3.5a:	Tie-line pattern of ph-chl pairs in rocks containing G_{2A}, G_{2B}, G_{2C} and in garnet-free rocks	80
FIGURE 3.5b:	Tie-line pattern of ph-chl pairs in rocks containing G_{2-4} garnet	81
FIGURE 3.6:	Core and rim compositional ranges of the analysed (a) M_2 garnet, (b) M_{2-4} garnets.	92

		Page
FIGURE 3.7:	Compositional profile from centre to edge of a G_{2A} garnet crystal, specimen (1)	103
FIGURE 3.8:	Compositional profile from centre to edge of G_{2A} garnet, specimen (2)	104
FIGURE 3.9:	Compositional profile from edge to edge across a G_{2A} garnet crystal, specimen (8)	105
FIGURE 3.10:	Compositional profiles across two G_{2B} garnet crystals in specimen (11)	106
FIGURE 3.11:	Compositional profile of a G_{2B} garnet porphyroblast	107
FIGURE 3.12:	Compositional profile of a G_{2B} garnet in specimen (10)	108
FIGURE 3.13:	Compositional profile across two G_{2C} garnets in specimen (25)	109
FIGURE 3.14:	Compositional profile from centre to edge across a G_{2A} garnet in hornblende schists, specimen (9)	110
FIGURE 3.15:	Compositional profile of an M_{2-4} garnet porphyroblast in specimen (18)	112
FIGURE 3.16:	Compositional profile of an M_{2-4} garnet in specimen (14)	113
FIGURE 3.17a:	Compositional profile from edge to edge in M_{2-4} garnet in specimen (16)	114
FIGURE 3.17b:	Compositional profile from centre to edge in M_{2-4} garnet in specimen (16)	115
FIGURE 3.18:	Compositional profile in an M_{2-4} garnet in specimen (17)	116

		Page
FIGURE 3.19:	Compositional profile of M2-4 garnet in specimen (5)	117
FIGURE 3.20:	Schematic representation of product (garnet)-reactant (chlorite) equilibria in T-X space	120
FIGURE 3.21:	Modal % of biotite *vs* Al_2O_3% in the bulk rock composition	124
FIGURE 3.22	Compositional profile of an albite porphyroblast crystal from specimen (25) showing type (a) zoning pattern	132
FIGURE 3.23:	Compositional profile in albite crystal in specimen (17) showing asymmetrical type (a) pattern	133
FIGURE 3.24:	Compositional profile in albite crystal from specimen (11) showing symmetrical type (a) pattern	134
FIGURE 3.25:	Compositional profile in albite crystal in garnet-free rock showing type (b) pattern, specimen (29)	135
FIGURE 4.1:	Plot of LnK *vs* 10^4 / T(K^o) for 3 garnet-biotite thermometers	144
FIGURE 5.1a	Geological map of the Balquhidder area showing temperatures in ^oC derived from garnet-biotite and garnet-hornblende geothermometry for rocks containing G_{2A}, G_{2B} and G_{2C} garnet phase (*cf.* Fig. 1.4 for sample numbers)	166

Page

FIGURE 5.1b Geological map of the Balquhidder area showing temperatures in °C derived from garnet-biotite geothermometry for rocks containing the G_{2-4} garnet phase (*cf.* Fig. 1.4 for sample numbers). 167

LIST OF TABLES

(abbreviated titles)

		Page
1.1:	Modal analyses of rocks for the Balquhidder district	9
1.2a:	Major element analyses	11
1.2b	Trace element analyses	13
1.3a	Means (X) and standard deviations (σ) for the Scottish Dalradian pelites, and rocks from the Balquhidder district	16
1.3b	Average values for trace elements for shales, and rocks of Balquhidder district	17
2.1	Average length-breadth (mm) measurements of garnets	41
2.2	Grain sizes (lengths) and MnO core-rim composition in representative garnets	42
2.3	Sequence of mineral growth-Balquhidder area	48
3.1a	Chemical composition of matrix chlorite (m) in rocks containing G_{2A} garnet in Pitlochry Schist	55
3.1b	Chemical composition of matrix chlorite (m) in rocks containing G_{2B} garnet in the Ben Lui Schist	56
3.1c	Chemical composition of matrix chlorite (m) in rocks containing G_{2C} garnet in the Pitlochry Schist	57
3.1d	Chemical composition of matrix chlorite (m) in garnet-free rocks in the Pitlochry Schist	58

		Page
3.1e	Chemical composition of matrix chlorite (m) in rocks containing the M_{2-4} garnet	59
3.2a	Chemical composition of chlorite (r) replacing G_{2A} garnet	60
3.2b	Chemical composition of chlorite (r) replacing G_{2B} garnet	61
3.2c	Chemical composition of chlorite (r) replacing G_{2C} garnet	62
3.2d	Chemical composition of chlorite after biotite	63
3.2e	Chemical composition of chlorite (r) replacing the post-D_2 - pre-D_4 garnet	64
3.3a	Muscovite composition in rocks containing G_{2A} garnet	69
3.3b	Muscovite composition in rocks containing G_{2B} garnet	72
3.3c	Muscovite composition in rocks containing G_{2C} garnet	73
3.3d	Muscovite composition in garnet-free lithologies	74
3.3e	Muscovite composition in G_{2-4} garnet-bearing lithologies	75
3.4a	Composition of the phengite-chlorite pairs co-existing in G_{2A} garnet-bearing Pitlochry Schist	82
3.4b	ph-chl pairs in G_{2B} garnet-bearing Ben Lui Schist	84
3.4c	ph-chl pairs in G_{2C} garnet-bearing Pitlochry Schist	85
3.4d	ph-chl pairs in garnet-free Pitlochry Schist	86

		Page
3.4e	ph-chl pairs with the post-D_2 - pre-D_4 garnet-bearing lithologies	87
3.4f	X_{mg} for phengite (ph) - chlorite (chl) pairs and the distribution coefficient K_D	89
3.5a	Chemical composition of G_{2A} garnet	94
3.5b	Chemical composition of G_{2B} garnet	96
3.5c	Chemical composition of G_{2C} garnet	98
3.5d	Chemical composition of G_{2-4} garnet	99
3.6a	Chemical composition of biotite in rocks containing G_{2A} garnet	125
3.6b	Chemical composition of biotite in rocks containing G_{2B} garnet	126
3.6c	Chemical composition of biotite in rocks containing G_{2C} garnet	127
3.6d	Chemical composition of biotite in rocks containing G_{2-4} garnet	128
3.6e	Chemical composition of biotite in garnet-free rock	129
3.7	Analysis of albite porphyroblasts	136
3.8	Chemical analysis of hornblende from the garnet-hornblende schists	139
4.1a	Temperature estimates based on garnet (core)-biotite (Matrix) compositions	149

		Page
4.1b	Temperature estimates based on garnet (rim)-biotite (matrix) compositions	150
4.2a	Mole fractions of Fe, Mg, Mn, Ca in garnet (rim) composition and Fe^{2+}, Mg, Ti, Al^{+6} in matrix biotite	151
4.2b	X_{Mn-ca}, $X_{Ti-Al+6}$, K_D values and temperature estimates obtained by using 3 calibrations	152
4.3	Temperature estimate of hornblende schists (sp. 9) using garnet-hornblende geothermometerof Graham and Powell (1984)	153
4.4	Garnet-biotite geothermometry; corrected form	154
4.5a	Estimated temperature of retrogression using garnet rim (Rr) composition and matrix biotite composition based on Ferry and Spear (1978) calibration	155
4.5b	Estimated temperature of retrogression using garnet rim (Rr) composition and hornblende composition based on Graham and Powell (1984) calibration	156
4.5c	Estimated temperature of retrogression using garnet rim (Rr) composition and biotite (R.G.) composition based on Ferry and Spear (1978) calibration	157
4.6	Estimated pressure using Biotite-muscovite-chlorite-quartz assemblage, based on Powell and Evans (1984)	158

ACKNOWLEDGEMENTS

I am indebted to my supervisor Professor D.R. Bowes for all his help, considerable interest, enthusiasm and constant advice.

My grateful thanks to Professor B.E. Leake for his helpful support, and for the numerous ways in which he rendered assistance during the difficult times of my research.

All staff members at the Department of Geology and Applied geology of the University of Glasgow also deserve sincere thanks and much appreciation.

I would like to thank Mr Roddy Morrison, the Departmental Superintendant, who was a constant source of inspiration; the technical staff for their assistance, and in particular, Mr Douglas Maclean for his skill and instruction in photography, and Mrs Sheila Hall for her skill in tracing the figures. Technical assistance was also provided by Mr George Bruce, for which he is thanked.

I am grateful to the secretarial staff, Mrs Irene Wells and Mrs Mary Fortune for their friendly help, and in particular Mrs Betty Mackenzie who typed this thesis with patience and enthusiasm, for which she is sincerely thanked

I wish to express my grateful thanks to the Egyptian Government and the Egyptian Education Bureau for their continuous support and sponsorship during my stay in Britain.

Lastly, but by no means least, I would like to express my undying gratitude to my wife, Enas, for her continual support and encouragement, and my son Ahmed, for his never-ending cheer.

ABSTRACT

The metamorphic rocks at Balquhidder are polyphase deformed and polymetamorphosed with the $D_1 - D_4$ sequential development of structures and the $M_1 - M_4$ development of minerals generally corresponding to that expressed in nearby areas. Garnet is found throughout the area and the Barrovian garnet-isograd must have been at least 2Km above the present topography. There is no garnet-biotite boundary present. The incoming of garnet was controlled by the bulk rock composition so that garnetiferous and non-garnetiferous schists can occur in the same, or adjacent outcrops.

Textural studies have shown that two phases of garnet growth occurred. The more prominent of these was during M_2 when three different types were formed (G_{2A}, G_{2B}, G_{2C}), two only in lithologies of the Pitlochry Schist (G_{2A}, G_{2C}) and the other (G_{2B}) only in the Ben Lui Schist. Growth of garnet was related to particular mineral reactions, non-instantaneous nucleation and reaction partitioning. This has been substantiated by the determination, using the electron microprobe of chlorite, muscovite, garnet, biotite, albite and hornblende compositions. Garnet-biotite and garnet-hornblende pairs permit temperatures of M_2 metamorphism to be determined: 530°C – 482°C for type G_{2A} (almandine), 423 – 410°C for type G_{2B} (almandine) and 370°C for type G_{2C} (spessartine-rich). The 530°C estimate for G_{2A} is considered to represent climactic conditions and, when considered with a pressure estimate of 7Kb based on the biotite-muscovite-chlorite-quartz geobarometer, indicates a typical Barrovian heat flow of *c.*, 27°C/Km and mid-amphibolite-facies conditions. On the basis of regional correlation of structures, the M_2 metamorphism (and $D_1 - D_2$) is related to the pre-590Ma Grampian Orogeny and was followed by elevation of temperature to its peak during crustal thickening during D_1 (Tay Nappe formation).

A second phase of garnet growth took place post-D_2 – pre-D_4 (possibly post-D_2 – pre-D_3). Temperature of development of G_{2-4} ($?G_{2-3}$) was 377°C for a spessartine-rich type, i.e. in the green schist facies. The elevation of temperature is related to the *c.* 500Ma event demonstrated elsewhere in the Highlands on the basis of isotopic studies and during which crustal thickening is postulated.

Previous interpretations of the presence of an inverted garnet isograd are not substantiated by this investigation. The structural development does not permit inversion of M_2 or M_{2-4} geotherms by tectonic activity, while the distribution of garnet throughout the area does not permit the presence of any isograd to be demonstrated. Rather the whole area is within the garnet zone. Two of the previous interpretations, which suggest an inverted zonal distribution, recognized neither the composition – nucleation – reaction partitioning controls nor the polyphase development of garnet. One sets out a position for a "garnet isograd" that corresponds to the prominent development of G_{2A} and G_{2C} garnets in particular flat-lying units of the Pitlochry Schist. The other sets out a position for a "garnet isograd" that corresponds to the prominent development of G_{2B} and G_{2-4} garnets in particular units of the Ben Lui Schist. These interpretations are rejected on the basis of the detailed evidence set out here.

D_4 and post-D_4 mineralogical expressions only result in minor modifications to the earlier formed features. D_4 is correlated with the regionally expressed *c.* 460Ma period of uplift and post-D_4 mineral growth was both prograde and retrograde.

The deformation and metamorphic history in the Balquhidder area generally corresponds to, and may be representative of, Caledonian activity in at least considerable parts of the SW Highlands.

DECLARATION

The material presented herein is the result of independent research by the author undertaken between October 1985 and November 1989 at the Department of Geology and Applied Geology, University of Glasgow. Any published or unpublished results of other workers have been given full acknowledgment in the text.

Sherif M.A. Fawzy

CHAPTER 1

GEOLOGICAL SETTING, ROCK UNITS AND STRUCTURAL FRAMEWORK.

1.1. Isograds: their distribution and disposition

The outcrop traces of planes which represent the positions at which different mineralogical reactions take place, and so separate different metamorphic mineral assemblages, are commonly referred to as isograds. They have been mapped in different lithologies by many workers all over the world following the pioneer work of Barrow (1893, 1912) in the SE Highlands of Scotland, which set out the distribution of what have become referred to as Barrow's or Barrovian zones. Tilley (1925) and Elles and Tilley (1930) continued Barrow's zones in the Dalradian assemblages of the Caledonides and along with Harker (1939), they considered that an isograd reflected the operation of particular physical conditions (especially pressure and temperature) in rocks of specific compositions.

Much subsequent work has evaluated the roles of temperature (*e.g.* Turner and Verhoogen, 1960) and of pressure (*e.g.* Loomis, 1986,) in influencing the development of those zone boundaries while various authors have presented evidence to show that, at least in places, they do not correspond to isothermal or isobaric surfaces (*cf.* Chinner, 1966; Thompson, 1976; Bhattacharyya and Das, 1983).

The present near-vertical disposition of the Barrovian zones in the SE Highlands of Scotland occurs in the region of the Highland Border downbend, a late Caledonian major structure that post-dates the peak of metamorphism in that region (*cf.* Harte *et al.*, 1984, fig.1). Further W, through the Central Highlands and in much of the SW Highlands N of the downbend, the garnet (almandine) isograd, for example, is shown on maps depicting the regional isograd pattern as a generally WSW- to SW-trending line with the overall zonal pattern of isograds indicative of an elongate thermal dome (Fig.1.1). However locally in the Balquhidder district of western Perthshire the garnet (almandine) isograd is shown by Tilley (1925), Elles and Tilley (1930), Trendall (1953) and Watkins (1984) as

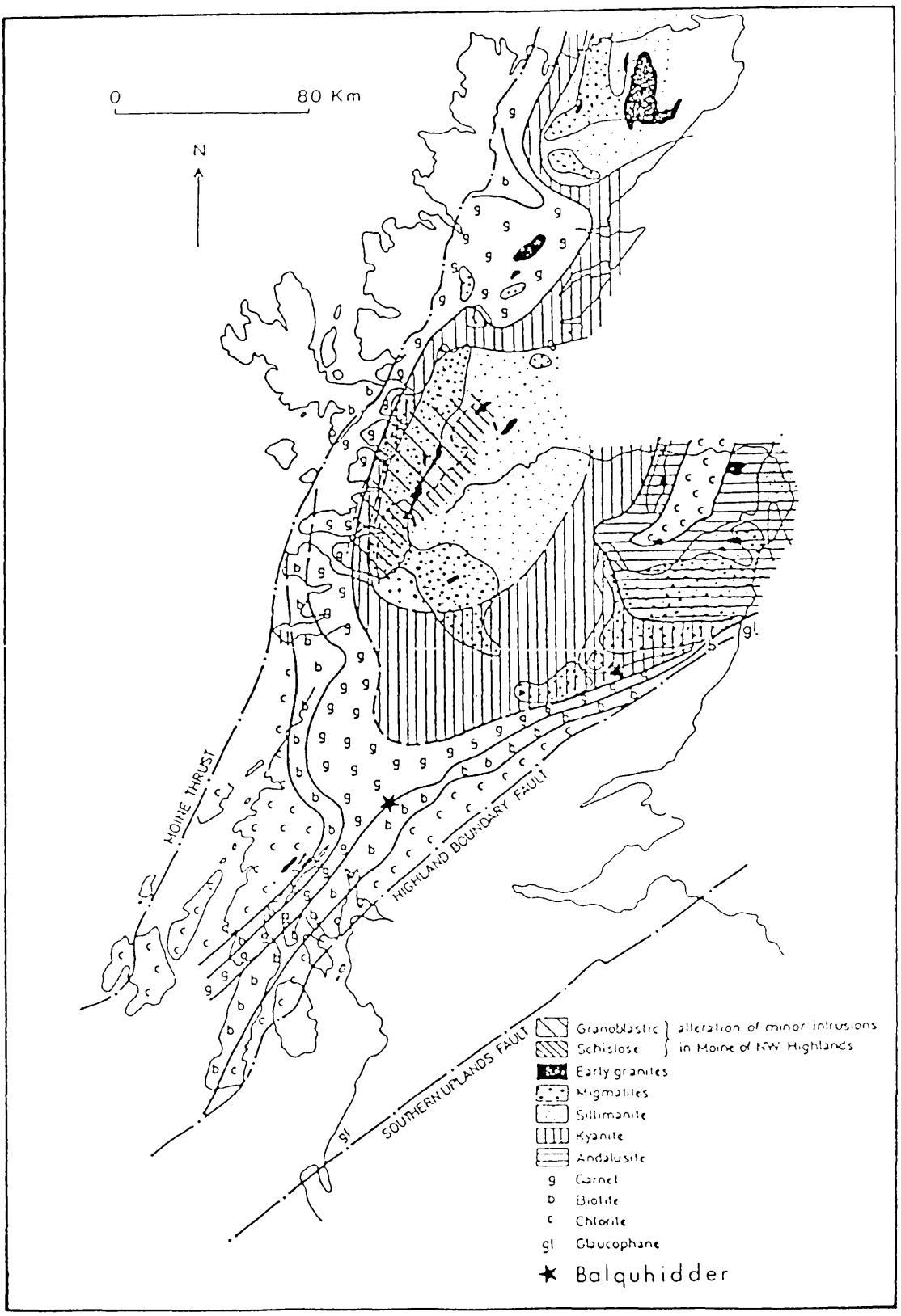

FIG. 1.1 Metamorphic zones in the Scottish Caledonides; from Johnson (1983)

being both flat-lying and inverted with garnet grade rocks shown as overlying biotite grade rocks (see Fig.1.2). While there are significant differences in the location of the isograd given by the different authors they all show the isograd surface to be gently NNW- to NW-dipping and with higher grade rocks above rocks of lower grade.

Elles and Tilley (1930) considered that the disposition of the zone boundary was intimately related to nappe emplacement during which both the stratigraphy and metamorphic zones were inverted. Such an interpretation implies that garnet growth in the Balquhidder district was very early, *i.e.* before or during the formation of the Tay nappe (*cf.* Fig.1.3b). The explanation of Watkins (1984) was that metamorphism had occurred in a negative thermal gradient with the same author (Watkins, 1985) suggesting that the initial temperature inversion was related to the emplacement of the Tay nappe with the subsequent modification being the result of convective transfer of heat by fluids derived from metamorphic reactions taking place at depth.

The thermal model of Watkins (1984, 1985) is apparently unique in studies of Caledonides in SW Scotland and it does not appear to explain either why the effects of the negative thermal gradient (in the Balquhidder district) are so very localized or why it had no apparent effect on the isograd disposition in adjacent areas. There, according to Watkins (1985, p.163); the shallowly-northerly dipping and inverted disposition of the isograd in the Balquhidder district changes westwards to a vertical disposition while southwards towards the Highland Border region (but at a higher level now not seen because of erosion) it changes again to having a "normal" non-inverted disposition, (Fig.1.2, section A-A). Likewise the interpretation of Tilley (1925) and Elles and Tilley (1930) does not account for the very localized nature of the suggested inversion, nor why the westward continuation of its surface trace is nearly straight through the area towards Crianlarich where there is considerable topographic relief (*i.e.* the disposition of the isograd is near vertical - Fig. 1.3; *cf.* Jones 1964; Atherton, 1964). Certainly its disposition is in marked contrast to the generally S-dipping attitude of metamorphic zones (*c.* 16km "down dip" demonstrated by Atherton (1968) in the flat-belt of central Perthshire.

The disposition of isograds is of major importance in determining the history of the Caledonides. It is also of importance in relation to the

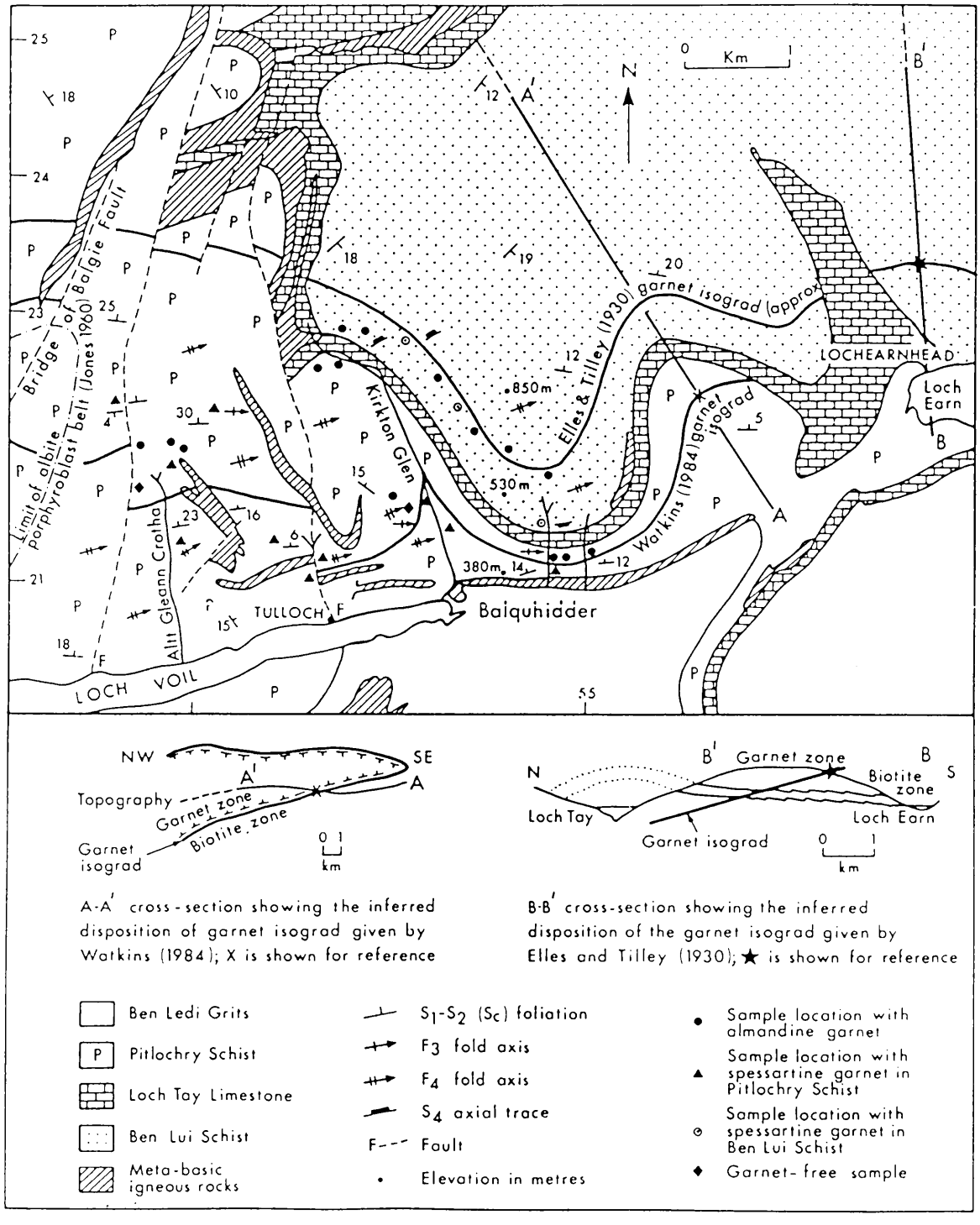

FIG. 1.2 Outline geological map of the Balquhidder district showing location of samples (cf. Fig. 1.4) and the inferred distribution of the garnet isograd given by Elles and Tilley (1930) and Watkins (1984)

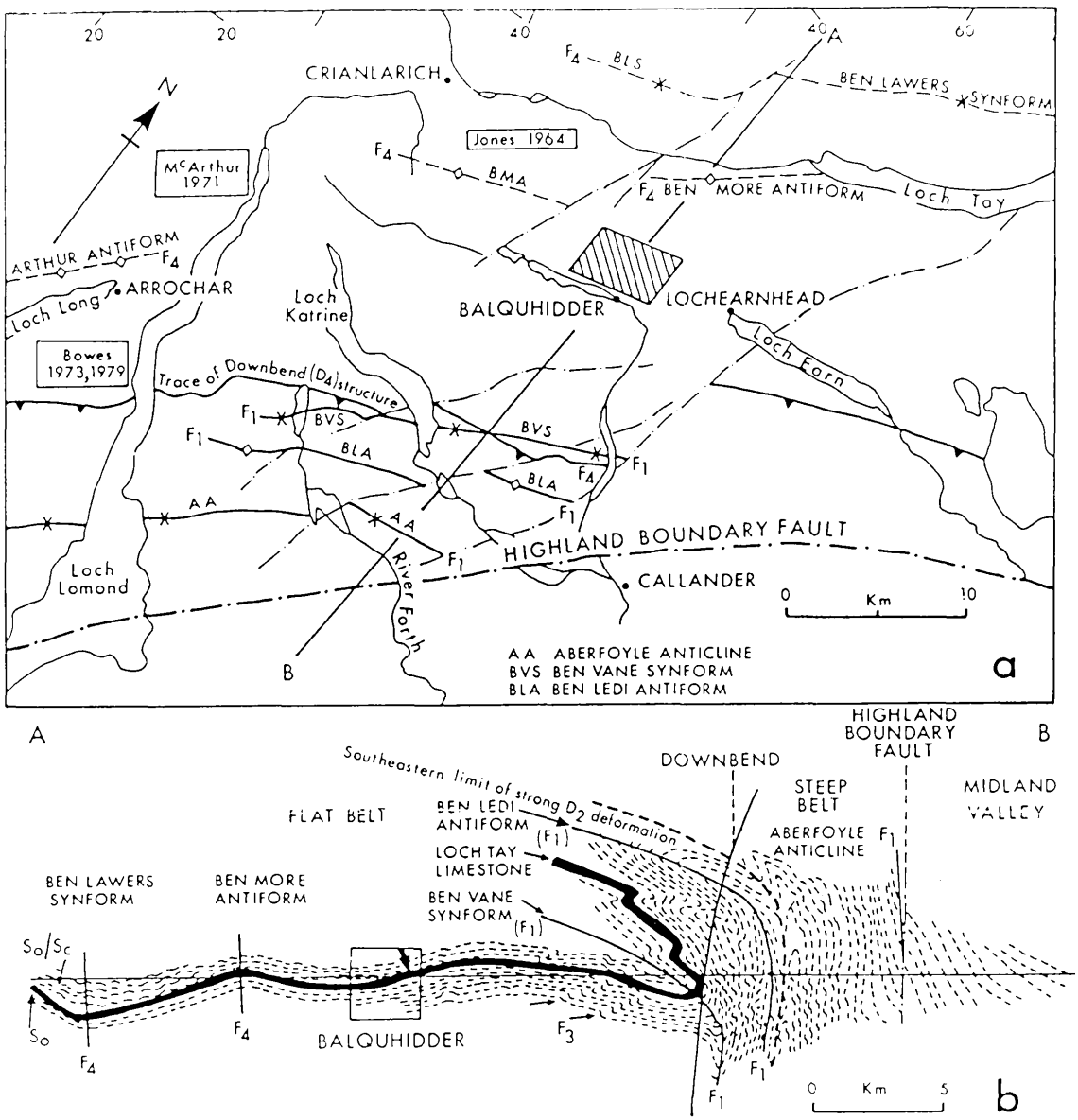

FIG. 1.3 (a) Map showing the Balquhidder area (hatched) in the context of major structures in the SW Highlands, and location of nearby areas where other workers have established structural successions; line of section (A-B) given in (b) (modified from Harte *et al.*, 1984)

nature and development of isograds in dynamothermal metamorphism as the existence of inverted isograds in other orogenic belts related to collison tectonics has been variously ascribed to (1) rotation of isograds by folding (*e.g.* Mason, 1984; Boyle, 1987), (2) heat generation associated with thrusting (*e.g.* Scholz, 1980), (3) advection of fluids along the fault surfaces (*e.g.* Peacock, 1986), (4) conductive transfer of heat from a hot upper plate to a cooler lower plate (*e.g.* Oxburgh and Turcotte, 1974), and (5) the effects below a high level igneous mass (*e.g.* St. Onge, 1981). Demonstration of any such effects in the Caledonian terrane would necessitate rethinking of concepts of Barrovian metamorphism.

1.2. Geological setting and rock units.

The rocks of the Balquhidder district are on the lower limb of the Tay nappe. The lithological units which are generally flat-lying (Fig. 1.3b) make up parts of the Argyll and Southern Highland groups of the Dalradian Supergroup and are now seen in inverted stratigraphic succession. The Loch Tay Limestone is a marker horizon. It generally dips at shallow angles to the N and approximately follows the contours from the head of Kirkton Glen (N of Balquhidder) to Lochearnhead (Fig. 1.2). Stratigraphically below it (but now structurally above it) is the Ben Lui Schist; stratigraphically above it is the Pitlochry Schist (see Mendum & Fettes, 1985, fig. 2). It is in these two dominantly pelitic and semipelitic units in which garnet and biotite variably occur and the samples used for mineralogical and petrological studies come from the *c.* 300m of the Ben Lui Schist immediately above (structurally) the Loch Tay Limestone and the *c.* 150m of the Pitlochry Schist immediately below (structurally) it (Fig. 1.4). Where this calcareous marker horizon is nearby, the stratigraphical control on the sampling is better than where it is further away (W of Kirkton Glen).

The pelitic and semipelitic types are mainly represented by garnet-quartz schists and garnet-quartz-mica schists. Also present, but of patchy distribution, are garnet-free chlorite-mica schists, garnet-free epidote-chlorite schists, and garnet-hornblende schists; these mainly occur W of Kirkton Burn. The more psammitic lithologies were not sampled for mineralogical studies but are important in the recognition of the various sets of structures (*cf.* Figs 1.6, 7). Thinly-bedded marble with psammitic and

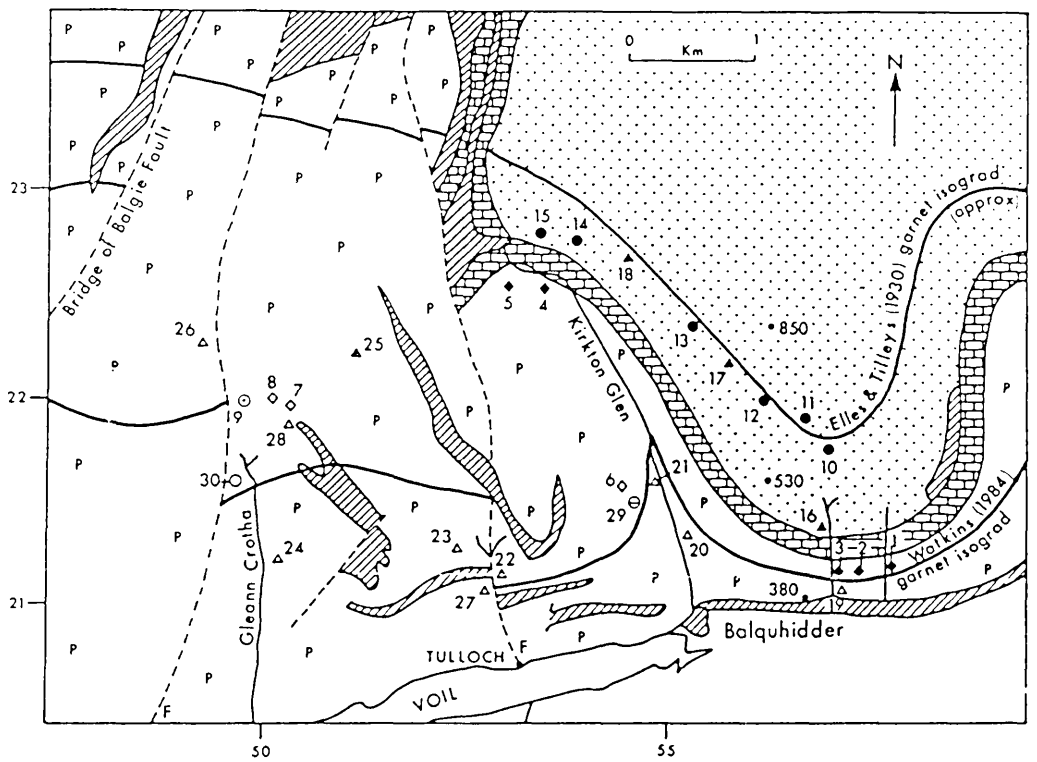

FIG.. 1.4 Sample locality map (cf. Fig.1.2); (♦) Alm-bearing Pitlochry Schists; (◊) Alm-bearing calc-rich Pitlochry Schist; (△) Sp-bearing Pitlochry Schist; (▲) sp-bearing calc-rich Pitlochry Schist; (⊙) Alm-bearing hornblende Schist; (○) garnet-free epidote-chlorite Pitlochry Schist; (⊖) garnet-free Pitlochry Schist; (●) Alm-bearing Ben Lui Schist; (▲) sp-bearing Ben Lui Schist

semipelitic layers and associated metadoleritic and metadioritic massive to foliated lithologies representing metamorphosed basic igneous rocks also occur (Fig. 1.2; *cf.* Wiseman, 1934; Ball, 1965) but were not used in the present investigation.

The predominant garnet-bearing lithologies consist of various combinations of garnet (0 - 14%); chlorite (0.5 - 45%); phengite (2 - 44%)(hereafter referred to as muscovite except where actual mineral composition is discussed); biotite (0 - 19%); quartz (14 - 35%) and albite (3 - 14%). Epidote (0 - 5%) and calcite (0 - 7%) also occur, the former occurring mainly as inclusions in the garnet and albite porphyroblasts while the latter is mainly present in some rocks W of Kirkton Burn (modal analyses given in Table 1.1). Garnet-hornblende schists are recorded at only one locality W of Gleann Crotha (sample 9). The garnet-free epidote schists were found mainly to the W of Kirkton Burn (*e.g.* sample 30). These are finer-grained than many of the other lithologies. They are light to dark green micaceous rocks that contain chlorite (36%), biotite (3%) and abundant epidote (21%). Accessory minerals in both the Ben Lui Schist and Pitlochry Schist are sphene, iron oxide, rutile, tourmaline and zircon. In addition there are iron sulphides, particularly in the garnet-hornblende schists.

The modal data indicates a negative correlation between quartz and phyllosilicates and a positive correlation between quartz and albite, and a general decrease in the proportions of phyllosilicate minerals relative to albite as the rock becomes more siliceous. The index minerals biotite and garnet occur in both the Ben Lui Schist and the Pitlochry Schist. However in the samples studied biotite is more common in the latter while the proportion of garnet varies considerably throughout both units, and both its grain size and habit vary greatly even within short distances up or down the succession. This is illustrated by the presence of elongate skeletal garnets in rocks with no biotite (*e.g.* 6, 7; see Fig. 1.4) and the association of very large (up to 6mm across) equigranular garnet porphyroblast in rocks with abundant biotite (*e.g.* 8; see Fig. 1.4). Both of these types of garnet occur only in the calc-rich lithologies, but in the case of the former the amount of chlorite in the studied samples is 0.5 - 1%, while in the latter it is *c.* 17%. In addition, within the stratigraphic section sampled the largest garnets occur in the Pitlochry Schist.

TABLE 1.1 Modal analysis, specimen localities shown in Figure 1.4;

	Almandine-bearing															Spessartine-bearing													Garnet-free	
	Pitlochry Schist									Ben Lui Schist						Ben Lui Schist				Pitlochry Schist									Pitlochry Schist	
	1	2	3	4	5	6	7	8	9	10	11	12	13	14	15	16	17	18	19	20	21	22	23	24	25	26	27	28	29	30
Gar	5.6	6.1	4.4	1.3	1.4	14	5	9	7.6	4.8	4.6	4	15	4.9	1.5	5.3	6	4.5	0.3	X	X	X	0.3	0.2	1.3	1.9	X	X	-	-
Chl	13	14	26	37	26	1	0.5	17	17	21	16	24.5	30	28	31	26	25.5	25	19	X	X	X	18	45	22	24	X	X	18	36
Mus	34.7	27	14	28	44	29	24	25	28	22	10	28.5	23	36	19	43	24	39	29	X	X	X	33	28	2.1	29.6	X	X	39	4.5
Bio	10.7	15	21	-	0.3	-	-	15	1.2	8.7	16	8	0.8	-	-	0.5	4.5	-	1.5	-	-	X	3.4	-	19	6.6	X	-	-	2.8
Qz	22.5	29	26	24	15	43	50	24	21	26	36	17	20	18.5	32	14	24	19.8	34	X	X	X	35	18	25	32	X	X	30	24
Alb	3.9	3.2	4.7	3.8	7.5	2.9	5.5	4.5	3.5	13.5	14	14.6	7.4	7.7	13	4.7	10	5.5	13	X	X	X	7.2	3.2	3.2	3.2	X	X	8.5	3.7
Tour	3.4	2.2	-	-	1.3	0.8	1.8	0.3	4.8	1.7	0.3	0.9	0.4	1.4	0.5	2.9	0.8	1.6	0.2	X	X	X	0.7	-	-	0.4	X	X	1.5	-
Epid	0.6	-	1.3	-	-	0.4	1.7	-	4.9	-	1.3	-	-	-	-	-	1.2	-	-	-	-	-	-	-	22	-	-	X	-	21
Calc	-	1.3	-	3.4	-	6.4	6.9	3.8	-	-	-	-	-	-	0.3	-	-	-	-	X	-	X	-	0.2	2.6	0.8	-	-	0.5	5.3
Ore	5.6	2.2	2.6	2.5	4.5	2.5	4.6	1.1	1.3	2	1.8	2.5	2.6	3.5	2.1	3.6	3.6	4.6	3	X	X	X	2.4	5.4	2.1	2.2	X	X	2.2	1.8
Hb	-	-	-	-	-	-	-	-	9.3	-	-	-	-	-	-	-	-	-	-	-	-	-	-	-	-	-	-	-	-	-
Sph	-	-	-	-	-	-	-	-	1.4	-	-	-	-	-	-	-	-	-	-	-	-	-	-	-	-	-	-	-	-	-
Zir	-	-	-	-	-	-	-	0.3	-	-	-	-	0.8	-	0.6	-	0.4	-	-	-	X	-	-	-	0.7	0.4	X	-	-	-

Explanation of Tables 1.1, 1.2a, b

1 - 9: Almandine-bearing Pitlochry Schist

10 - 15: Almandine-bearing Ben Lui Schist

16 - 18: Spessartine-bearing Ben Lui Schist

19 - 28: Spessartine-bearing Pitlochry Schist

29,30: Garnet-free Pitlochry Schist

These petrographic features point to the possible control of bulk chemical composition on modal expression of various minerals and possibly a relationship between metamorphic grade and mineral chemistry. To investigate the former, major and trace element analysis was carried out on the 23 representative samples on which modal analysis was also carried out. The latter is dealt with in Chapter 3.

1.3. Rock chemistry

The proportions of major elements are presented in Table 1.2a; trace element compositions (16 elements) are given in Table 1.2b. On the basis of these data the following features can be established for the schists:

1. There is strong correlation between K_2O and modal proportions of muscovite (except for 15).

2. Rocks with 48 - 50% SiO_2 contain relatively high K_2O but increased proportions of Na_2O; this is related to the proportions of albite present.

3. The Al_2O_3 generally shows a general antipathetic relationship with the modal percentage of biotite, but there are some exceptions.

4. Fe^{tot} shows regular distribution in relation to modal proportions of quartz and phyllosilicates, but there is no such regular distribution in FeO/Fe_2O_3.

5. There is a correspondence between CaO proportion and distinctions between calc-rich and calc-poor samples demonstrated solely on petrographic grounds.

Plots of Niggli values calculated from the chemical data are used here as a basis for comparison with other sedimentary assemblages, with the following features being particularly significant.

TABLE 1.2a Chemical composition (major elements) of rocks of the Balquhidder district

	Pitlochry Schist							Almandine-bearing		Ben Lui Schist					
	1	2	3	4	5	6	7	8	9	10	11	12	13	14	15
SiO_2	57.75	69.33	77.91	60.17	58.09	77.20	76.83	52.72	54.40	70.51	77.70	-	67.20	47.92	44.86
TiO_2	1.26	0.64	0.56	0.90	1.10	0.52	0.69	1.08	1.33	0.65	0.63	-	0.60	1.41	1.37
Al_2O_3	20.16	14.75	10.63	19.30	21.17	10.44	10.74	17.17	21.97	14.31	11.22	-	14.25	27.14	28.80
Fe_2O_3	2.38	1.07	1.43	1.62	1.72	1.81	1.08	1.85	3.09	1.11	2.28	-	1.13	2.67	2.53
FeO	5.09	3.49	6.39	5.09	6.02	2.28	2.83	8.23	6.22	3.69	1.87	-	6.08	6.86	7.30
MnO	0.14	0.09	0.11	0.13	0.09	0.07	0.11	0.16	0.17	0.09	0.07	-	0.14	0.14	0.05
MgO	2.00	1.51	2.80	2.17	2.50	0.68	0.53	4.61	2.23	1.48	1.25	-	1.63	2.88	3.60
CaO	0.89	1.26	0.64	1.12	0.34	2.76	3.15	4.63	1.93	0.34	0.69	-	0.95	0.42	0.30
Na_2O	3.07	2.82	1.28	3.25	2.30	1.10	1.24	3.09	3.34	3.95	3.04	-	2.02	1.32	1.53
K_2O	4.45	2.59	2.19	3.78	4.79	2.05	2.27	2.15	3.74	1.87	1.47	-	1.96	6.14	6.10
P_2O_5	0.25	0.11	0.08	0.12	0.16	0.07	0.09	0.15	0.20	0.09	0.08	-	0.05	0.18	0.19
H_20	2.39	2.07	1.86	2.22	1.17	1.32	1.05	1.40	2.54	1.24	1.17	-	1.70	3.10	3.45
CO_2	0.48	0.86	0.20	0.23	0.12	0.21	0.22	1.53	1.07	0.14	0.63	-	1.16	0.18	0.17
Total	100.31	100.59	101.08	100.1	99.57	100.51	100.83	98.77	102.23	99.47	102.1	-	98.87	100.36	100.25
O.R.	29.06	22.22	17.85	21.43	21.43	38.71	27.59	16.51	30.51	21.43	51.85	-	14.81	26.09	24.56
$Mg/Mg+Fe^{2+}$	0.41	0.44	0.44	0.43	0.43	0.35	0.25	0.50	0.39	0.42	0.54	-	0.32	0.43	0.47
Fe^{2+}/Fe^{3+}	4.75	7.25	9.93	6.98	7.78	2.80	5.82	9.89	4.47	7.39	1.82	-	11.96	5.71	6.41

- = Not analysed

TABLE 1.2a (contd)...

	Ben Lui Schist			Spessartine-rich			Pitlochry Schist							Garnet-free Pitlochry Schist	
	16	17	18	19	20	21	22	23	24	25	26	27	28	29	30
SiO_2	48.96	73.20	62.89	-	-	-	58.36	66.18	48.71	47.04	-	-	-	71.28	48.92
TiO_2	1.29	0.62	0.91	-	-	-	1.06	0.71	1.30	1.25	-	-	-	0.58	1.17
Al_2O_3	25.92	13.07	19.15	-	-	-	15.17	16.77	25.61	20.90	-	-	-	13.63	15.39
Fe_2O_3	1.84	0.70	2.47	-	-	-	2.30	1.05	0.87	4.55	-	-	-	0.59	1.73
FeO	7.39	2.80	3.67	-	-	-	6.24	4.81	8.35	6.96	-	-	-	4.23	7.41
MnO	0.20	0.05	0.09	-	-	-	0.16	0.06	0.10	0.21	-	-	-	0.03	0.17
MgO	2.92	1.19	1.84	-	-	-	4.38	2.31	2.67	4.86	-	-	-	1.93	7.08
CaO	0.65	0.55	0.19	-	-	-	2.86	0.21	0.65	5.06	-	-	-	0.79	8.06
Na_2O	1.53	2.68	1.15	-	-	-	5.48	3.66	2.77	4.24	-	-	-	2.81	3.16
K_2O	5.84	2.84	4.54	-	-	-	0.51	3.24	5.34	2.97	-	-	-	2.47	0.21
P_2O_5	0.14	0.10	0.14	-	-	-	0.14	0.11	0.29	0.15	-	-	-	0.08	0.21
H_2O	2.39	1.95	3.16	-	-	-	2.62	1.88	1.56	1.48	-	-	-	2.10	2.76
CO_2	1.18	0.39	0.12	-	-	-	0.92	0.13	0.83	0.53	-	-	-	0.46	1.30
Total	100.25	100.14	100.32	-	-	-	100.2	101.03	99.05	100.2	-	-	-	100.98	97.57
O.R.	18.18	16.51	16.51	-	-	-	24.56	16.51	7.69	36.07	-	-	-	11.32	18.18
$Mg/Mg+Fe^{2+}$	0.41	0.43	0.47	-	-	-	0.56	0.46	0.36	0.55	-	-	-	0.45	0.63
Fe^{2+}/Fe^{3+}	8.93	8.89	3.30	-	-	-	6.03	10.18	21.33	3.40	-	-	-	15.94	9.52

TABLE 1.2b Trace element analyses of rocks for the Balquhidder district

	Almandine-bearing														Spessartine-bearing														Garnet-free	
	Pitlochry Schist										Ben Lui Schist				Ben Lui Schist				Pitlochry Schist										Pitlochry Schist	
	1	2	3	4	5	6	7	8	9	10	11	12	13	14	15	16	17	18	19	20	21	22	23	24	25	26	27	28	29	30
Zr	309	196	988	226	242	222	249	153	267	234	273	-	242	191	225	283	234	200	-	-	-	176	162	177	185	-	-	-	166	104
Y	37	19	102	27	32	17	18	31	29	15	21	-	14	11	33	29	15	20	-	-	-	20	18	31	37	-	-	-	15	24
Sr	195	100	192	162	171	71	86	156	378	116	359	-	55	167	203	145	201	116	-	-	-	117	78	162	316	-	-	-	106	381
U	3	2	6	3	3	3	3	2	3	3	2	-	1	2	2	4	2	2	-	-	-	2	3	4	3	-	-	-	2	1
Rb	155	86	78	115	174	84	82	87	142	70	61	-	66	219	233	207	102	157	-	-	-	15	105	181	91	-	-	-	71	9
Th	14	8	14	13	12	9	7	8	12	9	7	-	7	15	18	14	7	8	-	-	-	5	7	13	12	-	-	-	7	5
Pb	23	23	20	14	25	19	17	8	38	17	9	-	15	87	29	27	8	42	-	-	-	8	17	26	20	-	-	-	33	14
Ga	28	16	21	22	26	11	12	20	29	16	14	-	17	32	32	31	17	22	-	-	-	18	18	27	24	-	-	-	14	15
Zn	130	82	316	86	132	65	64	110	116	73	61	-	98	131	159	148	60	97	-	-	-	119	95	166	114	-	-	-	80	102
Cu	27	28	23	53	29	5	5	44	36	14	10	-	5	24	45	20	5	18	-	-	-	50	28	71	44	-	-	-	20	31
Ni	43	30	5	81	58	15	11	78	50	21	24	-	28	27	45	63	18	11	-	-	-	69	29	57	79	-	-	-	32	48
Co	22	12	11	20	28	5	3	42	29	12	23	-	12	19	25	31	6	10	-	-	-	31	16	28	39	-	-	-	16	41
Cr	102	84	34	100	116	49	49	173	124	90	84	-	78	146	145	151	73	95	-	-	-	186	87	147	208	-	-	-	80	236
Ce	126	63	293	90	137	53	54	63	126	45	58	-	47	8	152	127	49	67	-	-	-	36	63	144	90	-	-	-	45	20
Ba	893	373	925	732	1368	573	595	416	975	348	656	-	416	794	801	1079	945	489	-	-	-	160	580	897	1161	-	-	-	519	120
La	31	31	131	46	88	24	23	28	43	11	33	-	18	-	69	61	21	24	-	-	-	8	19	69	43	-	-	-	10	9

1. On a c *vs.* mg plot most samples plot within the field for pelitic rocks of Van de Kamp (1970)(Fig. 1.5a). Those samples that plot outside of this field have modal compositions showing high calcite and epidote.

2. On a *k vs. mg* plot most samples fall within the field for pelitic rocks of Atherton and Brotherton (1982), a field that includes the majority of pelites of the Dalradian Supergroup. Those that do not show high $Na_2O:K_2O$ are mainly those having considerable proportions of albite. This is consistent with the observation of Atherton and Brotherton (1982) that other Dalradian rocks with a considerable proportion of albite plot below the $k = 0.3$ line.

The geochemical similarities of the analysed Balquhidder rocks to other Scottish Dalradian pelites and to the shales are also shown by averages for major and trace elements (Tables 1.3a,b). Hence, for the samples used in this study, the geochemical characteristics can be taken as being normal and used with confidence in the assessment of the nature and distribution of the mineral composition resulting from metamorphism. The influence of original chemical composition on mineral paragenesis and the relationships of mineral and rock chemistry are discussed in Chapter 3.

1.4 Structural framework

Regionally the rock assemblage lies on the inverted limb of the Tay nappe within the "flat belt" where not only lithological units So but also the dominant schistosity Sc are generally flat-lying. The general gentle NNW dip of both lithology and Sc defines one limb of a very open major upright fold with a NE-SW-trending subhorizontal axis that forms one of the regionally expressed F_4 folds of which the Ben More antiform and Ben Lawers synform are prominent representatives further north. Even later faults of the Loch Tay fault set transect the district (Fig. 1.3a,b).

Within the Balquhidder district the rocks show clear evidence of polyphase deformation and the structural succession was determined in the

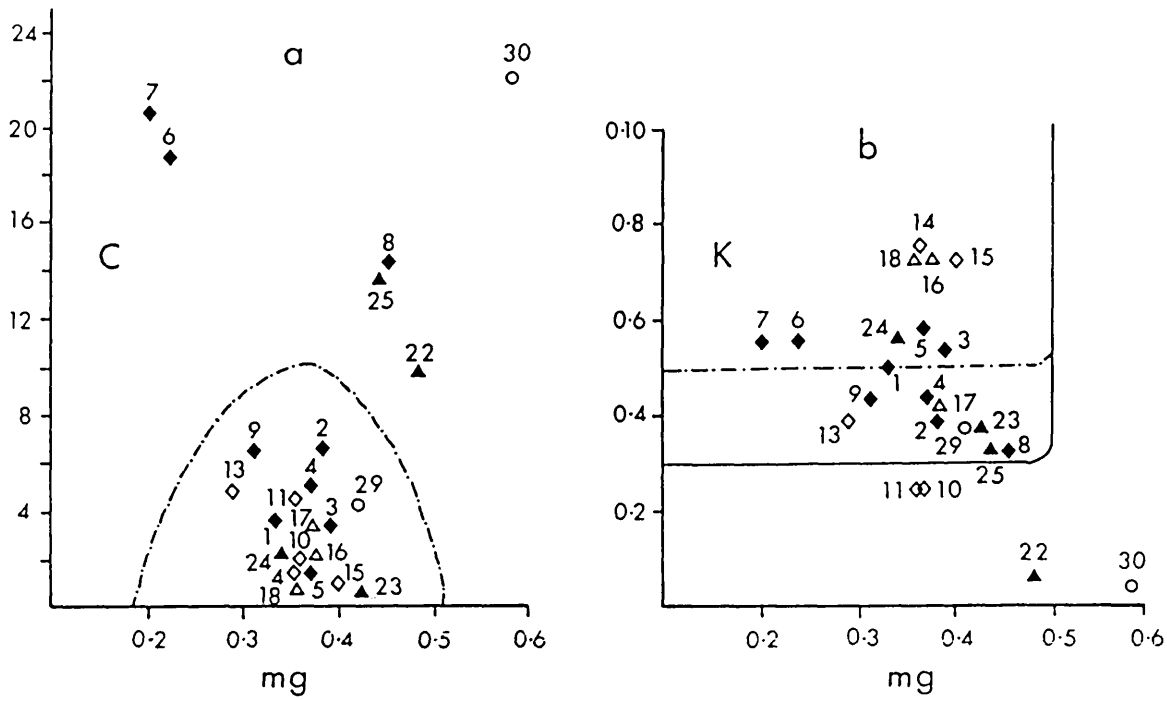

FIG. 1.5 Niggli plots and compositional fields

(a) Plot of c *vs.* mg with field for pelitic rocks after Van de Kamp (1970)

(b) Plot of k *vs.* mg with field for pelitic rocks that includes the majority of pelites of the Dalradian Supergroup (solid line) from Atherton and Brotherton (1982)

(♦) Alm-bearing Pitlochry Schist; (◊) Alm-bearing Ben Lui Schist

(▲) sp-bearing Pitlochry Schist; (△) sp-bearing Ben Lui Schist

(○) garnet-free Pitlochry Schist

TABLE 1.3a: Means ($\bar{x}$) and standard deviations (σ) for the Scottish Dalradian pelites: from Atherton and Brotherton (1982, table 1), and rocks from the Balquhidder district (from Table 1.2a)

	Scottish Dalradian Pelites		Rocks of Balquhidder district	
	$\bar{x}$	σ	$\bar{x}$	σ
SiO_2	59.88	10.87	61.44	10.67
TiO_2	1.03	0.46	0.94	0.32
Al_2O_3	19.15	6.02	17.70	5.36
Fe_2O_3	2.49	2.28	1.80	0.89
FeO	5.15	2.56	5.36	1.90
MnO	0.12	0.09	0.11	0.05
MgO	2.34	1.07	2.57	1.48
CaO	1.03	0.75	1.67	1.93
Na_2O	2.10	1.05	2.64	1.11
K_2O	3.50	1.52	3.20	1.66
H_2O+	2.55	1.12	2.59	0.81
No. of analyses	230		23	

TABLE 1.3b: Average values for trace elements for shales (A: Krauskopf, 1983; B: Turekian and Wedepohl, 1961; C: Rocks of Balquhidder district) of 23 analyses given in Table 1.2b.

	A	B	C
Zr	180	160	248
Y	35	26	-
Sr	400	300	175
U	3.5	3.7	-
Rb	140	140	113
Th	12	12	-
Pb	20	20	21
Ga	25	19	20
Zn	90	95	113
Cu	50	45	27
Ni	80	68	37
Co	20	19	20
Cr	100	90	114
Ce	70	59	85
Ba	600	580	687
La	-	92	-

field, and confirmed by thin section study, using refolding and cross-cutting (*e.g.* of cleavages) relationships as bases. It has been used as a framework into which the metamorphic mineral growths have been integrated.

D_1

No small F_1 folds have been recognized around Balquhidder but the presence of a large structure (Tay nappe) is indicated by the inverted stratigraphical sequence. If there were any related small-scale structures they must have been dissected and destroyed during D_1 or the later D_2 deformation, or isolated by tectonism so that they cannot be distinguished from F_2 folds. The earliest recognized schistosity (S_1) has no observed geometrical relationship to any folds but is deformed by intrafolial tight to isoclinal folds (F_2)(Pl. 1.2a; Fig. 1.6a,b) to which the second recognised schistosity (S_2) has an axial planar relationship. It is on these bases that S_0-S_1 - S_2-F_2 relationships are established. In addition penetrative (S_2) schistosity is discordant to remnants of an earlier schistosity (Pls 1.1a, b; 1.2b).

D_2

Folds (F_2) deform the first recognized schistosity (S_1) and quartz segregation veins are generally intrafolial, tight to isoclinal, and commonly strongly dissected. They are best preserved in the more psammitic lithologies. Commonly fold noses are much thicker than fold limbs (Fig. 1.6c), and many occur as detached and isolated fold hinges (Fig. 1.6a,b). There is a prominent axial planar schistosity (S_2) but in fold limbs there is a composite schistosity (Sc - S_1+S_2) with evidence for foliation transposition. Locally a strong mineral lineation (L_2) is developed. Many of the F_2 fold axes have a general N - S trend but others trend NW. It is not known whether this variation represents (1) the presence of isolated F_1 hinges as well as F_2 hinges, (2) the result of rotation of some dissected F_2 hinges, or (3) a multiple deformation during D_2. If D_2 is itself polyphase then the successively-formed folds must have been co-axial planar (or approximately so) as only one axial planar fabric (S_2) is recognized.

Within, or at a very low angle to Sc, are abundant quartz masses with lensoid sections having the appearance of boudinaged quartz veins (Pl.

1.1c). There are also sigmoidal quartz veins while others are arranged in an *en echelon* pattern. Textural observations point to these veins being the result of syntectonic metamorphic segregation during D_1 with subsequent tectonic modification during D_2.

A lineation seen as a fine colour banding formed by the alignment of mica and other mineral aggregates is present within the composite foliation. Its expression is only patchy, being best shown in pelitic units in contrast to the expression of F_2 fold hinges that are best seen in the more psammitic units. It is deformed by F_3 folds and on their generally flatly-disposed long limbs it trends NNW - SSE to NW - SE, the variation in attitudes being the result of the effects of open F_4 folds and crenulations. This lineation is likely to be equivalent to the "stretching lineation" (*cf.* Voll, 1960, p.544-560) that is so widely expressed in the SW Highlands and trends generally NW - SE. It also appears to correspond to the lines of stretching of Clough (1897, p.49-51, 76-82) although no evidence was observed for pull-apart features. Whether it is solely related to D_2 has not been determined. Certainly it pre-dates D_3 and is expressed in S_c.

D_3

Folds that are generally asymmetrical with gently to moderately inclined axial planes, and deform S_c, F_2 and the mineral lineation, are present throughout the area (Pls 1.1c, d, 2c; Figs 1.6d; 7a, d). They are not major structures, with a maximum wavelength of about 1.5m. Limb thickness tends to be less in the shorter limb than in corresponding longer limbs. The folds consistently face towards the SSE to S and in places there is evidence for axial planar thrusts with movement that is consistently towards the SSE or S (Fig. 1.7b). Fold axes plunge at low angles W or E and axial planes mainly dip at low to moderate angles to the N, although due to D_4 folding they sometimes dip S. However some curvature of fold axial planes and the related thrust planes appears to be unrelated to superposed structures and in places this curvature is like that shown by ramps in thrust duplexes (Ramsay & Huber, 1987, fig.22.14). Associated axial palanar cleavage is only rarely developed (Pl.1.2c) and restricted to the more pelitic lithologies. The planar character of the short fold limb is commonly far better retained than the long limbs which are generally much affected by F_4 folds. The proportion of F_3 fold hinge to limbs is extremely small so that in

many outcrops the superimposed F_4 folds are seen as first deforming the S_C composite foliation.

D_4

These folds are the most common mesoscopic fold structure throughout the area (Pl. 1.1e, f; Fig. 1.7c-e). They are generally open and asymmetrical with a well-developed strain-slip cleavage (Pl. 1.2d). S_4 - S_C intersection lineation and minor fold crenulation are almost ubiquitous, particularly in the more pelitic lithologies. There is clear evidence of refolding of F_3 folds (Pl. 1.3a) but the most commonly expressed relationship, seen at almost every outcrop, is that of F_4 minor folds and crenulations deforming S_C (Pl 1.1e, f). In some places where F_3 and F_4 hinges are of similar amplitudes and juxtaposed, fold interference structures resembling box folds are seen (Pl.1.3c). However, the structures are not conjugate and curvature of F_3 axial planes is sometimes evident. In other places F_4 folds die out against F_3 hinge zones (Pl. 1.3b). F_4 folds have subhorizontal SW or NE plunges. Most have axial planes that dip 50-70° SE but there are some with NW-dipping axial planes. The dips are generally at a lower angle than for the SE-dipping set. No example of F_4 box folds has been seen.

D_{Fault}

A number of NNE - SSW-trending faults dissect the rocks of the district, in places with marked off-set. These are part of the Loch Tay fault set, and are expressions of the transcurrent fault regime which was active in the late stages of the Caledonian episode with the Great Glen Fault a major expression.

1.5 Comparison with structures in nearby areas

Both the determined structural sequences and the nature of the various structures in the Balquhidder district correspond with those expressed throughout the "flat belt" (see Harte *et al.* 1984, table 1). To the W, in the Crianlarich-Loch Lomond region (Fig. 1.3a) Jones (1964),

FIGURE: 1.6 Structural features and relationships.

(a), (b) S_1 deformed by F_2 folds that are now much dissected associated with the development of axial planar S_2 and S_{1+2} (Sc) in limbs; local development of F_4 folds in more pelitic layers is shown, almandine-bearing Ben Lui Schist [545 224].

(c) F_2 folds defined by early (presumed D_1) quartz segregation veins and psammitic layers; S_2 is developed axial planar to F_2 and Sc is developed in fold limbs, F_4-Sc_1 is weakly developed in the more pelitic layers; Pitlochry Schist [534 215].

(d) Intrafolial F_2 folds, dissected F_2 fold hinges, S_2 and Sc deformed by asymmetrical F_3 folds; spessartine-bearing Pitlochry Schists [546 212].

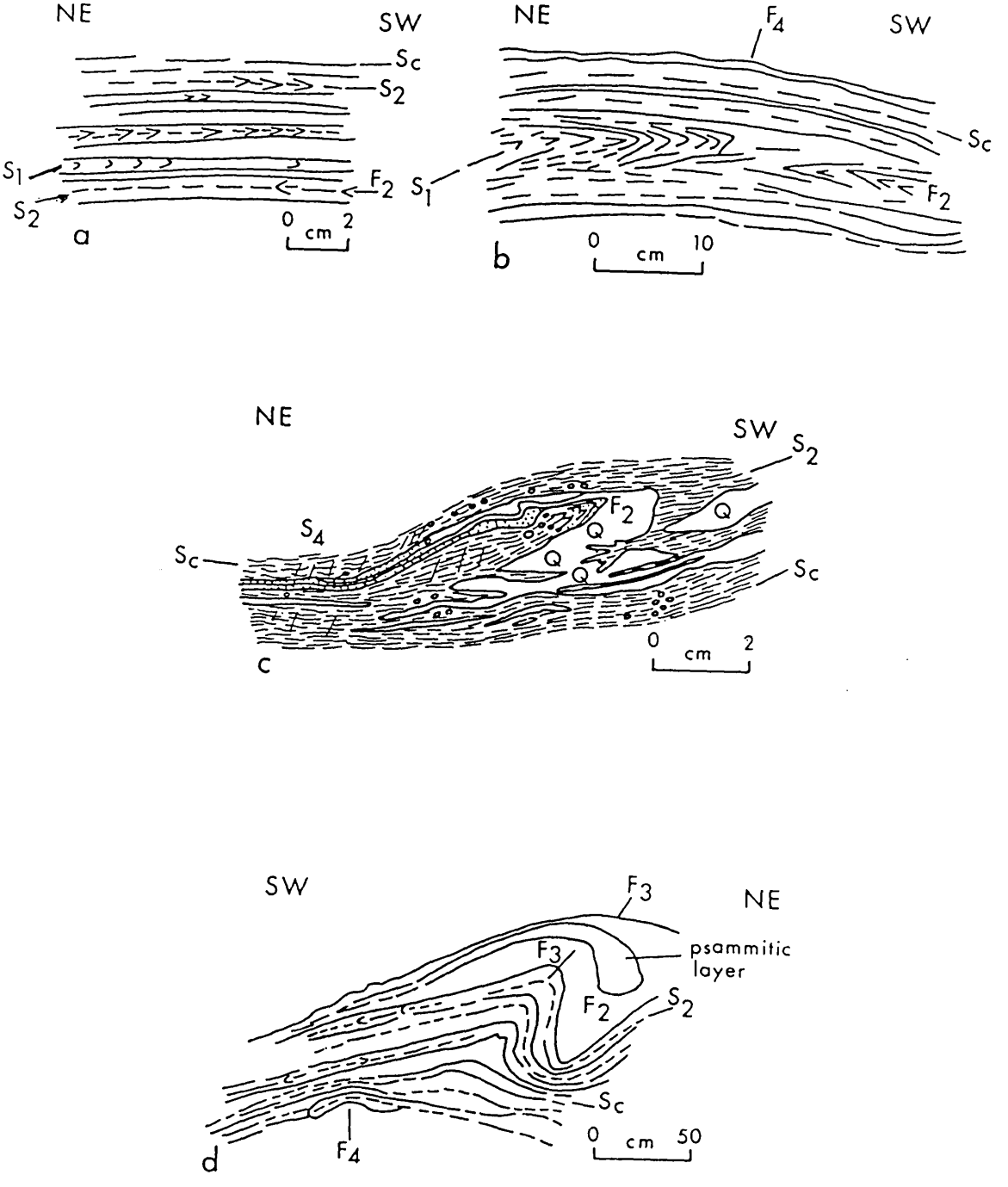
NE
SW
S_c
S_2
S_1
F_2
S_2
0 cm 2
a
NE
F_4
SW
S_c
S_1
F_2
0 cm 10
b
NE
SW
S_2
S_4
F_2
Q
Q
Q
Q
S_c
S_c
0 cm 2
c
SW
F_3
NE
psammitic layer
F_3
F_2
S_2
S_c
F_4
0 cm 50
d

FIGURE 1.7 Structural features and relationships.

(a) F_3 asymmetrical folds expressed in psammitic rocks with thin semipelitic interbeds, Pitlochry Schist .

(b) Structural pattern dominated by F_3 asymmetrical folds with moderately inclined axial planes and axial planar thrust that show curvature not realted to superposed F_4-S_4; Pitlochry Schist .

(c)-(e) Contrasting (F_4) fold styles; spessartine-bearing Pitlochry Schist [Grid reference shown].

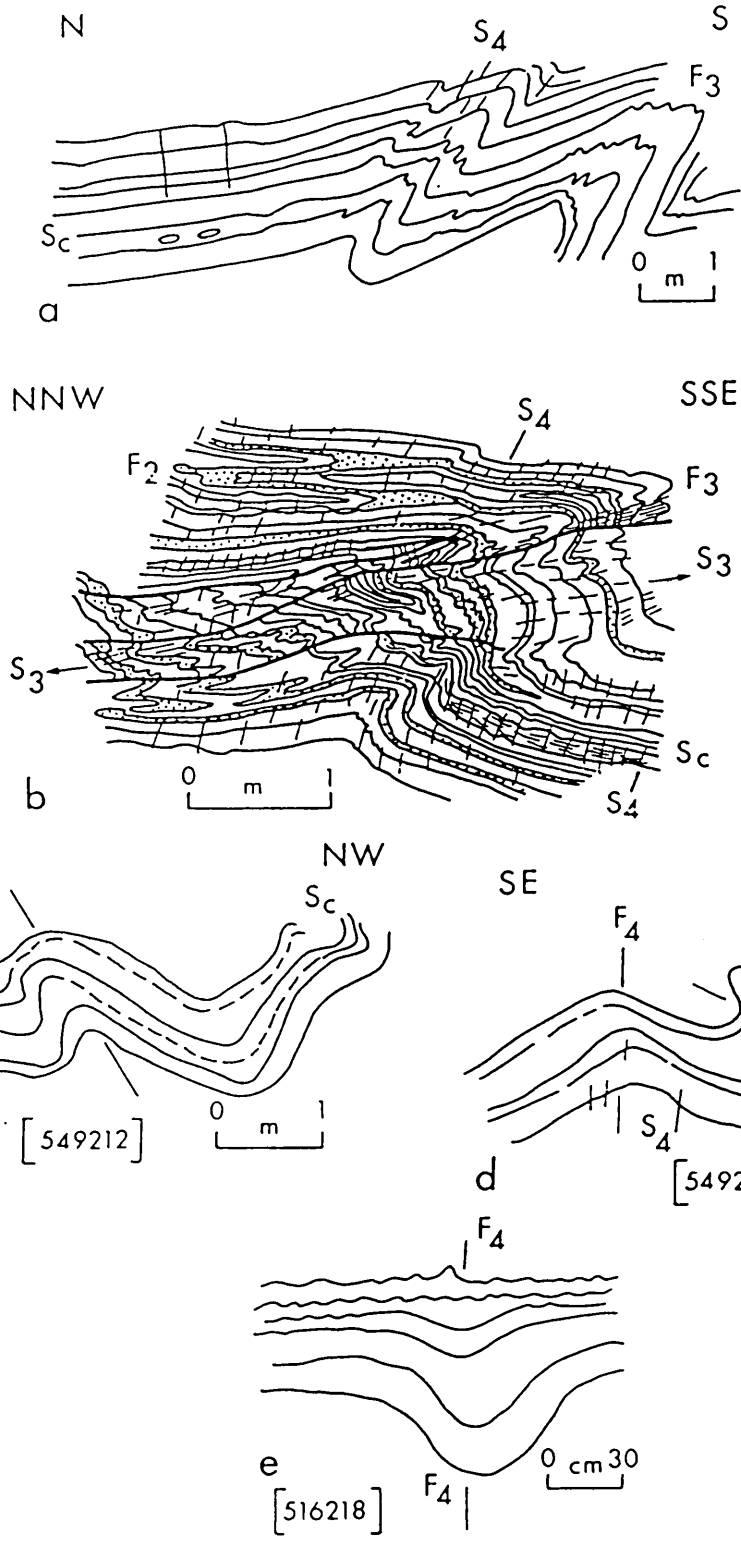
N
S
S_4
F_3
S_c
0 m 1
a
NNW
SSE
S_4
F_2
F_3
S_3
S_3
S_c
0 m 1
S_4
b
SE
NW
F_4
S_c
c
[549212]
0 m 1
SE
NW
F_4
S_4
S_c
F_3
S_4
0 cm 50
d
[549212]
F_4
0 cm 30
e
F_4
[516218]

PLATE 1.1: Structural features and relationships

(a) S_1 discordant to S_2 preserved in more psammitic layers with S_{1-2} (Sc) folded by F_4; SE-facing outcrop [505 218].

(b) Close-up of part of (a).

(c) F_3 folds deforming Sc and boudined quartz vein parallel to Sc; psammitic spessartine-bearing Pitlochry Schist; scale bar 2mm, E-facing outcrop [505 227].

(d) F_3 folds with no associated axial plan fabric affecting the composite foliation Sc with the later small very open F_4 folds; on the limb of a large F_3 fold; garnet-free Pitlochry Schist, W-facing outcrop [505 214].

(e) F_4 folds affecting the composite foliation (Sc), and parallel discontinuous quartz lenses; spessartine-bearing Pitlochry Schist, NE-SW facing outcrop [505 218].

(f) Strong S_4-F_4 crenulation; spessartine-bearing pelitic Pitlochry Schist, scale bar 2mm; NE-SW facing outcrop [515 214].

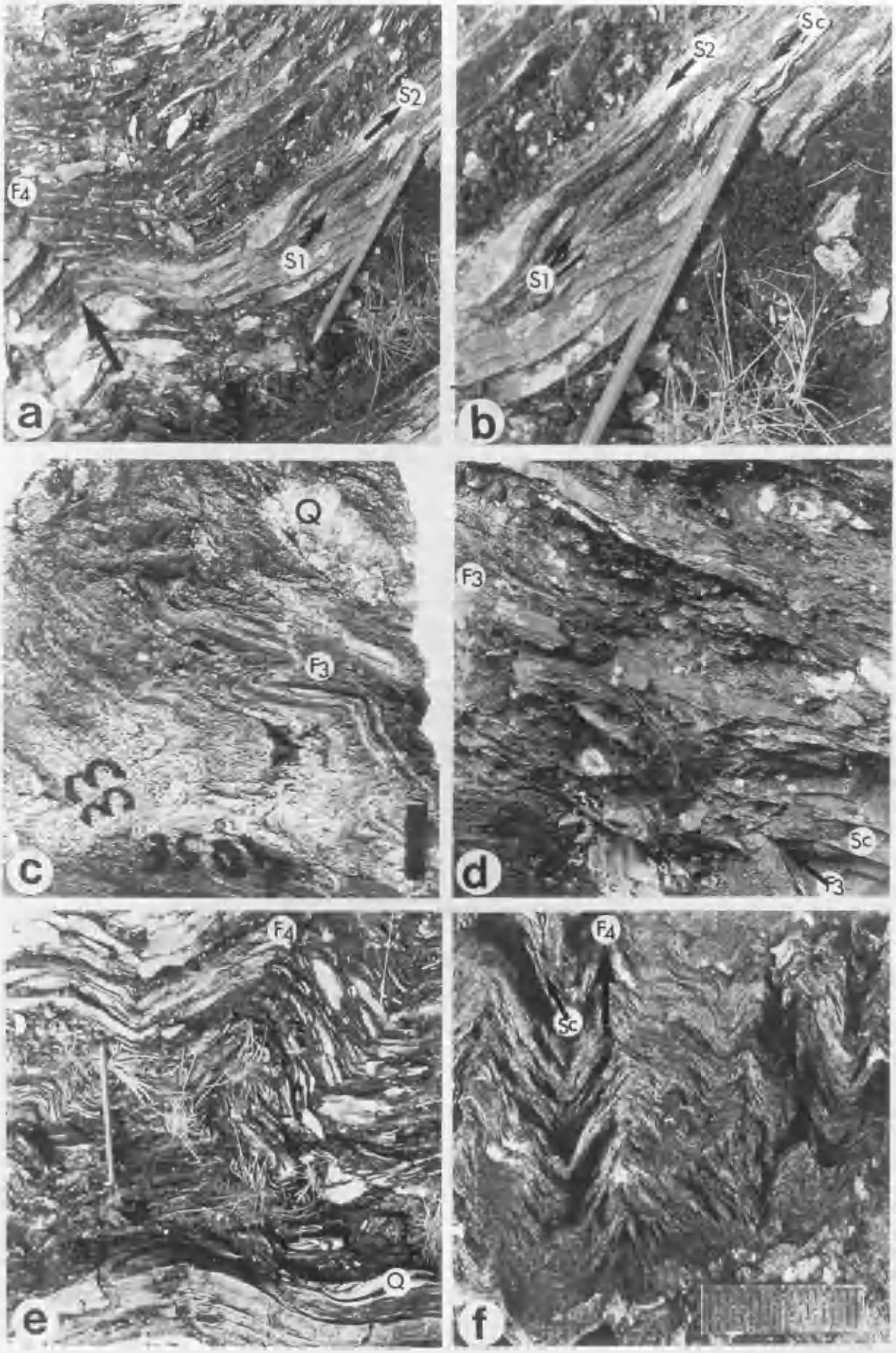
a
S2
F4
S1
b
Sc
S2
S1
c
Q
F3
d
F3
Sc
F3
e
F4
Q
f
F4
Sc

PLATE 1.2: Photomicrograph of structures and structural relationships.

(a) F_2 fold deforming S_1 composed of muscovite and chlorite, sometimes with intergrowths of the two, grain size of the micas making up S_1 is smaller than those of the micas making up S_2. Later muscovite and chlorite growths are indicated by unlabelled arrows; garnet-free Pitlochry Schist [525 214].

(b) Relict S_1 fabric between S_2; garnet-free Pitlochry Schist [525 214].

(c) S_3 crenulation cleavage weakly developed at angle to the Sce garnet-free Pitlochry Schist [525 214].

(d) S_4 crenulation cleavage associated with asymmetrical F_4 fold; spessartine-bearing Pitlochry Schist [505 218].

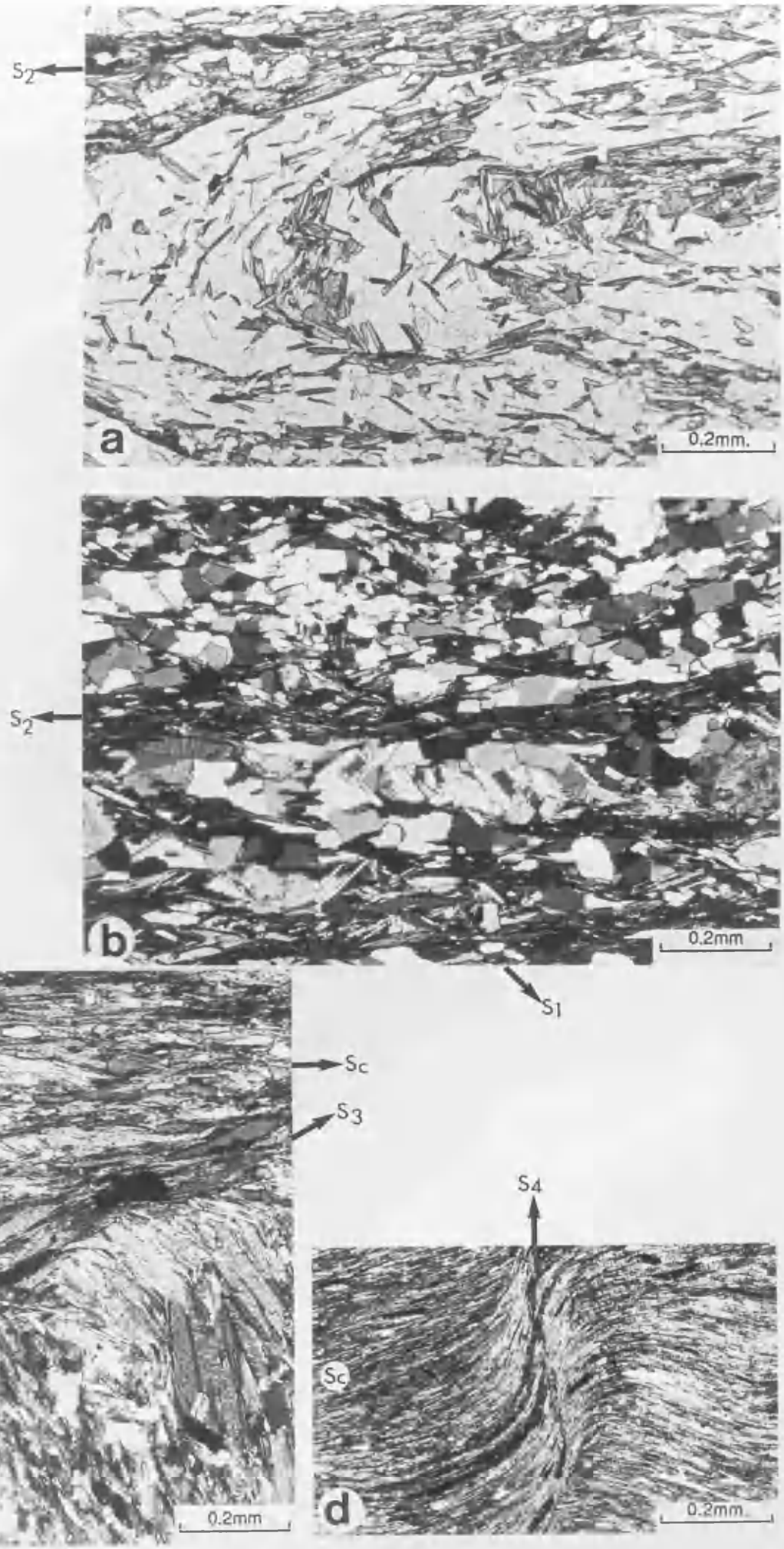
S2
a
0.2mm.
S2
b
0.2mm
S1
Sc
S3
S4
Sc
c
0.2mm
d
0.2mm.

PLATE 1.3: Photomicrographs of structures and structural relationships.

(a) F_3 deforming Se composed of muscovite and chlorite; slight curvature of F_3 axial planes and more pronounced folding of Se in F_3 limbs by F_4; spessartine-bearing Ben Lui Schist [546 213].

(b) F_4 fold dying out against F_3 fold hinges, spessartine-bearing Ben Lui Schist, [546 213].

(c) F_3 - F_4 interference pattern shown by Se; spessartine-bearing Pitlochry Schist [511 215].

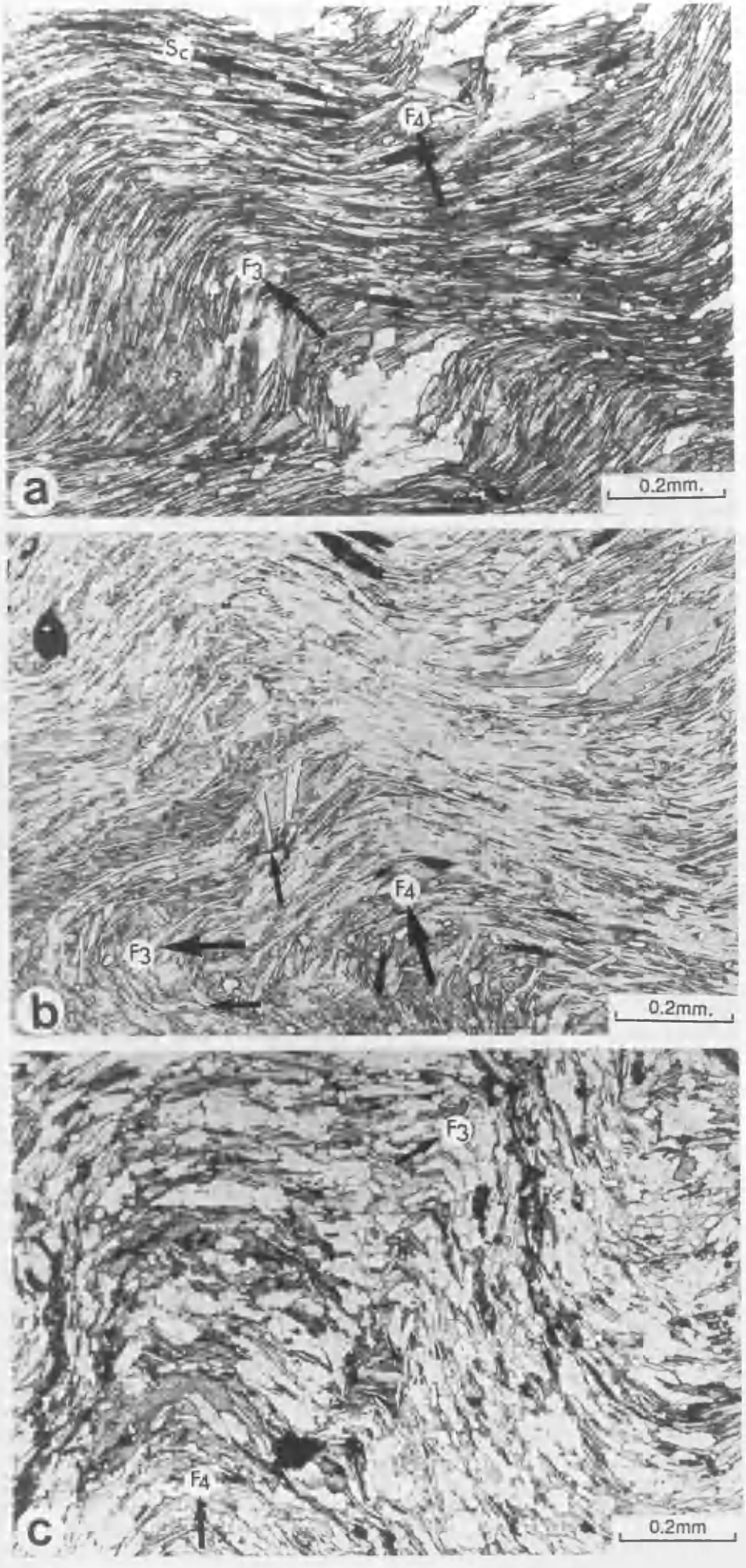
Sc
F4
F3
a
0.2mm.
F4
F3
b
0.2mm.
F3
F4
c
0.2mm

McArthur (1971) and Bowes (1973, 1979) have recorded corresponding structural successions. They have also described many corresponding details of similar structures. Consistently only small remnants of S_1 are seen, F_2 folds are tight to isoclinal, intrafolial, and much dissected (*cf.* Bowes, 1979, pls 1,2,3), F_3 folds are asymmetrical, face SSE and have thinned shorter limbs and northerly-dipping axial planes (*cf.* McArthur, 1971, pl.III 2a,b,c), S_3 is rarely seen, while F_4 and S_4 are very prominent (*cf.* McArthur, 1971, pl.III 2a,b,c; Bowes, 1979, pl.9), and over large areas F_4 folds and crenulations affecting S_c are the dominant structures.

Accordingly the various structural features recorded in the Balquhidder district and the established structural succession can be used with confidence as bases for a detailed study of metamorphic mineral growth and in the knowledge that conclusions reached in this study are likely to be applicable widely in the SW Highlands.

1.6 Scope of present investigation

There are many aspects of the garnet-biotite boundary recorded in the Balquhidder district that indicate that further investigation is needed.

1. The very local expression of proposed inverted isograd zones in a region where these features are generally not inverted needs explanation, as do the proposed changes in disposition from subhorizontal and inverted to subvertical and to subhorizontal and not inverted.

2. Any possible control of rock chemistry on metamorphic mineral growth requires investigation.

3. The index minerals, particularly garnet, show marked differences in size, habit, and modal proportions both in closely spaced samples and throughout the district generally.

4. There has been scant attention paid in previous investigations to the relationships of different expression of garnet to the successively formed structures in the polyphase deformation sequence.

5. There has been no investigation of mineral composition to position in the polyphase metamorphic history of minerals such as garnet.

6. The geochronological studies of Rogers *et al.* (1989) have shown that there are two widely separated (*c.* 100Ma) peaks of metamorphic activity shown in the Dalradian assemblage in the Scottish Highlands and the various imprints of the *c.* 600Ma and *c.* 500Ma events require elucidation.

As a basis for a study of the metamorphic rocks in the Balquhidder district the structural succession was established (Section 1.4). Then on the basis of textural studies the successively-formed metamorphic mineral assemblages were established and integrated with the structural succession (Chapter 2). Also in Chapter 2 are descriptions of the various grain sizes, habits and textural expressions of the various metamorphic minerals, with particular emphasis on garnet, while in Chapter 3, the relationships between rock chemistry (see 1.3) and growth of garnet (and other minerals) is dealt with. Also in this chapter the mineral chemistry of different minerals is used to (1) provide the recognition of chemically compatible and incompatible assemblages, (2) establish the degrees of attainment of chemical equilibrium, (3) demonstrate the presence of any geochemical gradient and, or, re-arrangement during late retrograde metamorphic activity and, (4) determine the variables that contribute to index mineral growth and (5) to elucidate the character of index mineral-forming reaction(s). In Chapter 4 mineral textural relationships and garnet zoning profiles are used to (1) determine peak metamorphic conditions, and (2) to evaluate P-T conditions during metamorphism. These studies, and those incorporated in Chapters 1, 2, 3 and 4, permit the metamorphic history of the rocks at Balquhidder to be established and integrated with their structural development. This in turn forms a basis not only for assessing the disposition and nature of the garnet-biotite boundary at Balquhidder, but also for contributing to an understanding of the overall tectono-metamorphic evolution of the Scottish Caledonides, with particular reference to the Dalradian terrane. These aspects are set out and discussed in Chapter 5, while Chapter 6 presents the main conclusions derived from this study.

1.7. Use of abbreviations.

For convenience a number of abbreviations used frequently throughout the thesis are defined below.

D	Deformational phase, these are qualified by use of numbers to indicate polyphase development.
F	Folds
S	Schistosity - cleavage
L	Lineation
M	Metamorphism, these are qualified by use of numbers to indicate polyphase metamorphism.
G_2	Refers to garnet growth during $D_2 - M_2$.
G_2A, G_2B, G_2C	When successive development of garnet can be demonstrated within a single phase, i.e. during $D_2 - (M_2)$
G2-4	Garnet growth during post-D_2 - (M_2) – pre D_4 (M_4)
M_{2-4}	Metamorphism when only a time range can be bracketed between M_2 and M_4.
m	Matrix mineral growth.
P	Porphyroblastic growth expression.
r	Composition of chlorite after garnet and, or biotite
R r	Composition of garnet edge replaced by chlorite
R.G.	Muscovite and, or, biotite composition in direct contact with garnet or in its pressure-shadow areas.

CHAPTER 2

SEQUENCE OF MINERAL GROWTHS

2.1 Introduction

The time relationships of mineral growth to deformation have been an essential part of the elucidation of the metamorphic history of the polyphase deformed Dalradian terrane of the Scottish Caledonides (*e.g.* Rast, 1958; Sturt and Harris, 1961; Johnson, 1962, 1963; Harte and Johnson, 1969; Harte *et al.*, 1984; Dempster, 1985). Much of this work has been done in relatively high grade rocks and particularly related to prograde metamorphism whereas in the Balquhidder district the rocks only reach the almandine grade and commonly exhibit the product of retrograde metamorphism. However, the textural criteria used are the same (see Rast, 1958; Zwart, 1962; Spry, 1963, 1979; Bell *et al.*, 1986; Vernon, 1988). The same ambiguities can also cause difficulties (*e.g.* Vernon, 1977, 1978) but misleading interpretation of textural relationships can be avoided, or at least largely so, if precautions such as those set out by Vernon (1977) are applied.

The demonstration of relations between porphyroblasts and cleavage-schistosity-foliation, and elucidation of the mineral growth sequence are essential for meaningful calculation of successive P-T conditions of mineral equilibration and hence the determination of a P-T path. They provide a means of recognition of, and discrimination between individual mineral phases (*e.g.* garnet, chlorite) which grew at more than one stage and which must be treated as separate mineral constituents (or cognate groups of constituents) rather than in a "bulk" manner.

2.2. Methods of textural investigation

The criteria commonly used involve the study of porphyroblasts and, or, porphyroblast internal fabrics (Si) and their relationship with fabric elements in the surrounding external matrix (Se).

2.2.1. **Porphyroblast *vs* matrix relations**

Rast (1958) and Zwart (1962) considered that porphyroblasts were formed later than the S-surface when the latter abuts and is not disturbed in the vicinity of the porphyroblast, *i.e.* the growth process had an element of matrix replacement. Where the S-surface is disturbed, and particularly where it bows around a porphyroblast, it is considered by these authors to be of later development (see also Ramsay, 1962; Spry, 1963; Zwart, 1963).

However Prior (1987) attributed the warping of intensified cleavage around porphyroblasts to be the result of the following three syn-tectonic processes: (1) deformation partitioning around a developing rigid porphyroblast, (2) heterogeneous deformation prior to porphyroblast growth, and (3) deformation of cleavage during porphyroblast growth. Of the above three possible mechanisms, the ability of a growing porphyroblast to push aside its surrounding matrix has been much debated (*e.g.* Misch, 1971, 1972a; Shelley, 1972; Spry, 1972; Ferguson and Harvey, 1972; Ferguson *et al.* , 1980). Rast (1965) suggested that the force of crystallization was only applicable in the case of some idioblastic forms of some minerals, particularly garnet while Prior (1987) considered force of crystallization to be applicable to porphyroblasts "rounded off" by pressure solution, a process considered to be incompatible with the crystallization force. Vernon and Powell (1976) also considered force of crystallization to be unimportant because any effects were only shown in limited boundary positions and did not extend laterally into the matrix.

Several explanations have been presented to account for an S-surface both bowed around and truncated by the porphyroblasts (Spry, 1972) with Ferguson and Harvey (1972) suggesting straightforward Syn-Se development. The following factors were noted by Ferguson and Harte (1975) as influencing the arrangement of (Se) adjacent to porphyroblasts: (1) the manner of growth of porphyroblasts and their interaction with the matrix, (2) the history and mechanism of Se modification, (3) the timing of porphyroblast development with respect to the Se, and (4) the mineral species of the porphyroblast and its competence relative to the matrix species during deformation.

2.2.2. Internal (Si) *vs* external (Se) fabrics.

The presence of inclusion fabrics in porphyroblasts is an important aid to the elucidation of mineral growth sequences as the relationship between inclusion and matrix fabrics is commonly used to infer the time relationship between porphyroblast growth and deformational phases (*e.g.* Zwart, 1962; Spry, 1969; Elliott, 1972; Ferguson and Harte, 1975; Bell *et al.* , 1986; Rice and Roberts, 1988). The interpretations both of the nature and geometrical relations of such a fabric to the external fabric mainly depends upon the assumption that a fabric within a porphyroblast truly reflects the morphology of the earlier external fabric and was not directly affected by the growth of the porphyroblast (see Vernon and Powell, 1976; Schoneveld, 1977; Olesen, 1978; Ferguson *et al.* , 1980).

Ferguson and Harte (1975) suggested the following petrographic features for the correct recognition of the true inclusion fabrics (*i.e.* those that represent an earlier matrix fabric, and by which they can be distinguished from other replacement and, or, exsolution fabrics): (1) the Si forms continuous trails which extend from margin to margin of the porphyroblasts, (2) these trails are not deflected when crossing twin boundaries of the host mineral, and (3) the preferred orientation of the inclusion fabric is unrelated to the crystal structure of the porphyroblasts. These three features together can be used to identify a true inclusion fabric present in an earlier matrix fabric.

The reasons for marked differences in the inclusion density and configuration in different porphyroblasts is not clear but they are thought to be related to differences in the interfacial tension between the mineral phase forming porphyroblast and the matrix, this being produced by change in the intergranular fluid composition (Galway and Jones, 1962). Vernon and Powell (1976) pointed out that a porphyroblast and its inclusions may nucleate at the same time with different nucleation rates, the included minerals forming many stable nucleii while the porphyroblast forms only one, *i.e.* both the inclusions and the porphyroblast belong to the same compatible mineral assemblage.

The reasons given for the occurrence of Si oblique to Sc, of S-shaped inclusion trails within porphyroblasts, and of rotated porphyroblasts, have ranged from the extremes of rigid syn-tectonic rotation of porphyroblasts (*e.g.* Zwart, 1960; Spry, 1963; Rosenfeld, 1968, 1970, 1985; Olesen,

1982, Reymer and Oertel, 1985, pp.629-630) to the rotation of the matrix around a growing but static crystal (*e.g.* Ramsay, 1962, pp.322-323). Curved inclusion trails have also been interpreted as the result of microfolds having been overgrown.

Spry (1969, p.254) pointed out the difficulties of distinguishing between rotational and overgrowth inclusion trails and also that the two extremes have been given explanations of similar inclusion patterns. He did suggest, though, that when porphyroblasts all have the same sense of rotation, as indicated by their trails, rotation of the porphyroblasts could be a reasonable interpretation (see *e.g.* Olesen, 1982). Hence the presence of crenulations inside the porphyroblasts that are similar to those outside gives support to the possibility of microfold overgrowth rather than rotation. However extensive deformation may occur after the growth of a porphyroblast, resulting in the common obliteration of former matrix crenulations (*e.g.* see Bell and Rubenach, 1983). Accordingly the obliquity of Si and Sc, even where Si curvature is consistent in many porphyroblasts, is considered to be insufficient evidence to demonstrate the porphyroblast rotation (see Vernon, 1988). However, Ramsay (1962, pp.322-323) showed that this microstructural relationship can be explained equally well by flattening and consequent rotation of the matrix around static porphyroblasts, and that this is the only correct interpretation when the Si of all crystals is parallel. He also set out the possibility of strain shadow development by this process (a basic form of the bulk heterogeneous shortening model discussed in more detail by Bell, 1981) and also illustrated how growing porphyroblasts can incorporate remnants of a progressively curving external foliation as inclusion trails that are typically straight in the centres of the porphyroblasts but curve into the matrix foliation at their edges: this is the main microstructural criterion for syndeformational growth of porphyrobnlasts discussed by Bell and Rubenach, 1983; and Bell *et al.*, 1986.

Bell *et al.* (1986) suggested that except for "snowball" garnets, porphyroblasts do not rotate during deformation and that the apparent rotation is due to overgrowth of a crenulated and, or, reactivated foliation. They also suggested that porphyroblast rotation only occurs when the deformation involves only simple shear and that the progressive shortening component cannot be partitioned out in regions adjacent to porphyroblasts.

An earlier fabric can also be preserved in the pressure shadow areas around opposite sides of porphyroblasts and this can be used in the same way as a fabric preserved inside porphyroblasts. Such a fabric represents either a fabric of an earlier deformational phase or the early stages of development of a fabric which later intensified and warped around a porphyroblast whose growth was early syndeformational.

2.3. Growth of muscovite and chlorite.

2.3.1. Introduction

Muscovite and chlorite are the most abundant rock-forming minerals in the Balquhidder rocks. Their grain size and expression differ in the different lithologies but they faithfully represent most of the rock fabrics developed by successive responses to deformation and metamorphism. They constitute the main minerals in the main schistosity (S_2) and show generally comparable variations in grain size and expression. Where S_2 are comparatively less transposing there are enclaves in which pre-S_2 muscovite and chlorite growths are preserved.

As the S_2 phyllosilicates possess a pronounced anisotropy they are a particularly sensitive register of the later overprinted very weak D_3 and the strong D_4 crenulation fabric (Plate 1.2, c,d).

2.3.2. Pre-S_2 growth

Pre-S_2 muscovite and chlorite are identified by their definition of the shapes of F_2 fold hinges (Plate 1.2a). They are also seen in an arrow-like arrangement in lenses and layers between S_2 planes (Plate 2.1a), *i.e.* as a static growth: this is interpreted to have taken place either very late during D_1 or, more probably, post-D_1 and pre-D_2. The present grain size is presumed to express D_2 grain coarsening, particularly in view of the marked difference in the grain size of the oriented quartz fabric (presumed to be S_1 or very early S_2) within the garnet porphyroblasts when compared to the grain size of quartz in S_2.

2.3.3. S_2-growths

Generally S_1 is strongly transposed by the development of the dominantly muscovite-chlorite (and biotite, or hornblende in the hornblende schists) S_2 schistosity (Plates 2.1b, 16c). Large chlorite is only seen in the hornblende schists, whereas in most lithologies the muscovite forms plasts up to 1.4 x 0.63mm across, set in a finer grained matrix (Plate 2.1c). Other muscovite is present as microboudin-like individual linsoidal grains with relatively narrow tapering necks and showing evidence of rotation (Plate 2.1d). The development of plasts in addition to the main matrix muscovite is indicative of non-instantaneous growth during S_2-M_2, with late D_2 modification of the main dynamic growth as the result of recrystallization on pre-existing grains by grain boundary migration along their length, *i.e.* by accretion recrystallization (see Bell *et al.*, 1986).

The shape transformation of the muscovite plasts is intepreted as due to solution. The shape change and associated slight rotation is not due to the presence of micro-shear zones because there are plasts with cleavage parallel to length and no evidence for internal deformation of the plasts (Lister and Snoke, 1984). In addition microshear zones are unfavourable sites for phyllosilicate growth where they are amenable to solution effects.

The muscovite plasts have not been seen deformed by F_3 but similar S_2.M_2 biotite plasts are deformed (Plate 2.11c).

2.3.4. S_2-deformation and later growths

The S_2 muscovite and chlorite define the shapes of F_3 folds and new axial planar muscovite is interpreted as expressing a very weak S_3 (Plate 2.2a). The muscovite and chlorite also define open F_4 folds (Plate 2.1b) and the associated S_4 (Plate 1.2d), the former also seen as undeformed and interlocking growths at F_4 crests (Plate 2.2b), are interpreted as representing late D_4 recrystallization. Randomly oriented muscovite flakes are also seen to overprint the S_2 matrix (Plate 2.2c). There is no evidence that they were affected by F_3 or F_4 and they are interpreted as representing post-D_4 (or very late D_4) static growth.

Chlorite also occurs as the product of retrogression of garnet and biotite. It is mainly after garnet occurring as rims of clear chlorite around

garnet with partial to complete pseudomorphism. Different garnet crystals in one thin section show various stages of chloritization (Plate 2.3). As this phase of mineral growth post-dates the M_{2-4} garnet. it is late in the overall sequence. However it cannot be closely tied into the metamorphic-tectonic framework and it is possible that the retrogressive effects shown by both garnet and the biotite span a range of time.

2.4 Growth of garnet

Textural investigations provide evidence that two major periods of garnet porphyroblast growths are associated with D_2 and the other post-D_2 but pre-D_4.

2.4.1. D_2 growth

Some syn-D_2 garnets are free of inclusion trails, but most preserve an earlier fabric, consisting mainly of quartz, and often in minute detail. This internal fabric (Si) is present in a range of porphyroblast sizes (Plate 2.4) and it shows considerable variation in expression and of relations with the external fabric (Se). The various sizes, habits and relationships are consistent with non-instantaneous nucleation under conditions of variable growth and strain rates and early-formed syndeformational porphyroblasts can appear similar to pre-tectonic porphyroblasts.

The following relations between garnet porphyroblasts free of useful inclusion trails and matrix foliations are consistent with syn-D_2 growth both where (1) the S_2 is disturbed and deflected in the vicinity of the porphyroblast and granoblastic quartz occurs in symmetrical pressure shadow areas (Plate 2.5a), and (2) the S_2 is both deflected and truncated by porphyroblasts and asymmetrical strain shadows are seen (Plate 2.5b). These features are interpreted as indicating stress heterogeneity and reactivation of the matrix foliation (see Bell *et al.,* 1986, fig. 7).

2.4.1.1. Textural types-description

Garnet porphyroblasts containing Si, show four main Si expressions and Si-Se relationships. For convenience of description these are referred to as types 1 - 4. It is appreciated that different directions of cutting through identical garnets can result in very different thin section characteristics.

Type 1: Si occurs as continuous straight trails and even bands that extend from margin to margin of the porphyroblast. Si is either continuous with and parallel to Se (Plate 2.6a) or abuts against Se at the porphyroblast matrix interface (Plate 2.6b). The same Si-Se relationship may be shown by all the garnet porphyroblasts in the same section (Plate 2.5c), or only some of them (Plate 2.6a,d).

The quartz present as inclusions in garnet has a significantly smaller grain size than that in corresponding matrix as is usual in most metamorphic rocks. In addition, it is smaller in garnet cores than in the rims especially in case large garnet porphyroblasts. The quartz grains in Si also differ in shape from those in Se, with those of Si commonly elongate with arcuate corners, whereas the quartz grains in the adjacent matrix are dominantly rectangular or polyhedral.

Type 2: Si is curved and continuous with Se even in the outermost rim of the garnet porphyroblast. Se itself shows curvature (matrix crenulation) and deflection around the porphyroblast (Plate 2.7a,c). In some porphyroblasts distinct curvature of Si is shown only in the outermost rim (Plate 2.7b) and porphyroblasts with curved and straight Si can occur in the same thin section (Plate 2.7c). The intensity of expression of Si varies markedly from uniform (Plate 2.7a) to irregular (Plate 2.7c).

Type 3: Si is sigmoidal with a number of quartz spirals (Plate 2.8a). Si shows direct continuation with the Se which, in turn, shows degrees of deflection as well as truncation with the porphyroblast (Plate 2.7a). Se also shows curvation (matrix crenulation) but this is neither as prominent as that shown by Si nor with the same disposition. The grain size of the Si quartz is generally similar to that of the Se quartz in Se.

Type 4: Si in the skeletal garnet porphyroblasts is both parallel to the Se and to the garnet elongate edges. The Si quartz accommodated in the garnet rims are smaller and elongate than Si in cores which are larger and commonly rectangular but also show degrees of preferential orientation parallel to Se Both Si quartz, either in cores or rims of the skeletal garnets are smaller than in the quartz matrix, the latter being commonly polygonal, and showing considerable embayment in the serrated garnet ends (Plate 2.8c, 2.9).

2.4.1.2 Textural types - interpretation

The existence of these four textural types can be accounted for, on the basis of non-instantaneous nucleation and growth of garnet porphyroblasts during D_2 and the overprinting of an earlier fabric, S_1 and, or, very early S_2.

Type 1 is interpreted as due to deformation partition and movement during the Se_2 foliation modification. The garnet porphyroblasts either rotated differentially or all suffered an equal amount of rotation (see Olesen, 1982; Bell *et al.*, 1986, figs 9,11).

Type 2 is interpreted as resulting from garnet overprinting open warps of Se. The more prominent expression of Si curvature than Se curvature is explained on the basis of crenulations being overprinted at an early stage of S_2 development with later stages during which the Se_2 deflection around the garnet porphyroblast took place, also being the time at which matrix crenulation was obliterated, or largely so. Those garnets in which Si shows distinct curvature only in the outermost rim are interpreted as indicating the initiation of garnet growth at an early stage of D_2, so that the garnet cores overprinted a very weakly curved fabric; at a later stage when Se_2 warped around the growing garnets, the garnet rims overgrew parts of the warped S_2. The coexistence of weakly curved Si, even only at the garnet rim together with straight Si occurring in the same thin section (*e.g.* Plate 2.7c, grains i,ii), can be explained as due to (1) that the garnet overgrew partly (*e.g.* grain (ii)), or as a whole (*e.g.* grain (i)) an earlier fabric, (2) that the smaller grain (ii), having grown later than the larger grain (i), consequently overprinted the more intensified Se, (3) the lack of rim

development in grain (ii), or (4), that the rims as well as the inclusion were dissolved. The possible rim dissolution is supported by the presence of opaque-rich rims at some porphyroblast-matrix boundaries parallel to the deflected Se (Plate 2.6a) (Bell and Cuff, 1989).

Type 3 indicates either (1) rotation during growth with the Si representing enveloped Se_2, or (2) growth over already crenulated Se, *i.e.* not associated with rotation. Both explanations imply syndeformational growth with respect to D_2. Such "snowball" garnet structure (Plate 2.8a) has been described and its development discussed in detail by many authors (*e.g.* Rast, 1958; Zwart, 1960; Spry, 1963; Powell and MacQueen, 1976; Cox, 1969; Kennan, 1971; Williams and Schonevelde, 1981; Bell *et al.*, 1986; Jamieson and Vernon, 1987; Bell and Johnson, 1989), with various explanations given for the Si pattern, *viz.* (1) the porphyroblasts were in the shortening component sites of the deformation portion, (2) the cut effect and whether or not such planes consistently comprise the rotation axes, (3) the shape of the porphyroblasts when near spherical are much more susceptible to rotation than the discoidal for a given amount of strain, and (4) their position with respect to their structural situation, *i.e* limbs or hinge of a fold.

Type 4 Si pattern and expression indicates that Si quartz recrystallization was continued even after the time they were included in the garnet core. But this does not explain their sizes and expression at the garnet rims. The particular morphology of the skeletal garnet porphyroblast probably suggests its growth, originally in an elongate habit (Bell *et al.*, 1986), with the later modification due to solution, strain and diffusion rates. Evidence for garnet dissolution is indicated by rounded porphyroblast ends and indentation into their neighbours juxtaposed garnet crystals (Plate 2.8c, 2.9). For other interpretations regarding the growth of skeletal garnets see *e.g.* Powell and Treagus, 1970; De Witt, 1976; Bell *et al.* 1986; Jamieson and Vernon, 1987.

2.4.1.3. **Matrix-grain coarsening**

Generally the quartz present as inclusions in garnet porphyroblasts has a significantly smaller grain size than in the corresponding matrix, while the quartz grain size in the cores of the porphyroblasts (except the skeletal

garnets) is generally smaller than that in the rims. In addition the included quartz grains are commonly elongate with arcuate corners, probably suggesting growth during deformation (*e.g.* Voll, 1960), with the possible shape modification after inclusion (*e.g.* Toriumi, 1979), whereas quartz grains in the adjacent matrix are dominantly rectangular or polyhedral. Also they consistently show approximately equal angle triple junctions, suggesting isotropic interfacial energy conditions (see Vernon, 1979).

These features indicate grain coarsening both during and after garnet porphyroblast growth reflecting either an increase in metamorphic grade or the existence of elevated temperature both during and after garnet growth. The differences in grain size of quartz in the cores and rims of the porphyroblasts are interpreted as indicating their successive inclusion while grain coarsening was operative. The differences in grain size of Si minerals in various porphyroblasts are interpreted as indications that garnet growth was non-instantaneous and that progressive nucleation of porphyroblasts proceeded, along with progressive increase in matrix grain size.

2.4.1.4. **Tectonic environment**

The existence of homogeneous inclusion patterns in garnet porphyroblasts (*e.g.* Plate 2.7a) indicates a uniform intensity of deformation, at least locally, on the scale of the porphyroblast. The presence of inhomogeneous Si patterns even in the same thin section suggest that the nucleation of garnet could have taken place at different times and grew relative to each other during D_2. The presence of Si showing curvature only at the crystal rim supports the above explanation. Otherwise, the presence of Si showing curvature only at crystal rims is indicative of increase of strain rate at the end of each individual grain growth which is considered unlikely. Alternatively the occurrence of curved Si only at the grain rims is indicative of slow growth. The principal variation of the syn-D_2 microstructural relationships, even in the absence of Si, mainly depends on whether the pre-existing foliation was in the extension field or in the shortening of D_2. Hence, if S_1 (or early S_2), for instance, was in the D_2 shortening field it became crenulated and the garnet grew early during D_2 preserving these crenulations at their early stages of development, continued deformation in the matrix, caused S_2 to warp around the porphyroblasts. However if S_1 (or early S_2) was in the D_2 extension field, pressure shadow

developed on either side of the porphyroblasts at right angles to the earlier fabric. Otherwise, rotated inclusion trails formed, indicating growth during non-co-axial stress.

2.4.2 Post-D_2 - pre-D_4 growth

The garnets that grew during this period are generally of limited size range and mostly appear equidimensional relative to the D_2 garnets and they are concentrated in the more micaceous domains. They do contain various inclusions, mainly quartz, but these are neither common nor uniformly distributed in the garnet porphyroblasts and no inclusion trails (Si) patterns have been observed. The garnet porphyroblasts show sharp cross-cutting relations with the adjacent Se. The following additional features have been observed (Plate 2.10).

(1) The garnet porphyroblasts overprinted the S_2 fabric.

(2) The S_4 fabric, where developed, warps around the porphyroblasts and commonly without the development of mica-free haloes.

(3) Some quartz inclusion in garnet shows obliquity to the Se_2 fabric.

These textures indicate that the second period of garnet growth took place post-D_2 but pre-D_4. The general absence of D_3-M_3 metamorphic mineral growth, except in very localized places where S_3 is only very weakly developed, means that unequivocal demonstration of the relationship of garnet growth to D_3 is not possible. However the observation that some inclusions in these post-D_2 garnets are oblique to the Se_2 fabric could be interpreted as indicating rotation during D_3. In addition post-D_2 garnet grew as replacements without disturbing the surrounding minerals, i.e. they represent static mineral growth. Accordingly, it is probable that they were a post-D_2 - pre-D_3 growth but they might have developed in the interval between D_3 and D_4 and no conclusive evidence to distinguish the two interpretations is known.

2.4.3. **Grain size variation of garnet**

The following factors are significant in the interpretation of the garnet size distribution:

1. Garnet is a unique phase that acts during polymetamorphism in a way that resists the re-equilibration (due to its low cationic diffusivity), overprinting and, or, the erasure of earlier metamorphic phenomena. Therefore this mineral preserves important information concerning the nature of the metamorphism and provides a basis for estimating the P-T history of the rock during its growth using element distribution coefficients and, or chemical zoning profiles (Spear and Selverstone, 1983).

2. Garnet can also assist in elucidating the progressive deformation of the matrix in which it occurs. This is because it is rigid, equant and commonly inclusion-bearing and thus can be used in establishing sequential change in temperature, strain and chemical reactions.

Thus the quantitative measurements of garnet sizes may provide an indirect measure of growth rate, P-T changes, chemical reaction and deformation. Throughout the region the size of garnet porphyroblasts differs significantly in outcrops in close proximity. There is also marked variation in the shapes of the garnets from outcrop to outcrop, from sample to sample in individual outcrop and even within a single thin section. Most are elongate, especially the larger grains (Plate 2.4b) while in some rocks they have a skeletal habit (Plate 2.9). Both size and expression appear to be linked to particular structural-stratigraphic "bands" or "units".

To elucidate the significance of the variability in grain size of the garnet the length and breadth of unbroken grains were separately measured: the syn-D_2 and post-D_2 - pre-D_4 porphyroblasts. To ensure that different cut orientations were studied, two thin sections were used for each sample. The number of grains measured varied greatly from thin section to thin section so that statistical techniques could not be applied. However the results show (1) a marked grouping of grain size distribution and (2) that the larger the garnets, the wider is the range of sizes represented.

The size data (Table 2.1) indicate the existence of three (average) grain size groups for the syn-D_2 garnets and a grouping of grain size with lithology. For convenience of subsequent description these size groups are

referred to as G_{2A}, G_{2B} and G_{2C}. With the post-D_2 - pre-D_4 garnets the size distribution is limited and the crystals are generally close to being equidimensional; these are referred to as G_{2-4} (See Plates 2.4a, b, c, d; 2.10 for representatives of G_{2A}, G_{2B}, G_{2C} and G_{2-4} respectively and Fig. 1.4 for sample locations). Examples of the garnet size variability existing within a single thin section are also shown in Plate 2.4a, b, with the larger grains generally containing quartz inclusions that are inhomogeneous and unsorted, while the relatively smaller grains include the elongate quartz in trails extending from margin to margin of the porphyroblast.

The chemical compositions of representative garnets showed that the G_{2A} ones are almandine-rich, the G_{2C} garnets are spessartine-rich with both being confined to the Pitlochry Schist. While the G_{2B} ones are almandine-rich but confined to Ben Lui Schist. Mostly the G_{2-4} garnets are confined to the Ben Lui Schist with both almandine-rich and spessartine-rich garnets occurring in relatively close outcrops. In addition the compositional profiles of garnets of different sizes in a single thin section (Fig. 3.10) showed that the larger garnets, have the lowest rim MnO and the most pronounced chemical zonation even within the same sample.

The occurrence of different sizes of garnets of comparable composition in the same thin section can be explained if the larger grains grew earlier than the smaller ones which commonly accommodate the more intensified matrix foliation (Se) (Plate 2.4a, b). The apparent slight elongation of the smaller grains suggests growth in a shortening regime, or else is due to dissolution of garnet rims (Bell*et al.* 1986). The relationship between garnet core and rim MnO, as well as garnet compositional profiles (Chapter 3), which systematically vary with the relative crystal size in the same thin section also indicate progressive garnet growth (Finlay, 1976; Bell and Rubenach, 1983: Mathavan, 1984). This interpretation is supported by temperature estimations for each size-group (Chapter 4) that show G_{2A} grew at the highest temperature, G_{2B} at an intermediate temperature and G_{2C} at the lowest temperature.

This interpretation is in accord with the nucleation and growth model of Galwey and Jones (1963) who showed that garnet nucleation occurs over a period of time to be followed by growth whose rate is determined by temperature and the concentration of the reactants (Kretz, 1966; Jones and

Galwey, 1966; Spry, 1969: Jones *et al.* 1972; Ridley, 1986; Christensen *et al.,* 1989).

TABLE 2.1. **Average length-breadth (mm) measurements of garnets.**

	Sp. No.	Mean length (mm)	Mean breadth (mm)
	1	1.58	1.28
	2	2.56	1.66
	3	1.52	1.22
G_{2A}	6	2.46	1.10
	7	2.54	1.24
	8	2.86	2.14
	9	1.89	1.51
	10	0.59	0.47
G_{2B}	11	0.52	0.40
	13	0.74	0.53
	22	0.28	0.22
G_{2C}	23	0.26	0.22
	24	0.26	0.20
	25	0.33	0.27
	14	1.37	1.18
G_{2-4}	15	1.31	0.99
	16	1.56	1.26
	17	0.75	0.57
	18	1.26	1.10

Table 2.2. Garnet sizes (lengths) and MnO core-rim composition in representative garnets

	Sp. No.	Size (mm) Length	MnO% Core	MnO% Rim
	3	1.49	4.74	0.95
		1.66	5.10	0.78
		2.76	6.24	0.71
G_{2A}	8	1.19	1.47	0.23
		3.49	2.34	0.19
		3.66	2.63	0.14
	9	1.19	1.89	0.78
		2.53	2.26	0.66
G_{2B}	13	0.63	3.34	0.65
		0.83	3.90	0.22
G_{2C}	25	0.33	7.99	6.46
		0.40	8.58	5.18
G_{2-4}	17	1.06	5.52	1.86
		1.29	8.26	1.36

2.5 Growth of biotite

No biotite has been found that can be assigned to S_1 fabric. However it is a component of S_2 in many rocks, particularly the D_2 garnet-bearing lithologies in the Pitlochry Schist. In rocks that contain the D_{2-4} garnet (mostly Ben Lui Schist) the biotite is rather sporadic or absent (Table 1.1). Mostly biotite occurs with its (001) cleavage plane trace parallel to the S_2 fabric and was deformed by F_3 (Plate 2.11a, c). Occasionally rare small biotite flakes occur in the pressure shadow areas of syn-D2 garnet porphyroblasts. In places biotite occurs as lens-like (up to 1.23 x 0.33mm across) some of which contain inclusion trails (Si), mainly of elongate quartz, that extend from margin to margin (Plate 2.11b). These trails are parallel to Se which shows both deflection and truncation against the biotite. Such biotites have not been seen to be deformed by either F_3 or F_4. In rocks with relatively high biotite mode, the flakes occur in apparent biotite-rich and biotite-poor domains defining S_2 and deformed by F_3 (Plate 2.11c). In rocks containing the G_{2-4} biotite defines the S4 more dominantly than S_2 (Plate 2.11d). In contrast to muscovite, biotite does not occur as random, radial aggregates or interlocked and undeformed crystals at F_4 hinge zones (Plate 2.2b).

The absence of biotite in S_1 probably suggests that P-T conditions were outside the biotite stability field during D_1. Its existence in S_2 and deformation by F_3 suggest growth during D_2. The very few small biotite flakes that occur in pressure-shadow areas of the G_2 garnet probably represent a by-product of the major garnet-forming reaction (Section 3.5.5). On the other hand, the sporadic occurrence of biotite in most G_{2-4} garnet-bearing lithologies probably suggests the involvement of D_2 biotite in the G_{2-4} garnet-forming reaction.

The textural relationships of such lens-like biotites, based on their orientation, transgressive relationship to biotite in the Se_2, their inclusion trails (Si) parallel to the external Se_2, and the amount of Se deflection, probably suggest their growth either earlier than those in the Se_2 matrix or later, during S_2 intensification. Either interpretation could be equally applied, assuming the non-instantaneous growth of biotite during the D_2 deformation which is responsible for the amount of matrix flattening. The shape and orientation of such biotite lenses is probably the result of the shape change due to marginal solution and rotation, rather than by internal deformation. The lensoidal biotite did not seem to be deformed by F_3 or F_4.

However the relationship to either D_3 or D_4 has not been determined although growth during D_2 is surmised.

The biotite that define S_4 suggests growth during the D_4 deformational phase. There is no static growth expression of biotite with it all being tectonically controlled, i.e. S_2- S_4-biotite, along with the common occurrence in segregated domains could be interpreted in terms of metamorphic differentiation. This would suggest that biotite nucleation took place in the more deformed sites in which strain energy provoked nucleation and promoted the diffusion of biotite-forming components towards the nuclei in the deformed region. The less stressed domains develop very little biotite (Mathavan, 1984, p.27).

2.6 **Growth of albite**

Most lithologies studied contain albite, but the occurrence of albite porphyroblast is limited and they are absent from lithologies containing the G_{2A} garnet although albite porphyroblasts may occur, in relatively nearby outcrops, that contain either of the other D_2 garnets, and in rocks that contain no garnet. The albite exhibits textural relationships that indicate syn-D_2 growth. It may occur in different sizes including porphyroblasts within the same domain. Inclusions in albite porphyroblasts may occur as (1) weakly curved trails commonly extending over the major part of the crystals and terminating near the albite edge (Plate 2.12c), (2) defining a large inclusion-rich core and a narrow inclusion-free rim. Both inclusion-rich albites may occur adjoining inclusion-free albite. The inclusions in albite are essentially significantly smaller than the corresponding matrix minerals. The general absence of (Si), left the porphyroblast- matrix relationship as the most useful criterion to be used to elucidate the possible albite sequential growth. On the other hand albite-matrix relationships present in the Balquhidder rocks clearly demonstrate that some of the textural criteria commonly used to infer time relationships between porphyroblast growth and deformation are ambiguous: the albite porphyroblasts in one rock could appear, for instance, as syn-D_2 (Plate 2.13). However there is no textural evidence to indicate that the growth of albite accompanied either D_1-M_1 or D_3-M_3. In addition, the possible albite growth during the post-D_1 static period seems impossible to predict due to the lack of unequivocal textural evidence for these periods, mainly the result of the possible irregular rotation of the albite porphyroblasts shown by the diverse orientation of the inclusion trails in albite which are in contact with one another. The albite

porphyroblasts (up to 1.7mm x 1mm), their length lying parallel to the S_2 fabric which deflect around the porphyroblast with quartz-pressure-shadow areas being developed on the opposite sides, suggest growth during the early or main part of D_2.

The albite porphyroblasts that overprint the S_2 fabric (Plate 2.12b, c) suggest growth during the post-D_2 phase. The growth of albite during post-D_2 is also evident from the moulding relationship observed with the G_{2-4} garnets (Plate 2.12d) so that overlapping post-D_2 garnet and albite growth took place. Albite porphyroblasts also overprint F_4 crests which indicates post-D_4 growth. The occurrence of more than one albite growth phase, syn-D_2, post-D_2 or post-D_4 in a single domain (Plate 2.13) contrasts with the single phase of garnet growth in each domain.

2.7 Growth of quartz

Quartz is commonly found in syn-D2 garnet porphyroblasts as fine elongate trails (Si) (Plate 2.6b, c; 2.7). In the matrix it forms dimensionally elongate grains, often rectangular, between mica flakes that define S_2 in semipelitic lithologies (Plate 2.14a). Quartz recrystallization, shown at F_3 crests of polyhedral equidimensional quartz grains with approximately equal angle triple junctions approaching the stable low energy configuration, are found in F3 hinge zones; and quartz in S_2 is deformed around both F_3 and F_4 (Plate 2.14b, c). Locally dimensionally aligned quartz grains express S_4.

The elongate quartz that is included in the syn-D_2 garnet provides evidence of the pre-D_2 quartz growth; this is likely to represent D_1 growth. Alternatively, the size and shape of the quartz included in garnet cores and rims could indicate early D_2 and late D_2 growth, respectively. The late-D_2 growth probably accompanied matrix grain coarsening, with some quartz being accommodated in the garnet rims (Plate 2.9c). Quartz growth also took place syn-D_2 as is evident from elongate and rectangular occurrences within the S_2 mica layers, and was deformed by F_3. The polyhedral equidimensional quartz grains at F_3 crests indicate that some quartz recrystallized after D_3.

2.8 Growth of epidote

Epidote is present as inclusions mostly in garnet (particularly G_{2A} and G_{2B}) and albite porphyroblasts. Its presence in the matrix is rather sporadic, although in some lithologies epidote is a major constituent (Table 1.1). In rocks containing the G_{2C} garnets the epidote dominantly occurs in

the matrix and commonly shows overprinting relationships with S_2 (Plate 2.15a). The matrix epidote are commonly prismatic and larger than those included in garnet and albite porphyroblasts. They show two types of optical zoning, always distinct in the larger grains, which show bluish core and yellowing rim birefringence colours. The smaller grains commonly show only the low birefringence, and both types of such zoned epidote may occur in the same lithology. The epidote included in the garnet and albite is equidimensional and smaller, but both types of zoning are seen in the same host phase.

2.9 Growth of tourmaline

Idioblastic accessory tourmaline is present in a number of rocks, locally being enclosed in albite and garnet porphyroblasts but mainly occurring as larger grains in the rock matrix. The matrix grains are prismatic (Plate 2.15b, c) and some have quartz inclusions (Si) which are either parallel to, or truncate, the Se_2 with overprinting relationship. The very small tourmaline grains included in albite and garnet porphyroblasts may have grown during D_1 (or D_1-D_2 static phase) as it is enclosed in phases that have grown during D_2. Tourmaline in the matrix is seen to overprint the S_2 fabric, and is not seen to be affected by either D_3 or D_4, therefore the growth history is not certain, except that it was at least D_1 to post-D_2.

2.10 Growth of hornblende

Hornblende in the garnet-hornblende schists of Gleann Crotha (all other metabasites were not investigated) forms large prisms parallel to S_2 orientation, and S_2 mica layers deflect around the hornblendes developing quartz pressure-shadow areas (Plate 2.16a). Some hornblende shows lenticular-like shapes while others show relative rotation in relation to S_2 fabric (Plate 2.16b,c). The hornblende encloses most of the matrix phases; i.e. oxides, quartz, fine micas and epidote. Some of the hornblende partially included smaller garnet porphyroblasts than those in the matrix which are the G_{2A} garnet phase (Plate 2.16d). The following features suggest that hornblende grew simultaneously with the G_{2A} during D_2.

1. The similar textural relationship between S_2 and garnet or the hornblende, as they both show the same amounts of matrix deflection.
2. Inclusion trails in garnet (Plate 2.6a) and in the hornblende suggest their possible differential rotation with respect to S_2.

3. The chemical composition of matrix garnet, of similar size to that partially included in the hornblende, is identical to those larger grains in the matrix with core and rim MnO composition (Table 2.2, No.9) indicating that they have nucleated progressively. Therefore it cannot be due to the garnet growing earlier than the hornblende and then some being isolated from the rest of the rock system by the enclosing hornblende crystal. Some of the hornblendes have shape modification due to solution (Plate 2.16b).

2.11 Summary

The sequence of mineral growth in relation to the deformational phases established at Balquhidder are presented in Table 2.3.

The D_1 deformational phase is accompanied by the growth of muscovite, chlorite and quartz. There is no textural evidence to indicate that epidote and, or, tourmaline have grown during that phase of metamorphism. But their occurrence as inclusions in the syn-D_2 garnet and albite porphyroblasts is probably indicative of their growth during D_1 (or D_1-D_2) or early D_2 before enclosed. D_2 deformational phase was the period of climactic and porphyroblastic mineral growth. During this phase muscovite, chlorite, garnet, biotite, albite, quartz and hornblende have grown, and have developed porphyroblastic crystals. The growth of garnet porphyroblasts during D_2 was prolonged and produced three distinguishable size varieties, i.e. the G_{2A}, G_{2B}, G_{2C}. The D_3 deformational phase was not accompanied by any new mineral growths, but the annealing of pre-existing assemblages are difficult to predict. Very weak S_3 defined by muscovite and chlorite is recognized. A second period of garnet growth is interpreted as static post-D_2 - pre-D_4 (as to keep within limits of confidence provided by textural relationships) and may be pre-D_3. The D_4 deformational phase was accompanied by the recrystallization of most other phases (except garnet): muscovite, chlorite, biotite and albite and muscovite and albite are continued after D_4. The last metamorphic imprint that affected the Balquhidder rocks is a retrogressive phase which affected the previous assemblages, especially the garnets and biotites.

TABLE 2.3 Sequence of mineral growth - Balquhidder area

	D_1 syn-D_1	Post D_1 - pre D_2	D_2 syn-D_2	post D_2 - pre D_4	D_3 syn-D_3	post D_3	D_4 syn-D_4	post D_4
Quartz	_____		____			_____		
Muscovite	_____	_____	_____	_____	- - - - -		_____	_____
Chlorite	_____	_____	_____		- - - - -		_____	
Albite	?	?	_____	_____				
Garnet				_____				
Biotite			_____				_____	
Epidote	?	?		_____				
Tourmaline	?	?		_____				
Hornblende			_____					

Retrogressive chlorite after garnet (and biotite) are excluded.

PLATE 2.1

(a) Pre-S_2 arrow-like muscovite-chlorite fabric interfolial between S_2 planes (sp.27)

(b) Typical S_2 consisting of muscovite, chlorite, biotite and iron oxide, deformed by F_4. (sp. 24)

(c), (d) Partially dissolved muscovite plasts defining the S_2 fabric set in finer-grained muscovite-chlorite-quartz; in (d) the muscovite is slightly rotated as the result of a shear component. (sp. 3)

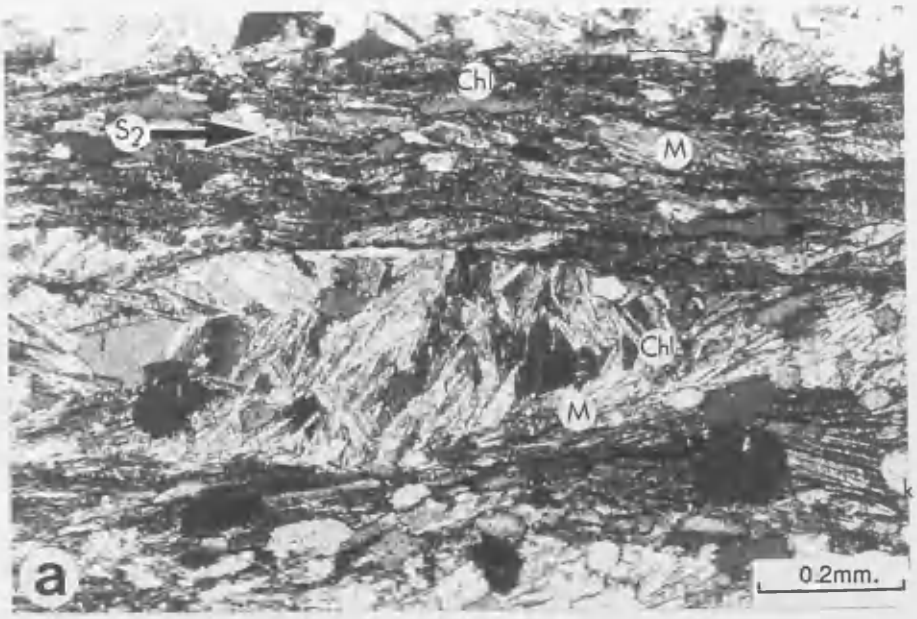
Chl
S2
M
Chl
M
a
0.2mm.

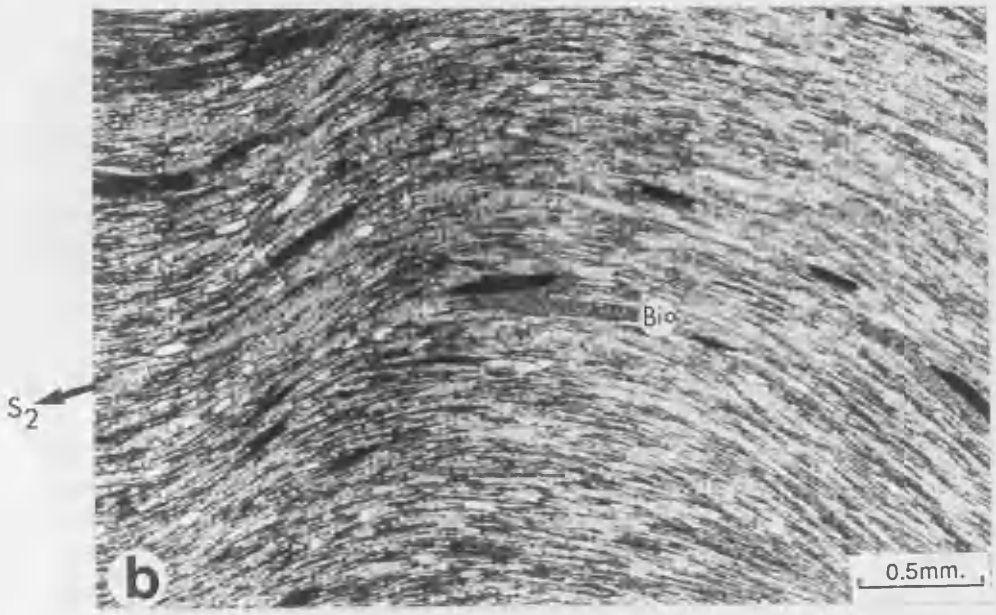
Bio
S2
b
0.5mm.

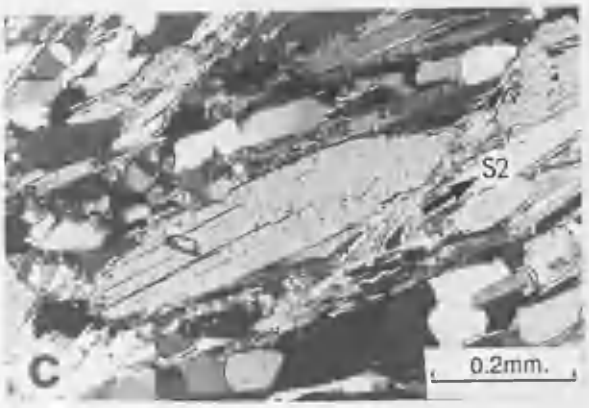
S2
c
0.2mm.


d
0.2mm.

PLATE 2.2.

(a) S_2 muscovite and chlorite defining an F_3 fold and F_4 microfolds in semipelitic schist; other undeformed flakes represent S_4 growth (cf. (b)). (sp. 29)

(b) Undeformed muscovite and chlorite interlocking at F_4 crests. (sp. 22)

(c) Randomly-oriented muscovite crystals across the S_2 matrix composed of muscovite and chlorite. (sp.29)

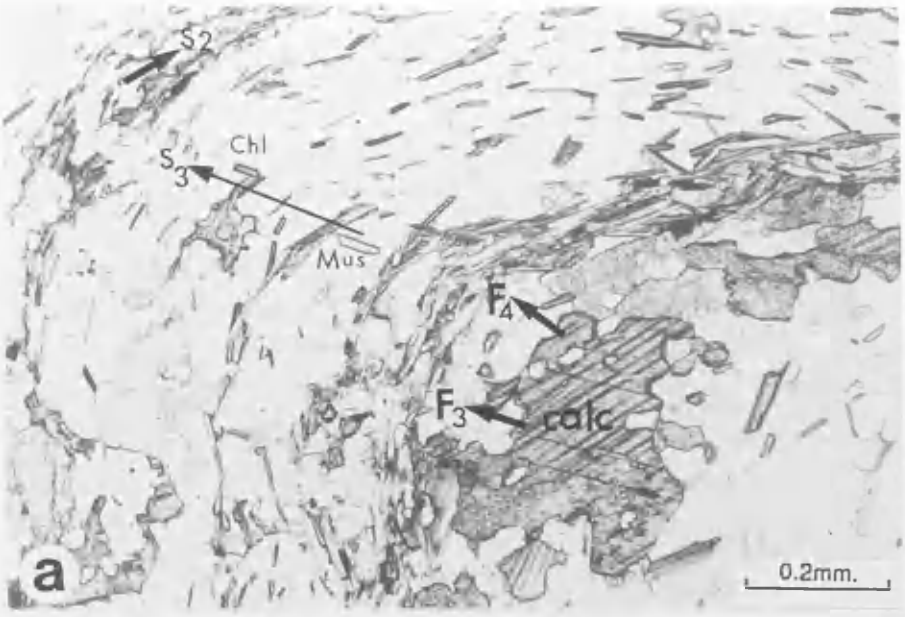
S2
S3
Chl
Mus
F4
F3
calc
a
0.2mm.

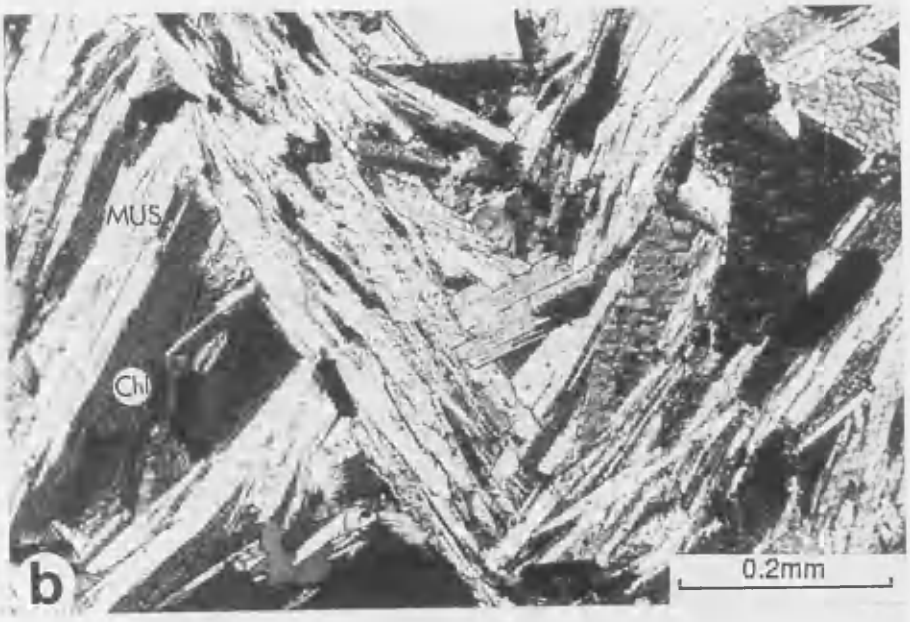
MUS
Chl
b
0.2mm

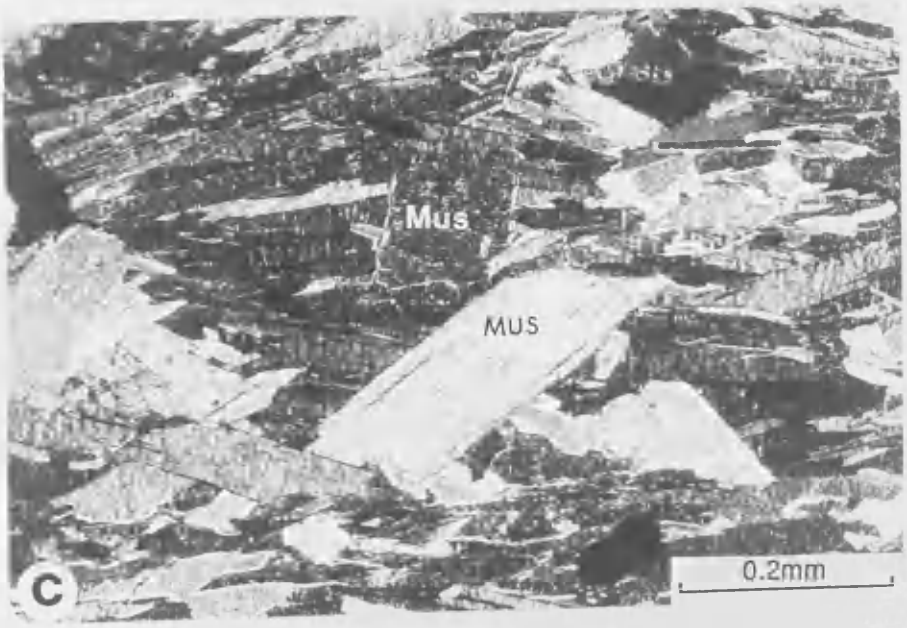
Mus
MUS
c
0.2mm

PLATE 2.3. **Garnet retrogression.** See text Section 2.4.3 for explanation

a) Partially to completely chloritized G_{2A} garnet porphyroblasts (sp. 2)

(b) Completely chloritized G_{2C} garnet grains (sp. 26)

(c) Partially chloritized G_{2-4} garnets; the removed and replaced parts are interconnected and extended throughout the remaining garnet and separate it into a number of disconnected islands (sp. 5)

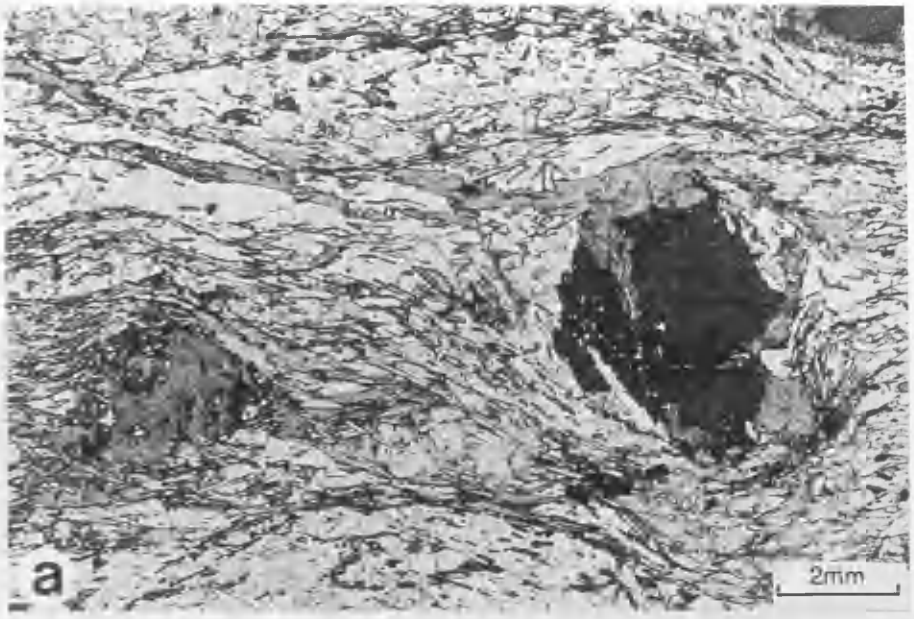
a
2mm

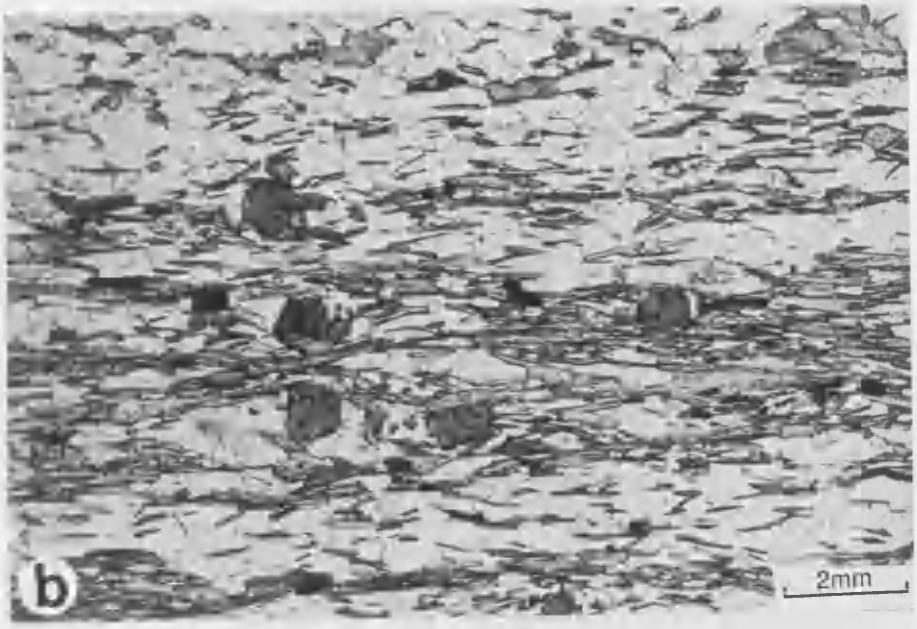
b
2mm


c
2mm

PLATE 2.4. Syn-D_2 garnets

(a), (b) Two garnet porphyroblasts in the same thin section; part of the larger crystal (a - 3.44 x 2.36mm) includes quartz and albite showing variable grain shapes and no dimensional alignment; the small crystal (b - 2.80 x 1.50mm) includes generally straight inclusion trails of quartz, muscovite, albite and biotite that are largely parallel Se which shows some deflection, at porphyroblast boundary. (sp. 8)

(c) Round garnet porphyroblast (0.7mm) with straight inclusion trails oriented at angle to Se which is warped round the garnet; quartz has grown in pressure shadow areas. (sp.13)

(d) Small garnet porphyroblast (0.30mm) with no inclusion trails, with Se deflected around it; small albite crystals overprint Se (sp. 26)

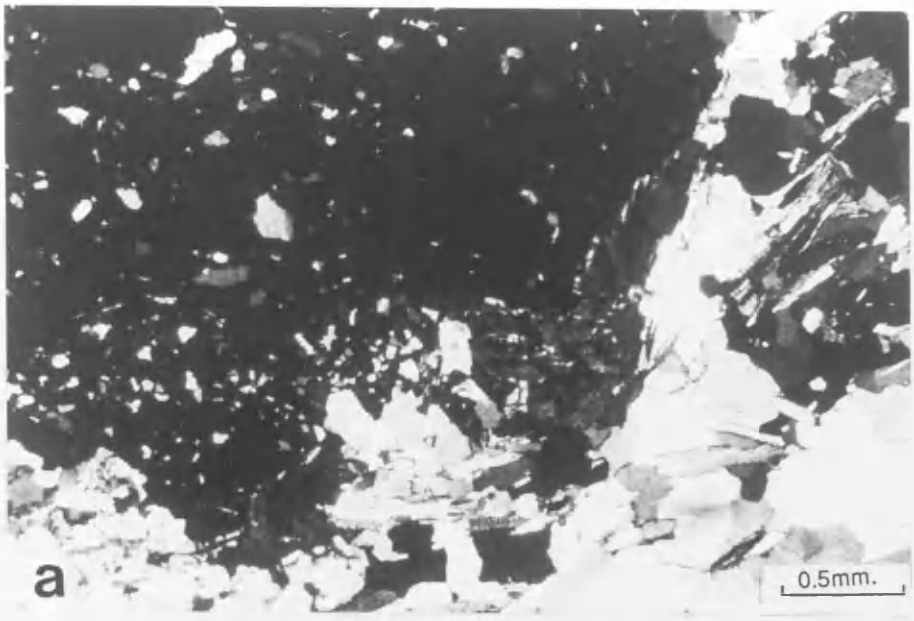
a
0.5mm.

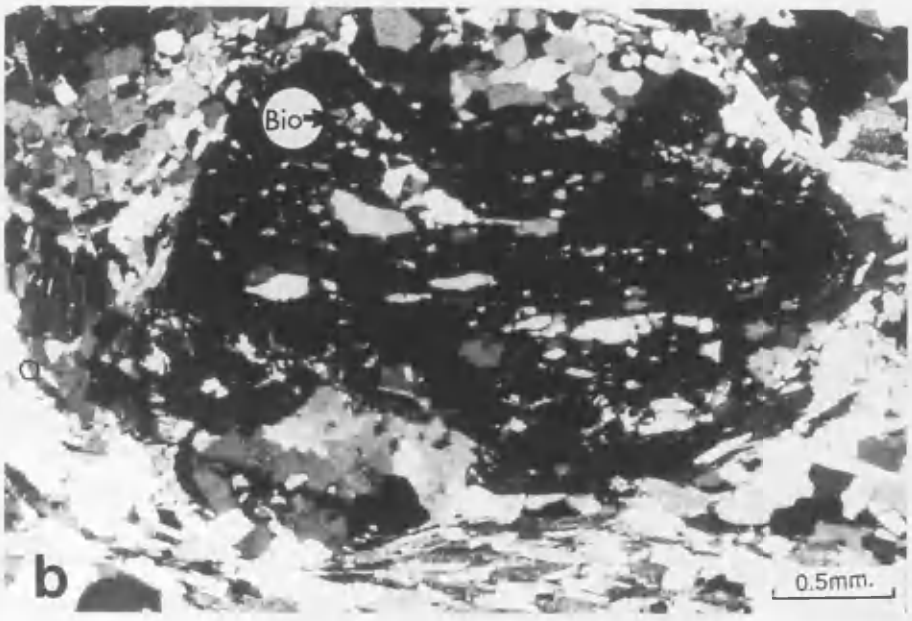
Bio
Q
b
0.5mm.


c
0.2mm

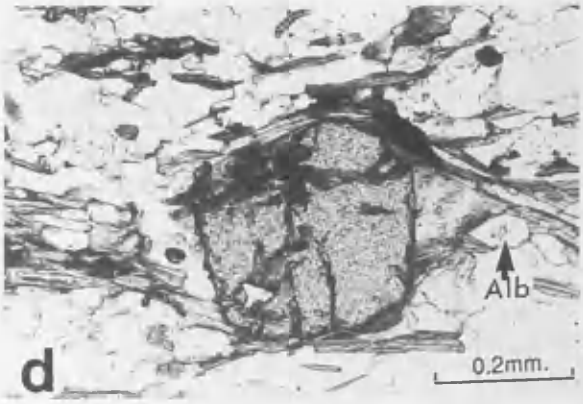
Alb
d
0.2mm.

PLATE 2.5. Syn-D_2 garnets

(a), (b) Syn-D_2 garnet porphyroblasts with few or no apparent inclusion trails showing, Se_2 is warped around them and with symmetrical (a) or asymmetrical (b) pressure shadow areas of quartz developed. (sp. 2)

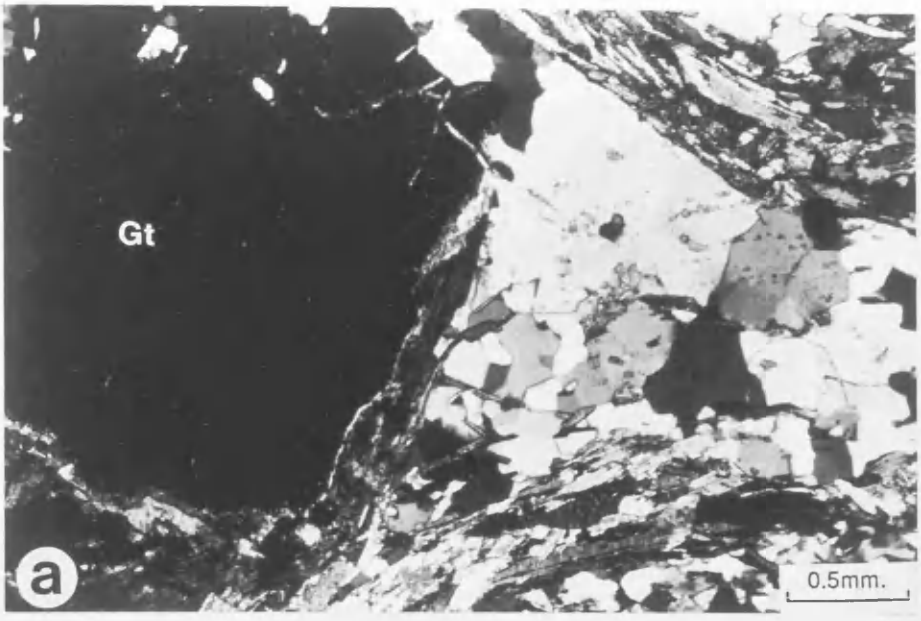
Gt
a
0.5mm.

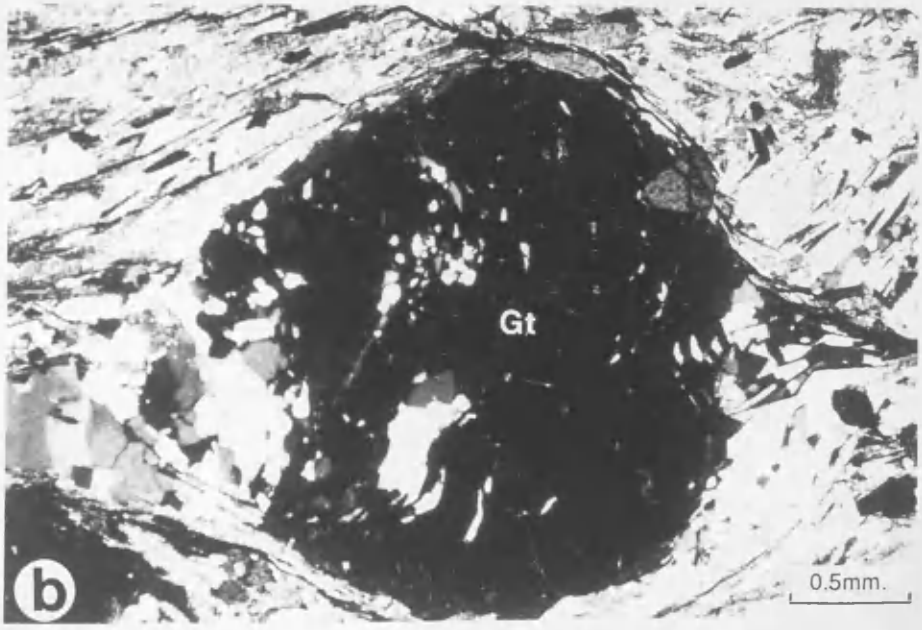
Gt
b
0.5mm.

PLATE 2.6. **Syn-D_2 garnets with type 1 inclusion patterns.**

(a) Garnet porphyroblast with linear inclusion trails (Si) shown by opaque iron oxide, that are generally parallel to Se. Locally rims rich in opaque minerals show parallelism to deflected Se. (sp. 9)

(b) Part of a garnet porphyroblast showing straight inclusion trails (Si) truncated by Se; larger quartz inclusions accommodated nearer to the garnet rim (sp. 2)

(c) Garnet porphyroblasts showing evidence of corresponding degrees of rotation as shown by Si-Se relationships; Se deflection around porphyroblasts is shown. (sp. 13)

(d) Garnet porphyroblast in the same section as in (a) with iron oxide inclusion trails at right angle iron oxide grains in Se. (sp. 9)

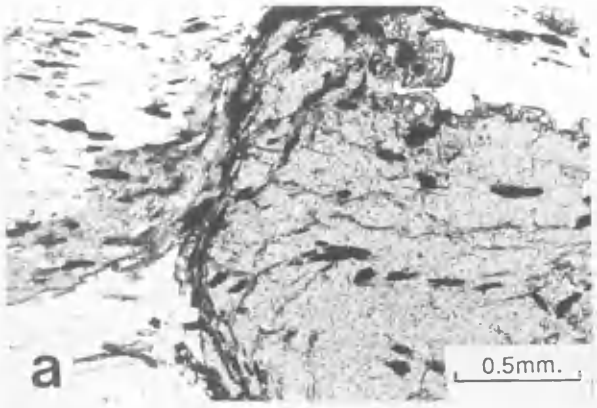
a
0.5mm.

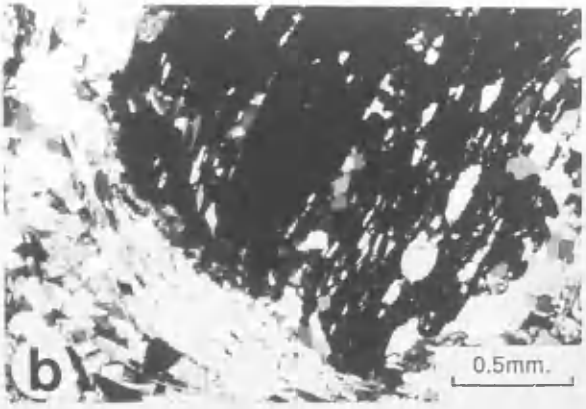
b
0.5mm.

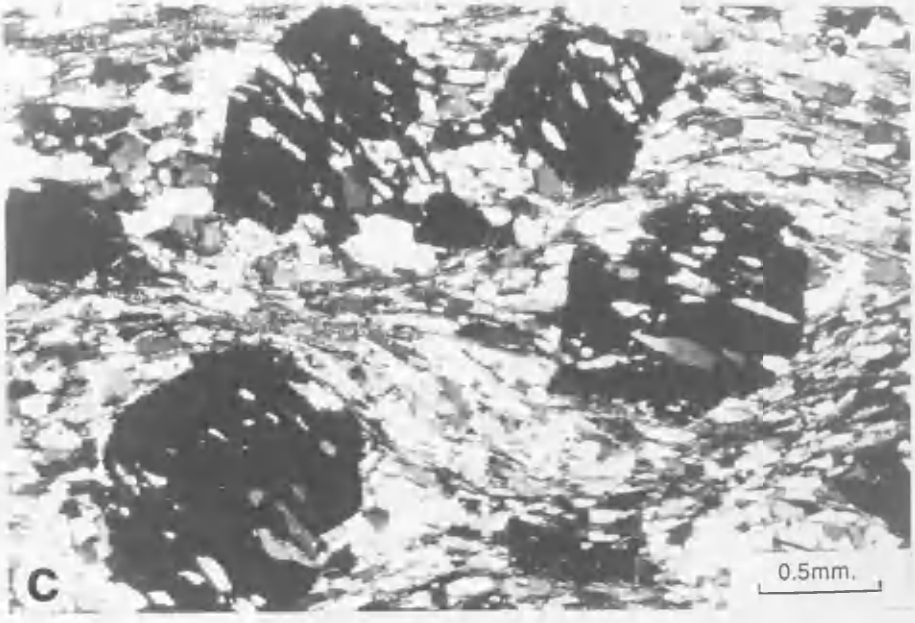
c
0.5mm.

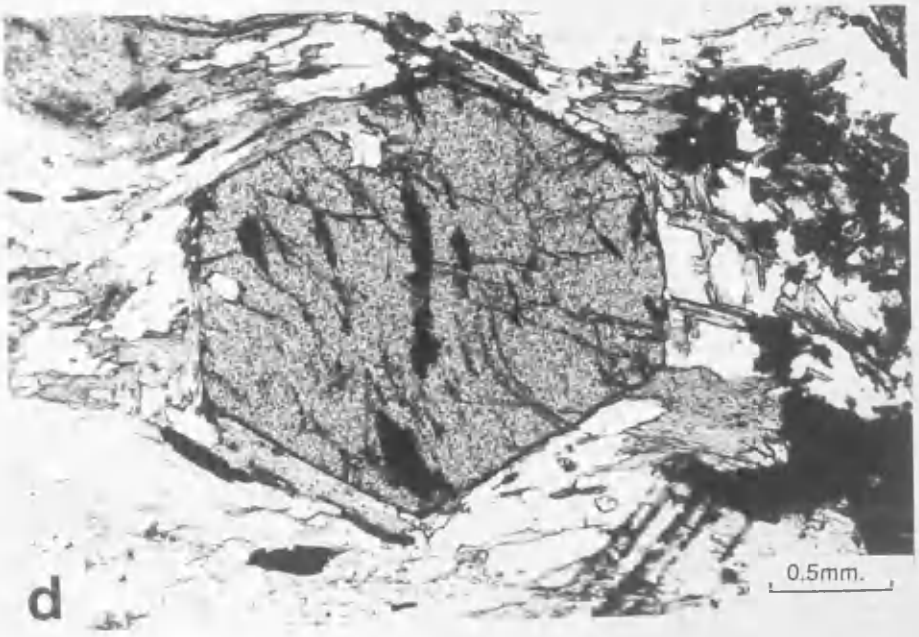
d
0.5mm.

PLATE 2.7. Syn-D_2 garnets with type 2 inclusion patterns.

(a) Garnet porphyroblast including bands of weakly curved Si composed of elongate quartz) that extend continuously from margin to margin and parallel to the Se. (sp. 3)

(b) Garnet porphyroblast with straight inclusion trails of quartz that show slight curvature towards the garnet edge. (sp. 3)

(c) Garnet porphyroblasts showing continuity of Si and Se; (i) incorporates weakly curved Si and (ii) straight Si showing no cuvature even at the rim; Si composed of quartz. (sp. 3)

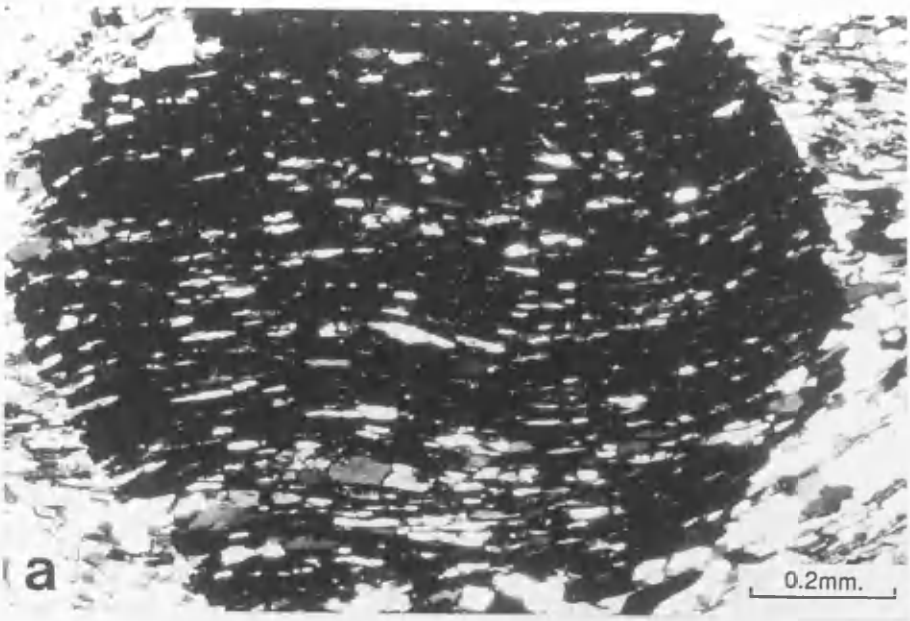
a
0.2mm.

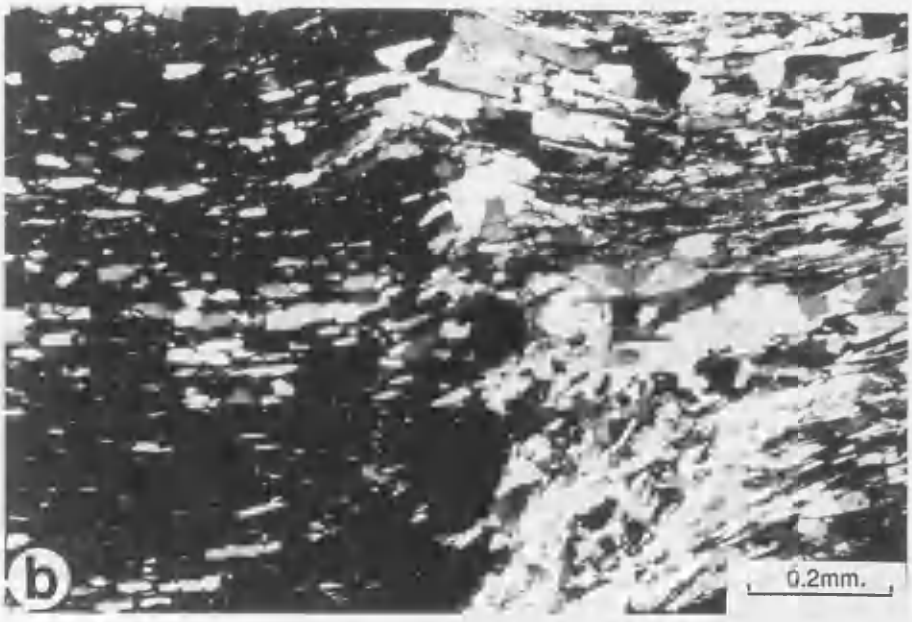
b
0.2mm.

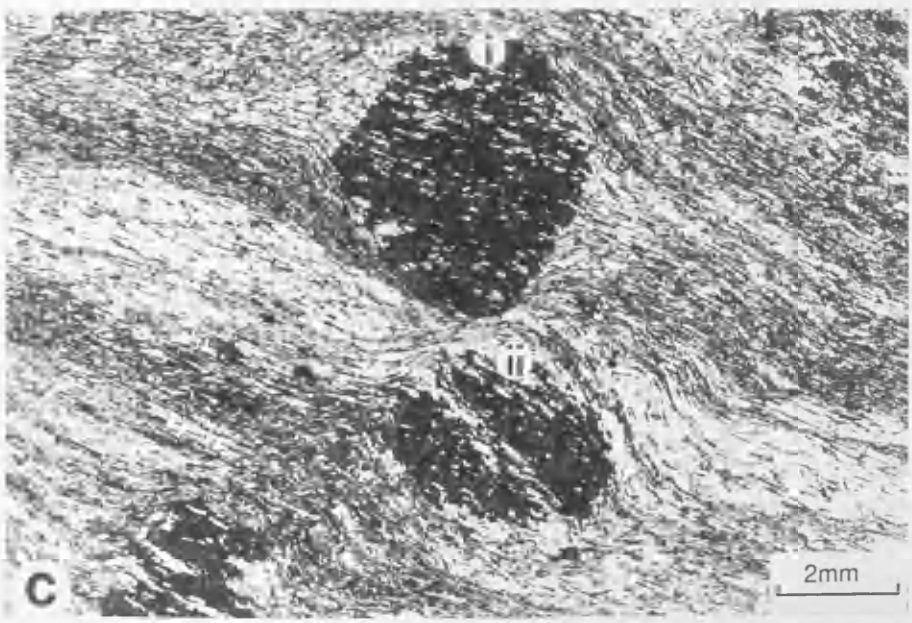
I
II
c
2mm

PLATE 2. 8. Syn-D_2 garnets with type 3 inclusion pattern

(a) Garnet porphyroblast with sigmoidal inclusion trails (Si); the Si quartz crystals showing the spiral are generally of similar size to that of Se quartz; Se_2 shows degrees of deflection and truncation. (sp. 3)

(b) Garnet porphyroblast incorporating spirals of quartz inclusions (Si) that are partially truncated by Se which itself is partially deflectd around the porphyroblast; the termination of the spiral away from the garnet edge is the result of the cut effect. (sp. 2)

(c) Elongate garnet porphyroblast with Si spiral trails of quartz; Se deflected around the garnet which shows much dissolution and indentation against quartz in the matrix. (sp. 6

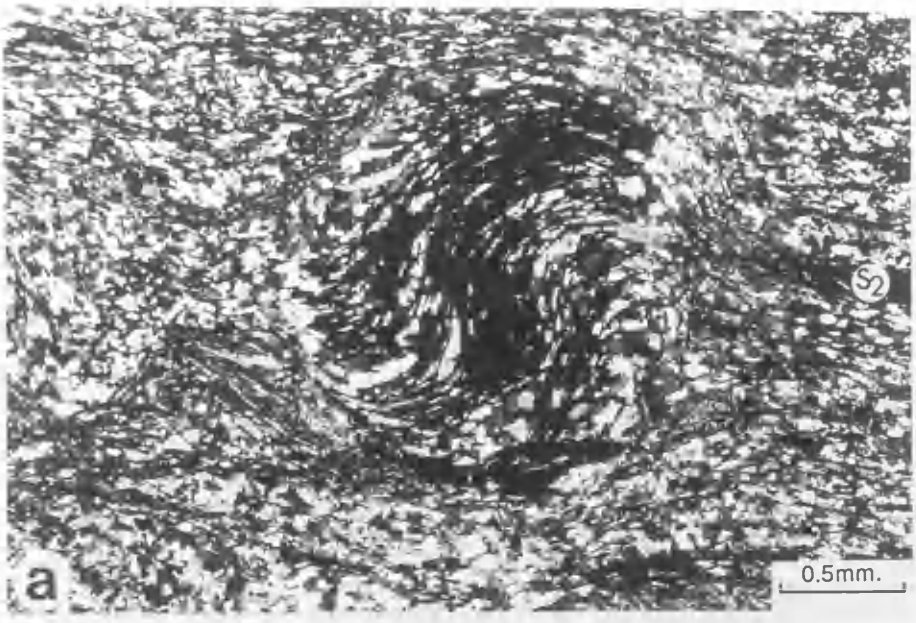
S2
a
0.5mm.

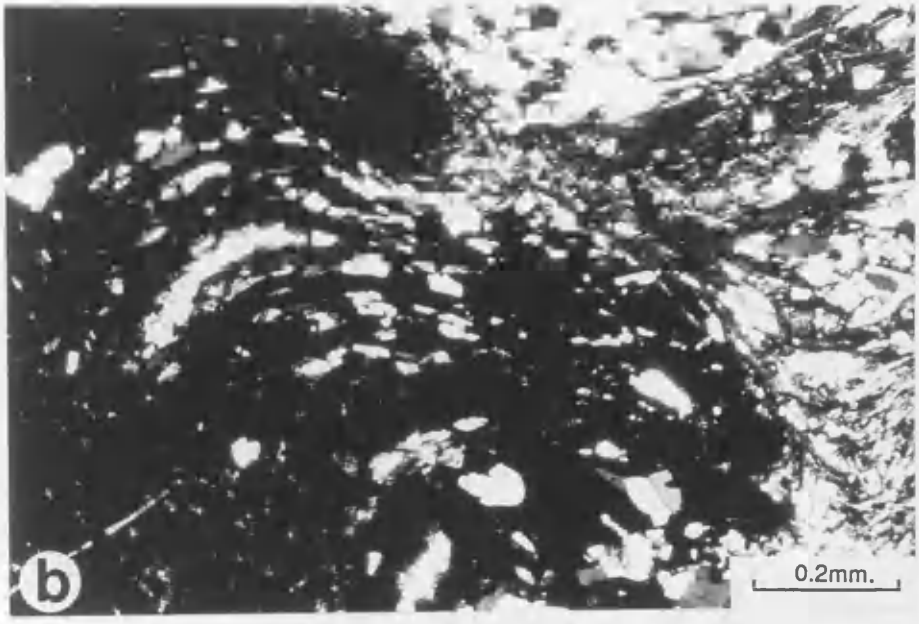
b
0.2mm.


c
0.2mm

PLATE 2.9. Syn-D_2 garnets with type 4 inclusion pattern.

(a), (b) Elongate skeletal garnet porphyroblasts with Si composed of quartz parallel both to Se and the garnet edges; the Si quartz crystals incorporated in the garnet rim are smaller and more elongate than those in the core. (sp. 6)

(c) Elongate skeletal garnet porphyroblast showing inclusion trails composed of quartz parallel to Se which, in turn, show deflection around the porphyroblast; recrystallized polyhedral quartz grains in pressure shadow areas are in direct contact with garnet edge. (sp. 7)

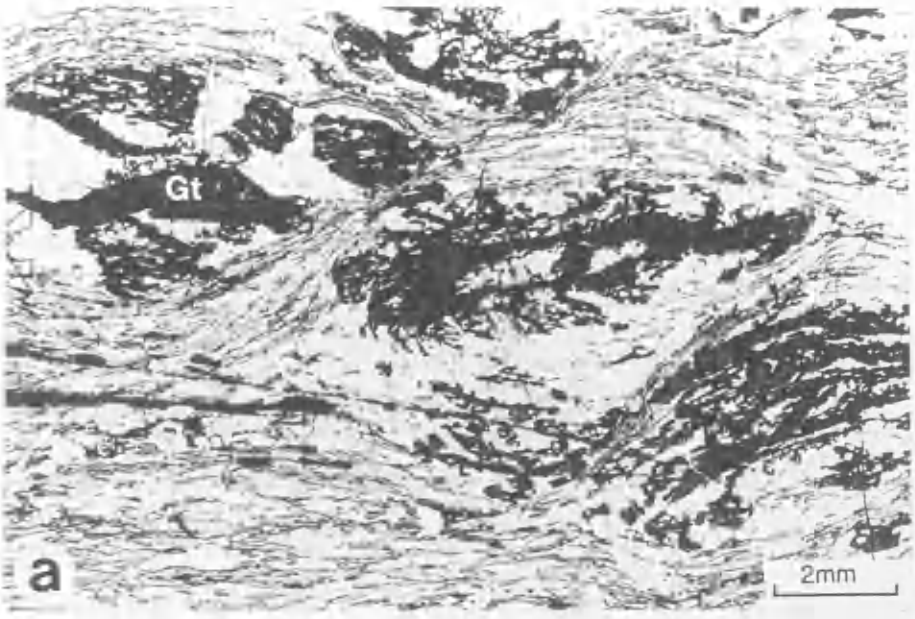
Gt
a
2mm

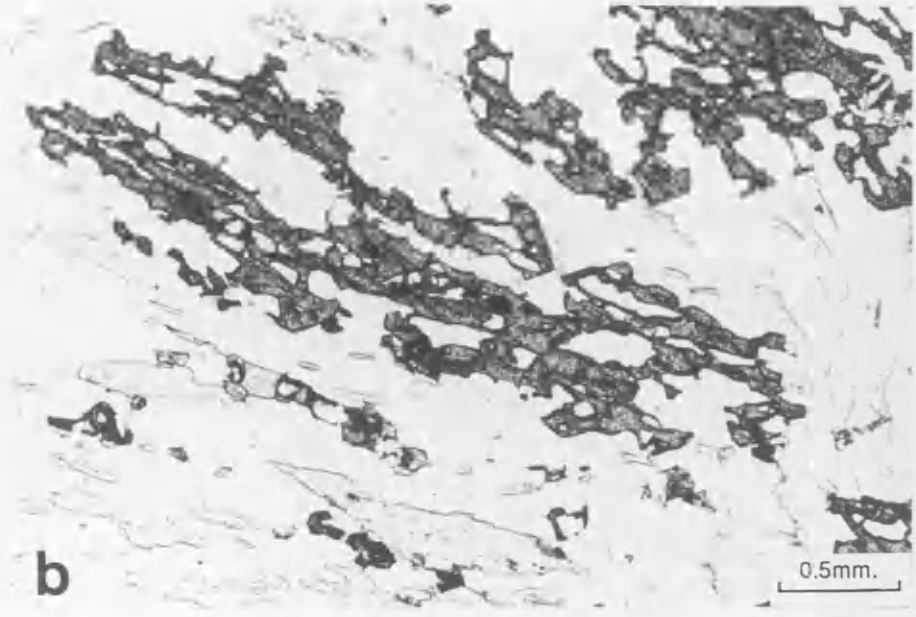
b
0.5mm.

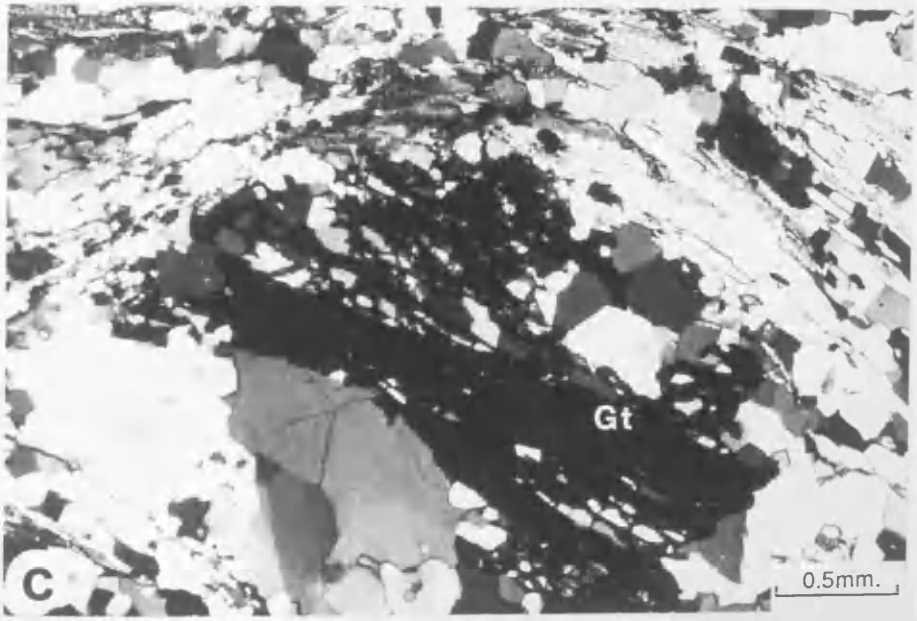
Gt
c
0.5mm.

PLATE 2.10. Post-D_2 pre-D_4 garnets.

(a) Garnet porphyroblasts showing overprinting relations with S_2; S_4 warps around them and there is no development of pressure shadows. (sp. 16)

(b) Garnet porphyroblasts showing overprinting relations with S_2 (right top) and strongly developed S_4 warped around them with no mica-free haloes developed (bottom). (sp. 17)

(c) Close-up of part of (b).

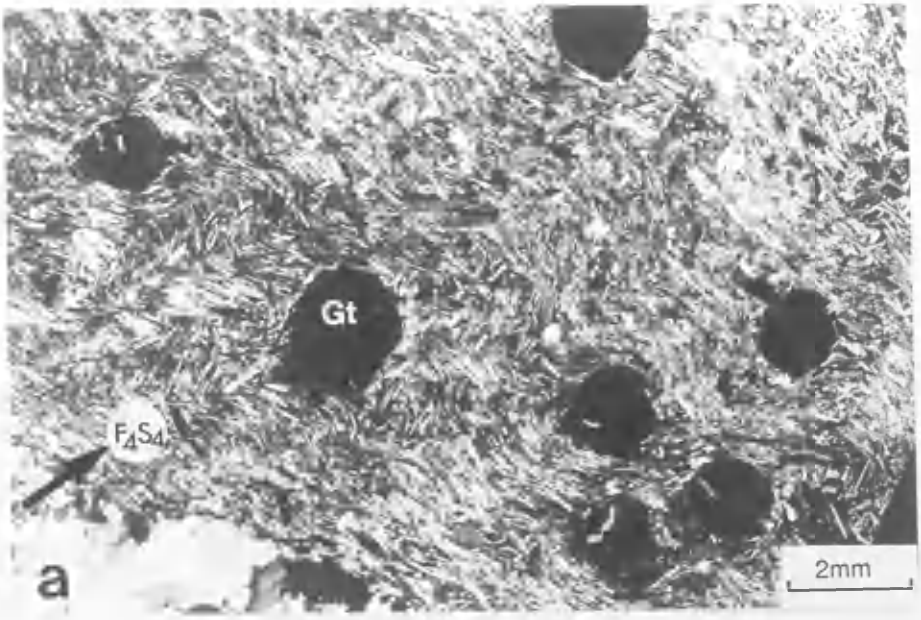
Gt
F_4S_4
a
2mm

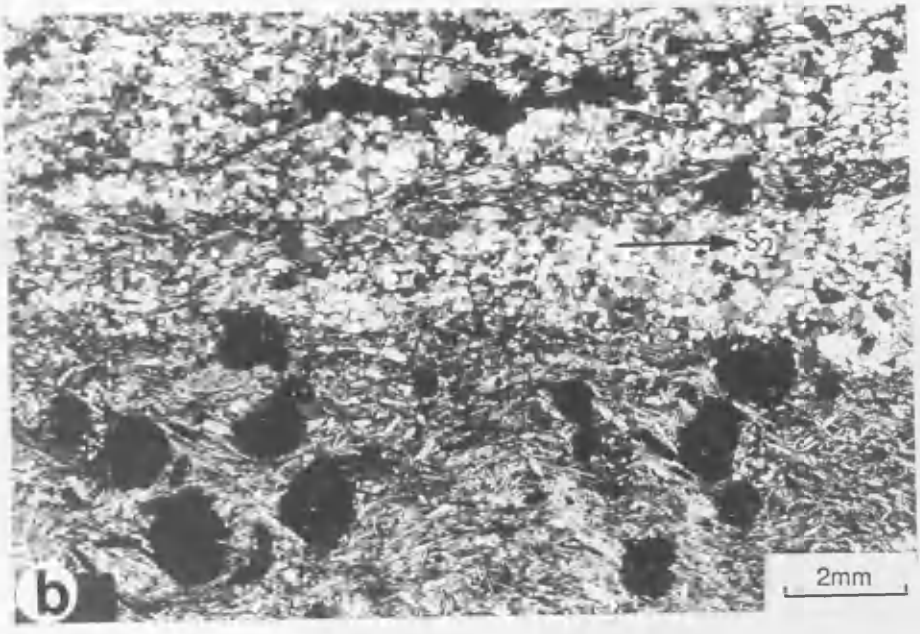
S_2
b
2mm

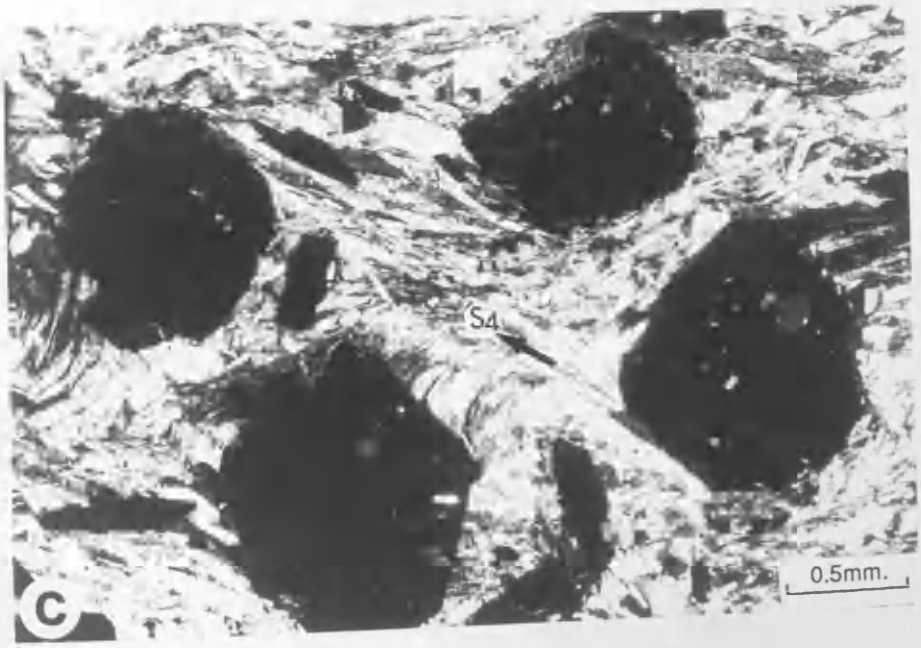
S_4
c
0.5mm.

PLATE 2.11

(a) Elongate biotite dimensionally oriented in S_2. The small garnets, which are partially chloritized occur in a quartz-rich layer which contains a smaller proportion of biotite than the biotitite-rich layers which have abundant epidote (below) and small albite (above), both overprint biotite in S_2 fabric. (sp. 25)

(b) Lens-like biotite plast with straight trails mainly of elongate quartz and muscovite oriented parallel to the S_2 matrix which shows slight deflection at the biotite edges (sp. 2)

(c) Quartz-rich layer with small biotite and thick clusters of biotite-rich layers both deformed by F_3. (sp. 25)

(d) Large biotite defining S_4 and axial planar to F_4 folds (sp. 17)

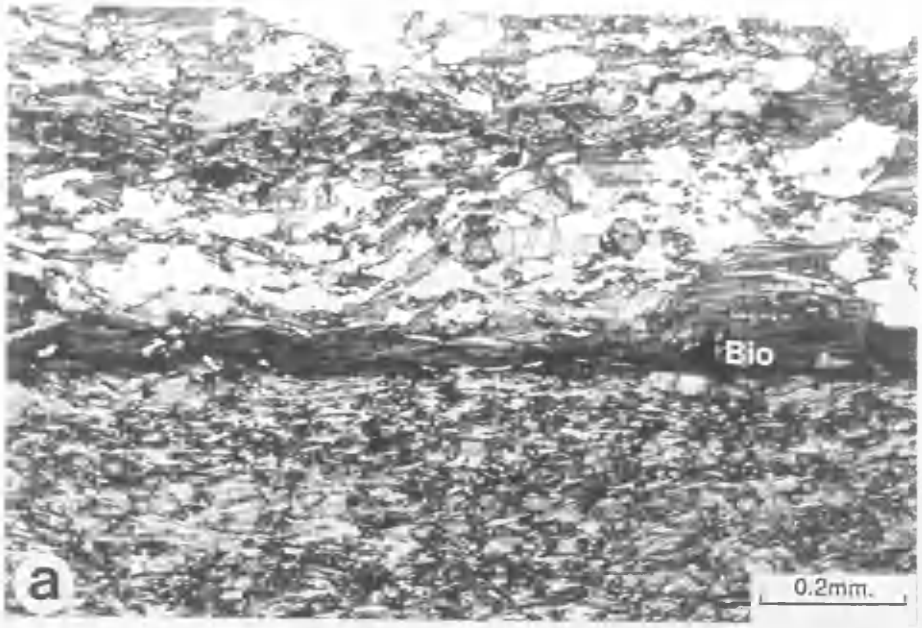
Bio
a
0.2mm.

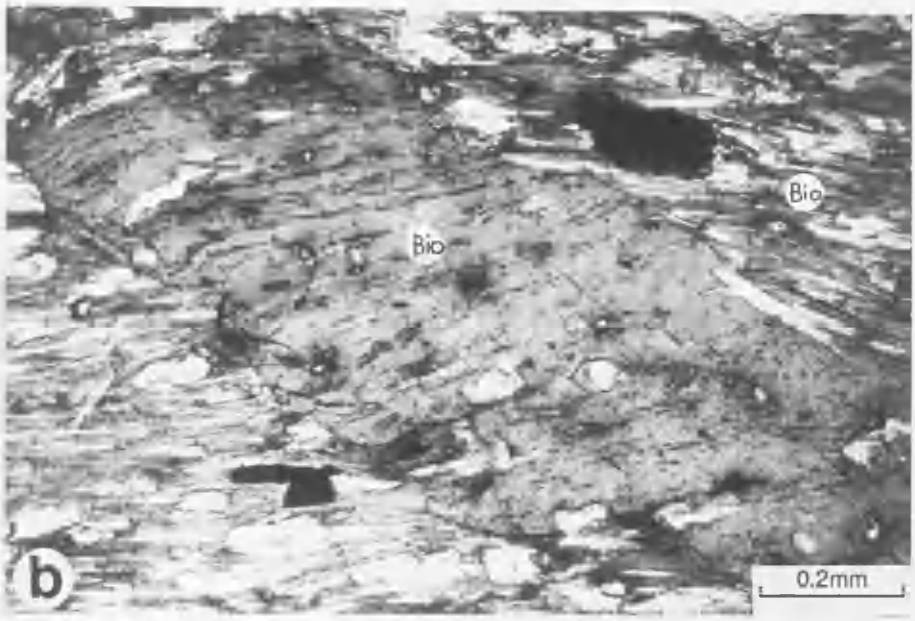
Bio
Bio
b
0.2mm

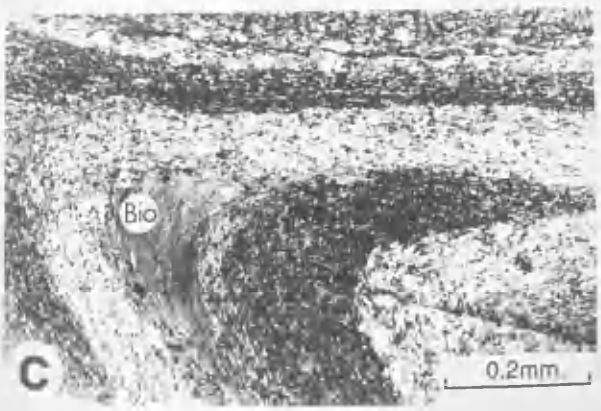
Bio
c
0.2mm.

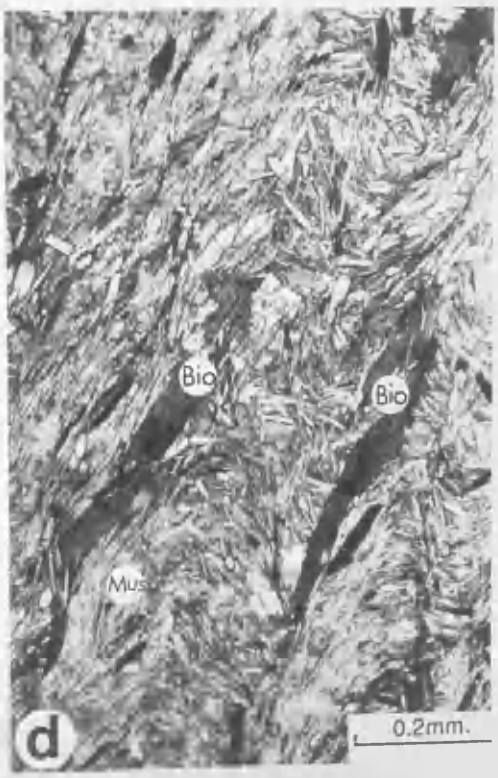
Bio
Bio
Mus
d
0.2mm.

PLATE 2.12

(a) Albite porphyroblast with inclusion-rich core and narrow inclusion-free rim and S_2 warped around it. (sp. 19)

(b) Albite microporphyroblasts (20%) overprinting the S_2 fabric made up of muscovite, chlorite, quartz and iron oxide (sp. 28)

(c) Albite porphyroblast overprinting S_2 fabric with curved inclusion trails oriented oblique to S_2 (sp. 29)

(d) Sutured albite porphyroblast grain with moulding relationship with the G_{2-4} garnet both of which overprint S_2. (sp. 17)

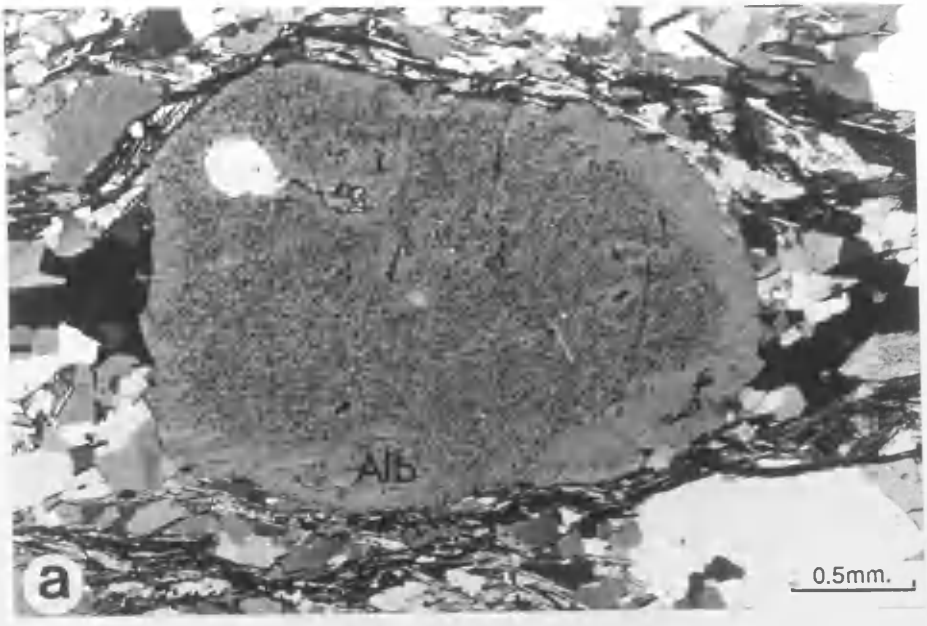
Alb
a
0.5mm.

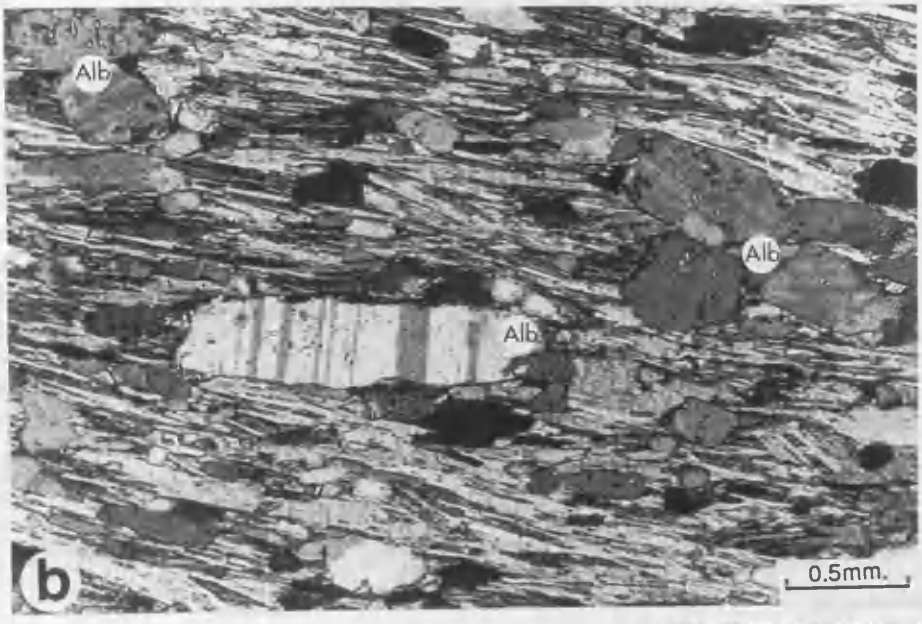
Alb
Alb
Alb
b
0.5mm.

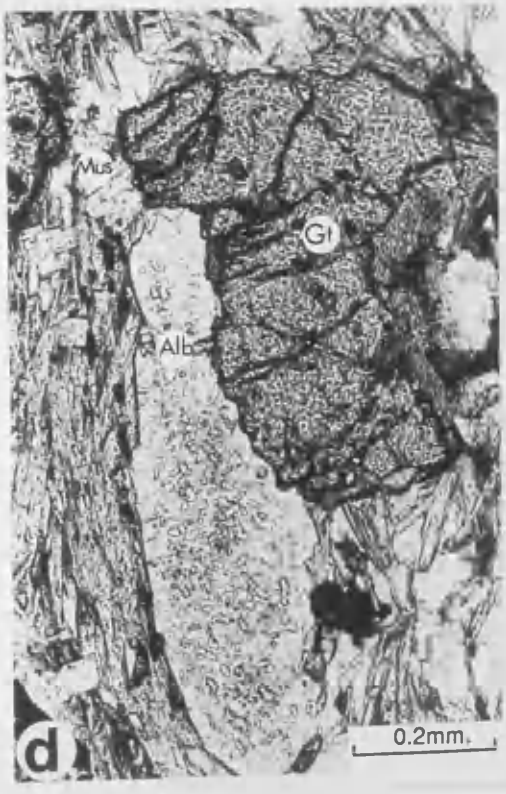
Mus
Gt
Alb
d
0.2mm.

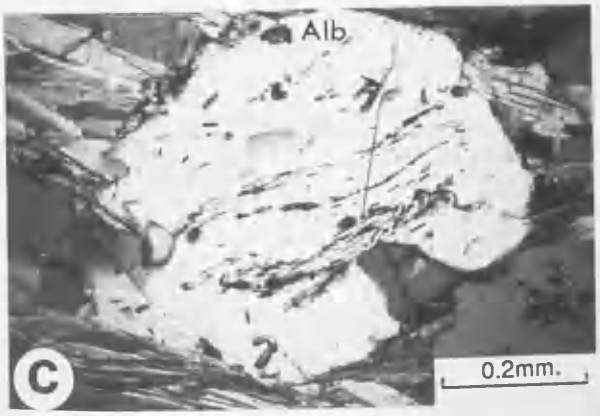
Alb
c
0.2mm.

PLATE 2.13 Albite grains showing various textural relationships (sp. 22)

(a) Adjacent albites show confliction in terms of conventional textural interpretations: grain (iii) and (iv) have overprinted the S_2 which deformed around F_4 with (Si) parallel and continuous with S_2 fabric; grain (i) with inclusion-rich core and at least two sets of trails, showing truncation against S_2, has overprinted the F_4 crest with no apparent physical pushing aside at the boundary of the grain and matrix; grain (ii) with straight inclusions truncated with S_2 which, in turn, shows both truncation as well as slight deflection around the albite grain.

(b), (c) Close-up of parts of (a)

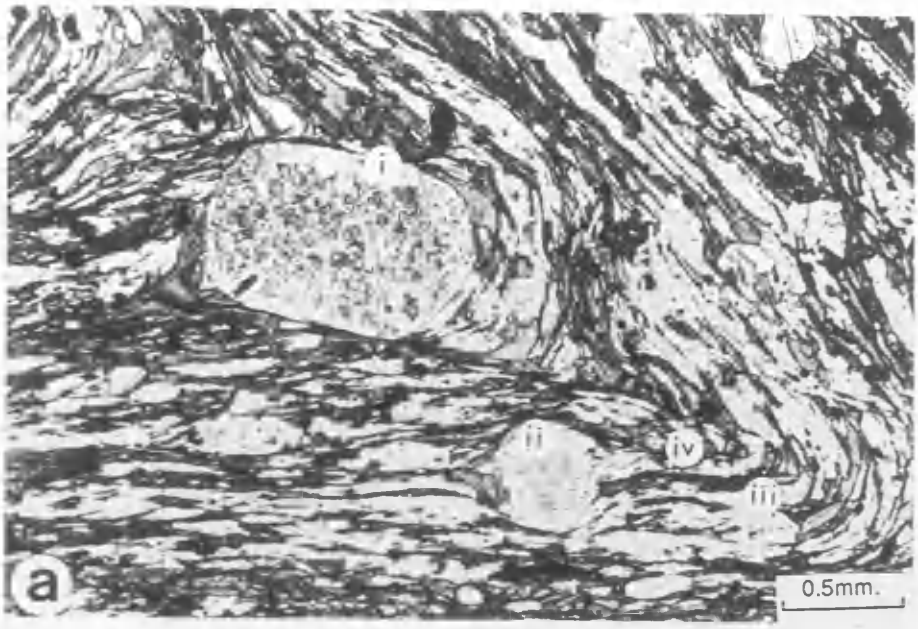
i
ii
iv
iii
a
0.5mm.


i
b
0.2mm.

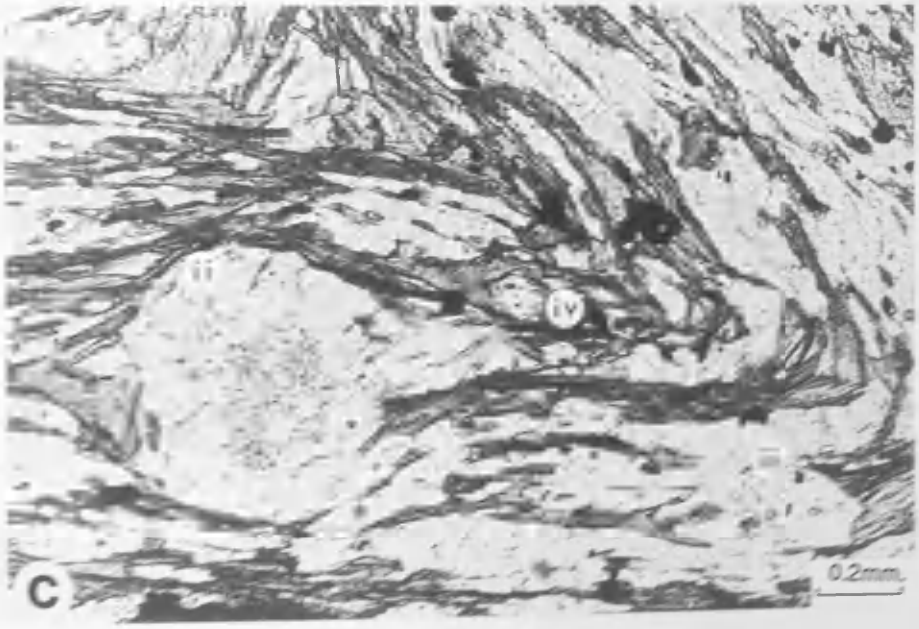
ii
iv
c
0.2mm.

PLATE 2.14

(a) Elongate to rectangular quartz grains between mica defining S_2 fabric. (sp. 6)

(b) Polyhedral quartz grains showing approximately equal angle triple junctions separated from mica domains by weakly defined quartz ribbons of slightly elongate and smaller quartz at an F_3 crest. (sp. 1)

(c) Deformed quartz grains of elongate and rectangular shapes against mica domains that define the short limb of open F_4. (sp. 23)

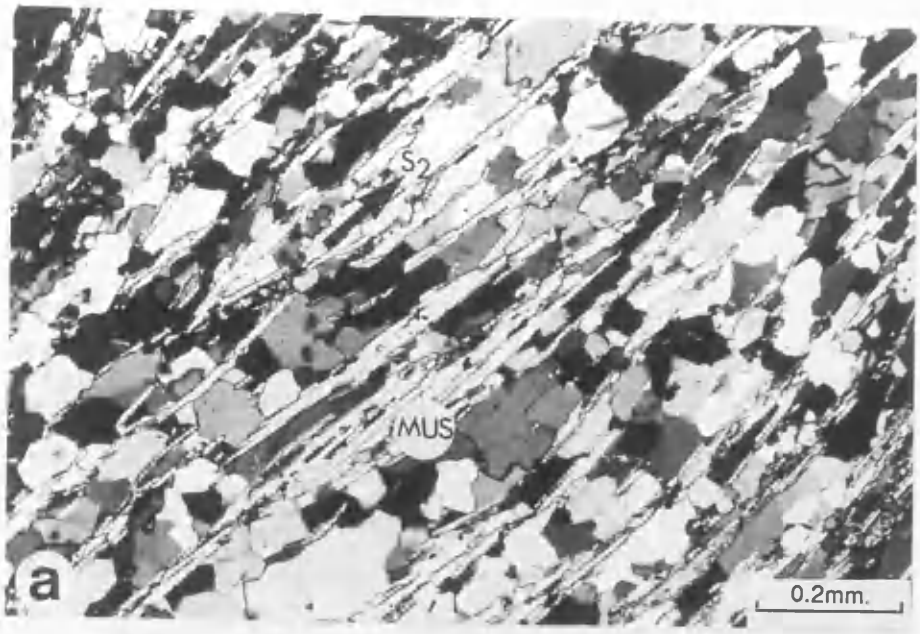
S2
MUS
a
0.2mm.

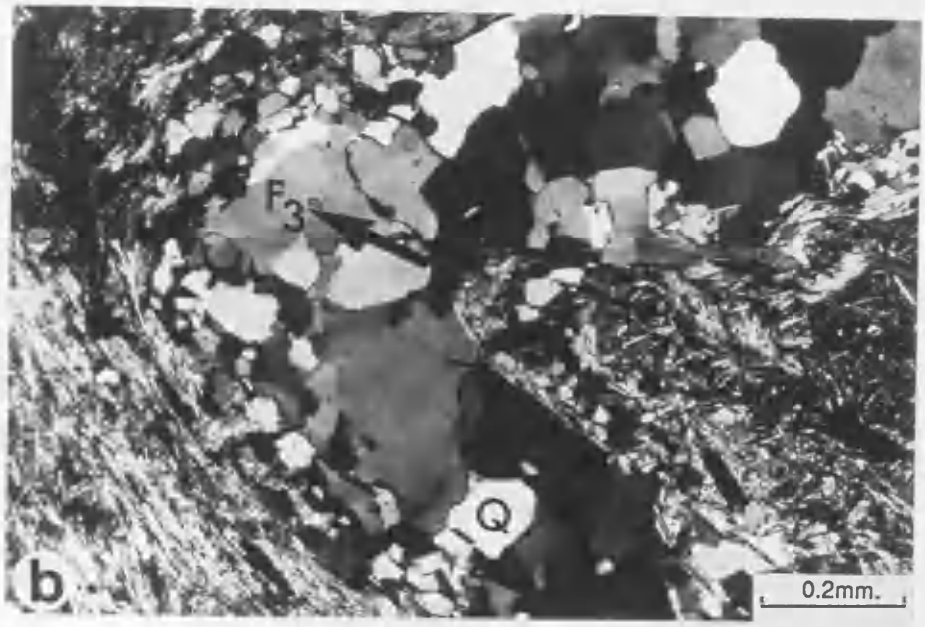
F3
Q
b
0.2mm.

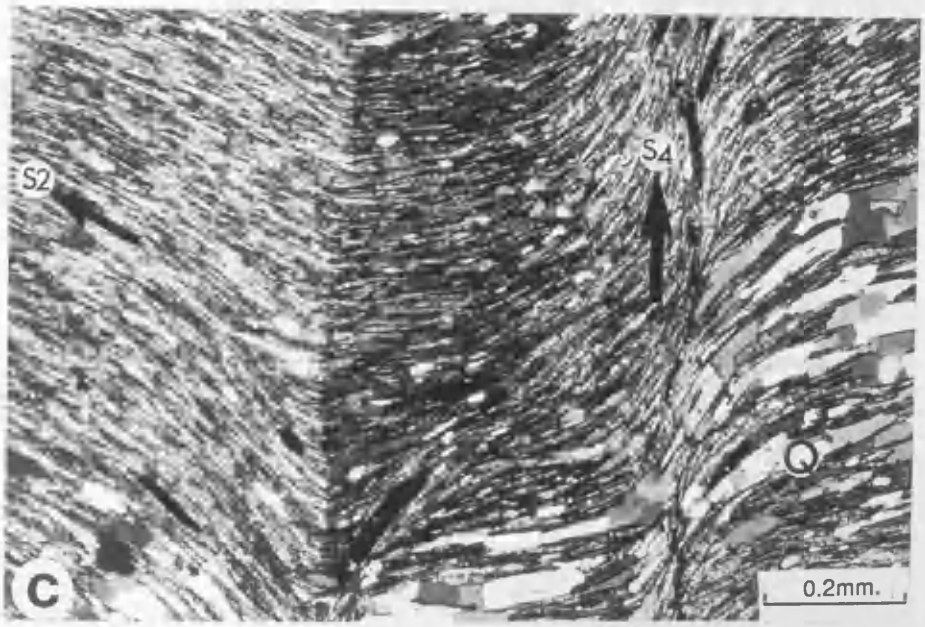
S2
S4
Q
c
0.2mm.

PLATE 2.15

(a) Epidote overprinting the S_2 fabric composed of muscovite, chlorite and biotite. (sp. 25)

(b) Tourmaline porphyroblast with straight quartz (Si) truncated against Se_2 with overprinting relationship. (sp. 7)

(c) Large prismatic tourmaline porphyroblast with straight inclusion trails (Si) composed of quartz overprinting S_2 fabric. (sp. 29)

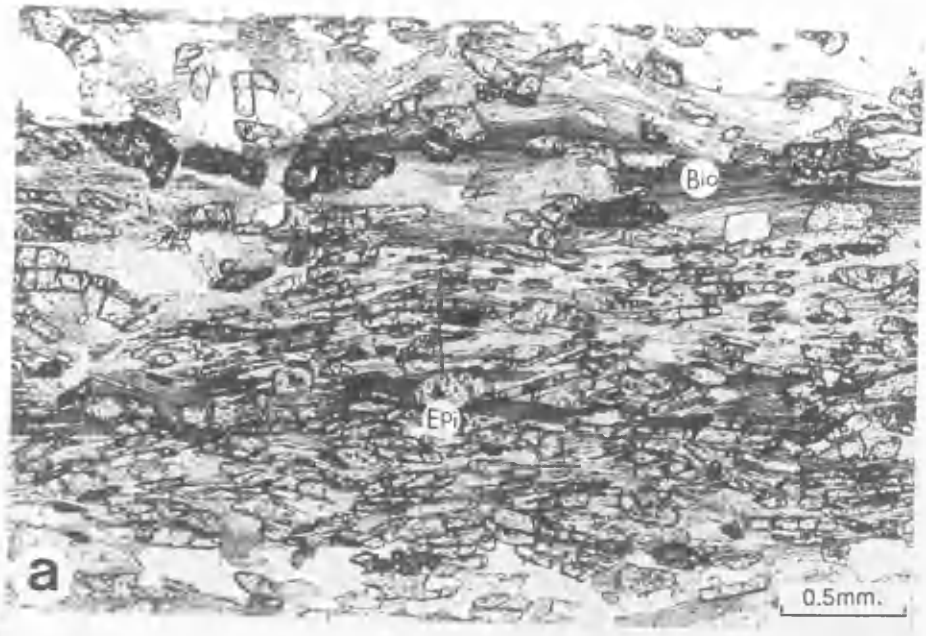
Bio
Epi
a
0.5mm.

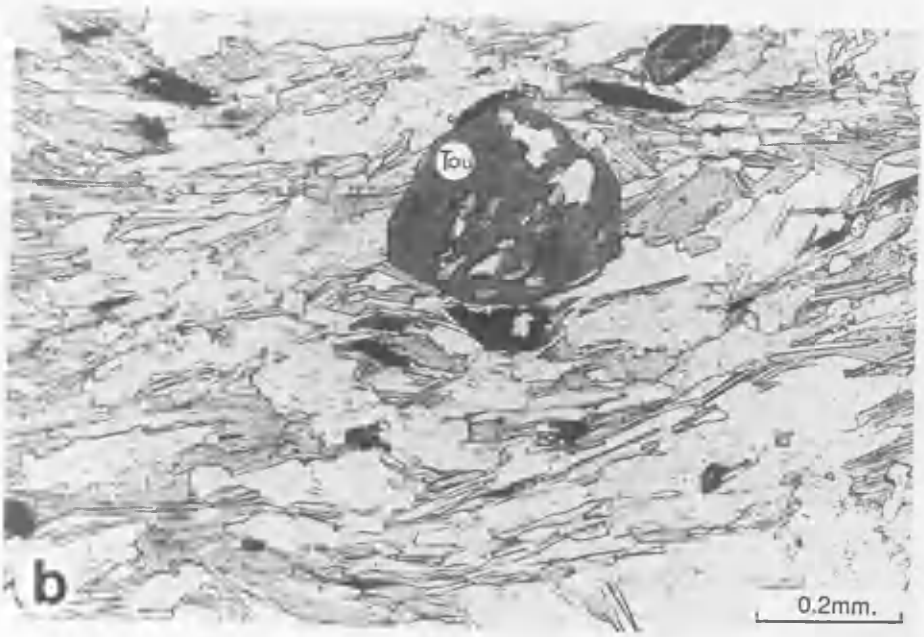
Tou
b
0.2mm.

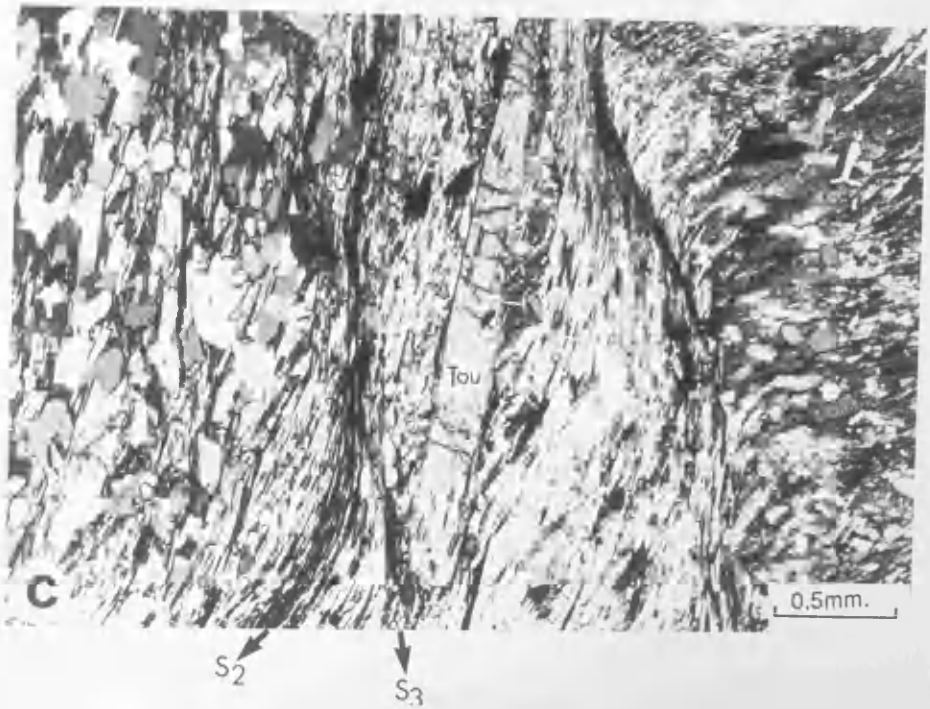
Tou
c
0.5mm.
S2
S3

PLATE 2.16 Hornblende growth; all microphotographs from sp. 9

(a) Se warped around a hornblende crystal with the development of pressure-shadow areas of quartz

(b) Lensoid-shaped hornblende porphyroblast with serrated boundaries; Se shows degrees of deflection and truncation.

(c) Hornblende and garnet porphyroblast (G_{2A}) showing comparable relationship to Se.

(d) Garnet partially included; enlargement of top centre of (c)

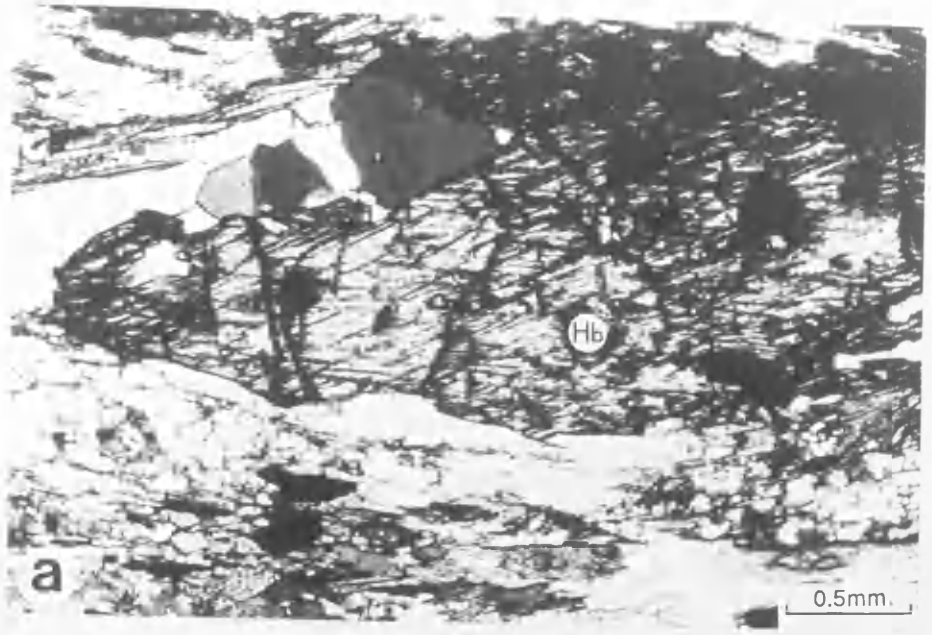
Hb
a
0.5mm.

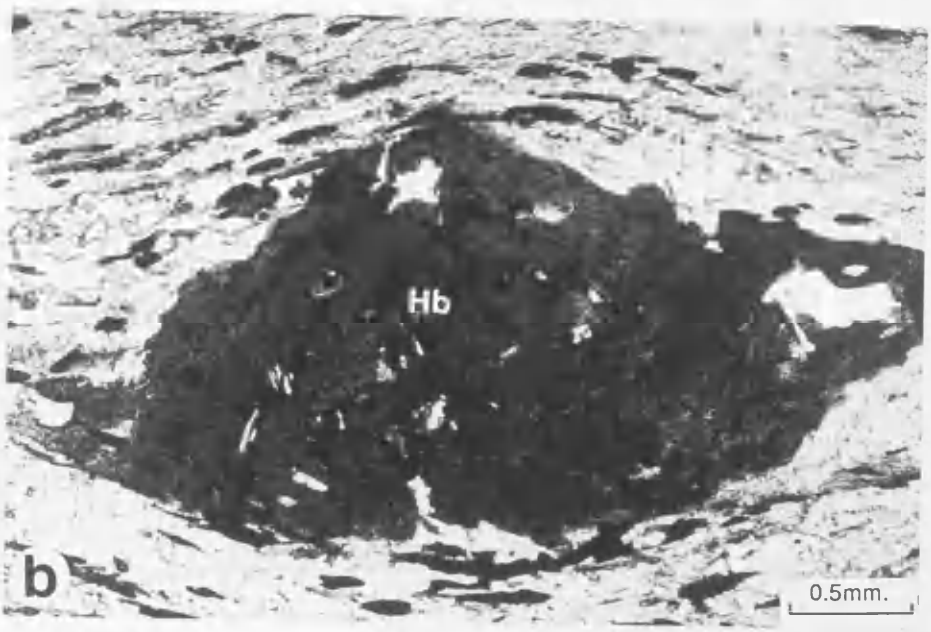
Hb
b
0.5mm.

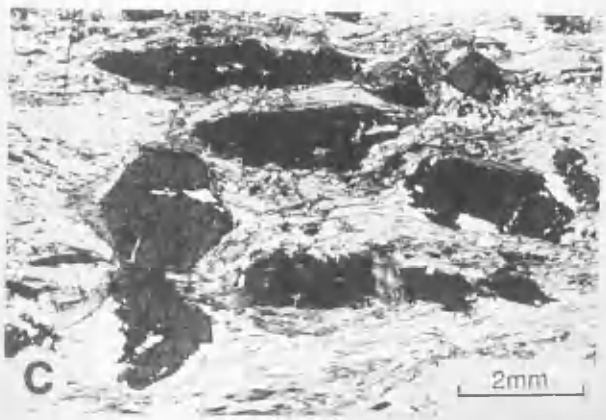
c
2mm


Gt
Hb
d
0.5mm.

CHAPTER 3

MINERAL CHEMISTRY

3.1 Introduction

Most of the lithologies at Balquhidder now consist of muscovite, chlorite, and quartz, together with garnet, biotite and albite. These minerals were variously developed during successive periods of mineral growth particularly syn-D_2, post-D_2 - pre-D_4 and D_4, that are referred to as M_2, M_{2-4} and M_4 metamorphic mineral growths respectively. D_1 (M_1), post-D_1 (M_{post-1}), D_3 (M_3) and post-D_4 (M_{post-4}) mineral growths, also took place. However each have only limited expression while the amount of post-D_2 - pre-D_4 mineral growth that corresponds to D_3 mineral growth cannot be assessed on the evidence available. Retrogressive metamorphism is seen with chlorite after garnet: the effects are shown by both M_2 and M_{2-4} garnets and they are presumed to represent a single, if extended, phase of retrogression after the second (M_{2-4}) garnet growth.

The chemical compositions of the various mineral phases have been determined using the electron microprobe. They are used (1) to investigate element distribution between co-existing mineral phases in very small volumes of rock, including at grain boundaries, as a basis of assessing the degree of attainment of chemical equilibrium and of the effect of any retrogression, (2) to determine possible garnet- and biotite-forming reactions, (3) to determine P-T conditions of metamorphic mineral growth, and (4) to establish other controls on mineral chemistry such as bulk rock composition and mineral assemblages.

In these investigations the following factors must be taken into account.

1. Due to the susceptibility of phyllosilicates to re-equilibration, their composition is likely to represent conditions operating during the last "phase" of metamorphism.

2. The products of retrogression represent disequilibrium.

3. There is a lack of even small measurable changes in the composition of albite.

4. Garnet compositions provide a record of progressive changes of conditions during its growth.

5. In many nearby outcrops the chemical distinction of a specific mineral phase in identical assemblages, the influence of T, P, P_{H2O}, P_{O2} etc. , (i.e. the conditions of metamorphism on the mineral chemistry), are best assessed when the influence of the bulk rock composition can be discounted. If the influence of the bulk composition of the rock on the mineral assemblages and the composition of the minerals can be specified, then the role of T, P, P_{H2O}, P_{02} etc., can more readily be identified.

3.2. Chlorite chemistry

3.2.1 Analytical data

Chemical analyses of chlorite are presented in Tables 3.1 and 3.2 which distinguish chlorite developed as the result of "prograde" reactions in the rock matrix (m) from those developed from garnet and biotite (r) by retrogression.

Generally each analysis is the average of about ten grains. The calculated structural formula considered only the Ti, Al, Fe, Mg and Mn in determining the number of the octahedral position occupied. The very small irregular "Ca" and "alkali" ions present in some chlorite analyses were neglected (Deer *et al.,* 1962, p.124; Foster, 1962). Because there is no reliable method of obtaining the wt. % of Fe_2O_3 from the probe analysis, this was estimated on the basis of formula normalized to 20 cation per 28 (0).

"Prograde" matrix chlorite

"Prograde" matrix chlorite is dealt with in relation to that which is present with garnets G_{2A}, G_{2B} and G_{2C} as these have been shown to represent different, but sequential, growth periods during D_2 - M_2 (Table 3.1a, b, c). The composition of matrix chlorite (m) in rocks containing G_{2-4} garnets is set out in Table 3.1e. In addition, analyses are given of chlorite present in

garnet-free rocks (Table 3.1d). Most of the chlorite forms part of the dominant S_2 fabric, i.e. texturally is M_2 chlorite. The exceptions are the chlorite at an F_4 fold hinge which probably represents M_2 - S_2 chlorite deformed by F_4 (Table 3.1c No. 22; see Plate 2.2b for the textural situation) and the pre-D_2 chlorite that possibly represents M_1 growth (Table 3.1d, No.29; see Plate 2.1a for the textural situation). Chlorite (M) that exhibits apparently different composition within the same thin section to be averaged, are set out separately (Table 3.1b, No.10).

Retrogressive chlorite

Compositional data for chlorite after G_{2A}, G_{2B}, G_{2C} are set out in Tables 3.2a, b, c, respectively, for chlorite after biotite in rocks containing G_{2A}, G_{2B}, G_{2C} and $G_{2\text{-}4}$ and in garnet-free rocks in Table 3.2d, and for chlorite after $G_{2\text{-}4}$ in Table 3.2e.

3.2.2 Data amplification

The analysed chlorite has oxide totals ranging from 83.62 to 89.99 (average 86.81 wt.%). The anhydrous cation totals, on the basis of 28(0) range from 19.19 (chlorite in G_{2C}-bearing lithologies) to 20.76 (chlorite in garnet-free lithologies) (average 19.86). These average cation totals are in good accord with the stoichiometric value of 20. The very small but variable proportions of K, Na and Ca are interpreted as representing phengite intergrowths and not part of the chlorite itself (Ernst, 1983). The very small proportions of Ti do not appear to show any systematic variation with bulk rock composition (see Table 1.2a) either in the matrix chlorite or the chlorite replacing garnet (or biotite). These data, together with the range of $[Si_{5.70}\ Al_{2.30}]$ to $[Si_{4.78}\ Al_{3.22}]$, are comparable to much other data for chlorite from similar and higher grade rocks (e.g. Atherton, 1968; Mather, 1970; Sivaprakash, 1979).

The following are the main compositional features of the "prograde" matrix chlorite (m) and the retrogressive chlorite (r):

Chlorite in garnet-bearing lithologies

Garnet phase	*Matrix (m)*	*After garnet (r)*
G_{2A} (Tables 3.1a; 3.2a)	repidolitic (1m, 2m, 3m, 6m, 8m, 9m)	repidolitic (1r, 2r, 6r, 8r, 9r)

G_{2B} (Tables 3.1b; 3.2b)	repidolitic (10m, 11m, 13m,)	repidolitic (10r, 11r, 13r)
G_{2C} (Tables 3.1c; 3.2c)	repidolitic to pseudothuringite (22m, 23m, 25m, & 24m)	repidolitic to pseudothuringite (22r, 23r, 25r, & 24r)
G_{2-4} (Tables 3.1e; 3.2e)	repidolitic (5r, 16r, 18r & 4r, 14r, 18r) 17m, 18m)	repidolitic to pseudothuringite (4m, 5m, 14m, 15m, 16m,

Chlorite in garnet-free lithologies

repidolitic (30m) transitional to pseudothuringite (29m) (Table 3.1d)

Chlorite after biotite (r)

repidolitic (9r, 10r, 23r, 15r, 30r) (Table 3.2d)

The other main feature is the absence of Mn in the matrix chlorite (m) and the retrogressive chlorite (r) in rocks containing the G_{2A} garnet phase.

The following features are significant in the interpretation of the compositional data of chlorite.

1. There is no simple compositional distinction in many analyses, either between chlorite that developed at different stages, or between the "prograde" chlorite and" retrograde" chlorite replacing garnet (and biotite); e.g. the pre-D_2 chlorite (m) is similar to chlorite (m) forming the S_2-fabric (Table 3.1d, m-29). Likewise chlorite (m) forming the S_2-fabric and that at F_4 crests are also similar (Table 3.1c, m-22). Therefore textural, not chemical distinction, is crucial for the recognition of the successive growth of chlorite in the "prograde" and "retrograde" conditions.,

2. The matrix chlorite (m) shows higher Mg/(Mg + Fe) than the chlorite replacing the garnets (r), e.g. m-1, m-2, m-6, m-8, m-9 and r-1, r-2, r-6, r-8, r-9 (Tables 3.1a, and 3.2a, respectively).

3. The Mg/(Mg + Fe) is generally higher in chlorite (r) that replaces G_{2A} than the chlorite (r) replacing G_{2B} and, or, G_{2C} garnet (Tables 3.2a, b, c).

4. Rocks with high MgO in the bulk composition have the highest Mg/(Mg + Fe) in the matrix chlorite (m),e.g. m-8, m-25, m-30.

5. A plot of matrix chlorite Mg/(Mg + Fe) against the modal percentages of biotite (Fig. 3.1) shows that the composition of the chlorite is certainly independent of the amount of modal biotite because rocks with widely varying amounts of biotite have chlorite with similar composition and Mg/(Mg + Fe).

3.2.3. **Discussion**

The best method of assessing the chemical data for the chlorites is to evaluate the chemical features in relation to the possible changes during the growth of the M_2 and M_{2-4} garnet porphyroblasts. The composition of prograde chlorite (m) is generally richer in Mg/(Mg + Fe) than the retrogressive chlorite (r) formed both from the garnet and biotite. However the (m) chlorite might represent a possible re-equilibration at least during either the two main prograde conditions or the subsequent retrogression. It is possible that the retrogression changed the composition of chlorite identified as being prograde on textural criteria to a composition stable under the retrograde conditions. However it is impossible to confirm or disprove this possibility so that the composition of the chlorite (m) during prograde mineral growth is uncertain. Perhaps the apparently wide range of the repidolitic compositional field (Hey, 1954) is not sufficiently critical to differentiate slight, but probably important, paragenetic trends. Thus the chlorites m-8 and m-3 (Table 3.1a), both from rocks of the Pitlochry Schist and both containing G_{2A}, each come within the repidolite group despite the considerable variations shown in MgO which can be correlated with variations in bulk rock composition.

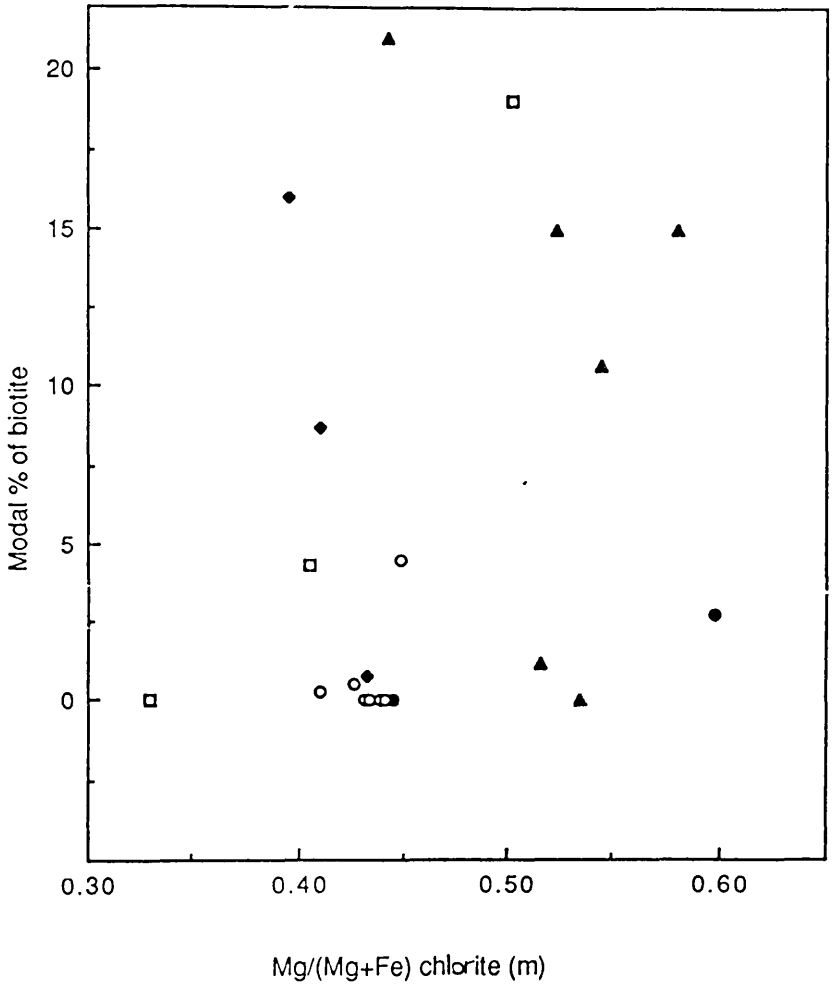

FIG. 3.1 Plot of Mg/(Mg+Fe) of the matrix chlorite (m) *vs.* modal % of biotite

▲ Rocks contain G_{2A}
♦ Rocks contain G_{2B}
□ Rocks contain G_{2C}
○ Rocks contain G_{2-4}
● Garnet-free rocks

TABLE 3.1a: **Chemical composition of matrix chlorite (m) in rocks containing G_{2A} garnet in the Pitlochry Schist** (see Fig.1.4 for specimen location).

Specimen No.	1	2	3	6	8	9
SiO_2	23.42	24.40	25.62	26.62	23.71	25.30	24.14
Al_2O_3	20.65	20.96	22.60	22.83	21.28	21.20	20.07
TiO_2	0.16	-	-	-	-	0.18	-
FeO	27.36	25.52	27.84	26.21	23.60	22.61	26.14
MgO	12.62	15.11	12.40	13.66	15.02	17.31	14.68
MnO	-	-	-	-	-	-	-
CaO	-		-	-	-	0.12	-
Na_2O	-	-	-	-	-	-	-
K_2O	-					0.13	-
TOTAL	84.45	85.98	88.46	88.40	83.62	86.85	85.02
Si	5.067	5.279	5.543	5.647	5.129	5.474	5.222
Al^{iv}	2.933	2.721	2.457	2.353	2.871	2.526	2.778
Al^{vi}	2.334	2.625	3.307	3.469	2.557	2.881	2.341
ΣAl	5.267	5.346	5.764	5.822	5.428	5.407	5.119
Ti	0.026	-	-	-	-	0.029	-
Mn	-	-	-	-	-	-	-
Mg	4.066	4.872	3.998	4.404	4.843	5.581	4.733
Fe^{2+}	4.844	4.438	5.037	4.742	4.227	4.049	4.446
Fe^{3+}	0.149	0.137	-	-	0.043	0.041	0.284
Mg/Mg+Fe	0.544	0.523	0.443	0.482	0.534	0.580	0.516
Σvi	19.419	20.072	20.340	20.620	19.670	20.581	19.805

TABLE 3.1b Chemical composition of matrix chlorite (m) in rocks containing G_{2B} garnet in the Ben Lui Schist

Specimen No.	10		11	13
SiO_2	27.59	24.26	24.19	23.88
Al_2O_3	23.79	21.82	21.64	20.44
TiO_2	0.15	-	-	-
FeO	26.02	29.17	31.10	28.39
MgO	10.16	12.00	11.32	12.17
MnO	0.17	-	-	-
CaO	0.11	-	-	-
Na_2O	-	-	-	-
K_2O	1.38	-	-	-
TOTAL	89.36	87.26	88.25	84.88
Si	5.701	5.251	5.233	5.166
Al^{iv}	2.299	2.749	2.767	2.834
Al^{vi}	3.495	2.818	2.753	2.379
ΣAl	5.794	5.567	5.520	5.213
Ti	0.023	-	-	-
Mn	0.029	-	-	-
Mg	3.127	3.869	3.650	3.924
Fe^{2+}	4.497	5.299	5.571	5.137
Fe^{3+}	-	-	0.056	-
Mg/Mg+Fe	0.410	0.442	0.396	0.433
Σvi	19.171	19.99	20.02	19.440

TABLE 3.1c Chemical composition of matrix chlorite (m) in rocks containing G_{2C} garnet in the Pitlochry Schist

Specimen No.	22		23	24	25
SiO_2	25.64	25.23*	24.21	22.79	24.07
Al_2O_3	21.09	20.16	21.10	21.39	20.52
TiO_2	-	-	-	-	-
FeO	27.13	27.47	31.43	33.16	26.19
MgO	14.46	14.38	11.51	9.34	13.96
MnO	0.37	0.42	0.34	-	0.48
CaO	-	-	-	-	0.10
Na_2O	-	-	-	-	-
K_2O	0.09	-	-	-	-
TOTAL	87.78	87.80	88.60	86.85	85.31
Si	5.331	5.392	5.238	4.930	5.207
Al^{iv}	2.669	2.608	2.762	3.070	2.793
Al^{vi}	2.710	2.469	2.619	2.386	2.441
ΣAl	5.379	5.007	5.381	5.456	5.234
Ti	-	-	-	-	-
Mn	0.068	0.076	0.062	-	0.088
Mg	4.662	4.579	3.711	2.902	4.501
Fe^{2+}	4.663	4.908	5.459	5.879	4.549
Fe^{3+}	0.245	-	0.228	0.120	0.189
$Mg/Mg+Fe^{2+}$	0.500	0.483	0.405	0.330	0.502
Σvi	20.350	20.030	20.080	19.290	19.768

*Chlorite at F4 crests

TABLE 3.1d Chemical composition of matrix chlorite (m) in garnet-free rocks in the Pitlochry Schist

Specimen No.	29		30
SiO_2	22.66*	22.75	25.35
Al_2O_3	20.78	20.98	21.32
TiO_2	-	-	-
FeO	29.98	29.51	22.45
MgO	12.11	11.59	17.80
MnO	-	-	0.20
CaO	-	-	-
Na_2O	-	-	-
K_2O	-	-	-
TOTAL	85.53	85.06	87.10
Si	4.902	4.922	5.484
Al^{iv}	3.098	3.078	2.516
Al^{vi}	2.202	2.273	2.922
ΣAl	5.300	5.351	5.425
Ti	-	-	-
Mn	-	-	0.037
Mg	3.905	3.737	5.739
Fe^{2+}	4.879	5.072	3.859
Fe^{3+}	0.542	0.267	0.203
$Mg/Mg+Fe^{2+}$	0.445	0.424	0.598
Σvi	19.530	19.350	20.76

*pre-D_2 chlorite

TABLE 3.1e Chemical composition of matrix chlorite (m) in rocks containing the M_{2-4} garnet, (4, 5) from the Pitlochry Schist and (14.-18) from the Ben Lui Schist.

Specimen. No.	4	5	14	15	16	17	18
SiO_2	23.72	23.52	23.77	24.02	24.13	24.31	23.39
Al_2O_3	21.03	22.04	21.61	22.75	22.01	20.90	22.00
TiO_2	-	-	-	-	-	-	-
FeO	29.53	30.99	29.93	30.61	29.63	28.47	29.30
MgO	12.33	11.49	12.26	12.53	12.25	12.76	12.58
MnO	0.16	0.24	-	-	-	0.15	-
CaO	-	-	-	-	-	-	-
Na_2O	-	-	-	-	-	-	-
K_2O	-	-	0.10	-	-	-	-
TOTAL	86.77	88.30	87.66	89.88	88.02	86.60	87.78
Si	5.132	5.088	5.142	5.196	5.220	5.259	5.168
Al^{iv}	2.868	2.912	2.858	2.804	2.779	2.741	2.832
Alvi	2.496	2.709	2.654	2.993	2.835	2.587	2.779
ΣAl	5.364	5.621	5.512	5.797	5.614	5.328	5.611
Ti	-	-	-	-	-	-	-
Mn	0.029	0.044	-	-	-	0.027	-
Mg	3.975	3.705	3.953	4.039	3.950	4.114	4.056
Fe^{2+}	5.076	5.327	5.199	5.261	5.308	5.048	5.142
Fe^{3+}	0.267	0.280	0.217	0.280	0.054	0.103	0.159
$Mg/Mg+Fe^{2+}$	0.439	0.410	0.432	0.434	0.427	0.449	0.441
Σvi	19.843	20.065	20.023	20.573	20.147	19.879	20.136

TABLE 3.2a Chemical composition of chlorite (r) replacing G_{2A} garnet in Pitlochry Schist - *cf.*Table 3.1a

Specimen No.	1	2 * r_1G	r_2G	6	8	9 * r_1G	r_2G
SiO_2	23.40	24.72	24.09	23.89	24.07	24.08	23.60
Al_2O_3	21.10	21.16	21.33	21.10	20.95	20.72	21.46
TiO_2	-	-	0.25	-	-	-	-
FeO	27.60	26.65	26.06	27.40	23.98	27.19	26.34
MgO	12.61	13.48	14.80	13.57	16.16	13.80	13.79
MnO	-	-	-	-	-	-	-
CaO	-	0.12	-	-	-	-	-
Na_2O	-	-	0.32	-	-	-	-
K_2O	-	-	-	-	-	0.10	-
TOTAL	84.71	86.41	86.84	86.30	85.16	85.89	85.19
Si	5.062	5.348	5.211	5.168	5.207	5.209	5.107
Al^{iv}	2.938	2.652	2.788	2.832	2.793	2.791	2.894
Al^{vi}	2.444	2.745	2.652	2.549	2.550	2.494	2.579
ΣAl	5.382	5.397	5.440	5.382	5.343	5.285	5.473
Ti	-	-	0.041	-	-	-	-
Mn	-	-	-	-	-	-	-
Mg	4.066	4.346	4.772	4.375	5.210	4.449	4.446
Fe^{2+}	4.894	4.822	4.526	4.761	4.035	4.723	4.623
Fe^{3+}	0.099	-	0.189	0.198	0.304	0.197	0.130
$Mg/Mg+Fe^{2+}$	0.454	0.474	0.513	0.479	0.564	0.485	0.490
Σvi	19.503	19.913	20.180	19.883	20.100	19.863	19.778

* r_1G, r_2G chlorite composition of the same grain close and away from the garnet contact, respectively.

TABLE 3.2b Chemical composition of chlorite (r) replacing the G_{2B} garnet in Ben Lui Schist. *cf.* Table 3.1b

Specimen No.	10	11	13
SiO_2	24.24	23.60	23.15
Al_2O_3	21.89	21.60	21.45
TiO2	-	-	-
FeO	29.45	29.77	29.96
MgO	12.69	11.85	11.23
MnO	0.20	0.22	-
CaO	-	-	-
Na_2O	-	-	-
K_2O	-	0.12	-
TOTAL	88.47	87.40	85.78
Si	5.244	5.106	5.008
Al^{iv}	2.756	2.894	2.992
Al^{vi}	2.827	2.615	2.479
ΣAl	5.583	5.509	5.471
Ti	-	-	-
Mn	0.037	0.041	-
Mg	4.091	3.821	3.621
Fe^{2+}	5.169	5.225	5.312
Fe^{3+}	0.160	0.162	0.108
$Mg/Mg+Fe^{2+}$	0.442	0.422	0.405
Σvi	20.280	19.860	19.520

TABLE 3.2c Chemical composition of chlorite (r) replacing G_{2C} garnet in Pitlochry Schist - *cf.* Table 3.2c

Specimen No.	23	24	25
SiO_2	24.25	22.10	23.90
Al_2O_3	21.82	21.10	20.73
TiO_3	-	-	-
FeO	31.70	33.36	27.33
MgO	12.10	9.10	14.33
MnO	-	0.33	0.45
CaO	-	-	-
Na_2O	-	-	-
K_2O	-	-	-
TOTAL	89.82	85.88	86.75
Si	5.246	4.781	5.171
Al^{iv}	2.754	3.219	2.829
Al^{vi}	2.811	2.163	2.458
ΣAl	5.565	5.382	5.287
Ti	-	-	-
Mn	-	0.060	0.082
Mg	3.901	2.934	4.620
Fe^{2+}	5.449	5.613	4.499
Fe^{3+}	0.287	0.423	0.445
$Mg/Mg/Fe^{2+}$	0.417	0.343	0.507
Σvi	20.450	19.190	20.104

TABLE 3.2d Chemical composition of chlorite after biotite

Spec. No.	9 G_{2A}-bearing Pitlochry Schist	10 G_{2B}-bearing Ben-Lui Schist	23 G_{2C}-bearing Pitlochry Schist	15 G_{2-4}-bearing Ben Lui Schist	30 Garnet-free Pitlochry Schist
SiO_2	24.37	23.97	24.50	24.49	25.62
Al_2O_3	20.60	22.15	20.97	23.35	20.64
TiO_2	0.17	-	-	-	-
FeO	25.50	29.16	30.91	29.85	22.04
MgO	14.79	12.70	11.10	11.77	17.50
MnO	-	-	0.37	-	0.30
CaO	-	-	-	-	-
Na_2O	-	-	-	-	-
K_2O	-	-	0.09	-	-
TOTAL	85.42	87.98	87.88	89.85	86.04
Si	5.272	5.186	5.300	5.298	5.543
Al^{iv}	2.728	2.814	2.700	2.702	2.457
Al^{vi}	2.526	2.834	2.649	3.253	2.807
ΣAl	5.254	5.648	5.348	5.955	5.264
Ti	0.028	-	-	-	-
Mn	-	-	0.066	-	0.055
Mg	4.769	4.095	3.579	3.795	5.642
Fe^{2+}	4.522	5.118	5.593	5.401	3.948
Fe^{3+}	0.092	0.158	-	-	0.040
$Mg/Mg+Fe^{2+}$	0.513	0.444	0.390	0.413	0.588
Σvi	19.937	20.21	19.890	20.449	20.49

TABLE 3.2e Chemical composition of chlorite (r) replacing the post-D_2 - pre-D_4 garnet; lithologies as in Table 3.1e.

Specimen No.	4	5		14	16		18	
		r_1G	r_2G		r_1G	r_2G	r_1G	r_2G
SiO_2	23.07	24.62	23.82	23.00	24.00	23.98	23.00	23.32
Al_2O_3	21.01	21.86	22.29	21.97	21.72	22.04	21.38	21.38
TiO_2	-	-	-	0.21	-	-	-	0.17
FeO	29.78	31.81	30.95	30.05	29.85	30.28	29.03	28.80
MgO	11.78	10.16	11.33	11.99	12.35	11.94	12.23	12.08
MnO	0.27	0.37	0.18	-	0.31	-	0.20	-
CaO	-	0.42	-	-	-	-	0.12	-
Na_2O	-	-	-	-	-	-	-	-
K_2O	0.11	-	0.11	-	-	-	-	-
TOTAL	86.03	89.26	88.67	87.23	88.23	88.25	85.96	85.76
Si^{iv}	4.991	5.326	5.153	4.976	5.192	5.188	4.976	5.045
Al^{iv}	3.009	2.674	2.847	3.024	2.808	2.812	3.024	2.955
Al^{vi}	2.349	2.901	2.838	2.579	2.732	2.809	2.428	2.498
ΣAl	5.358	5.575	5.685	5.603	5.540	5.621	5.452	5.453
Ti	-	-	-	0.034	-	-	-	0.028
Mn	0.049	0.068	0.033	-	0.057	-	0.037	-
Mg	3.798	3.276	3.653	3.866	3.982	3.849	3.943	3.895
Fe^{2+}	5.065	5.755	5.488	5.056	5.185	5.369	4.937	5.107
Fe^{3+}	0.323	-	0.112	0.381	0.216	0.109	0.315	0.104
$Mg/Mg/Fe^{2+}$	0.429	0.363	0.400	0.433	0.434	0.418	0.399	0.433
Σvi	19.584	20.00	20.124	19.916	20.172	20.172	19.66	19.632

3.3 Muscovite chemistry

3.3.1 Analytical data

As with chlorite, the chemical data for muscovite are grouped into muscovites co-existing with garnets G_{2A}, G_{2B}, G_{2C} and G_{2-4} (Tables 3.3a, b, c and e, respectively) and those in garnet-free rocks (Table 3.3d). Apart from one pre-D_2 muscovite (Table 3.3c, No.29; see Plate 2.1a for textural situation) and the S_4-muscovite undeformed at F_4 crests (Table 3.3e, No.16; 3.3d, No.22; see Plates 2.11d, 2.2b for textural situation) the analyses are of M_2 muscovite either matrix (m) or porphyroblasts(p)(see Plate 2.1c for textural situation). The different muscovite compositions within the same thin section are set out separately. The few muscovite flakes that occur in the garnet pressure shadow areas (R.G), particularly of the M_2 garnet porphyroblasts, are analysed to check if there are distinct compositional features.

The anhydrous totals are in the range 94% - which is low for a mica. The consistent occurrence of graphite in most specimens (Table 1.2a), and the scarcity of hematite and magnetite, supports the assumption that the iron is divalent (Ernst, 1963). The following are the main significant compositional features of the analysed muscovites.

1. Phengite compositions are usual with Si : Al^{iv}, being greater than 3 : 1 (Foster, 1956; Deer *et al.*,1962).

2. They are strictly dioctahedral micas, with cation totals varying from 13.92 to 14.03 and averaging 13.99 on the basis of 22 (0).

3. The paragonite (i.e. Na) content varies for grains in one thin section and is not linked to the bulk Na_2O of the rock (Table 1.2a; Fig. 3.2).

4. The K-content also varies for grains in the same thin section and is not linked to the bulk K_2O of the rock (Table 1.2a; Fig. 3.3).

5. The Ti-contents are generally fairly uniform.

6. There is no apparent relationship between SiO_2 and, or, Al_2O_3 in the rock composition and the phengite content. There is an antipathetic relationship between Al^{iv} and $\Sigma Mg + Fe$.

7. The octahedral occupancy is always greater than 4 per formula unit. This excess of the octahedral cation over the theoretical is a common feature in most phengitic muscovite and the overall composition is similar to typical metamorphic phengite in similar metamorphic grade. (e.g. Brown, 1967; Cipriani *et al.* ,1971; Guidotti and Sassi, 1976; Fletcher and Greenwood, 1979).

8. Although there is some chemical variation within single thin sections there is no distinct composition for each phase of muscovite, e.g. pre-D_2 muscovite is the same as the S_2 (Table 3.3d, No.,29) and post-D_4 muscovite (Table 3.3d, No.22). Also there is no simple difference between the matrix muscovite (m), plasts (p) in the same section, and flakes that occur in the pressure-shadow areas around the M_2 garnets.

3.3.2 **Discussion**

It is generally recognized that muscovite is a good petrogenetic indictor mineral which can reflect conditions and expresses variables during metamorphism. Many studies have demonstrated the effect of T, P including P_{H_2O}, and bulk rock composition on muscovite composition (Cipriani *et al.*, 1971; Guidotti and Sassi, 1976; Guidotti, 1978). Such studies have thrown light on the elucidation of these variables in metamorphic terranes.

However the present muscovite composition is the product of polyphase re-equilibration (see Section 2.3), especially during the two major periods of garnet growth, (D_2-(M_2) and post-D_2 - pre-D_4 (M_{2-4})). In addition, it represents the final re-equilibration during the subsequent retrogressive conditions. The possibility of all such variables being concomitant is far from rare. The similar relative heterogeneity of the muscovite composition within the same thin section has previously been interpreted as due to the co-existence of more than one distinct muscovite composition in a single rock (e.g. Crawford, 1965), or to a continuous range of muscovite composition (Brown, 1967) due to the ion exchange between muscovite crystals and intergranular fluid and not the consequence of a sequence of discontinuous reactions. The muscovite "equilibrium" composition presumably occurred during peak temperature when possibly, after the retrogression, both equilibrations occurred in a single rock, mainly

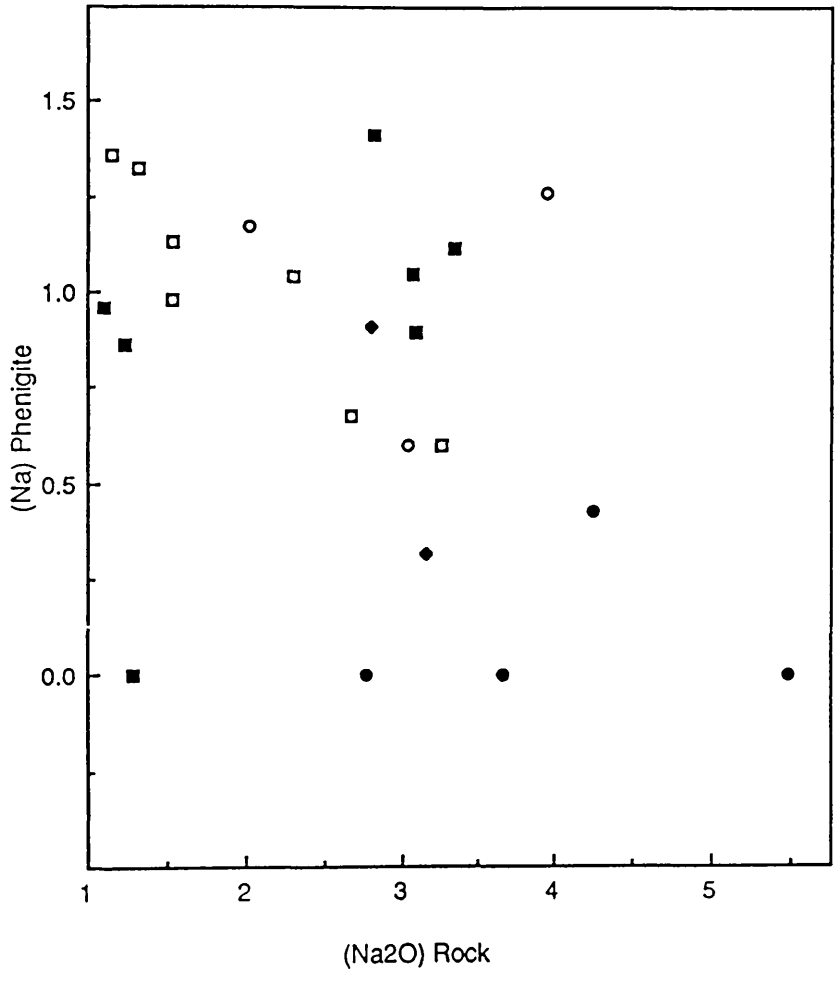

FIG. 3.2 Plot of (Na) phengite *vs.* (Na_2O) in the bulk rock

■ Rocks contain G_{2A}
○ Rocks contain G_{2B}
● Rocks contain G_{2C}
□ Rocks contain G_{2-4}
♦ Garnet-free rocks

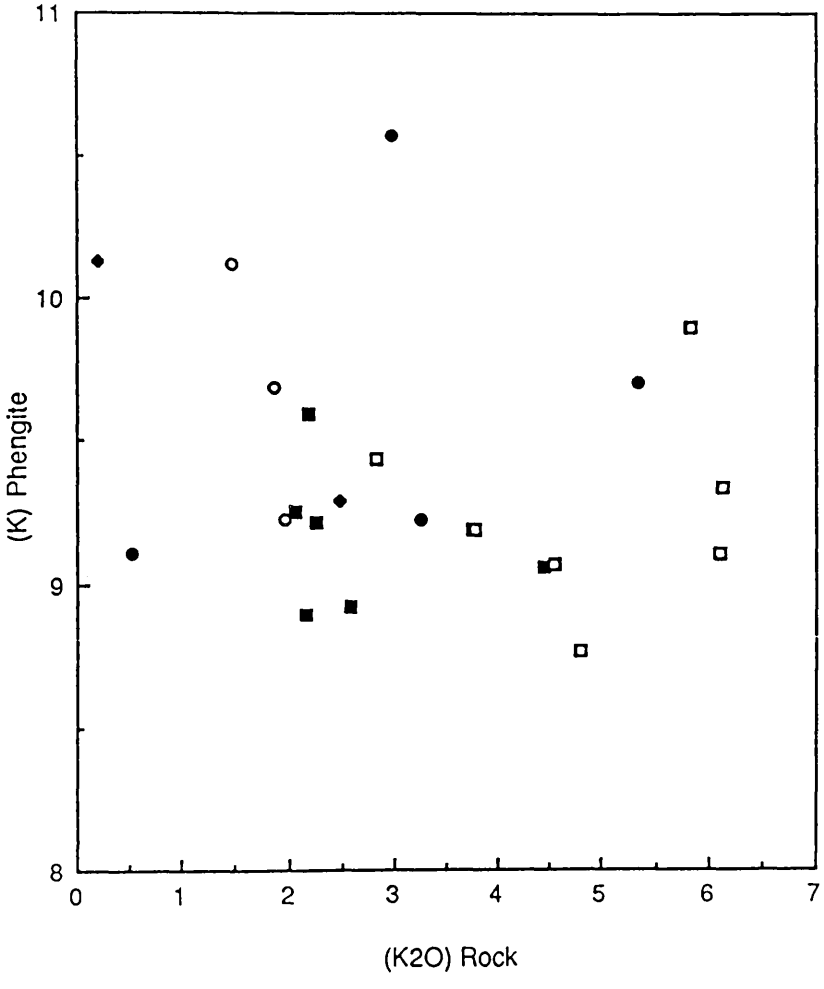

FIG. 3.3 Plot of (K) phengite *vs.* (K_2O) in the bulk rock

■ Rocks contain G_{2A}
○ Rocks contain G_{2B}
● Rocks contain G_{2C}
□ Rocks contain G_{2-4}
♦ Garnet-free rocks

TABLE 3.3a Muscovite composition in rocks containing G_{2A} garnet porphyroblast in Pitlochry Schist

	1				2		
	M	M	R.G.*	R.G.*	M	P	P
SiO_2	44.36	45.10	45.52	45.00	45.19	44.91	46.66
TiO_2	0.27	0.27	0.43	0.29	0.73	0.71	0.46
AL_2O_3	32.70	31.45	33.89	30.30	31.95	31.46	32.32
FeO	1.90	2.27	2.07	2.48	1.56	1.94	1.80
MgO	0.63	1.27	1.43	1.61	1.58	0.99	1.75
CaO	-	-	-	-	-	-	0.15
K_2O	9.06	9.65	9.65	9.56	8.93	9.54	9.42
Na_2O	1.05	0.51	0.59	0.54	1.41	0.54	1.10
TOTAL	90.14	90.82	93.57	89.79	91.34	90.10	93.65
Si^{iv}	6.238	6.315	6.174	6.383	6.265	6.323	6.317
Al^{iv}	1.762	1.685	1.826	1.617	1.735	1.677	1.683
Al^{vi}	3.660	3.506	3.593	3.449	3.486	3.546	3.475
Ti	0.029	0.060	0.043	0.031	0.076	0.075	0.047
Fe^{2+}	0.224	0.266	0.235	0.294	0.180	0.229	0.202
Mg	0.132	0.264	0.290	0.340	0.327	0.210	0.354
Σvi	4.045	4.096	4.161	4.114	4.069	4.060	4.078
K	1.625	1.724	1.670	1.729	1.579	1.713	1.627
Na	0.287	0.138	0.155	0.149	0.378	0.147	0.290
K+Na	1.912	1.862	1.825	1.878	1.957	1.860	1.917
Fe+Mg	0.356	0.530	0.525	0.634	0.507	0.439	0.556
ΣAl	5.422	5.191	5.419	5.066	5.221	5.223	5.158
Mg/Mg+Fe	0.371	0.498	0.552	0.536	0.645	0.478	0.637
Na/Na+K	15.01	7.41	8.49	7.93	19.32	7.90	15.13

Table explanation:
- (M) matrix, (P) porphyroblastic muscovite both forming the S2 matrix, except if stated otherwise.
- * R.G. represents muscovite composition in contact with garnet and, or, in garnet pressure shadow areas.

Cell contents calculated to 22 (0)

TABLE 3.3a (contd)

	3	6		7		
	M	M	P	M	M	R.G.*
SiO_2	43.97	46.40	45.18	45.92	45.14	45.62
TiO_2	0.50	0.81	0.80	0.79	0.65	0.57
Al_2O_3	31.33	31.95	32.33	32.47	32.69	32.00
FeO	4.50	1.85	1.71	1.82	1.61	1.60
MgO	1.37	1.61	1.35	1.30	1.33	1.25
CaO	-	-	-	-	-	-
K2O	9.60	9.26	9.00	9.22	9.38	9.57
Na_2O	-	0.96	1.39	0.86	1.28	1.00
TOTAL	91.26	92.85	91.77	92.38	92.10	91.63
Si^{iv}	6.200	6.329	6.240	6.289	6.222	6.313
Al^{iv}	1.800	1.671	1.760	1.711	1.778	1.687
Al^{vi}	3.409	3.466	3.505	3.532	3.534	3.535
Ti	0.053	0.083	0.084	0.081	0.067	0.059
Fe^{2+}	0.530	0.211	0.197	0.208	0.185	0.186
Mg	0.287	0.327	0.277	0.266	0.272	0.258
Σvi	4.279	4.087	4.063	4.087	4.058	4.038
K	1.728	1.612	1.587	1.610	1.650	1.690
Na	-	0.255	0.373	0.228	0.342	0.268
K+Na	1.728	1.867	1.960	1.838	1.992	1.958
Fe+Mg	0.817	0.538	0.474	0.474	0.457	0.444
ΣAl	5.209	5.137	5.265	5.243	5.312	5.222
Mg/Mg+Fe	0.351	0.608	0.584	0.561	0.595	0.582
Na/Na+K	-	13.66	19.03	12.40	17.17	13.69

TABLE 3.3a contd...

	8			9	
	M	M	P	M	M	P
SiO_2	46.69	46.11	46.28	44.03	45.37	45.42
TiO_2	0.72	0.62	0.60	0.37	0.57	0.52
Al_2O_3	32.28	33.74	32.64	32.48	30.99	30.56
FeO	1.72	1.34	1.68	2.96	3.16	3.39
MgO	1.65	1.68	1.72	0.69	1.34	0.97
CaO	0.13	-	-	-	-	-
K_2O	8.90	8.75	8.78	9.19	9.64	9.52
Na_2O	0.90	1.60	1.04	1.12	0.91	1.02
TOTAL	92.98	93.84	92.93	90.83	91.98	91.26
Si^{iv}	6.336	6.202	6.294	6.190	6.315	6.367
Al^{iv}	1.664	1.798	1.706	1.810	1.685	1.633
Al^{vi}	3.500	3.552	3.528	3.573	3.399	3.417
Ti	0.074	0.062	0.061	0.039	0.059	0.055
Fe^{2+}	0.196	0.151	0.191	0.348	0.368	0.397
Mg	0.333	0.337	0.349	0.144	0.278	0.202
Σvi	4.103	4.102	4.129	4.104	4.104	4.071
K	1.541	1.501	1.523	1.647	1.712	1.651
Na	0.234	0.418	0.275	0.306	0.245	0.277
K+Na	1.775	1.919	1.798	1.953	1.557	1.928
Fe+Mg	0.529	0.488	0.540	0.492	0.646	0.599
ΣAl	5.164	3.350	5.234	5.383	5.084	5.050
Mg/Mg+Fe	0.629	0.691	0.646	0.293	0.430	0.337
Na/Na+K	13.18	21.78	15.29	15.67	12.52	14.37

TABLE 3.3b **Muscovite composition in rocks containing G_{2B} garnet all specimens are in Ben Lui Schist.**

	10		11		13	
	M	M	M	M	M	M
SiO_2	46.08	46.72	45.26	45.81	45.84	44.02
TiO_2	0.46	0.43	0.69	0.59	0.55	0.36
Al_2O_3	34.22	32.77	31.15	32.51	33.58	34.35
FeO	2.48	2.42	3.28	3.21	1.48	1.58
MgO	1.24	1.80	1.75	1.32	1.12	0.75
CaO	-	-	-	-	-	-
K_2O	9.69	10.46	10.12	10.57	9.23	9.11
Na_2O	1.26	0.82	0.60	0.46	1.17	1.21
TOTAL	95.32	95.40	92.86	94.48	92.97	91.39
Si^{iv}	6.163	6.260	6.261	6.227	6.231	6.100
Al^{iv}	1.837	1.740	1.739	1.773	1.769	1.900
Al^{vi}	3.540	3.436	3.341	3.437	3.613	3.712
Ti	0.046	0.043	0.072	0.060	0.056	0.038
Fe^{2+}	0.277	0.271	0.379	0.365	0.169	0.183
Mg	0.248	0.359	0.360	0.268	0.227	0.154
Σvi	4.111	4.109	4.152	4.130	4.070	4.087
K	1.653	1.787	1.787	1.832	1.602	1.611
Na	0.327	0.213	0.162	0.122	0.309	0.326
K+Na	1.980	2.000	1.949	1.954	1.911	1.938
Fe+Mg	0.525	0.630	0.739	0.633	0.396	0.337
ΣAl	5.377	5.176	5.080	5.210	5.382	5.612
Mg/Mg+Fe	0.472	0.570	0.487	0.423	0.573	0.567
Na/Na+K	16.52	10.65	8.31	6.24	16.17	16.82

TABLE 3.3c **Muscovite composition in rocks contraining G_{2C} garnet, Pitlochry Schist.**

	2 4 M
SiO_2	43.99
TiO_2	0.47
Al_2O_3	31.80
FeO	1.97
MgO	0.66
CaO	-
K_2O	9.71
Na_2O	0.43
TOTAL	89.02
Si^{iv}	6.278
Al^{iv}	1.722
Al^{vi}	3.629
Ti	0.050
Fe^{2+}	0.235
Mg	0.140
Σvi	4.054
K	1.767
Na	0.118
K+Na	1.885
Fe+Mg	0.375
ΣAl	5.351
Mg/Mg+Fe	0.373
Na/Na+K	6.26

TABLE 3.3d **Muscovite composition in garnet-free lithologies, Pitlochry Schist.**

	22			29	
	M	M-F4	pre-D2	M	M
SiO_2	45.70	46.89	44.93	44.46	44.95
TiO_2	0.60	0.74	0.41	0.47	0.44
Al_2O_3	31.63	32.07	30.15	30.86	31.52
FeO	1.65	1.70	2.75	2.60	2.45
MgO	1.50	1.51	1.68	1.57	1.49
CaO	-	-	0.13	-	0.13
K_2O	9.29	9.37	10.35	9.99	10.13
Na_2O	0.91	0.98	-	0.32	0.79
TOTAL	91.29	93.26	90.40	90.29	91.91
Si^{iv}	6.337	6.360	6.363	6.294	6.261
Al^{iv}	1.663	1.640	1.637	1.706	1.739
Al^{vi}	3.508	3.488	3.397	3.307	3.437
Ti	0.063	0.075	0.043	0.051	0.046
Fe^{2+}	0.192	0.193	0.325	0.308	0.285
Mg	0.309	0.305	0.355	0.332	0.310
Σvi	4.072	4.061	4.120	3.998	4.078
K	1.644	1.622	1.869	1.805	1.801
Na	0.244	0.258	-	0.089	0.213
K+Na	1.888	1.880	1.869	1.894	2.014
Fe+Mg	0.501	0.498	0.680	0.640	0.595
ΣAl	5.171	5.128	5.034	5.150	5.176
Mg/Mg+Fe	0.617	0.612	0.522	0.519	0.521
Na/Na+K	12.92	13.72	-	4.70	10.58

TABLE 3.3e Muscovite composition in G_{2-4} garnet bearing lithologies in Pitlochry Schist (4,5) and Ben Lui Schist (14-18)

	4		5			14		15
	M	M	M	R.G.	P	P	M	M
SiO_2	45.73	46.51	46.38	42.75	45.71	45.11	45.27	46.77
TiO_2	0.32	0.58	0.33	0.42	0.33	0.24	0.31	0.32
Al_2O_3	31.90	34.04	31.97	32.02	34.12	34.05	32.15	34.52
FeO	2.41	2.56	2.98	5.11	1.90	2.29	2.38	1.89
MgO	1.40	1.05	1.24	1.00	0.60	0.42	1.00	0.97
CaO	-	-	-	-	-	-	-	-
K_2O	9.19	8.77	9.34	8.65	9.32	8.99	9.48	9.11
Na_2O	0.60	1.04	0.80	0.99	1.32	1.29	1.00	1.13
TOTAL	91.54	94.54	93.04	90.94	93.30	92.38	91.59	94.71
Si^{iv}	6.332	6.810	6.343	6.068	6.209	6.190	6.289	6.236
Al^{iv}	1.668	1.190	1.657	1.932	1.791	1.810	1.711	1.764
Al^{vi}	3.540	4.690	3.498	3.427	3.672	3.699	3.554	3.661
Ti	0.034	0.063	0.034	0.044	0.034	0.025	0.032	0.032
Fe^{2+}	0.279	0.314	0.341	0.606	0.216	0.263	0.276	0.211
Mg	0.288	0.229	0.253	0.213	0.120	0.085	0.207	0.193
Σvi	4.141	5.30	4.126	4.290	4.042	4.072	4.069	4.097
K	1.623	0.819	1.629	1.567	1.615	1.574	1.680	1.549
Na	0.159	0.148	0.212	0.271	0.348	0.343	0.272	0.292
K+Na	1.682	0.967	1.841	1.838	1.963	1.917	1.952	1.541
Fe+Mg	0.567	0.543	0.594	0.819	0.336	0.348	0.483	0.404
ΣAl	5.208	5.880	5.155	5.359	5.463	5.509	5.265	5.425
Mg/Mg+Fe	0.508	0.422	0.426	0.260	0.357	0.244	0.429	0.478
Na/Na+K	9.45	15.31	11.52	14.74	17.70	17.89	13.93	15.04

TABLE 3.3e contd

	16 M	16 P	M-S4	17 M	P	18 M	M
SiO_2	46.43	46.89	45.23	45.30	45.42	45.46	45.19
TiO_2	0.50	0.48	0.33	0.53	0.30	0.47	0.34
Al_2O_3	33.60	32.36	32.10	31.10	33.10	32.51	33.61
FeO	2.16	2.25	2.30	2.90	2.18	1.90	1.67
MgO	1.30	1.63	1.10	1.84	0.85	1.09	0.91
CaO	-	0.13	-	-	-	-	-
K_2O	9.90	10.00	9.36	9.44	9.07	9.14	9.19
Na_2O	0.98	0.73	1.12	0.86	1.36	1.24	1.03
TOTAL	94.81	94.46	91.49	91.94	92.25	91.80	91.92
Si^{iv}	6.230	6.318	6.287	6.293	6.247	6.275	6.217
Al^{iv}	1.770	1.682	1.713	1.707	1.753	1.725	1.783
Alvi	3.542	3.459	3.547	3.381	3.608	3.567	3.668
Ti	0.047	0.049	0.035	0.055	0.031	0.049	0.035
Fe^{2+}	0.243	0.253	0.268	0.339	0.251	0.217	0.192
Mg	0.260	0.327	0.218	0.380	0.174	0.224	0.186
Σvi	4.092	4.088	4.068	4.155	4.064	4.057	4.081
K	1.695	1.720	1.661	1.673	1.591	1.610	1.613
Na	0.259	0.190	0.302	0.230	0.363	0.332	0.274
K+Na	1.949	1.910	1.962	1.903	1.954	1.942	1.887
Fe+Mg	0.503	0.580	0.486	0.719	0.425	0.441	0.378
ΣAl	5.312	5.141	5.260	5.088	5.361	5.292	5.451
Mg/Mg+Fe	0.517	0.564	0.449	0.529	0.409	0.508	0.492
Na/Na+K	13.03	9.95	15.39	12.09	18.58	17.10	14.52

controlled by the stability field of "phengite", P-T conditions and P_{H_2O}, operating within the different lithologies (Velde, 1965b, p.909). In addition other mineral-forming reactions that may involve muscovite as a reactant, with increasing temperature, e.g. garnet and, or, biotite, may be the reason for the present muscovite compositional features, i.e. decreases the celadonite-content, or affects the paragonite content (Section 3.5.5 and 3.6.2).

The muscovite in rocks containing the G_{2A} garnet, for instance, is generally of uniform celadonitic-content despite significant differences in temperature as calculated from garnet-biotite e.g. $T_1 < T_2 < T_8$ (Table 3.3a, Nos 1, 2, 8 and Chapter 4 for temperature estimates) and the fact that lower celadonitic content would occur at higher temperatures.

The main control of muscovite composition was, however, probably temperature, as rock composition does not generally seem to be important.

3.4. **The coexisting phengite and chlorite**

Element distributions between co-existing minerals is controlled by the element distribution coefficient K_D which itself is influenced by temperature and pressure. The chemistry of the system and the degree of attainment of chemical equilibrium are also important (Phinney, 1963; Brown, 1967; Greenwood, 1967; Saxena, 1969, 1973; Ernst, 1983).

As the co-existence of phengite and chlorite is widespread, this pair offers the possibility of determining the degree of attainment of equilibrium. The chemical compositions of each mineral pair, which texturally co-exist within S_2, are established in relation to the presence of garnets G_{2A}, G_{2B}, G_{2C}, G_{2-4} (Table 3.4a, b, c, e) or garnet-absent assemblages (Table 3.4d).

The following expression (Rao, 1977) is used for the K_D of Mg between the coexisting phengite-chlorite-(as this is the dominant composition of the muscovite) pairs (Table 3.4f):

$$K_{Dmg} = \frac{X_{mg}}{1 - X^{ph}_{mg}} \Big/ \frac{X_{mg}}{1 - X^{chl}_{mg}}$$

where Xmg = Mg/Y where Y is the total cations. A plot of $K_D^{ph\text{-}chl}$ versus X^{ph} (Fig. 3.4) exhibits regular sympathetic variation between K_D which increases with the increase of X^{ph} in phengite.

Tie-line pattern between the coexisting phengite-chlorite

Tie-lines joining pairs of coexisting minerals are used to infer equilibrium conditions and check the effect of bulk composition and, or, grade on the equilibrium conditions during metamorphism.

The attitude of the tie lines of the phengite-chlorite pairs in rocks containing the M_2 garnets, i.e. G_{2A}, G_{2B}, G_{2C}, and in garnet-free rocks is shown in Figure 3.5a, while the pairs in rocks containing the $M_{2\text{-}4}$ garnets are shown in Figure 3.5b. In both figures the three co-ordinates represented are: S = Si, A= Al, and F= Fe^{2+} + Mg (atomic proportions) of the analysed pairs. In Figure 3.5a the tie-lines of the mineral pairs in rocks containing the G_{2A} (1,2,3,6,8,9) all show parallelism. On the other hand the tie-lines of the pairs in rocks containing G_{2B}, G_{2C}, as well as in garnet-free rocks (13, 24, 29, respectively), show tie-lines that cross each other and the tie-lines in rocks containing G_{2A}. The parallel tie-lines of the phengite-chlorite pairs in rocks containing the G_{2A} suggests the attainment of equilibrium with slight variations due to experimental error and bulk compositional changes (Saxena, 1969). However the crossing of the tie-lines of the pairs in G2A-bearing rocks with those with G_{2B} and G_{2C}, or in garnet-free rocks, and also the variation in rocks with $G_{2\text{-}4}$ garnet suggests that the pairs had equilibrated under varying P-T conditions in the different assemblages (Greenwood *et al.*, 1964), or possibly μH_2O : μCO_2 variation (Butler, 1969). This is consistent with the deductions that (1) the G_{2A}, G_{2B} and G_{2C} assemblages represent different growth periods during D_2 - M_2,

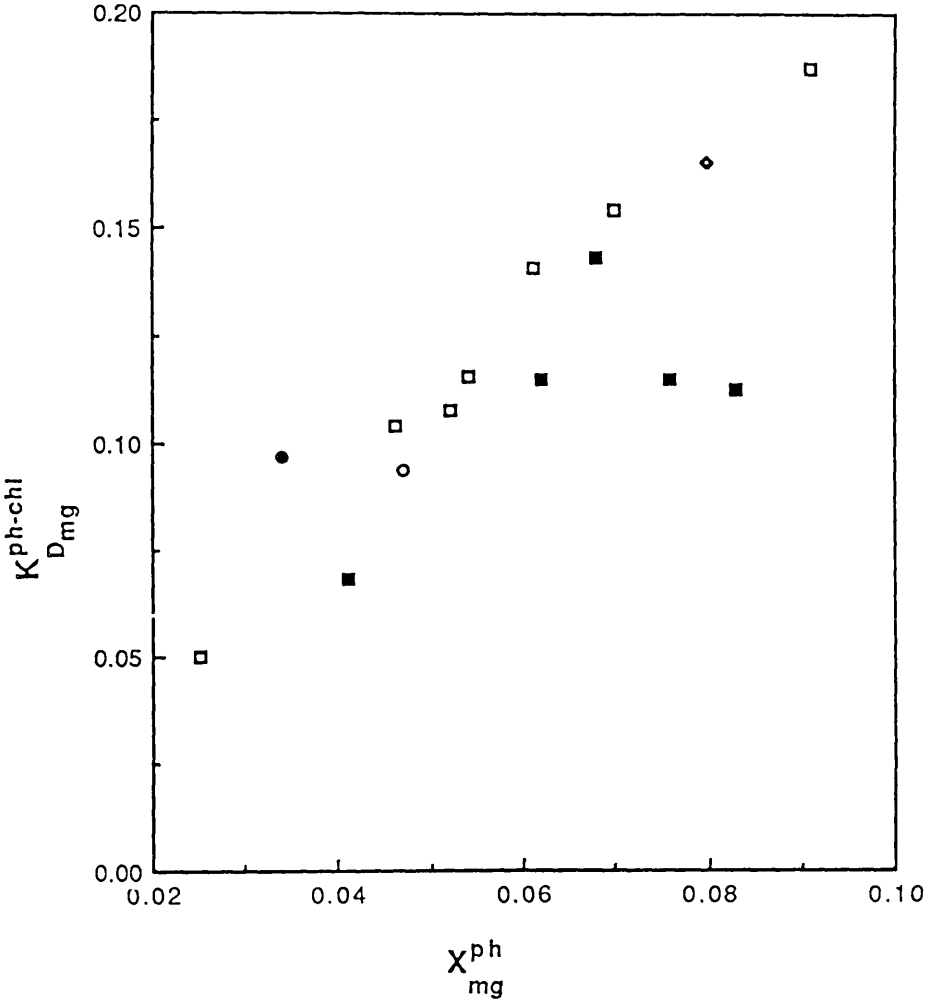

FIG.3.4 Plot of $K^{ph\text{-}chl}_{Dmg}$ *vs* X^{ph}_{mg}

■ Rocks contain G_{2A}
○ Rocks contain G_{2B}
● Rocks contain G_{2C}
□ Rocks contain $G_{2\text{-}4}$
♦ Garnet-free rocks

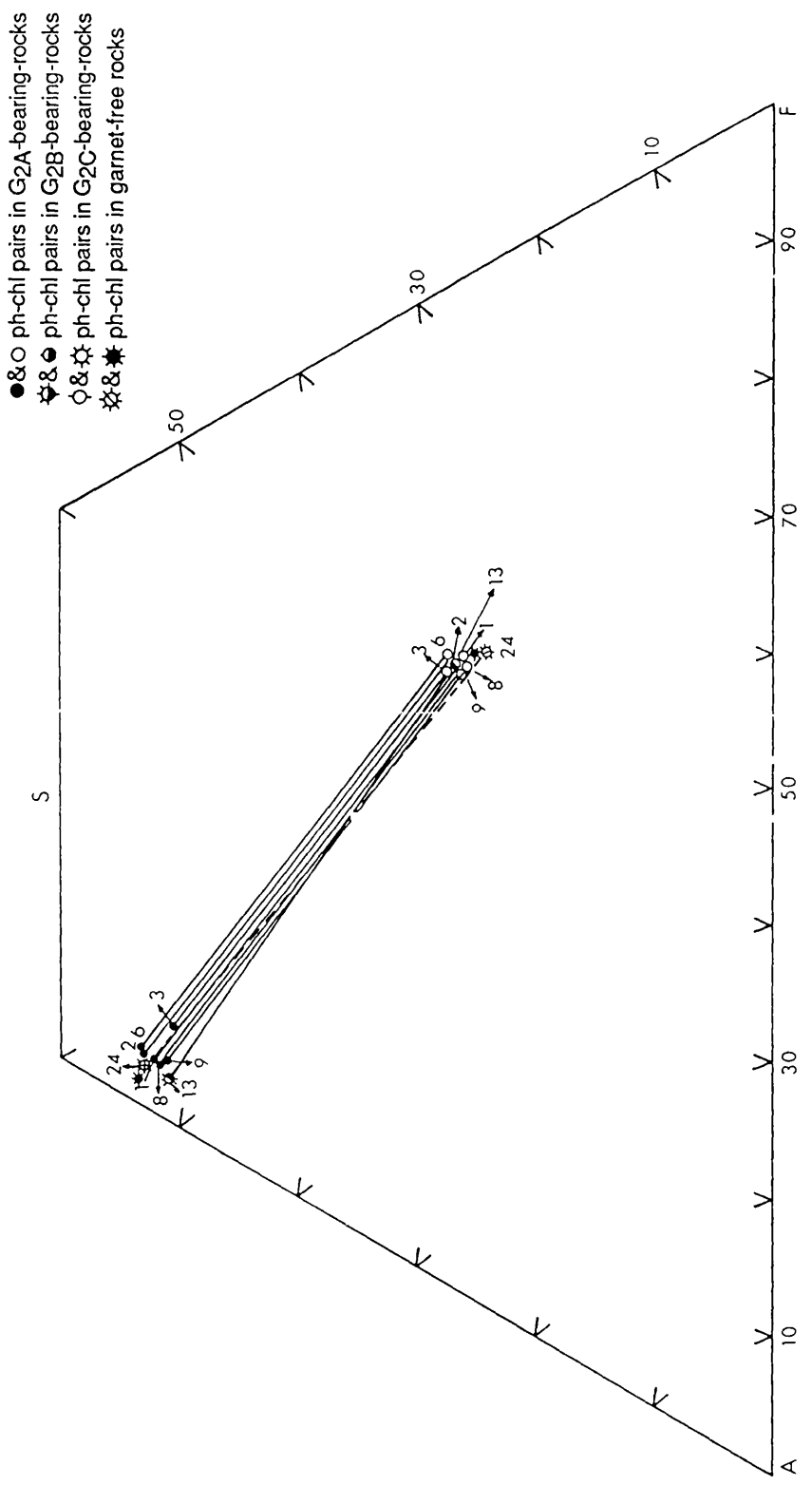

FIG. 3.5a Tie-line pattern of the co-existing phengite-chlorite pairs in rocks containing G_{2A}, G_{2B}, G_{2C} and in garnet-free rocks

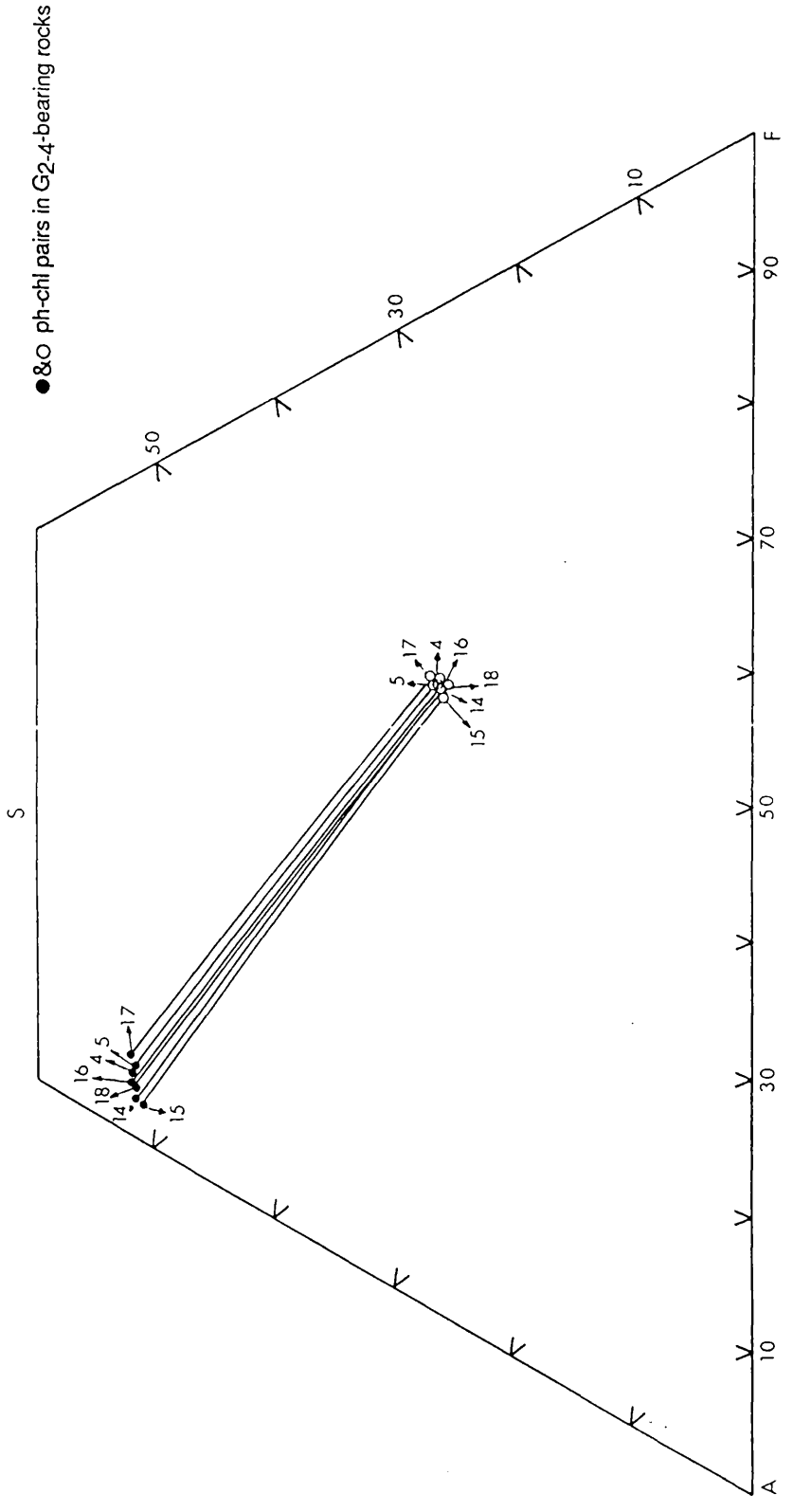

FIG. 3.5b Tie-line pattern of the co-existing phengite-chlorite pairs in rocks containing $G_{2\text{-}4}$ garnets

TABLE 3.4a Composition of the phengite-chlorite pairs coexisting in G_{2A} garnet-bearing Pitlochry Schist

	1		2		3	
	chl	ph	chl	ph	chl	ph
SiO_2	23.41	44.73	24.72	45.05	25.86	43.97
TiO_2	0.08	0.42	-	0.72	-	0.50
Al_2O_3	20.88	32.08	21.16	31.71	22.72	31.33
FeO	27.48	2.09	26.65	1.75	27.03	4.50
MgO	12.62	0.95	13.48	1.29	13.03	1.37
MnO	-	0.09	-	-	-	-
CaO	-	-	0.12	-	-	-
Na_2O	-	0.78	-	0.98	-	-
K_2O	-	9.36	-	9.24	-	9.60
TOTAL	84.58	90.48	86.41	90.72	88.64	91.27
Si^{iv}	5.07	6.28	5.35	6.49	5.60	6.200
Al^{iv}	2.94	1.72	2.65	1.51	2.40	1.800
Al^{vi}	2.38	3.59	2.75	3.72	3.39	3.409
Ti	0.02	0.04	-	0.14	-	0.053
Fe^{2+}	4.87	0.25	4.82	0.20	4.89	0.530
Mn	-	0.01	-	-	-	-
Mg	4.07	0.198	4.35	0.27	4.20	0.287
Ca	-	-	0.02	-	-	-
Na	-	0.21	-	0.26	-	-
K	-	1.69	-	1.65	-	1.728
Σvi	11.34	4.09	11.94	4.33	12.48	4.279
ΣAl	5.32	5.31	5.40	5.23	5.79	5.209

Cell content for phengite calculated to 22(0) and for chlorite to 28(0)

TABLE 3.4a Contd...

	6		8		9	
	chl	ph	chl	ph	chl	ph
SiO_2	23.71	45.96	25.30	46.40	24.14	44.45
TiO_2	-	0.64	0.18	0.67	-	0.46
Al_2O_3	21.28	31.66	21.20	33.01	20.07	31.81
FeO	23.60	1.73	22.61	1.53	26.14	3.21
MgO	15.02	1.50	17.31	1.67	14.68	0.82
MnO	-	-	-	-	-	0.08
CaO	-	-	0.12	0.07	-	-
Na_2O	-	0.90	-	1.25	-	1.19
K_2O	-	9.26	0.13	8.83	-	9.16
TOTAL	83.62	91.64	86.85	93.41	85.02	91.18
Si^{iv}	5.13	6.35	5.47	6.27	5.20	6.24
Al^{iv}	2.87	1.65	2.53	1.73	2.80	1.77
Al^{vi}	2.56	3.50	2.88	3.53	2.45	3.49
Ti	-	0.07	0.03	0.07	-	0.05
Fe^{2+}	4.23	0.20	4.05	0.17	4.63	0.38
Mn	-	-	-	-	-	0.01
Mg	4.84	0.308	5.58	0.34	4.46	0.17
Ca	-	-	0.01	0.01	-	-
Na	-	0.24	-	0.33	-	0.32
K	-	1.63	-	1.52	-	1.64
Σvi	11.63	4.08	12.55	4.12	11.54	4.10
ΣAl	5.43	5.15	5.41	5.26	5.25	5.26

TABLE 3.4b Ph - chl pairs in G2B garnet-bearing Ben Lui Schist

	13	
	chl	ph
SiO_2	23.88	44.93
TiO_2	-	0.46
Al_2O_3	20.44	34.07
FeO	28.39	1.53
MgO	12.17	0.94
MnO	-	-
CaO	-	-
N_2O	-	1.46
K_2O	-	9.17
TOTAL	84.88	92.18
Si^{iv}	5.17	6.17
Al^{iv}	2.83	1.83
Al^{vi}	2.38	3.67
Ti	-	0.04
Fe^{2+}	5.14	0.18
Mn	-	-
Mg	3.92	0.19
Ca	-	-
Na	-	0.32
K	-	1.61
Σvi	11.44	4.08
ΣAl	5.21	5.50

TABLE 3.4c Ph-chl pairs in G_{2C} garnet-bearing Pitlochry Schist

	24	
	chl	ph
SiO_2	22.45	43.99
TiO_2	-	0.47
Al_2O_3	21.25	31.80
FeO	33.26	1.97
MgO	9.22	0.66
MnO	0.17	-
CaO	-	-
Na_2O	-	0.43
K_2O	-	9.71
TOTAL	86.35	89.02
Si^{iv}	4.86	6.28
Al^{iv}	3.15	1.72
Al^{vi}	2.27	3.63
Ti	-	0.05
Fe^{2+}	5.75	0.24
Mn	0.03	-
Mg	2.92	0.14
Ca	-	-
Na	-	0.12
K	-	1.77
Σvi	10.97	4.06
ΣAl	5.42	5.36

TABLE 3.4d Ph-chl pairs in garnet-free Pitlochry Schist

	29	
	chl	ph
SiO_2	22.71	44.46
TiO_2	-	0.47
Al_2O_3	20.88	30.86
FeO	29.75	2.60
MgO	11.85	1.57
MnO	0.12	-
CaO	-	-
Na_2O	-	0.32
K_2O	-	9.99
TOTAL	85.31	90.29
Si^{iv}	4.91	6.29
Al^{iv}	3.09	1.71
Al^{vi}	2.23	3.44
Ti	-	0.05
Fe^{2+}	4.98	0.30
Mn	0.03	-
Mg	3.82	0.33
Ca	-	-
Na	-	0.09
K	-	1.81
Σvi	11.06	4.12
ΣAl	5.32	5.25

TABLE 3.4e Ph-chl pairs with the post-D2 - pre-D4 garnet-bearing samples, 4 and 5 are in Pitlochry Schists, 14-18 in Ben Lui Schist

	4		5		14		15	
	chl	ph	chl	ph	chl	ph	chl	ph
SiO_2	23.76	45.73	23.52	46.38	23.64	45.41	24.26	46.77
TiO_2	-	0.32	-	0.33	-	0.29	-	0.32
Al_2O_3	21.24	31.90	22.04	31.97	21.28	34.09	23.04	34.52
FeO	30.30	2.41	30.99	2.98	29.54	2.10	30.23	1.90
MgO	11.87	1.40	11.49	1.24	12.03	0.51	12.15	0.97
MnO	0.22	-	0.24	-	-	-	-	-
CaO	-	-	-	-	-	-	-	-
Na_2O	-	0.60	-	0.80	-	1.31	-	1.13
K_2O	-	0.19	-	9.34	0.05	9.16	0.20	9.11
TOTAL	87.38	91.54	88.30	93.04	86.63	92.84	89.87	94.71
Si^{iv}	5.14	6.33	5.08	6.34	5.11	6.20	5.25	6.24
Al^{iv}	2.86	1.67	2.92	1.66	2.89	1.80	2.76	1.76
Al^{vi}	2.56	3.54	2.70	3.50	2.59	3.69	3.11	3.67
Ti	-	0.03	-	0.03	-	0.03	-	0.03
Fe^{2+}	5.24	0.28	5.33	0.34	5.05	0.24	5.33	0.21
Mn	0.04	-	0.04	-	-	-	-	-
Mg	3.83	0.29	3.71	0.25	3.88	0.10	3.92	0.19
Ca	-	-	-	-	-	-	-	-
Na	-	0.16	-	0.21	-	0.35	-	0.29
K	-	1.62	-	1.63	0.01	1.59	0.11	1.54
Σvi	11.67	4.14	11.78	4.12	11.52	4.06	12.36	4.10
ΣAl	5.42	5.21	5.62	5.16	5.48	5.49	5.87	5.43

TABLE 3.4e Contd...

	16		17		18	
	chl	ph	chl	ph	chl	ph
SiO_2	24.19	45.66	23.31	45.30	23.32	45.32
TiO_2	-	0.41	-	0.53	0.17	0.41
Al_2O_3	21.77	32.78	20.90	31.06	21.38	33.06
FeO	29.52	2.17	28.47	2.91	28.80	1.78
MgO	12.28	1.09	12.76	1.84	12.08	1.00
MnO	-	-	0.15	-	-	-
CaO	-	-	-	-	-	-
Na_2O	-	0.93	-	0.86	-	1.14
K_2O	-	9.59	-	9.44	-	9.17
TOTAL	87.81	92.63	86.60	91.94	85.75	91.88
Si^{iv}	5.23	6.27	5.30	6.29	5.05	6.25
Al^{iv}	2.77	1.73	2.70	1.71	2.95	1.75
Al^{vi}	2.78	3.57	2.63	3.38	2.50	3.62
Ti	-	0.04	-	0.06	0.03	0.04
Fe2+	5.27	0.25	5.05	0.34	5.11	0.20
Mn	-	-	0.03	-	-	-
Mg	3.96	0.22	4.14	0.38	3.89	0.21
Ca	-	-	-	-	-	-
Na	-	0.25	-	0.23	-	0.30
K	-	1.68	-	1.67	-	1.61
Σvi	12.01	4.08	11.85	4.16	11.53	4.07
ΣAl	5.55	5.30	5.33	5.09	5.45	5.37

TABLE 3.4f X_{mg} for phengite (ph) - chlorite (chl) pairs, the distribution coefficient (K_D), and $X_{mg}/1-X_{mg}$ of each phase (from the analysis presented in Table 3.4a-e).

Sp.No.	X^{ph}	X^{chl}	K^{ph-chl}	$X_{mg}/1-X^{chl}$	$X_{mg}/1-X^{ph}$
1	0.049	0.359	0.92	0.560	0.052
2	0.062	0.363	0.115	0.573	0.066
3	0.068	0.337	0.143	0.508	0.073
6	0.076	0.416	0.115	0.713	0.082
8	0.083	0.445	0.113	0.801	0.091
9	0.041	0.386	0.068	0.629	0.043
13	0.047	0.343	0.094	0.522	0.049
24	0.034	0.266	0.097	0.362	0.035
29	0.080	0.345	0.165	0.527	0.087
4	0.070	0.328	0.154	0.488	0.075
5	0.061	0.315	0.141	0.460	0.065
14	0.025	0.337	0.050	0.508	0.026
15	0.046	0.317	0.104	0.464	0.048
17	0.091	0.349	0.187	0.536	0.100
18	0.052	0.337	0.108	0.509	0.035

with G_{2B} and G_{2C} developed at lower temperatures than G_{2A} and (2) the G_{2-4} growth was at a different time and also developed at lower temperatures than G_{2A}. Similar tie-line variations, i.e. showing varying inclination without cross-cutting relationships have been interpreted as due to varying grain sizes of the mineral pairs in the different lithologies (McNamara, 1965). However, lack of equilibrium is probably the reason for tie-line crossing. The relationship between $K_{D_{mg}}^{ph\text{-}chl}$ and X_{mg}^{ph} (Fig.3.4) suggests that in any individual rock Mg/(Mg + Fe) has exchanged by the mineral pairs had their own distribution coefficient, and their unique P-T dependence within their bulk compositional characteristics.

3.5 Compositional variations of garnets

3.5.1 Introduction

The multi-garnet growth sequence established in Chapter 2, suggests that more than one garnet composition may occur. In order to ensure that the garnet chemical characteristics obtained on the microprobe were representative, and minimise the cut effects, the following procedures were adopted: (1) the analysed garnets were those in which clear age relationships based on textures, were observed (2) the largest grains that showed good crystal faces were chosen, (3) the probe traverses attempted to cross the centre of the crystals and some reconnaisance probing assisted in identifying the centres based on chemical variation, and (4) in specimens where garnets were irregular (e.g. skeletal garnets), or those with abundant quartz inclusions, a sufficient number of scattered analyses were carried out to check for zoning and to spot the representative centre and rim composition, which were usually taken for the highest and lowest MnO content, respectively. The analytical results are given in Table 3.5a, b, c and d including the composition of garnet rims that shows textural replacement by chlorite for both M_2 and M_{2-4} garnets.

3.5.2 Compositional zonation in garnets

Both the D_2 garnets and the post-D_2 - pre-D_4 garnets are chemically zoned. MnO and CaO decreases from the centre towards the rim while FeO and

MgO show increase. This type of variation in garnet composition is commonly reported in almandine-rich garnet composition in the Dalradian Supergroup and from other metamorphic terranes (Atherton, 1968; Tracy *et al.*, 1976; Sivaprakash, 1981; Dempster, 1985). Such zonation is commonly referred to as "normal" and is a primary and intrinsic feature of the garnet growth mechanism under low and medium grade conditions.

All the garnets are almandine-rich (typically 63-74%) with grossular as the second largest constituent (typically 25-15%) Spessartine is typically 10-2%, but in the G_{2C} and G_{2-4} garnets the spessartine is higher, being 19-13% and 18-3% respectively . Pyrope in all garnets is typically 3-10%.

The core and rim compositions are plotted on a Mn-Ca-(Fe^{2+} + Mg) diagram, (Figs 3.6a, b). This shows that both M_2 and M_{2-4} garnets plot in the common field for garnet in metamorphic pelites (Müller and Schneider, 1971).

Numerous explanations have been proposed to account for the origin of the "normal" compositional zonation in garnet.

1. The fractionation (or segregation) of certain elements of the matrix during garnet growth, leads to the preferential depletion of some elements in the rock as they become incorporated into the growing garnet (Hollister, 1966; Atherton, 1968).

2. The growth of garnet during prograde metamorphism (Harte and Henley, 1966).

3. Exchange between initial homogeneous garnet and matrix minerals, i.e. post-crystallization diffusion (Anderson and Buckley, 1973).

4. The growth was produced by continuous and discontinuous reactions (Tracy *et al.*, 1976; Crawford, 1977; Trzcienski, 1977).

5. Changing oxygen fugacities with changing P-T conditions, i.e. by influencing the activity of the divalent iron (Müller and Schneider, 1971; Tewhey and Hess, 1976).

6. Combination and, or variations of the above models (McAteer, 1976; Finlay and Kerr, 1979).

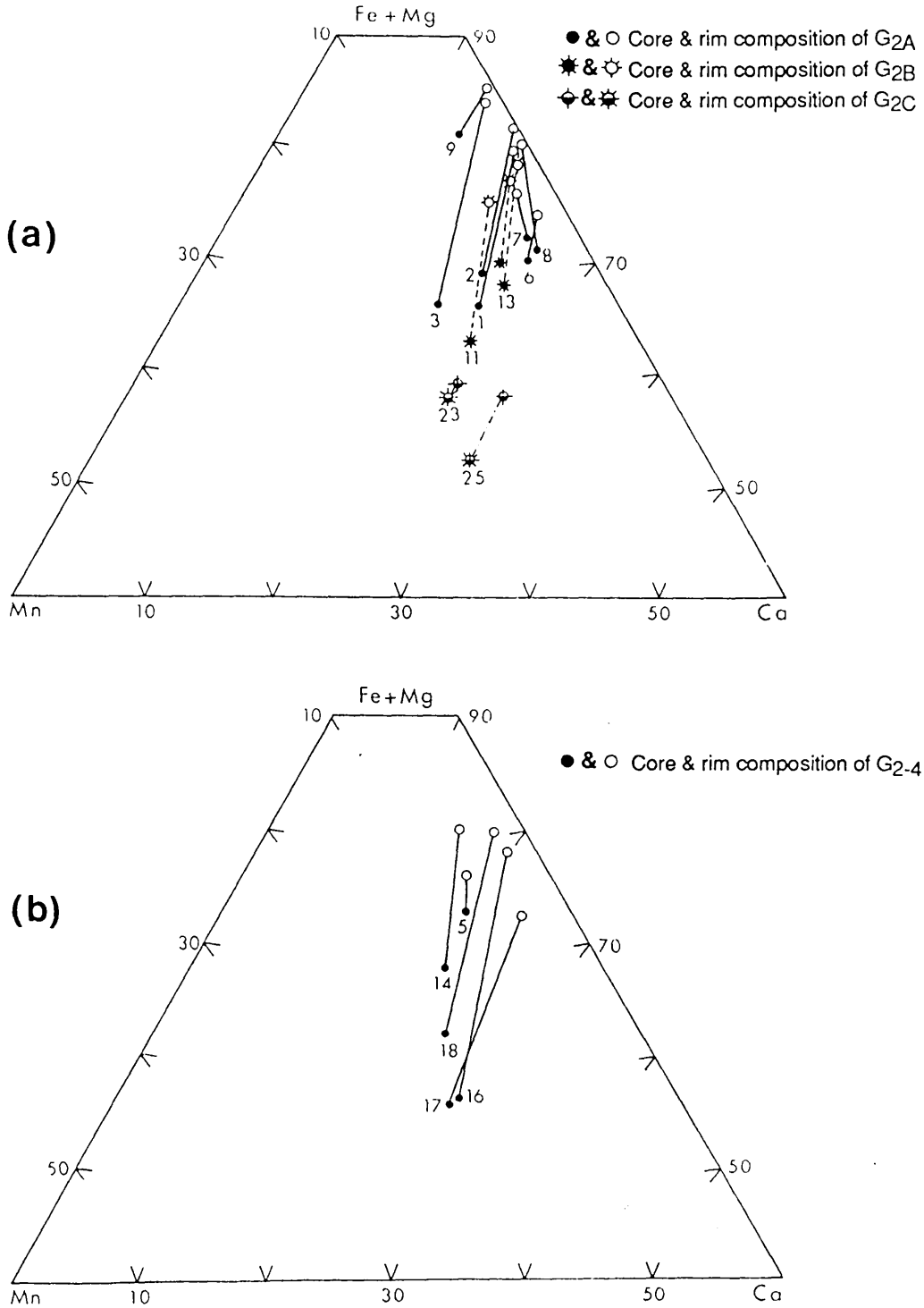

FIG. 3.6 Core and rim compositional ranges of the analysed (a) M_2 garnets, (b) M_{2-4} garnets

The depletion model, which is based on Rayleigh fractionation as proposed by Hollister (1966) is the most probable explanation of the MnO profiles. The model essentially postulates that the fractionation factor (λ), (where λ = MnO% in garnet/MnO% in the rock) is high implying that Mn is preferentially partitioned into garnet compared with its entry into other minerals. The Mn zoning therefore is the result of the progressive depletion of Mn from the surrounding rock. The model is thought to be less applicable to the CaO variation (Hollister, 1966): if the model applies to Mn then it must be at least influenced by other ionic variations. Both the depletion (Hollister, 1966) and the segregation (Atherton, 1968) models assume that diffusion in the garnet is negligible while diffusion in the surrounding matrix has to be faster to maintain homogeneity. Only the thin outer layer of the garnet could be in equilibrium with the rest of the matrix. The basic assumption in Hollister's model is that the fractionation factor is considered constant at fixed P-T conditions but that will only be correct at very low Mn concentration in both the reservoir and the garnet. λ Should change with changing temperature and pressure and may be able to give an indicator of these variables, although the growth of garnet probably took place over a range of P-T conditions (Tracy, 1982).

Trzcienski (1977) suggested that the zoning in garnet does not require a constant temperature, or a changing fractionation factor, but it occurs by the continuous and, or, discontinuous reaction over a given range of temperature. The zoned garnet developed while its surface composition was controlled by multivariant equilibrium with one or more reactant. This model is generally referred to as the "reaction partitioning" model (Tracy, 1982). This model indicates that the formation of garnet and the amount of zoning depends in part on the initial Fe/Fe+Mn of the host rock and, unlike the fractionation model, the MnO was not treated as a minor component (see 3.5.6, page 118).

Much of the present garnet analytical data are interpreted essentially on the basis of theTrzcienski (1977) model.

TABLE 3.5a Chemical analysis of G2A garnet porphyroblasts

	1			2			3		6	
	C	R	Rr	C	R	Rr	C	R	C	R
SiO_2	36.33	36.42	36.52	36.96	37.53	37.47	36.20	36.75	37.13	37.02
Al_2O_3	20.68	20.44	20.66	21.10	21.43	20.91	20.93	21.23	21.10	21.23
TiO_2	0.18	0.15	-	0.28	-	-	0.21	-	0.32	0.20
FeO	29.44	34.34	32.99	29.58	32.31	33.11	29.39	35.38	31.21	32.10
MgO	0.82	1.50	1.27	1.28	2.81	2.53	0.94	1.85	0.86	1.19
MnO	4.84	0.67	0.81	3.97	-	0.17	6.24	0.71	2.30	1.23
CaO	8.26	6.87	7.58	8.14	7.13	6.31	7.20	5.19	8.98	8.49
TOTAL	100.55	100.40	99.83	101.31	101.21	100.50	100.74	101.11	101.82	101.47
Si	5.880	5.902	5.927	5.898	5.933	5.984	5.869	5.898	5.906	5.898
Al^{iv}	0.120	0.098	0.073	0.102	0.067	0.016	0.131	0.102	0.094	0.1020
Al^{vi}	3.825	3.807	3.880	3.869	3.927	3.921	3.798	3.915	3.848	3.886
Ti	0.022	0.018	-	0.034	-	-	0.025	-	0.038	0.024
Fe	3.985	4.654	4.478	3.948	4.272	4.422	3.984	4.748	4.152	4.277
Mg	0.197	0.361	0.308	0.304	0.662	0.602	0.227	0.443	0.204	0.282
Mn	0.664	0.092	0.112	0.537	-	0.023	0.856	0.097	0.310	0.166
Ca	1.432	1.193	1.318	1.392	1.208	1.081	1.250	0.892	1.530	1.449
SUM	16.125	16.125	16.096	16.084	16.069	16.049	16.140	16.095	16.082	16.084
ΣFe+Mg+ Mn+Ca	6.278	6.300	6.216	6.181	6.142	6.128	6.317	6.18	6.196	6.174
Alm	63.48	73.87	72.04	63.87	69.55	72.16	63.07	76.83	67.01	69.27
Pyr	3.14	5.73	4.95	4.92	10.78	9.82	3.59	7.17	3.29	4.57
Sp	10.58	1.46	1.80	8.69	-	0.375	13.55	1.57	5.01	2.69
Gros	22.80	18.94	21.20	22.52	19.67	17.64	19.79	14.43	24.69	23.47
Mg/Mg+Fe	0.047	0.072	0.064	0.071	0.134	0.120	0.054	0.85	0.047	0.062

(C) = Core composition, (R) = rim composition, (Rr) = garnet rim composition that is essentially mantled by chlorite. The G_{2A} are all in Pitlochry Schist lithologies, specimen numbers of the rocks (ions calculated on the basis of 24 oxygens), molecular percentage of end members are also shown.

TABLE 3.5a Contd

	7		8			9		
	C	R	C	R	Rr	C	R	Rr
SiO_2	37.46	37.48	36.52	36.45	36.61	36.68	36.11	36.81
Al_2O_3	20.93	20.83	20.99	20.90	21.10	20.38	20.14	21.10
TiO_2	0.28	0.18	0.22	-	-	0.19	-	-
FeO	31.95	32.30	30.44	31.07	30.99	32.83	32.85	33.21
MgO	0.95	1.52	1.63	3.57	2.42	2.60	3.22	3.43
MnO	1.85	1.40	1.74	0.16	0.81	2.26	0.68	0.50
CaO	8.52	7.52	9.35	6.95	7.44	5.00	4.90	5.10
TOTAL	101.94	101.23	100.91	99.11	99.37	99.97	97.91	100.03
Si	5.913	5.973	5.848	5.881	5.908	5.935	5.939	5.909
Al^{iv}	0.087	0.027	0.152	0.119	0.92	0.065	0.061	0.091
Al^{vi}	3.809	3.887	3.810	3.857	3.922	3.823	3.843	3.886
Ti	0.033	0.021	0.027	-	-	0.023	-	-
Fe	4.180	4.306	4.077	4.193	4.182	4.445	4.517	4.458
Mg	0.223	0.361	0.390	0.858	0.582	0.627	0.789	0.821
Mn	0.248	0.189	0.236	0.022	0.110	0.310	0.095	0.069
Ca	1.442	1.284	1.604	1.202	1.287	0.868	0.864	0.864
SUM	15.935	16.048	16.144	16.132	16.083	16.096	16.108	16.103
ΣFe+Mg+Mn+Ca	6.093	6.14	6.307	6.275	6.161	6.25	6.265	6.212
Alm	68.60	70.13	64.64	66.82	67.88	71.12	72.10	71.71
Pyr	3.66	5.88	6.19	13.67	9.45	10.03	12.59	13.21
Sp	4.07	3.08	3.74	0.35	1.79	4.96	1.52	1.11
Gros	23.67	20.91	25.43	19.16	20.88	13.89	13.79	13.97
Mg/Mg+Fe	0.051	0.077	0.087	0.170	0.122	0.124	0.149	0.156

TABLE 3.5b Chemical analysis of G_{2B} garnet porphyroblasts

	10			11		
	C	R	Rr	C	R	Rr
SiO_2	37.17	36.22	37.00	36.92	35.87	36.92
Al_2O_3	20.71	21.32	20.94	20.47	20.38	20.75
TiO_2	-	-	-	-	-	-
FeO	30.53	34.03	32.95	28.22	32.03	30.89
MgO	0.78	1.35	1.28	0.83	1.25	0.78
MnO	3.30	1.26	1.26	5.90	2.54	3.33
CaO	8.33	7.32	7.71	8.90	7.12	8.18
TOTAL	100.82	101.50	101.14	101.24	99.32	100.85
Si	5.971	5.896	5.927	5.933	5.885	5.942
Al^{iv}	0.029	0.104	0.073	0.067	0.115	0.058
Al^{vi}	3.895	3.877	3.881	3.809	3.826	3.880
Ti	-	-	-	-	-	-
Fe	4.102	4.507	4.414	3.791	4.395	4.158
Mg	0.187	0.319	0.305	0.200	0.305	0.187
Mn	0.450	0.169	0.171	0.803	0.353	0.454
Ca	1.433	1.242	1.324	1.532	1.252	1.410
SUM	16.067	16.114	16.095	16.135	16.131	16.089
ΣFe+Mg+Mn+Ca	6.172	6.237	6.214	6.326	6.305	6.209
Alm	66.46	72.26	71.03	59.93	69.71	66.97
Pyr	3.030	5.12	4.90	3.16	4.84	3.11
Sp	7.29	2.71	2.75	12.69	5.60	7.31
Gros	23.22	19.91	21.32	24.22	19.86	22.71
Mg/Mg+Fe	0.044	0.066	0.065	0.050	0.065	0.043

(C), (R) and Rr as in 3.5a

TABLE 3.5b Contd...

	12		13		
	C	R	C	R	Rr
SiO_2	37.13	37.02	36.27	36.63	36.27
Al_2O_3	20.72	21.03	21.34	21.34	21.71
TiO_2	-	-	0.27	-	-
FeO	29.77	32.38	30.44	34.56	33.44
MgO	0.63	1.12	0.76	1.15	1.55
MnO	4.24	2.65	3.84	0.80	0.55
CaO	8.86	7.60	8.64	7.10	7.00
TOTAL	101.35	101.81	101.54	101.58	100.54
Si	5.948	5.909	5.894	5.945	5.916
Al^{iv}	2.052	2.091	0.106	0.055	0.084
Al^{vi}	1.860	1.865	3.873	3.920	3.979
Ti	-	-	0.032	-	-
Fe	3.988	4.322	4.025	4.566	4.439
Mg	0.150	0.267	0.179	0.271	0.367
Mn	0.570	0.359	0.514	0.107	0.074
Ca	1.521	1.300	1.463	1.202	1.192
SUM	16.089	16.113	16.085	16.066	16.051
ΣFe+Mg+Mn+Ca	6.229	6.248	6.181	6.146	6.072
Alm	64.02	69.17	65.12	74.29	73.11
Pyr	2.41	4.27	2.90	4.41	6.04
Sp	9.15	5.75	8.32	1.74	1.22
Gros	24.42	20.81	23.66	19.56	19.63
Mg/Mg+Fe	0.036	0.058	0.043	0.056	0.076

TABLE 3.5c Chemical composition of G_{2C} garnet, in Pitlochry Schist lithologies

	23		25			26	
	C*	R*	C	R	Rr	C	R
SiO_2	37.45	37.57	36.28	37.37	36.40	36.73	37.57
Al_2O_3	20.54	20.88	20.73	20.52	20.79	20.68	20.88
TiO_2	-	0.20	-	-	0.22	-	0.20
FeO	26.30	25.70	23.24	25.06	23.60	25.70	26.25
MgO	0.60	0.73	0.54	0.89	0.86	0.59	0.73
MnO	7.57	7.57	8.61	5.83	7.30	7.57	6.47
CaO	9.16	9.09	10.80	10.32	10.93	9.35	9.09
TOTAL	101.62	101.73	100.200	99.99	100.10	100.62	101.19
Si	5.978	5.967	5.870	6.007	5.870	5.941	5.967
Al^{iv}	0.022	0.033	0.130	-	0.130	2.059	2.033
Al^{vi}	3.843	3.878	3.825	3.888	3.823	1.885	1.878
Ti	-	0.024	-	-	0.027	-	0.024
Fe	3.511	3.414	3.145	3.369	3.183	3.414	3.550
Mg	0.144	0.172	0.131	0.213	0.208	0.143	0.172
Mn	1.024	1.018	1.180	0.794	0.997	1.018	0.887
Ca	1.567	1.546	1.872	1.777	1.889	1.621	1.546
SUM	16.089	16.052	16.153	16.048	16.127	16.081	16.057
ΣFe+Mg+Mn+Ca	6.246	6.15	6.328	6.153	6.277	6.196	6.155
Alm	56.21	55.51	49.70	54.75	50.71	55.10	57.68
Pyr	2.31	2.80	2.07	3.46	3.32	2.31	2.79
Sp	16.39	16.55	18.65	12.90	12.65	16.43	14.41
Gros	25.09	25.14	29.58	28.89	20.09	26.16	25.12
Mg/Mg+Fe	0.040	0.048	0.040	0.059	0.061	0.040	0.046

* Essentially represent core remnant

TABLE 3.5d Chemical analysis of G_{2-4} garnet porphyroblasts

	5 *			14			16		
	C	R	Rr	C	R	Rr	C	R	Rr
SiO_2	36.82	36.15	36.79	36.59	36.40	36.16	36.73	36.92	36.68
Al_2O_3	20.74	20.50	20.40	20.91	21.12	21.14	20.78	21.32	20.91
TiO_2	0.16	-	-	-	0.19	-	0.16	-	-
FeO	31.95	33.62	33.24	30.01	34.88	34.34	24.16	32.31	32.75
MgO	0.77	1.19	0.98	0.84	1.40	1.32	0.65	1.33	1.45
MnO	3.54	3.05	2.83	5.51	2.24	2.06	7.54	1.08	1.02
CaO	6.94	6.42	6.41	7.26	5.68	5.77	9.41	6.95	7.60
TOTAL	100.92	100.93	100.64	101.12	101.90	100.78	99.41	99.40	100.42
Si	5.936	5.898	5.959	5.896	5.836	5.851	5.953	5.950	5.912
Al^{iv}	0.064	1.102	0.041	0.104	0.164	0.149	0.047	0.050	0.088
Al^{vi}	3.879	3.838	3.855	3.867	3.828	3.882	3.923	4.001	3.885
Ti	0.019	-	-	-	0.024	-	0.019	-	-
Fe	4.307	4.496	4.503	4.044	4.677	4.648	3.275	4.355	4.415
Mg	0.185	0.285	0.235	0.202	0.334	0.319	0.156	0.319	0.349
Mn	0.484	0.413	0.388	0.753	0.304	0.282	1.035	0.147	0.139
Ca	1.199	1.101	1.112	1.254	0.977	1.00	1.634	1.200	1.313
SUM	16.073	16.133	16.093	16.120	16.144	16.281	16.042	16.022	16.101
ΣFe+Mg+Mn+Ca	6.175	6.306	6.238	6.253	6.292	6.249	6.1	6.021	6.216
Alm	69.75	71.42	72.19	64.67	74.33	73.38	53.69	72.33	71.03
Pyr	3.00	4.53	3.77	3.23	5.31	5.11	2.56	5.30	5.61
Sp	7.84	6.56	6.22	12.04	4.83	4.51	16.97	2.44	2.24
Gros	19.41	17.49	17.82	20.06	15.53	16.00	26.78	19.93	21.12
Mg/Mg+Fe	0.041	0.060	0.050	0.048	0.067	0.064	0.045	0.068	0.073

*C, R and Rr as in 3.5a, all in Ben Lui Schist lithologies except (5) which is in Pitlochry Schist

TABLE 3.5d Contd...

	17			18		
	C	R	Rr	C	R	Rr
SiO_2	37.46	36.89	37.04	36.89	36.7	36.49
Al_2O_3	21.00	21.11	20.34	21.04	20.97	20.66
TiO_2	-	0.15	0.24	0.24	-	-
FeO	24.99	31.28	30.06	27.42	34.59	34.08
MgO	0.43	0.98	0.72	0.83	1.69	1.29
MnO	8.26	1.86	2.21	6.89	1.22	0.99
CaO	9.26	8.32	8.76	8.26	6.53	7.14
TOTAL	101.89	100.69	99.38	101.57	101.27	100.65
Sl	5.942	5.922	6.011	5.894	5.839	5.900
Al^{iv}	0.058	0.078	-	0.106	0.161	0.100
Al^{vi}	3.869	3.917	3.391	3.857	3.819	3.838
Ti	-	0.018	0.029	0.029	-	-
Fe	3.316	4.199	4.080	3.664	4.657	4.608
Mg	0.102	0.235	0.175	0.199	0.404	0.310
Mn	1.110	0.253	0.304	0.932	0.166	0.136
Ca	1.618	1.431	1.524	1.414	1.126	1.237
SUM	16.015	16.053	16.003	16.095	16.172	16.129
ΣFe+Mg+Mn+Ca	6.146	6.118	6.083	6.209	6.353	6.291
Alm	53.95	68.63	67.07	59.01	73.30	73.25
Pyr	1.66	3.84	2.88	3.21	6.36	4.93
Sp	18.06	4.14	5.00	15.01	2.61	2.16
Gros	26.33	23.39	25.05	22.77	17.72	19.66
Mg/Mg+Fe	0.030	0.053	0.041	0.052	0.080	0.063

* Essentially represent core remnant.

3.5.3. Compositional variation of the syn-D_2 garnets

3.5.3.1 G_{2A} garnet porphyroblasts

The garnets of the G_{2A} phase shows normal zoning, with the MnO decreasing and the (FeO+MgO) increasing outwards from the centre towards the rim. CaO shows compositional variations that are similar to those shown by MnO in the general trend but the detailed variation is different from that of MnO. The G_{2A} garnet MnO rim concentrations are low and in some it approaches zero %, e.g. 2 (Table 3.5a, Figs 3.7-9). Compositional profiles through the G_{2A} garnet are given for two specimens (1) and (2), both of about the same bulk chemistry (Table 1.2a) and from nearby outcrops (see Fig. 1.4 for sample locations). The two specimens have similar mineralogy (Table 1.1), except that garnets in (1) contain only a few epidote grains while the garnets in (2) are epidote-free. The biotite in (1) is coarser than in (2), which has higher modal biotite. No biotite was seen enclosed in the garnets in either specimen. The compositional profiles in two representative and similar-sized garnets in each specimen are presented in Figures 3.7 and 3.8, with the edge and centre of the crystals being identified by minimum and maximum MnO, respectively. Towards the rim area all the elements exhibit a distinct break in slope located at different distances from the garnet edges; this being particularly distinct for the CaO and FeO profiles. In Figure 3.8 the CaO rises from 6.4% to 7.6% and then falls again at the garnet edge. Such CaO increases are usually compensated by a decrease in MnO and, or, FeO. The MnO reaches zero over the outmost edge of the garnet.

The G_{2A} in a Ca-richer rock e.g. sample 8 containing chlorite-biotite-muscovite-quartz and albite has also been studied. Both garnet and biotite are partly chloritized and the G_{2A} garnet porphyroblasts in this sample (see Table 1.2a) reach the largest sizes for garnet in the area (Plate 2.4a,b) and are full of quartz inclusions. Other calc-rich rocks commonly have the elongate skeletal garnets (e.g. 6,7, see Plate 2.9).

One of the G2A garnets in (8) shows a rather complex compositional profile (Fig.3.9). The CaO shows an antipathetic relation with FeO and generally mirrors that of the FeO. In addition the CaO shows a relatively more fractionated profile than that of the MnO which, in turn, has a rather flat profile away from the core region with distinct compositional breaks at the rim, while varying antipathetically with CaO. The MgO profile shows a

gradual increase towards the rim reaching a maximum content recorded for the G_{2A} garnet rim composition with 3.37% MgO, while at the chloritized garnet rim composition it reaches 2.42% MgO.

The garnet rim composition has the lowest MnO composition which is often not the case, particularly for G_{2A} garnet. These garnet-rim zonal inflections generally occur in the outer 5-10μm from the garnet edge, independent of garnet size but appear consistently where the garnet rim is mantled by chlorite. This element inflection shows as a direct continuation with the normal continuous zoning trends. Such rim compositions (R_r) are shown in Tables 3.5a-d.

3.5.3.2 G_{2B} garnet porphyroblasts

The G_{2B} garnet phases are generally small, euhedral and have a smaller grain size range than the G_{2A} garnet. The largest grains have the widest range of MnO, core to rim, with the smallest grains having the highest MnO at the rim (Fig.3.10a,b). The garnet profiles (Figs 3.10-12) show that FeO initially increases either abruptly (e.g. Figs 3.10a, 3.11) or gradually (e.g. Fig. 3.12) from the garnet centre, then decreases gradually before increasing again at the rim, which may show decreasing FeO. The CaO profile generally shows the reverse of FeO. MgO exhibits little variation, with a gradual increase towards the garnet edge. The MnO has also either rapid or gradual initial decline from the core followed by a slight decline towards the rim. These general patterns have been detected in the analysed G_{2B} garnet but with some variations in the precise shapes of the profiles. Generally the G_{2B} garnet phase has MnO rim composition higher than the G_{2A} phase.

3.5.3.3 G_{2C} garnet

Figures 3.13a, b, give the compositional profiles through two G_{2C} garnets. The profiles are generally flat with fall in MnO and CaO towards the edge, but with a compensating slight increases in FeO and MgO. Generally the G_{2C} garnets are low in FeO and have significantly higher MnO rim composition than any other D_2 garnets.

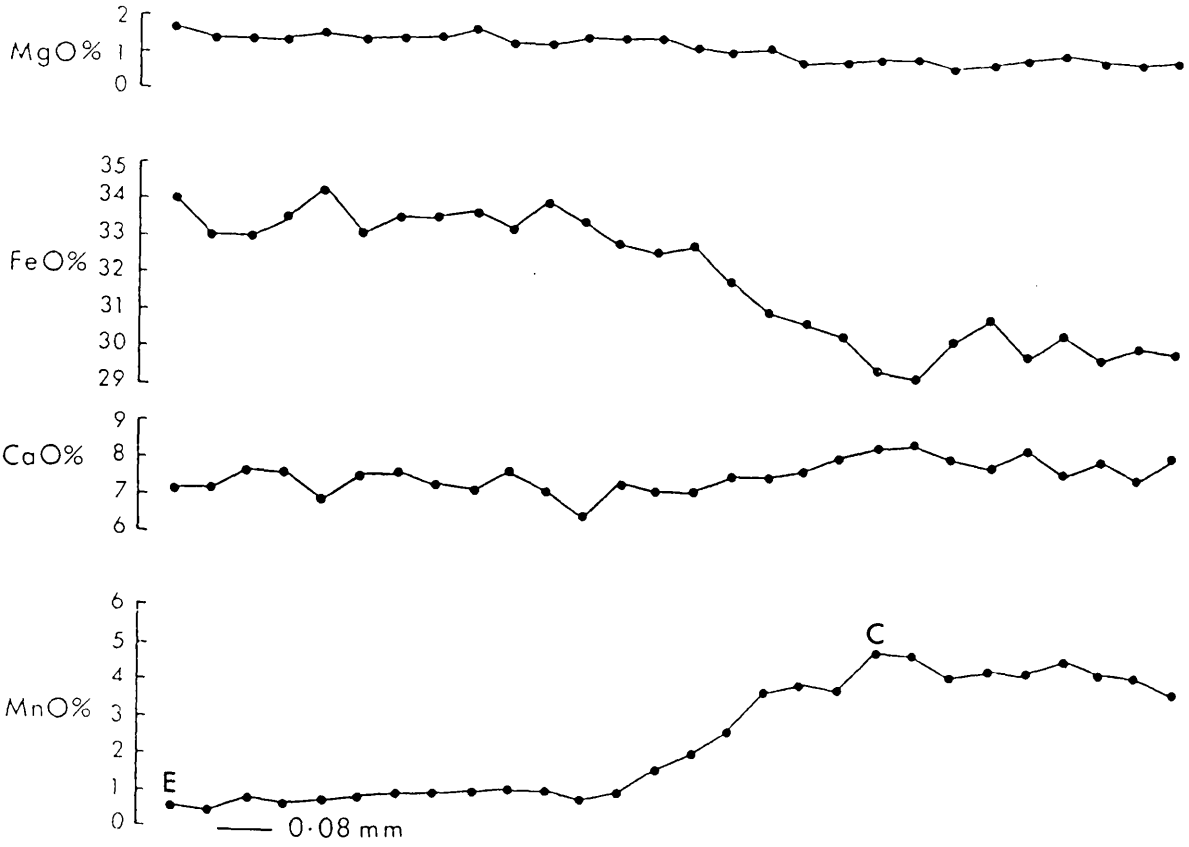

FIG. 3.7 Compositional profile from centre to edge of a G_{2A} garnet crystal, specimen (1)

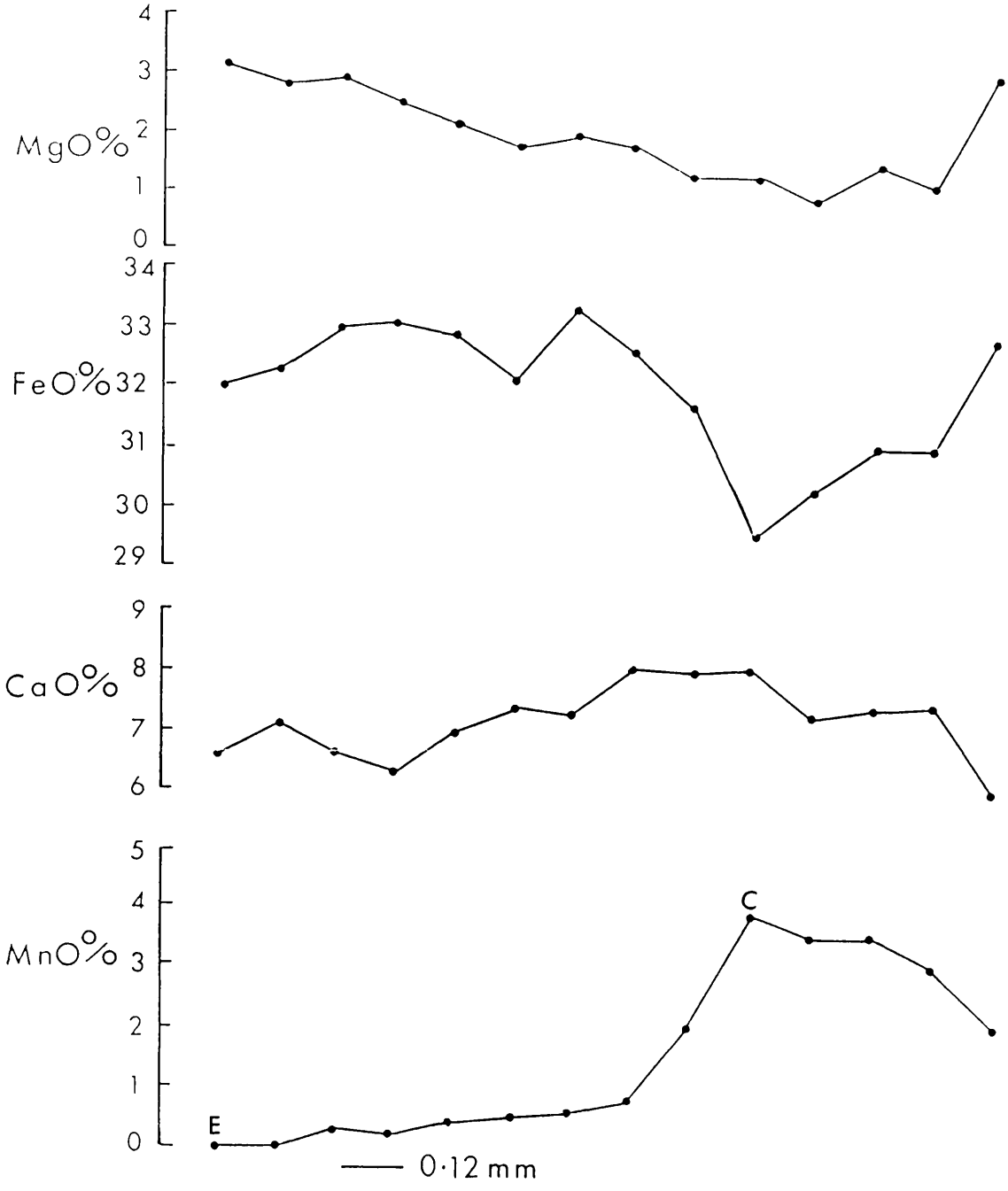

FIG. 3.8 Compositional profile from centre to edge of G_{2A} garnet, specimen (2)

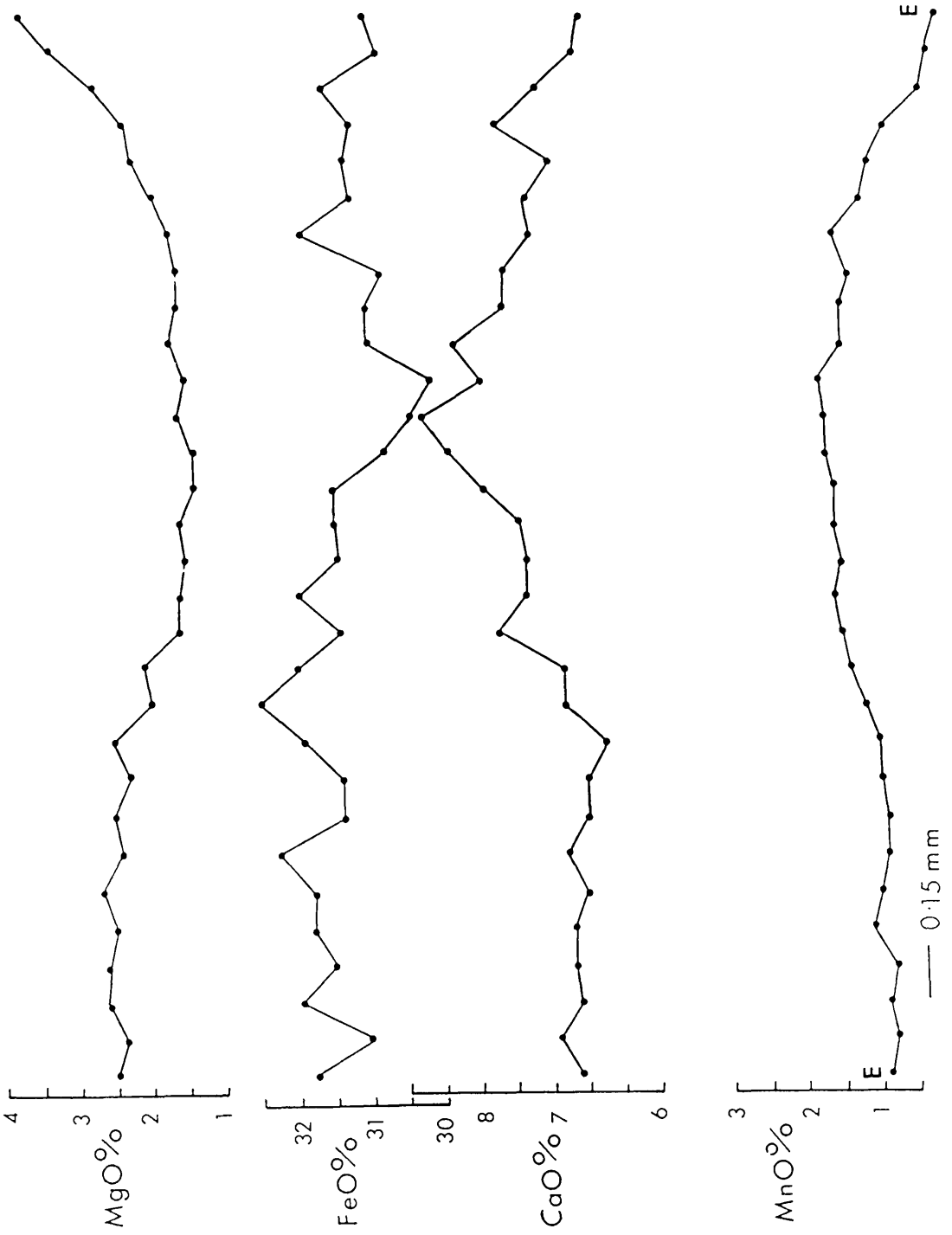

FIG. 3.9 Compositional profile from edge to edge across a G_{2A} garnet crystal, specimen (8)

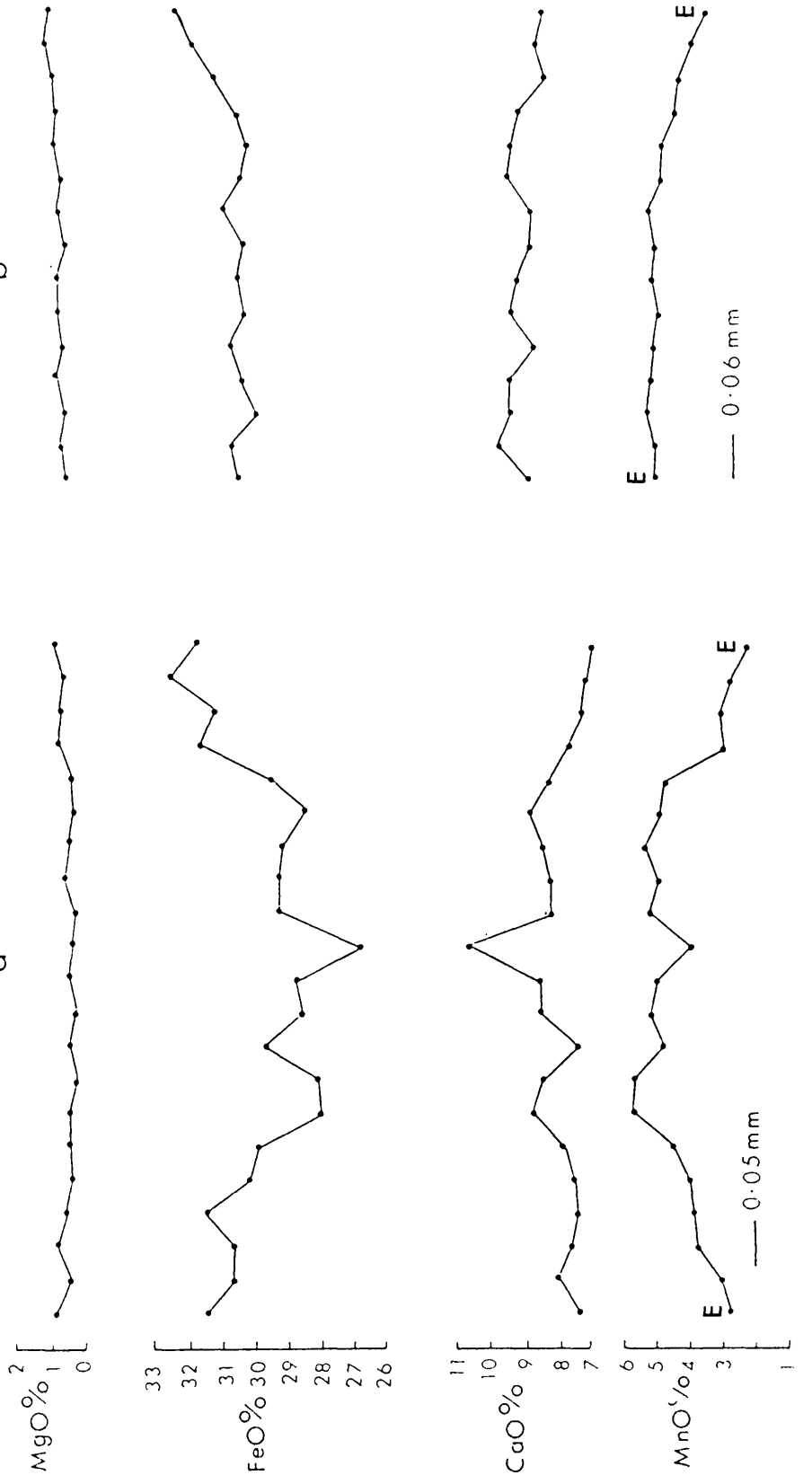

FIG.3.10 Compositional profiles across two G_{2B} garnet crystals in specimen (11)

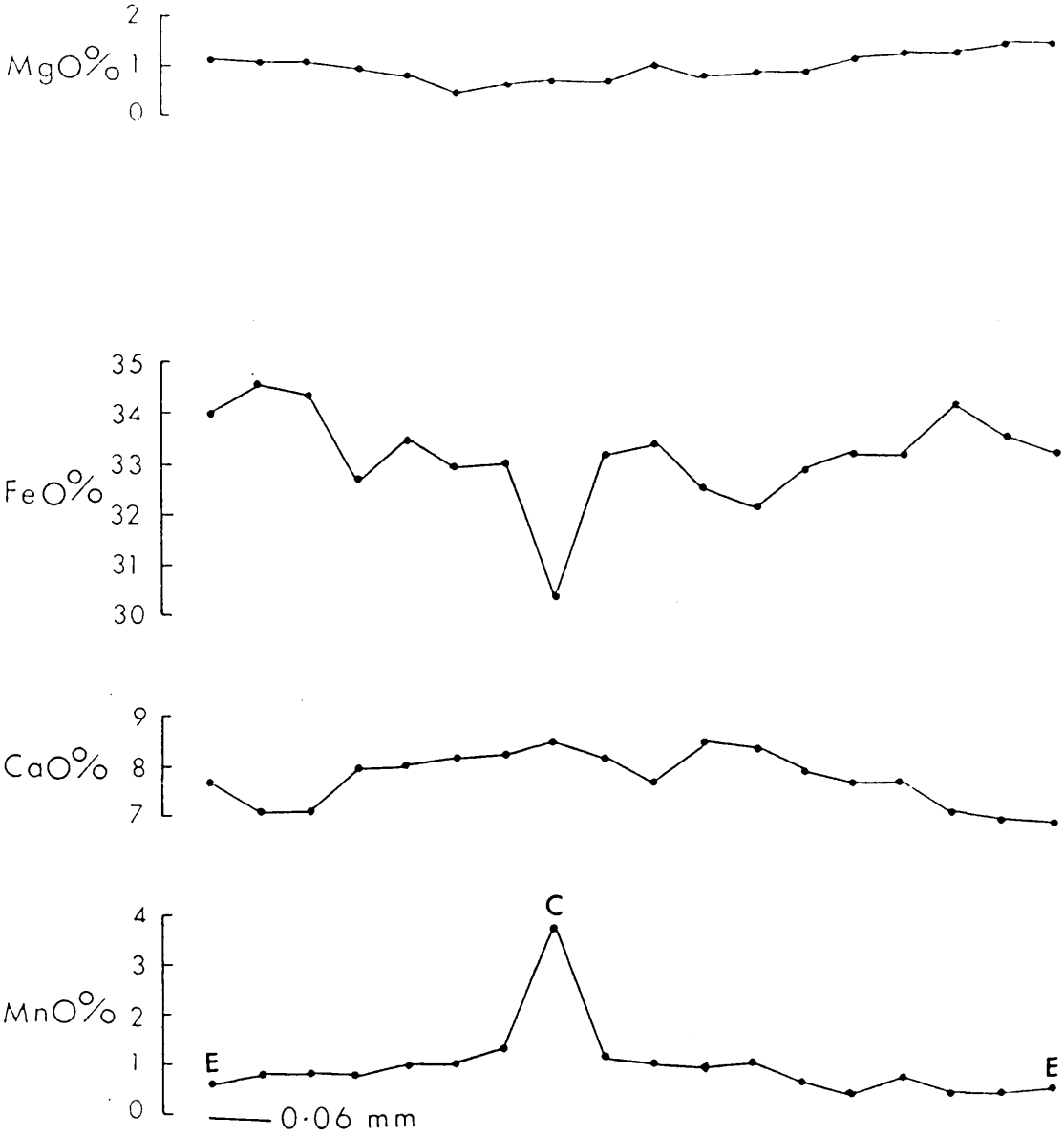

FIG. 3.11 Compositional profile of a G_{2B} garnet porphyroblast in specimen (13)

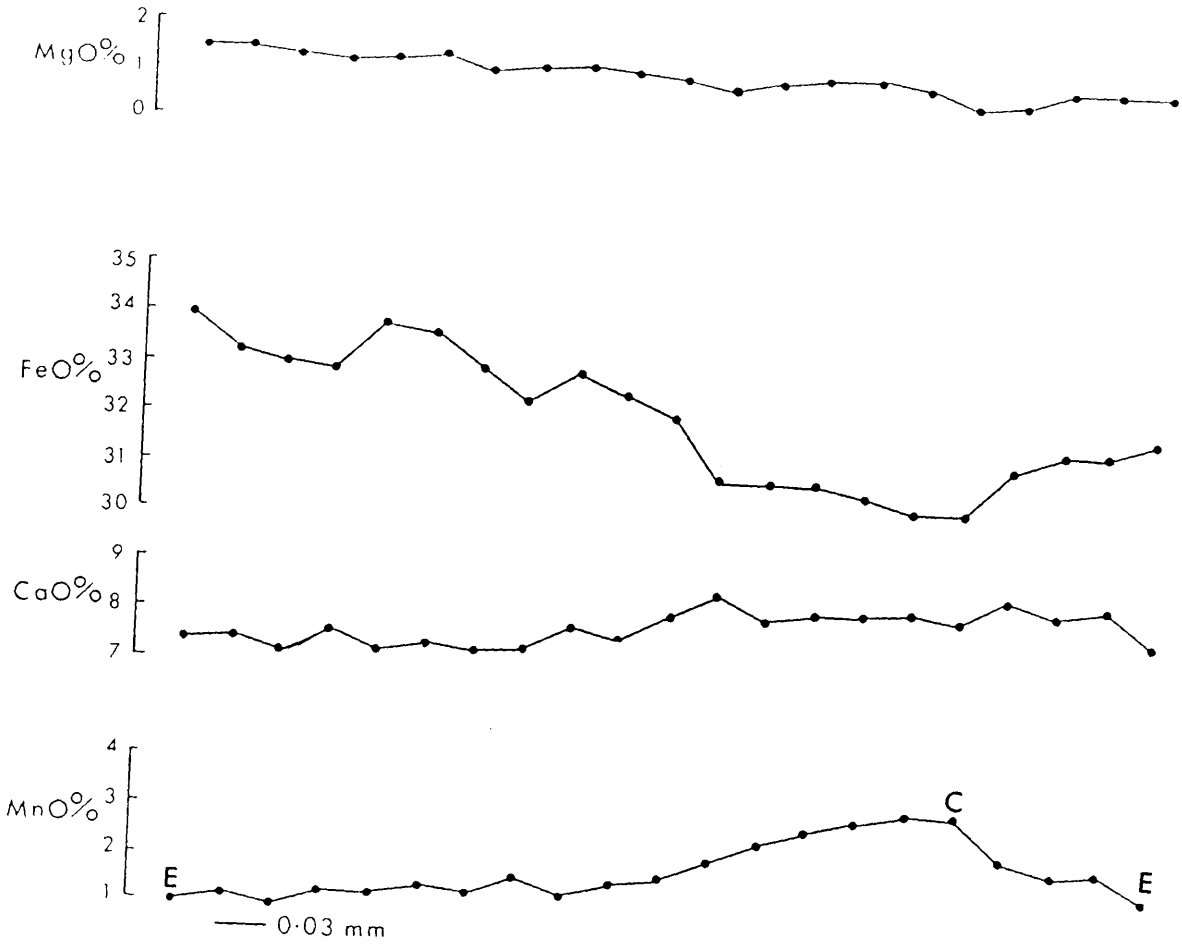

FIG. 3.12 Compositional profile of a G_{2B} garnet in specimen (10)

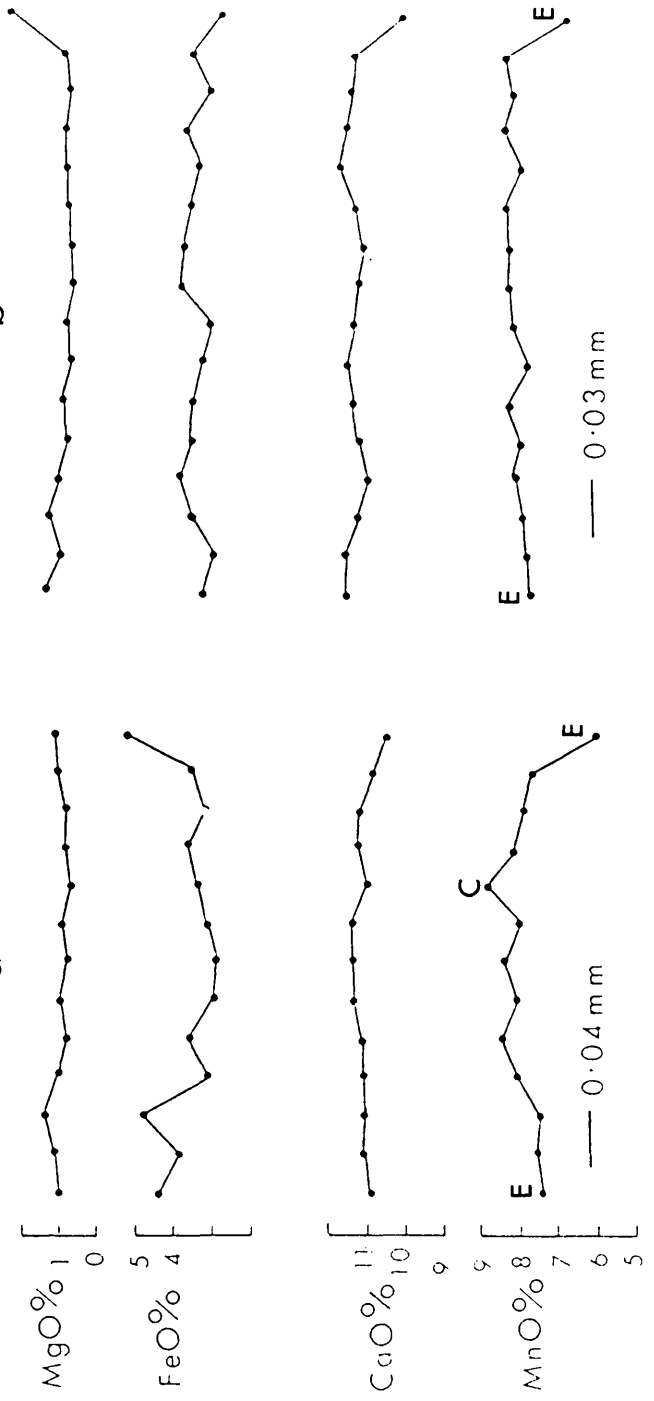

FIG. 3.13 Compositional profile across two G_{2C} garnets in specimen (25)

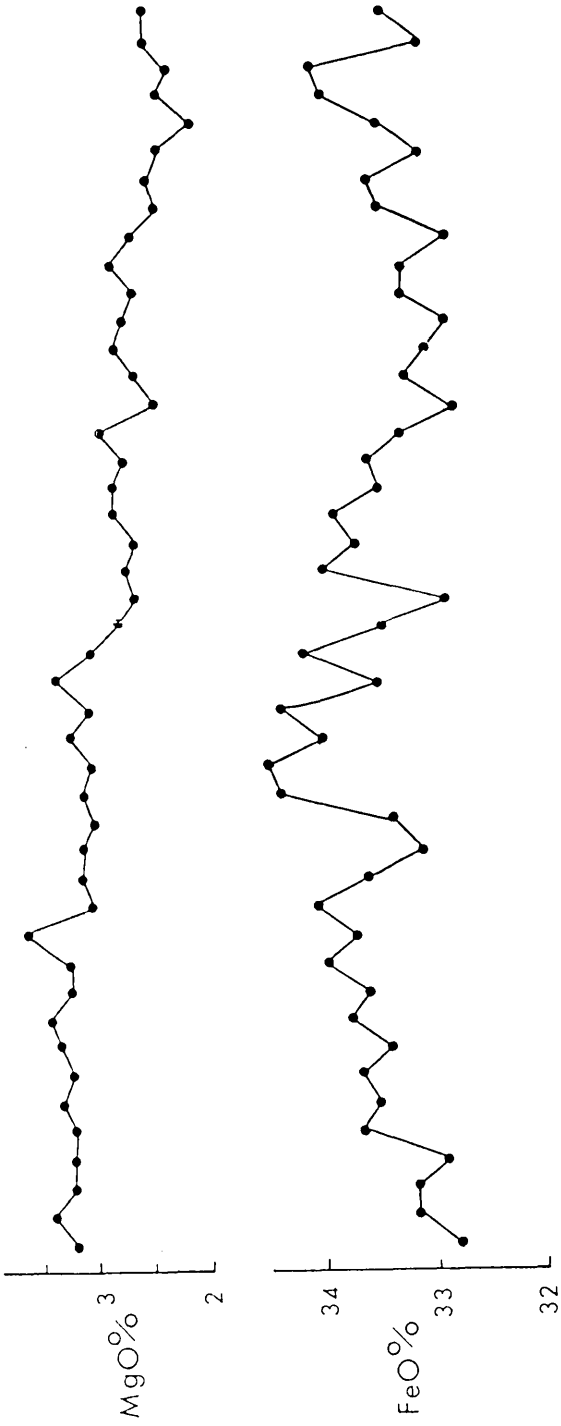

FIG. 3.14 Compositional profiles from centre to edge across a G_{2A} garnet in horblende schists, specimen (9)

3.5.3.4 D_2 garnets in the hornblende schists

A compositional traverse from the centre to the rim of D_2 garnet porphyroblasts (Fig.3.14; Table 3.5a, No.9) shows a general normal zonation but with a zig-zag pattern, particularly in FeO. This may be due to the presence of many quartz inclusions, but could also derive from a complex growth history (Atherton and Edmunds, 1966).

3.5.4 Compositional variation of the G_{2-4} garnet porphyroblasts

The G_{2-4} garnet porphyroblasts show a normal decrease in MnO outwards with either a regular decline (Figs 3.15-17) or abrupt decrease outwards from the garnet centre, then a gradual decrease towards the rim (Fig.3.18). MnO commonly shows antipathetic variation with FeO which mirrors that of FeO, sometimes very closely. The garnet grains that are most chloritized have the least Mn fractionation and the lowest core minus rim composition compared with the least chloritized grains (Table 3.5d, No.5; Fig.3.19; see Plate 2.3c) which lack MnO enrichment at the garnet edge. CaO generally shows an initial decrease from the core outwards with oscillations up to 1 wt% CaO superimposed on the profiles (Fig. 3.17a). In some garnets a single CaO maximum and minimum is followed by a gentle decrease to the edge, followed by a final increase (Fig.3.17b). The G_{2-4} garnet CaO variations generally do not follow the MnO variation.

3.5.5. Garnet-forming reaction(s)

Petrographic and compositional data enables the garnet-forming reactions, especially those forming M_2 garnets, to be deduced. From the mineral growth sequence (Chapter 2) chlorite and muscovite are the two major minerals involved in garnet formation following either

$$\text{Chlorite}_A + \text{quartz} \rightarrow \text{chlorite}_B + \text{garnet} + H_2O \quad 3.1, \text{ (Atherton, 1964)}$$

or

$$\text{Chlorite} + \text{muscovite} + \text{quartz} \rightarrow \text{garnet} + \text{biotite} + H_2O \quad 3.2,$$

(Sivaprakash, 1981)

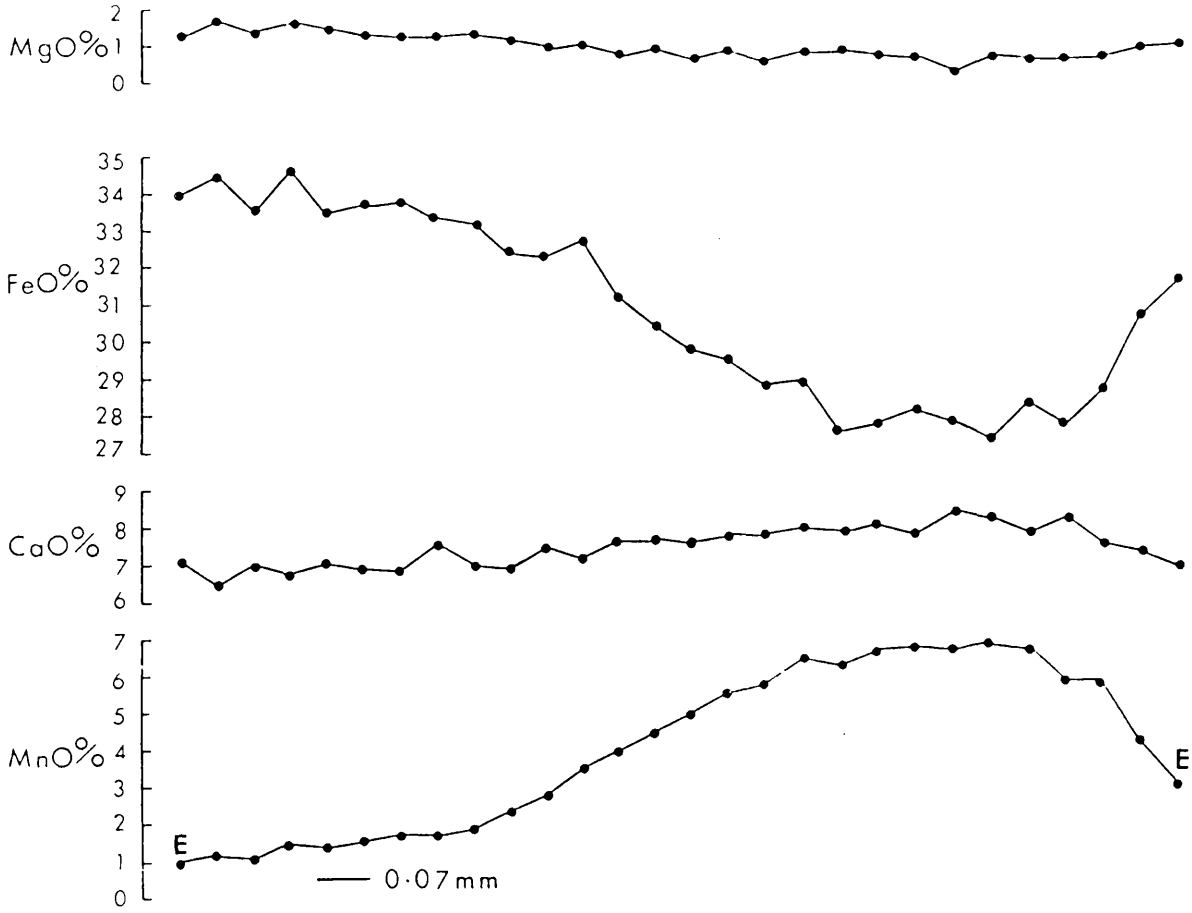

FIG. 3.15 Compositional profile of an M_{2-4} garnet porphyroblast in specimen (18)

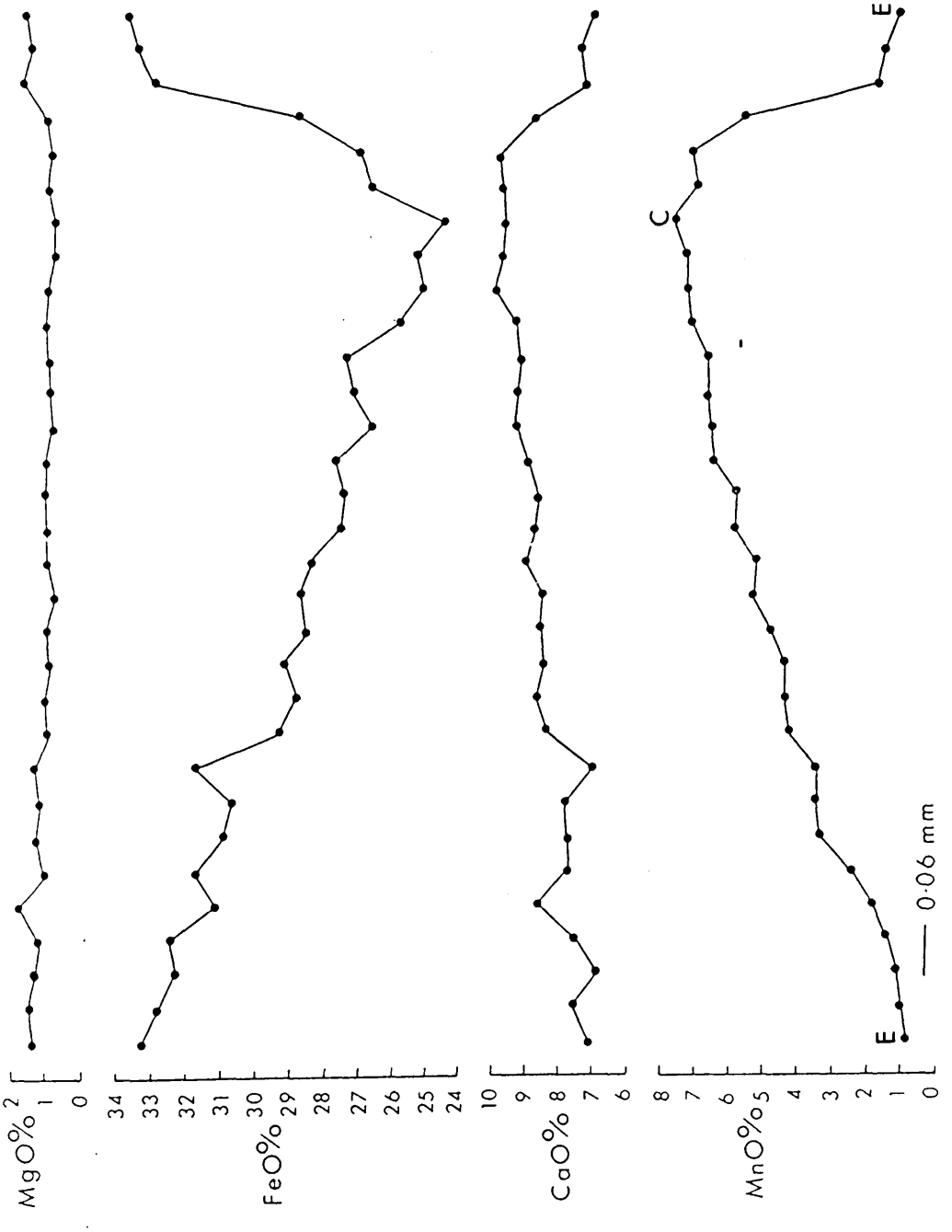

FIG. 3.16 Compositional profile of an M_{2-4} garnet porphyroblast in specimen (14)

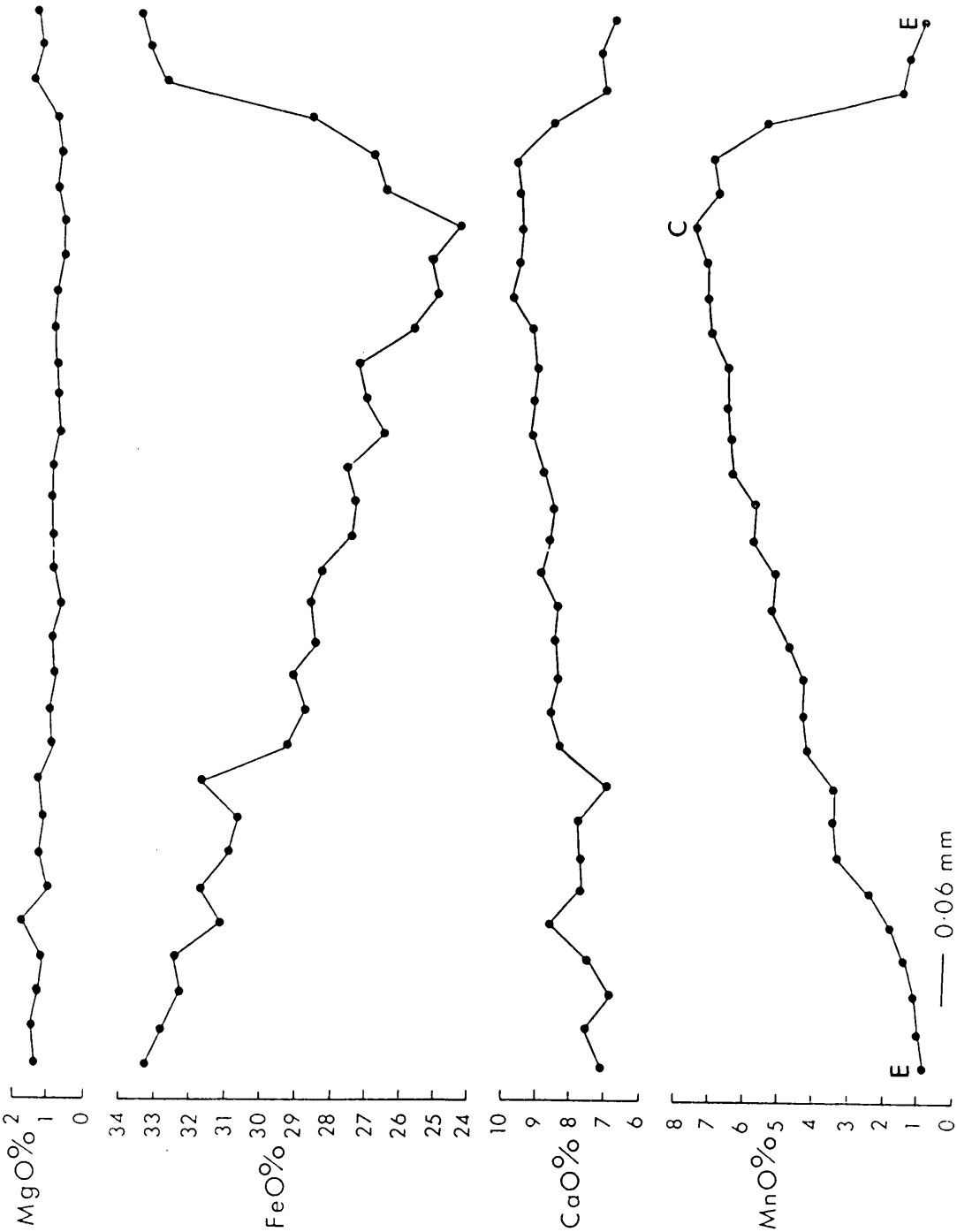

FIG. 3.17a Compositional profile from edge to edge in $M_{2\text{-}4}$ garnet in specimen (16)

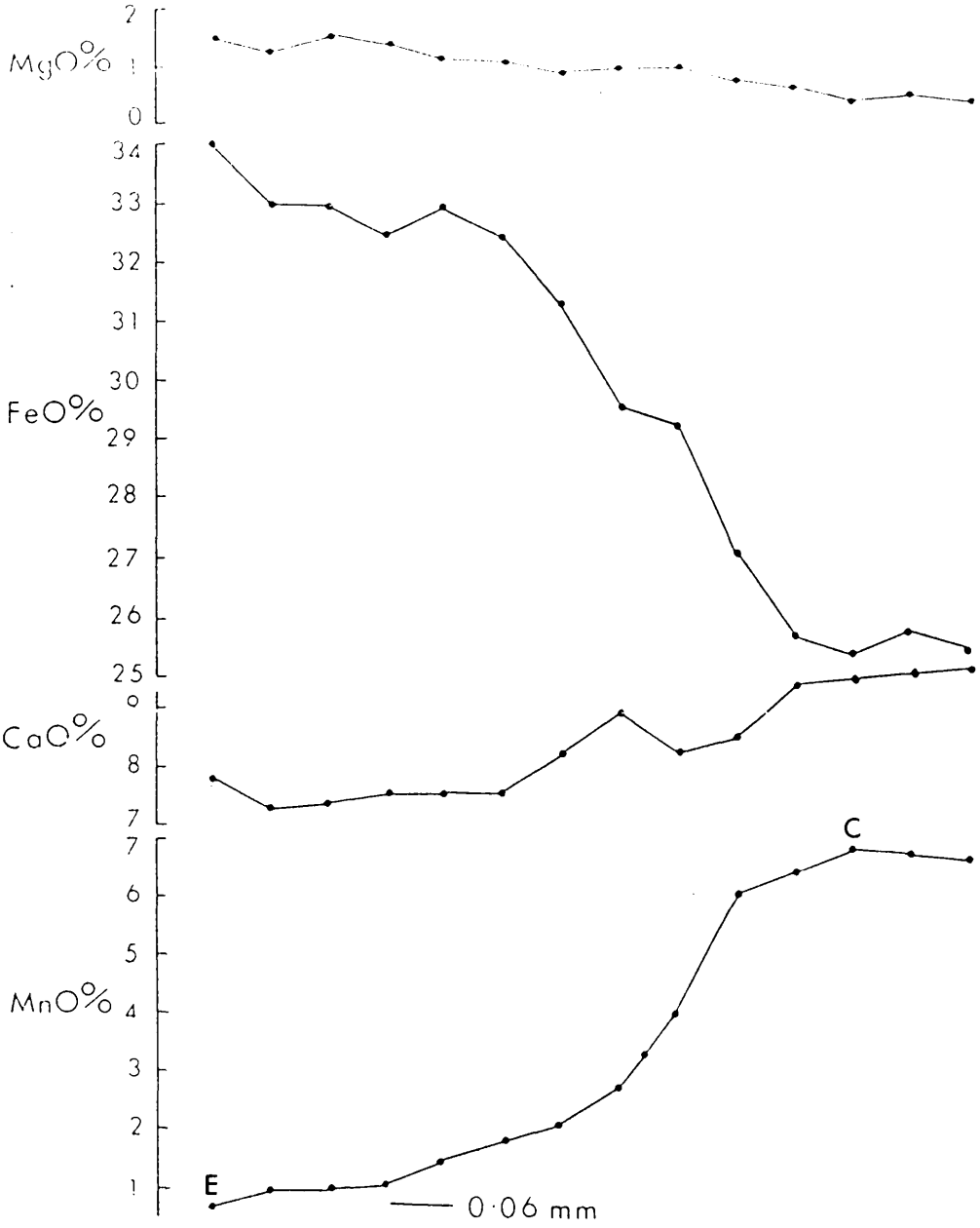

FIG.3.17b Compositional profile from centre to edge in M_{2-4} garnet in specimen (16)

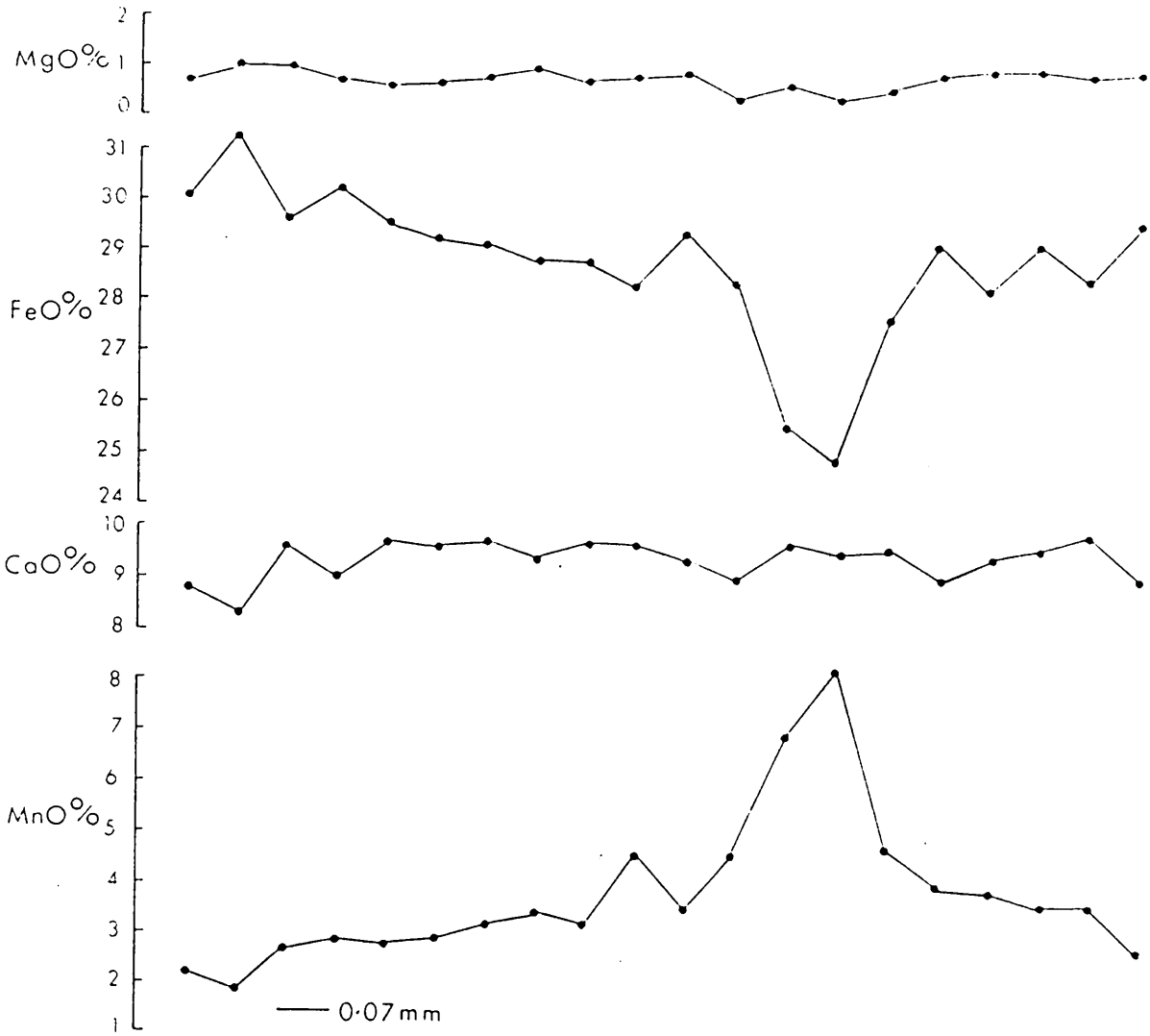

FIG. 3.18 Compositional profile in an $M_{2\text{-}4}$ garnet in specimen (17)

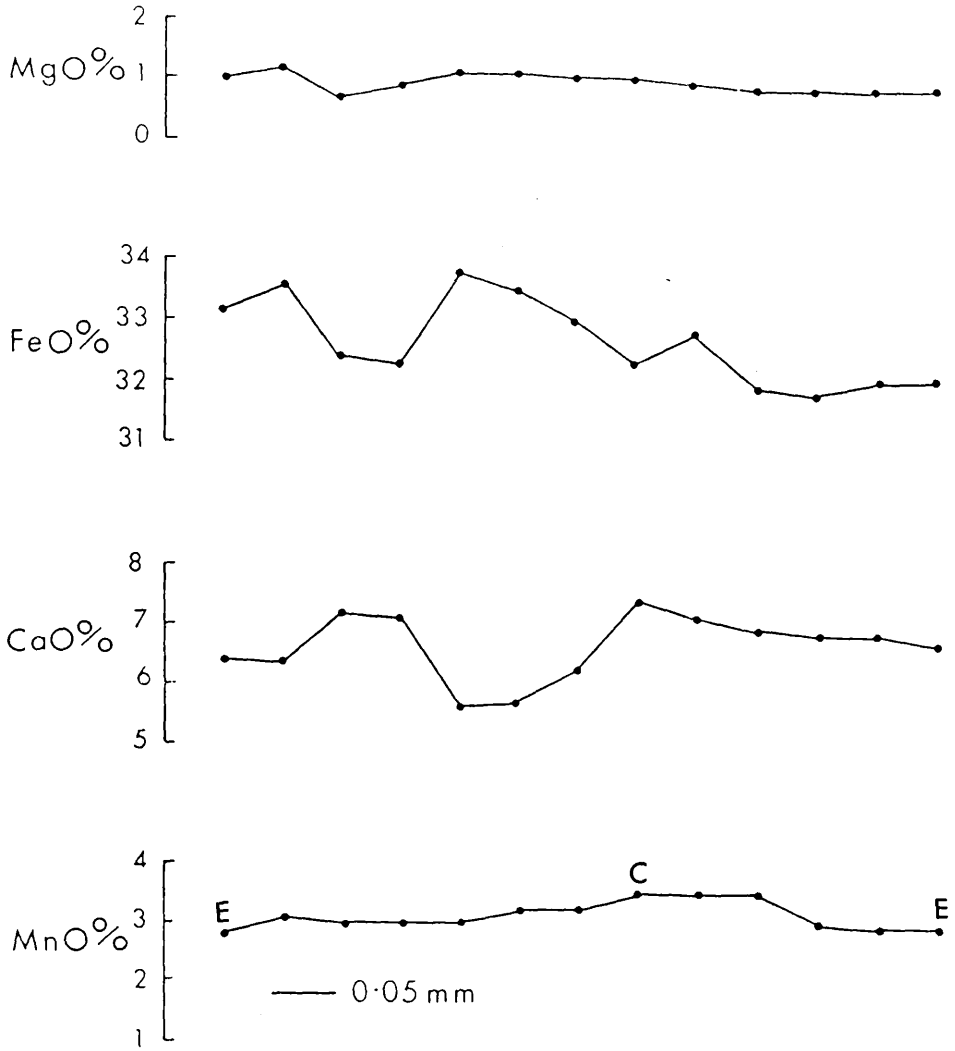

FIG. 3.19 Compositional profile of M_{2-4} garnet in specimen (5); the two edges are chloritized

Biotite (M_2) in the S_2 fabric warps around the M_2 garnet porphyroblasts indicating that the garnet pre-dates the biotite. However reaction of type 3.2 shows contemporaneous growth of biotite and garnet. In the most calcareous rocks the following may have occurred:

Muscovite + chlorite + calcite + quartz → epidote + biotite + CO_2 + H_2O 3.3 (Butler, 1967)

The presence of epidote as inclusions in the M_2 garnets and its virtual absence from the rock matrix suggests the following reactions (Brown, 1969):

Chlorite + quartz + epidote → garnet + H_2O + O_2 (3.4)

Chlorite + muscovite + epidote → garnet + biotite + H_2O (3.5)

Although some garnet and biotite growth may be contemporaneous, biotite growth probably extended over a longer period than garnet growth overlap growth periods (Rice and Roberts, 1988), and could also have proceeded in separate domains, dependent upon compositional inhomogeneities and coupled reactions (Carmichael, 1969). It seems unlikely that one single reaction is responsible for the garnet formation because some G_{2A} garnets are accompanied by abundant biotite while others have none, so a reaction producing garnet and biotite simultaneously (i.e. equation 3.2) could not always have occurred. Although M_2 biotite was not a reactant in the major garnet-forming reaction it is possible that garnet formed, in part, from biotite, thus explaining the general lack of biotite in rocks containing the M_{2-4} garnets, assuming that the M2 biotite is not absent due to rock composition.

3.5.6 **Discussion**

The normal compositional zoning with respect to Ca and Mn shown by the M_2 and M_{2-4} garnet is best explained by Rayleigh fractionation (Hollister, 1966) and involves preferential concentration of Ca and Mn in the garnet progressively depleting the matrix Mn and Ca available for incorporation in the outer part of the garnet. Irregularities in the profile

could result from other reactions involving the release or absorption of cations into the intergranular fluid. For instance, such a reaction involving epidote break-down (3.4, 5) would release Ca and force a decrease in Fe and Mn in the garnet unless significant Mn was also released from the epidote. The complexity of the detailed changes in the zoning patterns are not likely to be the result of fluctuating P-T conditions but might in part result from variations in the size and composition of the domains supplying reactant to the growing garnet. These domains could be influenced by sedimentary compositional layering and other variations, e.g. early reactants (Yardley, 1977).

Chemical zonation in garnet can be interpreted in terms of supposed continuous and, or, discontinuous reactions and is generally referred to as a reaction partitioning model (Tracy, 1982). This proposes that zoned minerals grow with the surface composition controlled by some multivariant equilibrium with one or more reactants. Tracy (1982), Trzceinski (1977) and Kretz (1973) have described this model.

Trzcienski (1977) suggested that the garnet-forming reaction in the Whetstone Lake area, Ontario, Canada was muscovite + chlorite + plagioclase + ilmenite → garnet + biotite + rutile + H_2O.

The equilibria between the chlorite and garnet defines a divariant loop similar to that found in numerous igneous systems (Fig. 3.20). Assuming an initial Fe/Fe+Mn at N, and temperature $< T_1$, there will be no reaction. At T_1, the reaction begins with the formation of products with a Fe/(Fe+Mn) ratio at C, and the reactant with a ratio N. With increase of temperature, the equilibria would move along the two solubility curves defined by the reactants and products. As the temperature increases to T_2, there is a gradual change in composition of all the participating minerals. As garnet remains refractory, it does not re-equilibrate and therefore it preserves the equilibrium composition, for each step of the prograde continuous reaction. Thus zonation in garnet results. The other minerals re-equilibrate at successive temperatures through which they pass and retain only the composition of the last equilibrium. On the basis of this model the presence of garnet and the amount of zoning in garnet depend greatly on the initial Fe/(Fe+Mn) ratio of the rock. Unlike for the fractionation model, Mn is not treated as a minor component in this model. Consideration of the reaction

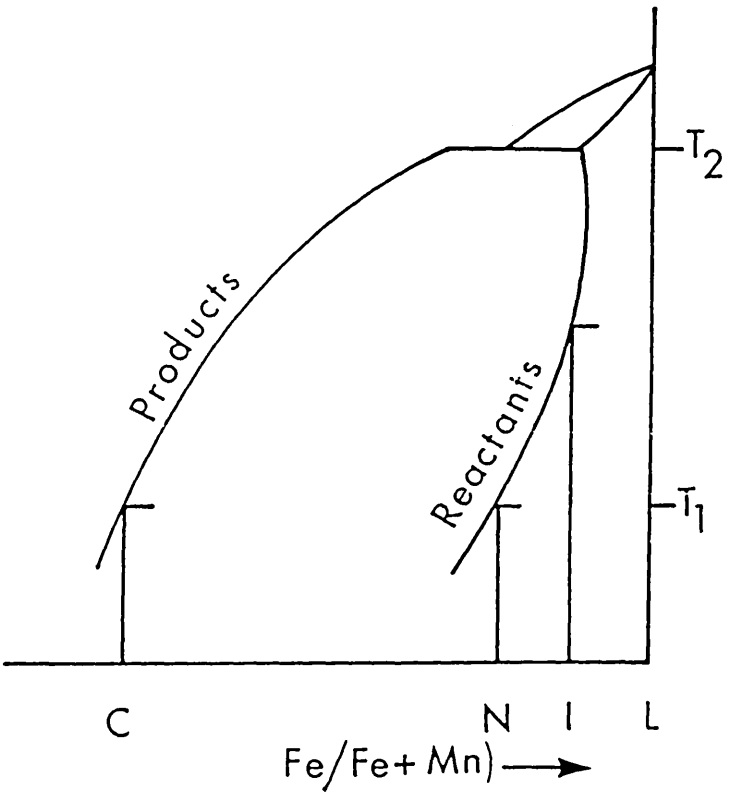

FIG.3.20 Schematic representation of product (garnet)-reactant (chlorite) equilibria in T-X space (After Trzcienski, 1977)

parititioning model (Trzcienski, 1977) also suggests that the relatively high Mn rim composition is the consequence of the incomplete growth of garnet due to temperature control. The high MnO rim composition does not suggest the termination of garnet growth because of exhaustion of the reactants, otherwise there would be a decline to zero MnO before the garnet ceased to grow.

The quantitative calibration of the relative temperature for Mg, Fe and Mn end members in various isobaric reactions is $T_{Mg} > T_{Fe} > T_{Mn}$ (Thompson, 1976), i.e. the temperature of the reaction with the Mg end member in the garnet system is higher than that of Fe and Mn, respectively. Since garnet has a higher preferential retention of Mn than any other FAM phase, high Mn garnet will grow at lower temperature than garnets with low Mn (Hsu, 1968; Loomis, 1986). Thus at least the rim composition of the G_{2B}, and certainly the G_{2C} garnets, was produced during a lower temperature than the G_{2A} phase (Table 3.5a-c; Table 4.2b).

Because magnetite and haematite are rare and graphite is common in these rocks it does not seem likely that high oxidation conditions were responsible for low Fe^{2+} values which might have promoted the incorporation of Mn at the expense of Fe^{2+} (Chinner, 1960, 1962). The fact that variations in the oxidation conditions took place during the later retrogression is not relevant to the growth history of the G_{2C} garnets.

The G_2C garnets are thought to have crystallized under different P-T conditions from the G_{2A} garnets because the chemical composition of the two garnets differs significantly and the rocks containing G_{2C} garnets do not have special chemical characteristics. The G_{2C} seems to have developed independently by a reaction of type 4.2 but at a lower temperature than G2A growth.

The general Mn edge enrichments", mainly found in G_{2A} mantled by chlorite (Table 3.5a) is straightforward retrogression of garnet to chlorite with incorporation of the released Mn into the edge of the relict garnet (Grant and Weiblen, 1971).

Several authors have discussed outer edge modifications of garnets and several interpretations have been made. These include (1) that the ilmenite breakdown results in increases in the Ti and Mn in the garnet rims (Evans and Guidotti, 1966; Hollister, 1969), and (2) simple exchange diffusion and

resorption, results in varying the Mg/Fe in the garnet rim (Müller and Schneider, 1971). The model envisaged by Grant and Weiblen (1971) explains the present occurrence with re-incorporation of Mn into the corroded garnets. This mechanism is enhanced by oxidizing conditions (Tewhey and Hess, 1976) so that the conversion of Fe^{2+} to Fe^{3+} near the garnet edge may have produced enough Fe^{2+} vacancies to enhance the diffusion rate for Mn, even under declining temperature, i.e. P_{O2} strongly influences diffusion rates (Bethune *et al.*, 1968; Woodsworth, 1977).

The biotite flakes that are in contact with, or, in the pressure shadow areas of the M_2 garnets, particularly garnet showing chloritization, have a different composition from the biotite in the matrix. Biotites in the vicinity of fresh M_2 garnet have the same composition as the matrix biotite. Thus compositional changes in the garnet edges are probably partly the result of late-stage exchanges with other FAM minerals and are not related to the prograde reaction developing the garnet.

3.6 Biotite chemistry

3.6.1 Analytical data

The biotite chemical analyses are given in Table 3.6a, b, c and d grouped according to the co-existing garnet type. Apart from one S_4-biotite (Table 3.6d, No.17, Plate 2.11d) the analyses are of M_2-biotites (m). An M_2-biotite (m).analysis in a garnet-free rock is presented in Table 3.7e. Biotite (R.G.) from the pressure shadow areas of the M2 garnets or in direct contact with M_{2-4} garnet are also given.

Biotite (m), is characterised by a homogeneous composition throughout each probe section, so that three to four flakes were analysed and the average calculated. In common with muscovite iron is assumed to be in the ferrous state. This is probably a good assumption as Atherton (1968) and Mather (1970) determined a number of biotite compositions from the SW Dalradian rocks by wet chemical methods and found that $Fe^{2+} \rangle Fe^{3+}$.

The following are the main compositional features of the analysed biotite.

1. Both biotite (m) and M_4-biotite have uniform composition within the field of the thin section both in garnet-bearing and in garnet-free rocks, although there is some chemical variation within biotite composition from sample to sample. Biotite (m) has a similar composition to M4-biotite, both with interlayer site occupancy, being consistently less than two (per formula unit) which is a common feature and found elsewhere in the SW Dalradian (Atherton, 1968; Mather, 1970).

2. The biotite (m) composition is different from biotite (R.G.) within the same section with the latter showing much more variation of composition from sample to sample than the former. The octahedral content (based on 22(0)) for the biotite (m) ranges from 5.767 to 5.863 while for the biotite (R.G.) it is from 4.724 to 6.690. Generally the biotite (R.G.) has higher Al_2O_3 and FeO and less K_2O, MgO and TiO_2 than biotite (m). Biotite (R.G.) has identical composition to biotite (m) only when the garnet is not chloritized, e.g. m-3 and R.G.-3, Table 3.6a.

3. Mn is consistently below detection limit in both biotite (m) and biotite (R.G.) in rocks containing G_{2A} or G_{2B} but is higher in biotite in rocks containing G_{2C} or G_{2-4}.

4. The modal percentages of biotite (m) in rocks containing G_{2A} are significantly higher than those containing G_{2-4} (Fig. 3.2) and generally the modal % of biotite is not consistently linked to the bulk Al_2O_3 of the rock (Tables 1.1 and 1.2a; Fig. 3.21).

3.6.2 **Possible biotite-forming reaction(s)**

The biotite-forming reaction in M_2 garnet-bearing and garnet-free rocks could be:

phengitic muscovite + chlorite -- less phengitic muscovite + chlorite + biotite + H_2O. 3.7 (Atherton, 1977)

The antipathetic relationship between the modal percentage of muscovite and that of the biotite (Table 1.1) in these rocks is compatible with the possible consumption of muscovite during the biotite-forming reaction as in 3.7 (Atherton, 1977). Variations in biotite modal percentage may be due to (1)

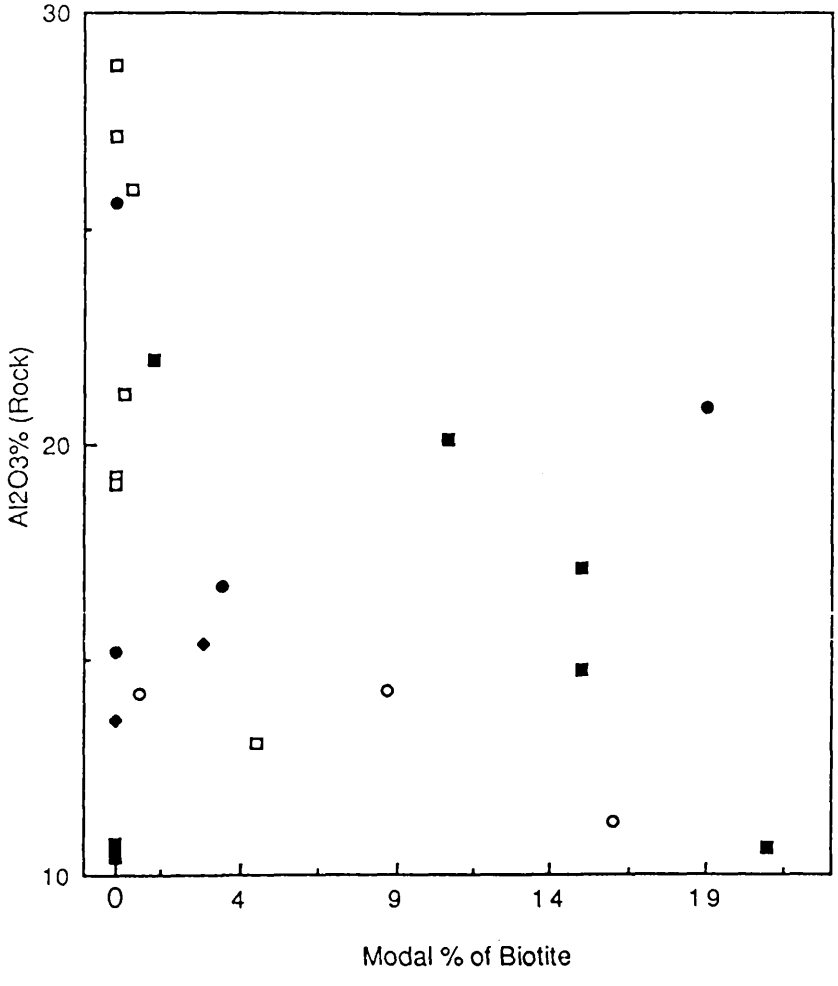

FIG.3.21 Modal % of biotite *vs* Al_2O_3 in the bulk rock composition

■ Rocks contain G_{2A}
○ Rocks contain G_{2B}
● Rocks contain G_{2C}
□ Rocks contain $G_{2\text{-}4}$
♦ Garnet-free rocks

TABLE 3.6a Chemical composition of biotitein rocks containing G_{2A} garnet in the Pitlochry Schist

Sp. No.	1	2		3		8		9
	m	m	R.G.	m	R.G.	m	R.G.	m
SiO_2	34.55	35.79	30.54	34.51	35.21	36.62	35.46	41.89
TiO_2	1.72	1.77	0.28	1.67	1.77	1.91	1.31	0.31
Al_2O_3	17.50	16.78	18.75	16.93	16.91	17.65	17.84	30.74
FeO	20.41	18.63	27.31	21.76	21.32	18.51	18.94	6.11
MgO	8.84	10.76	9.86	9.02	9.11	11.42	10.84	1.51
CaO	0.04	0.16	-	-	0.066	0.10	-	-
MnO	-	-	-	-	-	-	-	-
K_2O	7.26	8.23	4.40	8.68	9.01	8.76	8.99	8.10
Na_2O	0.27	0.33	0.36	-	-	0.10	-	1.30
TOTAL	90.59	92.45	91.49	92.57	93.40	95.07	93.38	89.95
Si^{iv}	5.515	5.566	4.965	5.476	5.525	5.532	5.488	6.047
Al^{iv}	2.485	2.434	3.035	2.524	2.475	2.468	2.512	1.953
Al^{vi}	0.808	0.642	0.557	0.643	0.653	0.675	0.742	3.279
Ti	0.207	0.207	0.034	0.199	0.210	0.217	0.152	0.034
Fe	2.725	2.422	3.712	2.889	2.797	2.338	2.452	0.737
Mg	2.103	2.493	2.388	2.132	2.131	2.570	2.500	0.326
Ca	0.007	0.026	-	-	0.011	0.012	-	-
Mn	-	-	-	-	-	-	-	-
Σvi	5.850	5.790	6.691	5.860	5.802	5.812	5.846	4.376
K	1.477	1.634	0.913	1.757	1.804	1.689	1.775	1.492
Na	0.084	0.099	0.112	-	-	0.028	-	0.364
K+Na	1.561	1.733	1.025	1.757	1.804	1.717	1.775	1.856
ΣAl	3.292	3.076	3.592	3.167	3.128	3.143	3.254	5.232
Mg/Mg+Fe	0.436	0.507	0.391	0.425	0.432	0.524	0.505	0.307

Ionic content calculated on the basis of 22(0). (See Fig. 1.4 for specimen location)
m = matrix biotite which is essentially that forming the S_2 fabric (except if stated otherwise)

TABLE 3.6b Chemical composition of biotite in rocks containing G_{2B} garnet in Ben Lui Schist

Sp No.	10	11		12	13
	m	m	R.G.	m	m
SiO_2	35.23	33.92	34.29	33.71	34.12
TiO_2	2.32	2.04	1.83	2.03	2.06
Al_2O_3	17.07	16.75	16.82	17.00	16.50
FeO	22.46	23.09	22.98	23.12	23.06
MgO	7.96	8.09	7.90	8.05	8.13
CaO	0.128	0.25	0.098	0.25	0.24
MnO	-	-	-	-	-
K_2O	8.63	7.81	8.09	7.32	8.30
Na_2O	-	-	-	-	-
TOTAL	93.79	90.93	92.01	91.47	92.41
Si^{iv}	5.520	5.430	5.482	5.421	5.439
Al^{iv}	2.480	2.570	2.518	2.579	2.561
Al^{vi}	0.672	0.592	0.653	0.644	0.439
Ti	0.274	0.246	0.224	0.245	0.247
Fe	2.942	3.092	3.074	3.110	3.074
Mg	1.858	1.930	1.883	1.930	1.931
Ca	0.021	0.042	0.017	0.042	-
Mn	-	-	-	-	-
Σvi	5.767	5.902	5.851	5.929	5.691
K	1.725	1.595	1.649	1.501	1.688
Na	-	-	-	-	-
K+Na	1.725	1.595	1.649	1.501	1.688
ΣAl	3.152	3.162	3.171	3.223	3.000
Mg/Mg+Fe	0.387	0.384	0.480	0.383	0.386

TABLE 3.6c Chemical composition of biotite in rocks containing G_{2C} garnet in the Pitlochry Schist

	22	23		25		26
	m	m	R.G.	m	R.G.	m
SiO_2	34.69	33.64	31.12	35.06	30.71	34.88
TiO_2	1.47	1.82	1.63	1.43	0.66	1.88
Al_2O_3	16.83	17.15	18.54	16.50	18.31	16.76
FeO	21.10	25.36	29.21	20.55	22.96	23.35
MgO	10.57	7.48	6.62	9.62	11.81	7.91
CaO	0.24	0.18	-	-	-	-
MnO	0.22	0.17	0.27	0.28	0.32	-
K_2O	7.25	7.03	3.74	9.04	5.23	8.44
Na_2O	-	-	-	-	-	-
TOTAL	92.37	93.84	91.14	92.48	90.00	93.48
Si^{iv}	5.456	5.348	5.093	5.550	4.996	5.500
Al^{iv}	2.544	2.652	2.907	2.450	3.004	2.500
Al^{vi}	0.577	0.563	0.672	0.629	0.509	0.616
Ti	0.174	0.218	0.201	0.170	0.081	0.223
Fe	2.774	3.505	3.999	2.720	3.125	3.080
Mg	2.477	1.774	1.616	2.270	2.864	1.858
Ca	0.040	0.030	-	-	-	-
Mn	0.029	0.023	0.037	0.037	0.044	-
Σvi	6.071	4.687	6.525	5.826	6.621	5.777
K	1.455	1.426	0.781	1.826	1.086	1.697
Na	-	-	-	-	-	-
K+Na	1.455	1.426	0.781	1.826	1.086	1.697
ΣAl	3.121	3.225	3.579	3.079	3.513	3.116
Mg/Mg+Fe	0.472	0.336	0.288	0.455	0.478	0.376

TABLE 3.6d Chemical composition of biotite in rocks containing the G_{2-4} garnet porphyroblast (5) from Pitlochry Schist lithologies; 16 and 17 are from Ben Lui Schist lithologies.

	5	16		17
	m	m	R.G.	*m-S4
SiO_2	34.56	40.02	29.18	35.11
TiO_2	0.20	0.51	0.26	1.88
Al_2O_3	27.92	29.56	24.23	17.16
FeO	18.06	7.64	24.95	21.61
MgO	5.01	3.07	7.68	8.37
CaO	0.16	-	-	-
MnO	0.93	0.16	-	-
K_2O	4.73	7.45	2.44	8.25
Na_2O	-	0.37	0.70	-
TOTAL	91.59	88.78	89.44	92.38
Si^{iv}	5.231	5.897	4.715	5.548
Al^{iv}	2.769	2.103	3.285	2.452
Al^{vi}	2.212	3.033	1.331	0.746
Ti	0.023	0.056	0.032	0.224
Fe	2.286	0.942	3.372	2.856
Mg	1.130	0.673	1.849	1.971
Ca	0.026	-	-	-
Mn	0.120	0.020	-	-
Σvi	5.797	4.724	6.584	5.797
K	0.914	1.401	0.502	1.664
Na	-	0.107	0.219	-
K+Na	0.914	1.508	0.721	1.664
ΣAl	4.981	5.136	4.616	3.198
Mg/Mg+Fe	0.331	0.417	0.354	0.408

*m-S_4 = matrix biotite that define the S_4 fabric

TABLE 3.6e Chemical composition of biotite in garnet-free lithology, Pitlochry Schists

	30 m
SiO_2	35.70
TiO_2	1.08
Al_2O_3	16.27
FeO	16.71
MgO	12.11
CaO	0.12
MnO	-
K_2O	8.97
Na_2O	-
TOTAL	90.97
Si^{iv}	5.622
Al^{iv}	2.378
Al^{vi}	0.643
Ti	0.128
Fe	2.202
Mg	2.843
Ca	0.021
Mn	-
Σvi	5.837
K	1.803
Na	-
K+Na	1.803
ΣAl	3.021
Mg/Mg+Fe	0.564

biotite destruction by reaction (Section 3.5.5), (2) significant differences in the activity of CO_2 affecting the promotion of the biotite-forming reaction (Graham *et al.* 1983) or (3) reversibility of the reaction of type 3.7, in lowering temperature. This suggests the M_{2-4} garnet-bearing assemblages with general sporadic biotite are more retrogressed than M_2-garnet-bearing assemblages, but it does not explain the absence of biotite in the M_2-assemblages with skeletal garnet porphyroblasts, e.g. 6, 7, Table 1.1).

The absence of D_1-M_1 biotite is probably due to the P-T conditions being outside those of biotite stability.

3.6.3 **Discussion**

The uniform M_2 and M_4-biotite (m) compositions within the same sample indicate homogeneous re-equilibration, even after the subsequent retrogression. Because biotite (R.G.) is compositionally different from biotite (m) only when chloritized garnet is present indicates the retrogression disturbed biotite composition in the vicinity of garnet. Generally such biotite (R.G.) composition is similar to the commonly reported metamorphic vermiculite composition (e.g. Black, 1975; Velde, 1978; Olives and Amouric, 1984; Maresch *et al.*, 1985; Woodland, 1985; Franceschelli *et al.*, 1986).

3.7 **Compositional variation of albite**

3.7.1 **Analytical data**

Microprobe analyses of porphyroblastic albite, including core and rim compositions, are given in Table 3.7 and Figures 3.22-25. The analyses are grouped in relation to the nature of the coexisting garnets G_{2B}, G_{2C}, G_{2-4} or garnet-absent. No albite porphyroblasts have been recognized in rocks with G_{2A} garnet.

1. Generally the porphyroblasts are unzoned with pure albite (An_O) cores and with slightly (An_1-An_3) anorthite richer rims (i.e. "reversely" zoned component with most metamorphic plagioclase). Two distinct types of rim zoning have been recognized.

a) The An_O core and the bulk of the crystal is surrounded by a narrow An_3 marginal zone which has a thin rim at the outermost edge of the crystal of An_0 (Figs 3.22-24).

b) The albite has a uniform core area (An_{1-2}) while at varying distances from the rim there is a zone with A_n richer (up to An_5) of variable composition (Fig. 3.24).

2. Both types of zoned albite occur in garnet-free rocks but only type a occurs in garnet-bearing rocks.

3. The first significant increase in An in both types varies from 30μm to 5μm from the albite edge. The zoned rims are better developed in micaceous matrix than in quartz-rich ones.

3.7.2 **Discussion**

"Reversely" zoned albite porphyroblasts are common in low grade metamorphic terrane and are considered to result from increase of grade with growth (Nord *et al* , 1978; Graps and Otsuki, 1983). Plagioclase is generally uniformly albitic in the Scottish Dalradian assemblage throughout the lower grade zones (Phillips, 1930; Ambrose, 1936) with no distinct compositional change across the garnet isograd (Jones, 1961; Misch, 1968; Atherton, 1977).

Plagioclase compositions in metamorphic rocks are generally thought to be controlled by internal structural mechanisms (e.g. growth rate influences) and external influences such as PT conditions and mineral reactions. Goldsmith (1982) has reviewed in detail the behaviour of plagioclase under metamorphic conditions and considered that both of the above mechanisms might operate.

However the absence of albite porphyroblasts in rocks containing G_{2A} garnets (although they occur in relatively nearby outcrops and grew syn-D_2 (Plate 2.12a)) probably suggests a rock compositional control. The lack of Ca in most of the porphyroblast shows that they cannot have been a reactant providing Ca to form G_{2B}, G_{2C} and G_{2-4} garnets. Presumably the garnet-forming reaction uses the available Ca in making the grossular component and

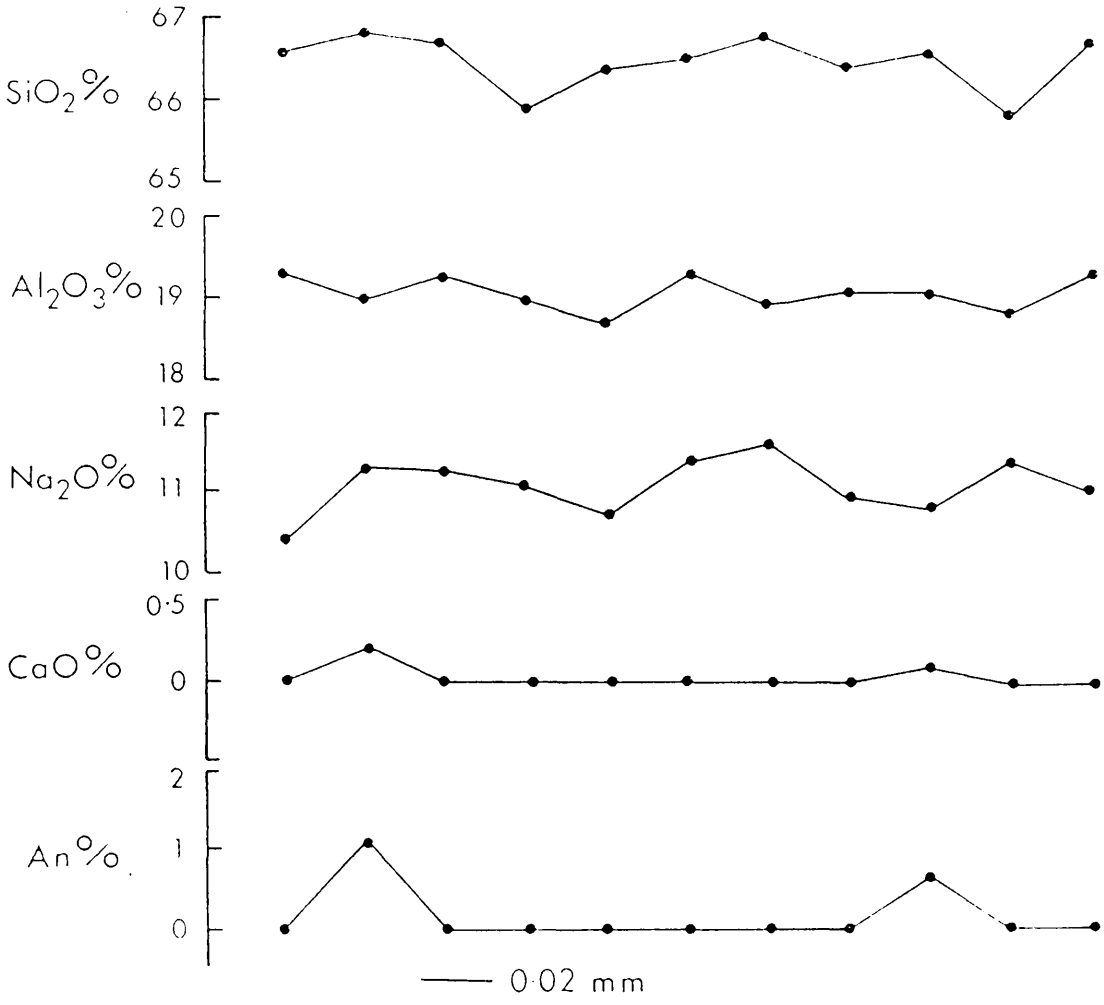

FIG. 3.22 Compositional profile of an albite porphyroblast crystal from specimen (25) showing type (a) zoning pattern

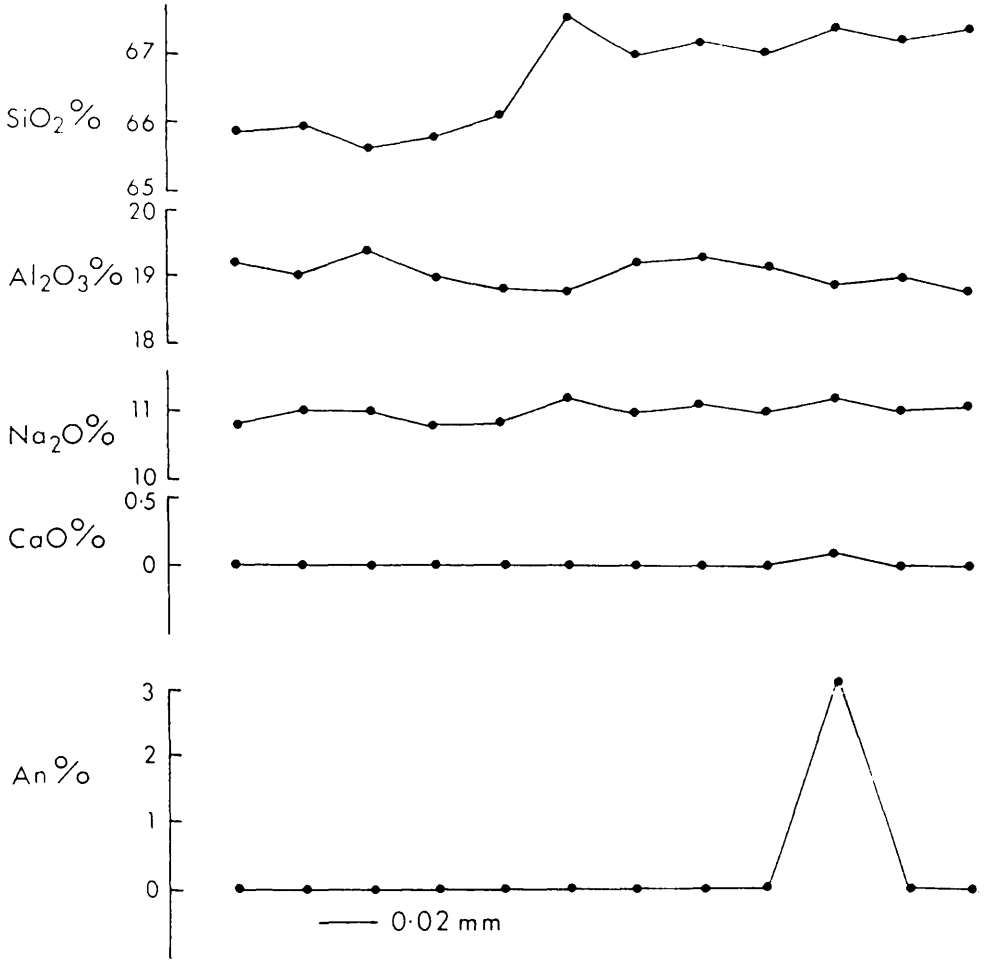

FIG.3.23 Compositional profile in albite crystal in specimen (17) showing asymmetrical type (a) pattern

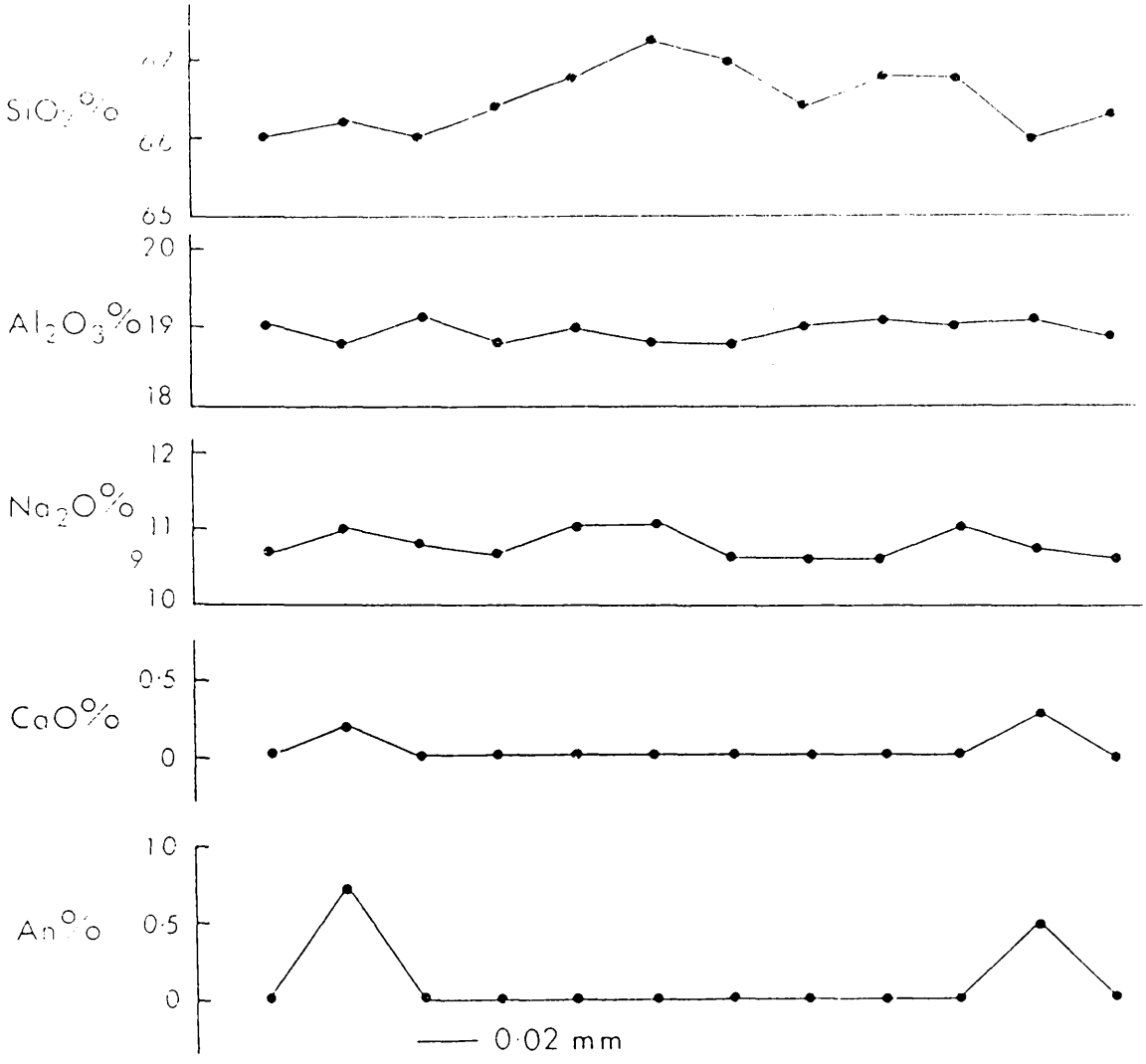

FIG. 3.24 Compositional profile in albite crystal from specimen (11) showing symmetrical type (a) pattern

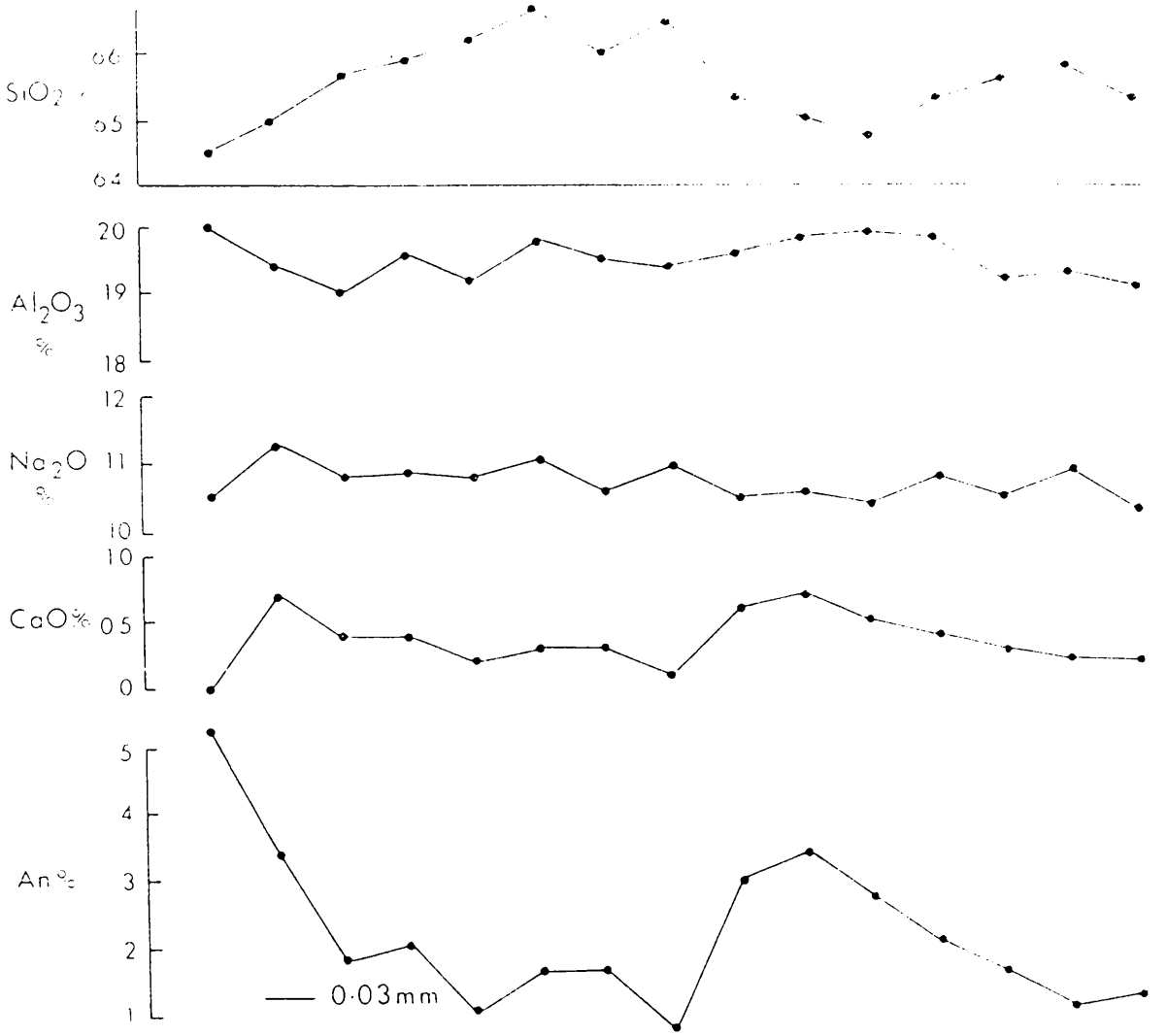

FIG. 3.25 Compositional profile in albite crystal in garnet-free rock showing type (b) pattern, specimen (29)

TABLE 3.7 **Analyses of albite porphyroblasts showing core and rim composition Specimen numbers are shown for reference (Fig. 1.4 for specimen locations)**

Sp.No.	10				11		22		23	
Lithological unit	G_{2B}-bearing Ben Lui Schist						G_{2C}-bearing Pitlochry Schist			
	rim	core	rim	rim	core	rim	rim	core	rim	core
SiO_2	68.20	67.35	67.94	66.82	67.30	67.61	68.05	69.16	67.74	67.93
Al_2O_3	19.86	19.38	19.60	19.54	19.41	19.42	20.67	19.88	19.68	18.91
CaO	0.11	-	-	0.154	-	-	0.87	-	0.35	-
K_2O	-	-	-	0.093	-	-	-	0.12	0.14	-
Na_2O	11.41	11.68	11.55	11.14	11.24	11.39	10.72	11.46	11.28	11.46
TOTAL	99.58	98.41	99.09	97.747	97.95	98.42	100.31	100.62	99.19	98.3
Si	11.932	11.937	11.955	11.931	11.977	11.945	11.817	11.985	11.921	12.035
Al	4.097	4.056	4.066	4.113	4.071	4.045	4.232	4.061	4.082	3.949
Ca	0.020	-	-	0.030	-	-	0.161	-	0.067	-
K	-	-	-	0.020	-	-	-	0.026	0.031	-
Na	3.870	4.018	3.939	3.857	3.878	3.901	3.609	3.850	3.846	3.934

TABLE 3.7 Contd...

Sp No.	16		17			29		
Lithological unit	G_{2-4}-bearing Ben Lui Schist					Garnet-free Pitlochry Schist		
	rim	core	rim	core	rim	rim	core	rim
SiO_2	67.50	67.74	65.98	67.61	67.40	65.80	66.20	65.91
Al_2O_3	19.18	18.91	19.97	19.30	18.85	19.10	19.10	19.16
CaO	-	-	0.63	-	-	0.13	-	0.10
K_2O	0.09	-	0.11	-	-	-	-	-
Na_2O	11.29	11.56	10.86	11.52	11.37	11.17	10.91	10.56
TOTAL	98.06	98.21	97.44	98.43	97.62	96.2	96.21	95.73
Si	12.006	12.021	11.824	11.985	12.039	11.941	11.986	11.981
Al	4.021	3.956	4.220	4.034	3.969	4.081	4.076	4.105
Ca	-	-	0.121	-	-	0.024	-	0.020
K	0.021	-	0.026	-	-	-	-	-
Na	3.892	3.977	3.774	3.960	3.936	3.929	3.830	3.720

only after garnet stops growing the Ca available goes to form the An-bearing outer part of some albites.

In many rocks epidote occurs as inclusions in albite, particularly in the core while it is absent or rare in the rock matrix. Hence a reaction of type 3.5 or 3.6 (see Section 3.5.5) could have operated which, after its cessation, allowed decomposing epidote to supply the An-component in a reaction of the following type:

albite + epidote + celadonitic muscovite + chlorite→zoned albite + less celadonitic muscovite + chlorite ± biotite ± oxides. 3.8

The better development of zoned albite rims in more micaceous layers than in quartz-rich layers suggests that reaction of type 3.8 were involved in the production of zoned albites (Jones, 1961; Bowes and Convery, 1966). There is no textural evidence to suggest that calcite was involved in formation of zoned albite.

Generally more data is needed to fully understand the development of the albite porphyroblasts.

3.8 Chemical composition of hornblende from the garnet-hornblende schists

The hornblende is generally bluish-green with a few crystals of a brownish-green colour.

The average chemical composition of both varieties (Table 3.8) exhibits no significant differences, with the brownish variety which is slightly richer in Fe and poorer in Ti than the bluish ones. The oxide totals of about 96% is generally low for a hornblende. This is probably due to the incorporation of much Fe^{3+}. The hornblende (both colour varieties) are generally subcalcic with CaO% very low. The generally high NaO and Al_2O_3 and low Ti indicate crystallization under relatively high pressure and low temperature conditions, respectively.

TABLE 3.8 Chemical analysis of hornblende from the garnet-hornblende schists

	Greenish-blue hornblende	Brownish-green hornblende
SiO_2	40.40	40.44
Al_2O_3	15.75	15.42
TiO_2	0.37	0.30
FeO	20.67	22.00
MgO	7.77	7.25
CaO	9.05	8.43
MnO	-	-
Na_2O	2.05	2.13
K_2O	0.36	0.38
TOTAL	96.42	96.35
Si	6.196	1.782
Al^{iv}	1.804	1.782
Al^{vi}	1.043	1.013
Ti	0.043	0.034
Fe^{2+}	2.651	2.829
Mg	1.775	1.662
Mn	-	-
Ca	1.485	1.388
Na	0.609	0.635
K	0.070	0.075
ΣAl	2.847	2.795

(Average of 3 analyses of each variety)

CHAPTER 4

PHYSICAL CONDITIONS OF GARNET GROWTH

4.1 Introduction

Essential to the main aim of this study is the determination of the physical conditions that operated during the growth of garnet which has been shown to have been during both the D_2 (M_2) and post-D_2 – pre-D_2 (M_{2-4} periods). The geothermometry and geobarometry used to establish these conditions is based on element partition between co-existing mineral pairs.

The partitioning of elements, particularly Fe^{2+} and Mg between garnet and biotite has been extensively investigated (e.g. Kretz, 1959; Frost, 1962; Albee, 1965; Saxena, 1969; Lyons and Morse, 1970), with advances in the last decade permitting reliable estimates of temperature to be made (e.g. Thompson, 1976; Ferry and Spear, 1978), although there is still considerable debate concerning the reliability of derived temperatures and efforts are still being made to extend their application at low grade conditions (e.g. Hynes and Foster, 1988). Reviews of the problems involved with P-T estimations are given by Essene (1982); Powell (1985); Hodges and Crawley (1985), and Hodges and McKinna (1987).

The distribution of elements between a pair of co-existing phases is a function not only of temperature, but also pressure and the composition of the phases. A critical component in the calibration is the equilibrium constant (K_D) which is related to the standard free energy (Gibb's energy) ΔG_o according to the equation (which provides the basis of P-T calculations).

$$\Delta G_o = -RT\,(K)\,\mathrm{Ln}\,K_D$$

where R = gas constant (1.987 cal. $mole^{-1}$ $degree^{-1}$)

T = temperature in degree Kelvin (K),

provided both the mineral phases form an ideal solid solution between end members.

4.2 Geothermometry

The partitioning of Fe^{2+} and Mg between co-existing garnet and biotite is temperature dependent and it has been calibrated using the following relationship:

$$\underset{(pyr.)}{{}^1/_3\ Mg_3\ Al_2\ SiO_3\ O_{12}} + \underset{(Ann.)}{{}^1/_3\ K\ Fe_3\ Al\ Si_3O_{10}\ (OH_2)} = \underset{(Alm.)}{{}^1/_3\ Fe_3\ Al_2\ Si_3\ O_{12}} + \underset{(phlo.)}{{}^1/_3\ K\ Mg_3\ Al\ Si_3\ O_{10}\ (OH)_2} \quad (4.1)$$

Such a cation exchange reaction is the basis of a potentially useful thermometer because (1) no fluid phase appears in the reaction and therefore the activity of volatile components such as H_2O and CO_2 are of less importance than in reactions involving the loss or gain of H_2O or CO_2 (Thompson, 1976), and (2) the reaction has a very small Δv of 0.019 cal/bar (Ferry and Spear, 1978), and thus is only slightly pressure dependent (Thompson, 1976), unless the pressure is very high (Albee, 1965; Perchuk, 1970). However where there is zonation shown by the garnet, caution is required (Yardley, 1977).

As this study is aimed at establishing the thermal history, as well as the peak metamorphic conditions reached, the least retrogressed compositions were considered separately from the retrogressed material (e.g. Dietvorst, 1982). In this regard the demonstration (Chapter 3) that the composition of biotite from the matrix is uniform, while that of the biotite near to garnet that shows retrogression may reflect some re-equilibration, is important. It cannot be shown unequivocally that the composition of the matrix biotite is that which was in equilibrium with the edge of the prograde garnet, but in the absence of evidence to the contrary, this has been assumed to be the case. The use of these matrix biotite compositions in estimation of temperature assumes that these compositions did not change during progressive re-equilibration that would be expected during the overall metamorphic history. However if there were changes to more Fe-rich compositions, the result would be smaller temperature decline than that calculated (Tracy *et al.*, 1976; Chamberlain and Lyons, 1983; Mohr *et al.*, 1986).

Thompson (1976) and Holdaway and Lee (1977) produced empirical calibrations of the garnet – biotite thermometer. The former is based upon analyses of cores of garnet crystals co-existing with biotite from metapelitic assemblages of low and medium grade. It uses independently determined temperatures for the studied rocks; and an empirical linear relationship between LnK_D and $10^4/T_k$ (op.cit, p. 429). This calibration is only well controlled at the lower temperature end with extrapolation by best-fit techniques to higher temperature regions. Hence any small error at the low temperature end will be magnified at a higher temperature.

The calibration of Holdaway and Lee (1977) is primarily based on the previous calibration. However these authors consider that the work of Osberg (1971), on which the lower temperature end of Thompson's calibration is mostly based, yields temperatures that are too low, and their calibration takes account of this.

Ferry and Spear (1978) published the only experimentally determined calibration of the garnet – biotite thermometer. It is based upon the partitioning of Fe^{2+} and Mg between pure end-members of the reaction of type 4.1 at 2.07Kb over the range of 550°C and 800°C. This calibration assumes that Fe^{2+} and Mg mix ideally in both garnet and biotite. However as it neglects the effect of posible octahedral substitution of Ca and Mn in garnet and Al^{vi}, Ti and Fe^{3+} in biotite its accuracy could be suspect (Hodges and Spear 1982; Pigage and Greenwood, 1982; Indares and Martignole, 1985). All three calibrations (Thompson, 1976; Holdaway and Lee, 1977; Ferry and Spear, 1978) have an uncertainty range of $\pm$ 50°C.

In the present study the three calibrations are initially used as they appeared in the literature (Table 4.1a, b) and then the mole fractions of Fe, Mg, Ca and Mn in garnet and Ti and Al^{iv} in biotite are considered (Table 4.2a), and the three calibrations applied again to the garnet rim compositions (Table 4.2b).

The estimated temperatures for the hornblende schists use the Graham and Powell (1984) geothermometer, which is based on the partitioning of Fe^{2+} and Mg between garnet and hornblende. This geothermometer is calibrated using the garnet – clinopyroxene thermometer of Ellis and Green (1979) applied to garnet – clinopyroxene – hornblende rocks. Its distribution coefficient (K_D) is also approximately independent of pressure. This thermometer is appropriate because of the abundance of the hornblende

and the non-ideal composition of biotite (Table 3.7, No.9). In addition textural investigation indicated that the garnet and hornblende are syngenetic M_2 growths.

The garnet core–matrix biotite temperatures are consistently lower than the garnet rim–matrix biotite temperatures (Tables 4.1a, b, respectively) which , except for sample 8, are similar to those obtained when the mole fractions of Fe, Mg, Ca and Mn in garnet and the Ti and Al^{+6} in biotite are considered (Table 4.2b). The Ferry and Spear (1978) calibration consistently yields temperatures lower than those of both Thompson (1976) and Holdaway and Lee (1977) which give comparable values. For sample 8 there is a marked difference in temperature between the original calculations and those obtained, when the mole fractions of octahedral components are used in the Ferry and Spear (1978) calibration. This sample initially yielded a temperature of $\underline{c}$. 600°C, (Table 4.1b) and, since the slope of Ln K_D versus T(K) of the Ferry and Spear (1978) calibration is markedly different from those of Thompson and Holdaway and Lee (Figure 4.1) it is to be expected that all three calibrations will yield very similar temperatures between 525° and 600°C; that of Ferry and Spear (1978) would yield higher temperatures above 600°C. If the calibration of Ferry and Spear (1978) is used (Table 4.2b) the highest temperature recorded (~660°C) is for sample 8 which contains the largest G_{2A} garnet porphyroblasts. Such high temperatures are substantially above those suggested by the mineral assemblage of the rock. The calcite-muscovite-quartz assemblage in this sample can be stable up to *c.* 600°C at uniform CO_2 and H_2O ratio (Sivaprakash, 1982, Fig. 5, Curve 4). This temperature is consistent with that obtained for Sample 8 (598°C) when only the mole fractions of Fe and Mg are calculated (Table 4.1b). Even so the notably higher temperature relative to the other G_{2A} bearing samples is considered to be due to the higher MgO in the garnet rim-composition used, which is directly correlated with the high MgO concentration in the bulk composition. Other G_{2A} garnet-bearing samples recorded 543C° (Sample 2), 482°C (Sample 3), and 423°C (Sample 1). The lowest temperature recorded, (~370°C) is for G_{2C}-bearing rocks, while the G_{2B}-bearing rocks recorded generally intermediate temperatures between the above values and ranged between 410°C and 450°C. Two samples containing the $G_{2\text{-}4}$ garnet recorded 482°C (Sample 5) and 377°C (Sample 17).

The garnet-hornblende schists (Sample 9) yielded temperatures of 517°C and 461°C for garnet-(rim)-hornblende and garnet-(core)-

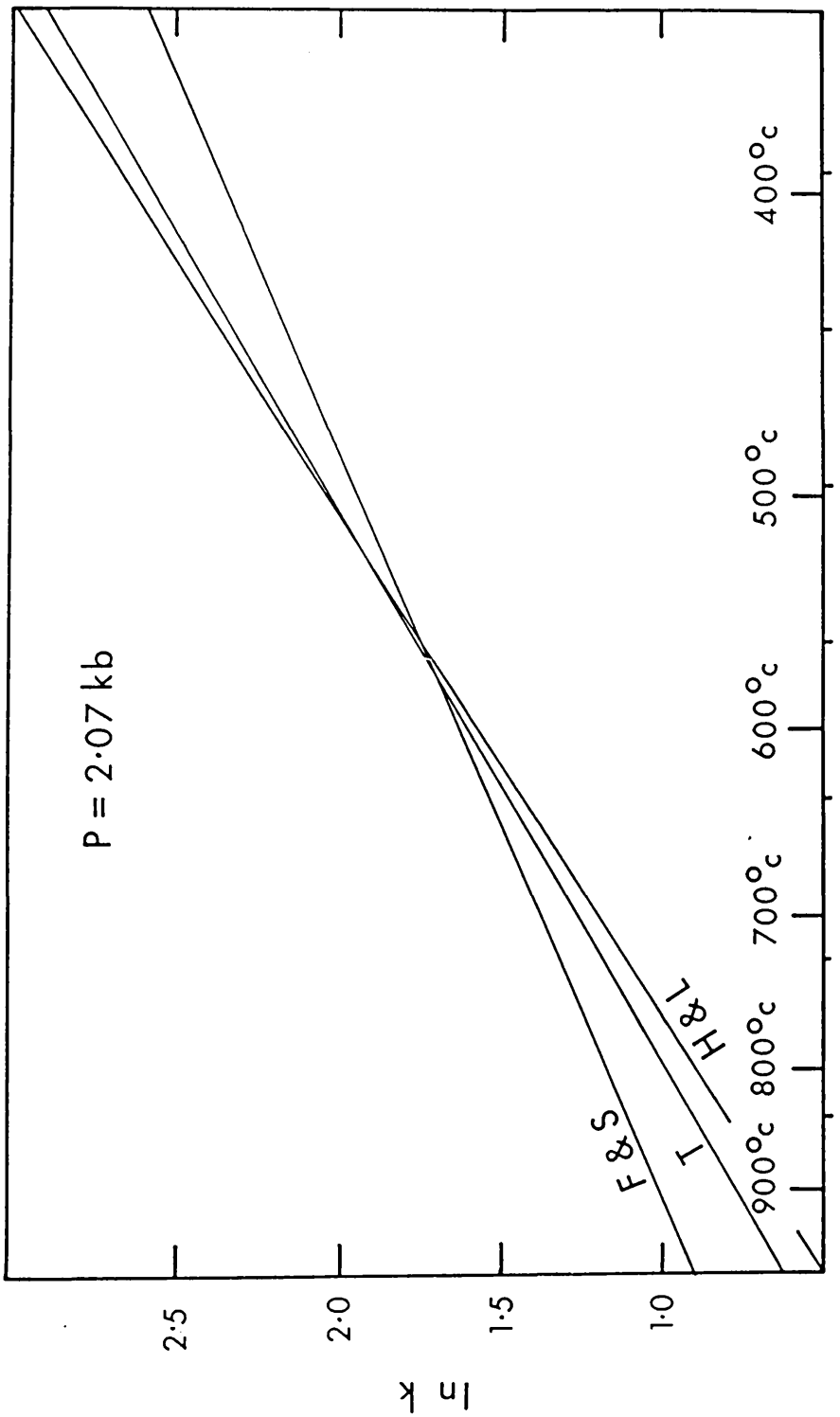

FIG. 4.1 Plot of LnK *vs* $10^4/T(K°)$

hornblende, respectively, using the Graham and Powell (1984) calibration (Table 4.3). As in the case of the garnet-biotite pairs, the temperature obtained using the garnet rim is higher than that using the garnet core, with the former considered to be the more meaningful temperature estimate for M_2.

4.3 Effect of octahedral substitution in garnet and biotite

The effect of octahedral substitution of Al^{vi}, Fe^{3+} and particularly Ti for Fe^{2+} and Mg in biotite decreases the K_D values of garnet-biotite pairs (Dallmeyer, 1974). This substitution increases the positive charges in the octahedral layers, an increase that is accommodated through increased Al^{3+} at the expense of Si^{4+} in the tetrahedral – and also by octahedral positions being left unoccupied (Foster, 1960). The result is a slight structural mismatch that favours the slightly larger Fe^{2+} over Mg in the octahedral layer. Therefore at constant temperature, increasing octahedral Ti, Al^{vi} and Fe^{3+} substitution results in the decrease of the K_D value and the overestimation of the temperature. This accounts for the temperature (449°C) calculated for the garnet G_{2B}-biotite pair for Specimen 10 (with higher Ti in the biotite) being higher than that calculated for Specimen 13 (410° – with lower Ti in the biotite). It is this latter temperature, determined in the specimen with the lowest Ti in the biotite that is considered to represent the best estimate of G_{2B} growth (Tables 4.2a, b).

Similarly the differences in temperatures calculated for the $G_{2\text{-}4}$ garnet-bearing rocks can be explained on the basis of the higher temperature recorded for Specimen 5B (with higher Al^{vi} in the biotite) than Specimen 17 (with lower Al^{vi} in the biotite), with the lower of the two temperature estimates (377°C) considered to be the better representative of the particular metamorphic conditions.

The effect of octahedral substitution of Mn and Ca for Fe^{2+} and Mg in garnet produces structural expansion that favours Fe^{2+} over Mg. This leads to increases in the K_D value that result in a lowering of calculated temperature (Dallmeyer, 1974). Such an explanation accounts for the temperature obtained for Specimen 1, in which $X_{Mn\text{-}Ca}$ in garnet is higher than in other G_{2A}-bearing samples.

The temperature derived using the calculation of Hodges and Spear (1982, equation 9) based on the composition-activity relationships in garnet has only been applied to data based on calibrations of Ferry and Spear (1978). The temperatures derived from this correction result in considerable increases in temperature estimates which, in the case of some of the samples, are inconsistent with the mineral assemblages present. For example, the 616°C value for Sample 2 is such that sillimanite development might be expected while the 821°C value for Sample 8 would be consistent with a high granulite facies mineralogy which is clearly not present. Accordingly it seems that this empirical correction of Hodges and Spear (1982) is unnecessary if the X_{Mn-Ca} in garnet is less than 0.2 and X_{Ti-Al}^{vi} in biotite is less than 0.15 (Ferry and Spear, 1978) with neither limit being exceeded for any of the samples investigated (Table 4.2b).

4.4 Temperature of retrogression

Temperatures of retrogression are based on garnet edge composition (Rr) and biotite matrix (hornblende for the hornblende schists)with data and temperatures for garnet – biotite schists and garnet – hornblende schists set out in Tables 4.5a and 4.5b, respectively. The very high difference between prograde and retrograde temperatures for Sample 8 (Table 4.5a) is mainly due to the lower MgO of the retrograde garnet composition relative to the higher MgO of the prograde garnet composition used in the calculations. Corresponding data when retrogressed biotite composition (R.G.) is used, and calculated temperatures, are set out in Table 4.5c. Although the data are limited, in the case of three samples, the temperatures of retrogression (and hence the difference between prograde and retrograde temperature estimates) are very similar to those determined when the composition of the unretrogressed matrix biotite is used in the calculations. The exception is Sample2 where a temperature higher than that determined for prograde metamorphism, and clearly inconsistent with the minerals present, is calculated (Table 4.2b) which is directly due to the non-ideal biotite composition used in the calculations. This biotite is quite different in composition from primary biotite in the rock matrix and has a chemical composition that is strongly constrained by its immediate environment with the retrogressed garnets.

4.5 Geobarometry

Metamorphic pressure estimates are generally rather imprecise compared with those for temperature. Among the geobarometers applicable to the Balquhidder rocks are those of Ghent and Stout (1981) and Powell and Evans (1983). The latter is preferred as the former (plagioclase-biotite-garnet-muscovite geobarometer) has the following disadvantages: (1) the activity composition relationships are such that where the anorthite content of the plagioclase is less than 8%, incomplete correction of deviations from the ideal molecular mixing is likely (Ghent and Stout, 1981), (2) the geobarometer was built on the geothermometry of Ghent *et al.,* (1982) in conjunction with the garnet-biotite thermometer of Ferry and Spear (1978) and assumes ideal mixing situations in all the participating minerals, which is clearly not the case for zoned garnets and plagioclase.

The biotite-muscovite-chlorite-quartz geobarometer of Powell and Evans (1983) is based on the Mg-Al celadonite substitution in muscovite in equilibrium with biotite and chlorite. Although it is insensitive to the oxidation state of the mineral phases it is, however, sensitive to within-sample variation in muscovite composition, which has been observed in the present samples.

Although, broadly, temperature and pressure increase together with increase of grade in metamorphic rocks, it is now well-known that P and T do not necessarily reach a peak together. Moreover mineral assemblages such as those with G_{2A}, G_{2B} , G_{2C} and G_{2-4} probably formed over a range of temperatures and pressures and since the prograde garnet rim compositions encompass syntectonic and post-tectonic growth temperatures and pressures were probably not precisely in step. Moreover, because the calculation of pressure is sensitive to the value of the temperature input to the formula calculating pressure, there is a strong correlation of high calculated pressure with high estimated temperature, which is an artefact of the method used. There is some constraint, however, on the estimates of pressure because they should be consistent with the petrogenetic grid results based on experimentally determined reactions (e.g. Harte and Hudson, 1979; Spear and Cheney, 1989) consequently a P-T-t path cannot readily be defined. In only one sample (3) are the essential requirements of the biotite-muscovite-chlorite-quartz geobarometer fulfilled and using the calibration of Powell and Evans (1983) a pressure estimate of 7Kb is calculated (Table 4.6), which is

likely to represent the peak metamorphic pressure. This is consistent with the pressure estimated for the most assemblages located in the Southern Highland Flat Belt (Dempster and Harte, 1986, p.99).

4.6 Summary

At pressures of 7 Kbar the following temperatures, based entirely on the calibration of Ferry and Spear (1978), were obtained (1) ~ 500°C for rocks containing G_{2A}, (2) ~410°C for rocks containing G_{2B}, (3) ~370°C for rocks containing G_{2C} and (4) ~370°C for rocks containing G_{2-4}. Because of the uncertainty of the degree of biotite re-equilibration during retrogression, it is not clear whether the temperature obtained represents a minimum or a maximum. Temperature estimates of retrograde metamorphism are generally slightly lower than prograde metamorphic temperatures, but in two samples (8 and 11) the retrograde temperatures are much lower than the prograde temperatures and indicate that retrograde equilibration has differentially changed much of the garnet edge-composition.

TABLE 4.1a Temperature estimates based on garnet (core) – biotite (matrix) compositions

Core	Sample No.	X^{gt}_{Fe}	X^{gt}_{Mg}	X^{gt}_{Fe}/X^{Bt}_{Fe}	X^{Bt}_{Fe}	X^{Bt}_{Mg}	X^{Bt}_{Mg}/X^{Bt}_{Fe}	K_D	LnK_D	T_1C^o	T_2C^o	T_3C^o
	1	0.953	0.047	20.274	0.564	0.436	0.773	15.673	2.752	394	397	334
G_{2A}	2	0.929	0.071	13.078	0.493	0.507	0.739	12.947	2.561	425	524	369
	3	0.946	0.054	17.519	0.575	0.425	0.739	12.947	2.561	425	524	369
	8	0.913	0.087	10.491	0.476	0.524	1.10	11.540	2.446	446	443	391
	10	0.956	0.044	21.736	0.613	0.387	0.630	13.694	2.617	416	416	358
G_{2B}	11	0.950	0.050	18.998	0.616	0.384	0.623	11.836	2.471	441	439	386
	12	0.964	0.036	26.778	0.617	0.383	0.621	16.629	2.811	385	388	324
	13	0.957	0.048	22.556	0.614	0.386	0.629	14.188	2.652	410	411	352
G_{2C}	25	0.960	0.040	24.00	0.545	0.455	0.825	20.040	2.998	358	363	294
	26	0.960	0.040	24.00	0.624	0.376	0.603	14.472	2.672	407	411	348
G_{2-4}	5	0.959	0.041	23.390	0.669	0.331	0.495	11.578	2.449	445	443	391
	17	0.959	0.041	23.390	0.592	0.408	0.690	16.139	2.781	390	393	329

T_1C^o = Thompson (1976) T_2C^o = Holdaway and Lee (1977) T_3C^o = Ferry and Spear (1978) assuming P = 6 Kbar
The garnet composition (core and rim) and the mean composition of matrix biotite used are those given in Tables 3.5a-d and Tables 3.7a-d, respectively.

$$K_D = \frac{X^{gt}_{Fe}}{X^{gt}_{Mg}} \cdot \frac{X^{Bt}_{Mg}}{X^{Bt}_{Fe}}$$

TABLE 4.1b Temperature estimates based on garnet (rim) – biotite (matrix) compositions

Rim	Sample No.	X^{gt}_{Fe}	X^{gt}_{Mg}	X^{gt}_{Fe}/X^{gt}_{Mg}	X^{Bt}_{Fe}	X^{Bt}_{Mg}	X^{Bt}_{Mg}/X^{Bt}_{Fe}	K_D	LnK_D	T_1C^o	T_2C^o	T_3C^o
	1	0.928	0.072	12.889	0.564	0.436	0.773	9.963	2.299	473	468	423
G_{2A}	2	0.866	0.134	6.461	0.493	0.507	1.029	6.649	1.894	560	545	529
	3	0.915	0.085	10.760	0.575	0.425	0.739	7.952	2.073	519	509	478
	8	0.830	0.170	4.883	0.476	0.524	1.10	5.371	1.681	615	593	598
	10	0.934	0.066	14.150	0.613	0.387	0.630	8.914	2.188	495	487	449
	11	0.935	0.065	14.386	0.616	0.384	0.623	8.963	2.193	494	486	448
G_{2B}	12	0.942	0.058	16.241	0.617	0.383	0.621	10.086	2.311	471	466	420
	13	0.944	0.056	16.857	0.614	0.386	0.629	10.603	2.361	461	457	410
G_{2C}	25	0.941	0.059	15.941	0.545	0.455	0.825	13.15	2.577	423	422	365
	26	0.954	0.046	20.74	0.624	0.376	0.603	12.506	2.526	432	430	375
G_{2-4}	5	0.940	0.060	15.673	0.669	0.331	0.494	7.743	2.047	525	514	485
	17	0.947	0.053	17.868	0.592	0.408	0.690	12.329	2.512	434	432	378

TABLE 4.2a Mole fractions of Fe, Mg, Mn and Ca in garnet (rim composition) and Fe^{2+}, Mg, Ti and Al^{vi} in matrix biotite

	Sample No.	Garnet				Biotite			
		X_{Fe}	X_{Mg}	X_{Mn}	X_{Ca}	$X_{Fe^{2+}}$	X_{Mg}	X_{Ti}	$X_{Al^{vi}}$
	1	0.739	0.057	0.015	0.189	0.466	0.360	0.035	0.138
G_{2A}	2	0.696	0.108	-	0.197	0.420	0.433	0.036	0.111
	3	0.768	0.072	0.016	0.144	0.493	0.364	0.034	0.110
	8	0.668	0.136	0.004	0.192	0.403	0.443	0.037	0.116
	10	0.723	0.051	0.027	0.199	0.512	0.323	0.048	0.117
G_{2B}	11	0.697	0.048	0.059	0.199	0.528	0.329	0.042	0.101
	12	0.692	0.043	0.057	0.208	0.525	0.326	0.041	0.112
	13	0.743	0.044	0.017	0.196	0.540	0.340	0.043	0.077
G_{2C}	25	0.534	0.034	0.126	0.282	0.470	0.392	0.029	0.109
	26	0.577	0.028	0.144	0.251	0.533	0.322	0.039	0.107
G_{2-4}	5	0.714	0.045	0.066	0.175	0.405	0.200	0.004	0.391
	17	0.686	0.038	0.041	0.234	0.493	0.340	0.039	0.129

The following are the formulae used to calculate the mole fractions (after Hodges and Spear, 1982, p.1127).

Garnet

X_{Fe} = Fe/Fe+Mg+Mn+Ca

X_{Mg} = Mg/Fe+Mg+Mn+Ca

X_{Mn} = Mn/Fe+Mg+Mn+Ca

X_{Ca} = Ca/Fe+Mg+Mn+Ca

Biotite

X_{Fe} = Fe/Fe+Mg+Ti+Al^{vi}

X_{Mg} = Mg/Fe+Mg+Ti+Al^{vi}

X_{Ti} = Ti/Fe+Mg+Ti+Al^{vi}

$X_{Al^{vi}}$ = Al^{vi}/Fe+Mg+Ti+Al^{vi}

TABLE 4.2b X_{Mn-Ca}, $X_{Ti-Al^{vi}}$, K_D values and temperature estimates obtained using 3 calibrations

Rim	Sample No.	X_{Mn-Ca}	$X_{Ti-Al^{vi}}$	K_D	LnK_D	T_1°C	T_2°C	T_3°C
	1	0.204	0.173	10.016	2.30	473	467	423
	2	0.197	0.147	6.644	1.89	561	546	530
G_{2A}	3	0.160	0.144	7.876	2.06	522	512	482
	8	0.196	0.153	4.505	1.51	665	635	663
	10	0.226	0.165	8.943	2.91	495	487	449
	11	0.258	0.143	9.050	2.20	493	485	446
G_{2B}	12	0.265	0.153	9.993	2.30	473	467	423
	13	0.213	0.120	10.632	2.36	461	457	410
G_{2C}	25	0.408	0.138	13.10	2.57	424	397	367
	26	0.395	0.146	12.449	2.52	432	431	377
G_{2-4}	5	0.241	0.395	7.835	2.06	522	512	482
	17	0.275	0.168	12.450	2.52	432	431	377

$$T_1(K) = \frac{2740 + 0.0234\ P\ (bars)}{LnK_D + 1.56} \pm 50^o \quad \text{Thompson (1976)}$$

$$T_2(K) = \frac{6150 + 0.0246\ P\ (bars)}{RLnK_D + 3.93} \pm 50^o \quad \text{Holdaway and Lee (1977)}$$

$$T_3(K) = \frac{4151 + 0.019\ P\ (bars)}{RLnK_D + 1.554} \pm 50^o \quad \text{Ferry and Spear (1978)}$$

TABLE 4.3 Temperature estimates for hornblende schists (sample 9) using garnet – hornblende geothermometer of Graham and Powell (1984)

	Garnet				Hornblende		K_D	LnK_D	T°C
	X_{Fe}	X_{Mg}	X_{mn}	X_{Ca}	X_{Fe}	X_{Mg}			
Core	0.665	0.030	0.073	0.232			12.523	2.53	461
					0.639	0.361			
Rim	0.710	0.049	0.028	0.213			8.186	2.10	517

$$K_D = X_{Fe} / X_{Mg} \cdot X_{Mg} / X_{Fe}$$

$$T(K) = \frac{2880 + 3280\ X_{Ca}}{LnKD + 2.426}$$

The garnet compositions (core and rim) and the mean composition of the hornblende used are those given in Tables 3.5a and 3.8,respectively.

TABLE 4.4 Garnet – biotite geothermometry; corrected form

	Sample No.	X^2_{Ca}	$X_{Fe} X_{Ca}$	$X_{Mn} X_{Ca}$	$X_{Mg} X_{Ca}$	LnK_D1	LnK_D2	LnK_DT	T°C*
	1	0.036	0.140	0.003	0.011	2.30	-0.310	1.99	501(+78)
	2	0.039	0.137	-	0.021	1.89	-0.259	1.631	616(+86)
G_{2A}	3	0.021	0.111	0.002	0.010	2.06	-0.208	1.852	542(+60)
	8	0.037	0.128	0.0007	0.026	1.51	-0.195	1.315	821(+158)
	10	0.040	0.144	0.005	0.010	2.19	-0.308	1.882	533(+84)
	11	0.040	0.139	0.012	0.010	2.20	-0.313	1.887	531(+85)
G_{2B}	12	0.043	0.144	0.012	0.009	2.30	-0.339	1.961	509(+86)
	13	0.038	0.146	0.003	0.008	2.36	-0.327	2.03	490(+80)
	25	0.080	0.151	0.036	0.010	2.57	-0.510	2.06	482(+115)
G_{2C}	26	0.063	0.145	0.036	0.007	2.52	-0.452	2.07	479(+102)
	5	0.031	0.125	0.012	0.008	2.06	-0.255	1.805	556(+74)
G_{2-4}	17	0.055	0.161	0.010	0.009	2.52	-0.423	2.097	472(+95)

* Temperature estimates based on Ferry and Spear (1978) calibration, corrected as suggested by Hodges and Spear (1982), where Margule parameter for Mg-Mn solid solution in garnet is taken to be equal to zero, as suggested by the authors (i.e. W_{Mg}-Mn = 0). Figures between brackets are the increased temperature from those calculated without correction in Table 4.2b

TABLE 4.5a Temperature estimates of retrogression based on Ferry and Spear (1978) calibration

Sample No.		Garnet				Biotite							
		X_{Fe}^{2+}	X_{Mg}	X_{Mn}	X_{Ca}	X_{Fe}	X_{Mg}	X_{Ti}	X_{Al}^{vi}	K_D	LnK_D	T°C	
	1	0.720	0.050	0.019	0.212	0.466	0.360	0.035	0.138	11.12	2.41	400	(-23)
	2	0.722	0.098	0.004	0.176	0.420	0.433	0.036	0.111	7.60	2.03	490	(-40)
G_{2A}	3	0.768	0.072	0.016	0.144	0.493	0.364	0.034	0.110	7.876	2.06	482	(0)
	8	0.679	0.094	0.018	0.209	0.403	0.443	0.037	0.116	7.94	2.07	479	(-184)
G_{2B}	10	0.710	0.049	0.028	0.213	0.512	0.323	0.048	0.117	9.14	2.21	444	(-5)
	11	0.670	0.030	0.073	0.227	0.528	0.329	0.042	0.101	13.92	2.63	356	(-90)
G_{2C}	25	0.507	0.033	0.159	0.301	0.470	0.392	0.029	0.109	12.81	2.55	371	(-7)
G_{2-4}	5	0.722	0.038	0.062	0.178	0.405	0.200	0.004	0.391	9.38	2.23	439	(-43)
	17	0.671	0.029	0.050	0.251	0.493	0.340	0.039	0.129	15.96	2.77	331	(-46)

Garnet edge (Rr) compositions are those listed in Tables 3.5a - d

Numbers between brackets are the difference between prograde and retrograde temperature estimates

TABLE 4.5b Temperature estimates of retrogression based on Graham and Powell (1984)

	Garnet				Hornblende				
Sample No.	X_{Fe}	X_{Mg}	X_{Mn}	X_{Ca}	XFe	XMg	KD	LnKD	ToC
9	0.720	0.051	0.027	0.199	0.639	0.361	7.976	2.08	511(-6)

Garnet (Rr) and hornblende compositions are those listed in Table 3.5a, No.9 and Table 3.8, respectively.

TABLE 4.5c Temperature estimates of retrogression based on Ferry and Spear (1978) calibration

		Garnet				Biotite							
Sample No.		X_{Fe}^{2+}	X_{Mg}	X_{Mn}	X_{Ca}	X_{Fe}^{2+}	X_{Mg}	X_{Ti}	X_{Al}^{vi}	K_D	LnK_D	T°C	
G_{2A}	2	0.722	0.098	0.004	0.176	0.555	0.357	0.005	0.083	4.739	1.556	645	(+115)
	8	0.679	0.094	0.018	0.209	0.419	0.428	0.026	0.127	7.379	1.999	498	(-165)
G_{2B}	11	0.670	0.030	0.073	0.227	0.527	0.323	0.038	0.112	13.690	2.617	358	(-88)
G_{2C}	25	0.507	0.033	0.159	0.301	0.475	0.435	0.012	0.077	14.070	2.644	353	(-14)

Garnet rim (Rr) composition and biotite (R.G.) compositions are those listed in Tables 3.5a-d and 3.7a-d, respectively

Numbers between brackets are the difference between prograde and retrograde temperature estimates

TABLE 4.6 Activity data and pressure estimate from biotite-muscovite-chlorite-quartz geobarometry.

Sample No.	X_{phl}	X_{mus}	X_{cel}	X_{clin}	L_nK	P (Kb) at
3	0.031	0.307	0.057	0.003	3.895	7.0

For equations used to calculate values of X, K ,see Powell and Evans (1983)

CHAPTER 5

SYNTHESIS AND DISCUSSION

5.1 Garnet distribution and development

Garnet occurs throughout the area north of Balquhidder - Loch Voil (Figs 5 1a,b). They are found below as well as above the so called "isograds" of both Elles and Tilley (1930) and Watkins (1984). Accordingly discussion of garnet distribution in relation to the position of an isograd in the area is not meaningful. In addition garnet growth is polyphase, having taken place during D_2 (the main growth of garnet) and post-D_2 – pre-D_4. This means that assessment of the position of isotherms – zones etc. must be made for more than one time period and studies that do not separate the different growths, and treat the distribution of garnet in a bulk manner, can only lead to confusion in assessment of the metamorphic development of this part of the Caledonides.

The distribution of garnet from outcrop to outcrop, and within individual outcrops, has a compositional control. This explains (1) the nearby occurrence of garnetiferous and non-garnetiferous rocks, (2) the occurrence of particular types of M_2 garnet (G_{2A}, G_2C) and the absence of the other type of M_2 garnet (G_{2B}) in the Pitlochry Schist and (3) the occurrence of only one type of M_2 garnet (G_{2B}) together with M_{2-4} garnet in the Ben Lui Schist. Evidence for this compositional control is set out in Chapter 3 and the various garnet expressions in different lithologies as set out and illustrated in Chapter 2.

The range (530 -367°C) determined for M_2 temperature from garnet-biotite and hornblende-biotite pairs must be assessed in the light of the controls of G_{2A}, G_{2B} and G_{2C} formations. On the basis of textural evidence all three expressions represent M_2 growth and the highest temperature determined (530°C for G_{2A}) is considered to be the peak temperature during D_2. It is not possible to state unequivocally the order of growth of G_{2A} *vs* G_{2B} *vs* G_{2C}, but the zoning profiles (Figs 3.7 - 19) represent typical prograde growth conditions. The 377°C temperature determination for the separate G_{2-4} growth is considered to approximate to peak conditions during the M_{2-4} "phase" (Chapter 4.3).

Any discussion of geothermal gradient based on temperature versus depth (elevation – there is *c.* 0.5km variation in topography in the area studied) can only be meaningful in the light of the above constraints. However the single determination of pressure of *c.* 7kb for a rock containing G_{2A} indicates a thermal

gradient of *c.* 27°C/Km during $D_2 - M_2$ on the basis that this pressure corresponds to the peak temperature (530°C) for M_2. Such a geothermal gradient is within the range of what is generaly accepted for Barrovian-type metamorphism (e.g. Miyashiro, 1973. One implication of this is that the M_2 almandine isograd ("boundary" of biotite and almandine zones) must be at least 2km away, presumed to be upwards on the basis of the regional flat-lying distribution of isograds in the Flat Belt. Another implication is that the staurolite isograd is not far away (downwards) or that staurolites might have formed in the Balquhidder district – had there been rocks of suitable composition.

The interpretation of Watkins (1984) of the existence of a flat-lying garnet isograd and of inverted zones near Balquhidder (Fig. 5.1a) and between Balquhidder and Lochearnhead (Fig. 1.2) would appear to be related to the development of G_{2C} in a particular flat-lying lithological unit in the Pitlochry Schists. This conclusion is based on the correspondence both in grain size and temperature of growth of G_{2C} determined in this rock with that of the size and temperature of the garnets determined by Watkins (1985, fig.2, p.159). His statement (1985, p.163) that the garnets are post-M_2 is unsupported by any textural evidence. The differently placed flat-lying "isograd" and the "inverted" zones of Elles and Tilley (1930) would appear to be related to the development of G_{2B} and G_{2-4} in particular flat-lying lithologies in the Ben Lui Schists.

The representation by Watkins (1984 Fig. 1) of a steeply-dipping to vertical isograd further W (e.g. Gleann Crotha - Fig. 5.1c) could have been influenced by the localized occurrence of prominent G_{2A} garnets: it has no basis from the mapped distribution of all types of garnet. The westward continuation of this "isograd" is depicted by Watkins (1984, Fig. 1) in a way which, when put on a contoured map, indicates variation from steeply-dipping to shallowly-dipping and from southerly-dipping to northerly dipping. It can only be assumed that such an irregular pattern, that is unlike any other known for an isograd in Barrovian-type terrane, results, at least in part, from treating all types of garnet in a bulk manner and excluding compositional controls of growth.

5.2 Conditions of metamorphism

5.2.1 M_1

There is no mineral assemblage that permits P-T conditions for M_1 to be closely constrained. However the very small amounts of M_1 muscovite (phengite) and chlorite (a Fe-rich chlorite, Table 3.1d, No.29) that survived M_2 are indicative of a low metamorphic grade (see Plates 1.2a and 2.1a). This conclusion is supported by the fine grain size of the inclusions in M_2 porphyroblasts: quartz, epidote and micas in garnet, albite, biotite and hornblende (see Table 2.3).

5.2.2 M_2

D_2 deformational phase was particularly strong concomitant with the widespread development of S_2-fabric and M_2 metamorphic reconstitution. During the M_2 phase muscovite, chlorite, garnet, biotite, albite, quartz and hornblende grew, with all except chlorite and quartz expressed, at least in part, as porphyroblastic crystals. Matrix grain-coarsening took place, probably mainly late in D_2. This has been shown by the size of the Si quartz inclusions in syn-D_2 garnet cores relative to those at the rims (see Plate 2.6a). The S_2-mica schistosity which is the dominant fabric expression in the area was used as a "datum" for determination of the relative time of mineral growth, particularly garnet. From garnet-biotite and garnet-hornblende pairs a maximum of *c.*530°C has been determined for M_2 temperature, and from biotite-muscovite-chlorite-quartz assemblage the pressure has been determined as being *c.* 7Kb. These values mean that M_2 can be considered generally as being of mid-amphibolite facies. They are consistent with the quartz-chlorite-almandine ($\pm$ biotite) mineral assemblage on the basis of known data for the chlorite + quartz = garnet and chlorite + muscovite + quartz = garnet + biotite reactions, *c.* 450-500°C and 6.7Kb – e.g. Spear and Cheney (1989, Fig. 1).

5.2.3 Post-M_2 – pre-M_4 (including M_3)

The static growth of post-M_2 garnet that can be definitely constrained to be pre-M_4 could have been pre-M_3 (see Chapter 2, p.). The 377°C determined for

its temperature of growth is considered to be a temperature near to the maximum conditions, which thus correspond to upper green schist facies.

The only known metamorphic mineral growth that can be unequivocally assigned to M_3 is that of a few flakes of muscovite and chlorite defining weakly developed S_3 (Plate 2.2a) and thus a dynamic (D_3) growth.

This is also likely to represent greenschist facies conditions but there is no evidence on which to base specific P-T or whether temperature increased or decreased following garnet growth. It is possible that there was continued growth of muscovite, chlorite, epidote and probably tourmaline growth at this stage (Table 2.3) but the textural evidence is unavailable in the rocks examined. Some such continued growth could have been post-M_4.

5.2.4 M_4

D_4 is characterised by open flexural folds, kink bands and crenulation cleavage. These features are indicative of low temperature, possibly spanning the zone of the beginning of metamorphic mineral growth into the lowermost parts of the greenschist facies. At this stage some further mimetic recrystallization, particularly of phyllosilicates, could have taken place. The presence of very localized S_4 muscovite and biotite possibly indicates the existence of local fluid flow.

5.2.5 $M_{post\text{-}4}$ (Prograde)

The development of late muscovite and albite (Plates 2.2c and 2.13, respectively) which are prominent in places, marks the last recognized prograde mineral growth at Balquhidder. These $M_{post\text{-}4}$ static growths of muscovite would suggest a thermal regime but there is no evidence concerning the nature of the heat source. Detailed evidence relating to the growth of albite is outside the scope of the present investigation as it does not materially affect studies of earlier-formed Barrovian zones. There is much controversy concerning the heat source, but there is general agreement that the large albite porphyroblast growth is late in the metamorphic-deformational history (Jones, 1960; Mathavan, 1984)

The limits of albite porphyroblasts given by Jones (1961) (see Fig. 1.2) point to an essentially post-tectonic development.

5.2.6 $M_{post\text{-}D4}$ (Retrograde)

Other post-D_4 metamorphic activity is retrogressive and most noticeably is seen as the alteration to chlorite of the M_2-garnet, M_2-biotite, $M_{2\text{-}4}$ garnets and M_4-biotite. The beginning of the retrogressive alteration may be related to D_4 deformational phase (which is associated with regional uplift - see 5.3) and continues thereafter. It is possible, however, that late development of both the regional chloritization and the growth of $M_{post\text{-}4}$ albite porphyroblasts genetically related (Jones, 1964). However as yet this is uncertain. Generally the retrograde conditions of metamorphism cannot be explained solely by decreasing temperature of deformation, because chloritized and unchloritized minerals often occur together in variable proportions and, commonly in the same thin section. Since all samples are from a generally restricted area, and approximately the same structural level, similar P-T conditions during uplift and cooling are assumed. The variability of development of retrograde textures, however suggests that the different minerals may have re-equilibrated at different times, and thus under different P-T conditions, which may also reflect local variation in the availability of fluids for hydration reactions.

5.3 Balquhidder in the Scottish Caledonides

In common with many other parts of the Dalradian flat belt the rocks at Balquhidder reveal evidence of a polyphase deformational and a polyphase metamorphic history. Both the field and microstructural evidence e.g. (Plate 1.1, 2, 3) indicate a $D_1 - D_4$ sequence of progressive fold and foliation development. Although the intensity of expression of the different structural elements varies from place to place the overall $D_1 - D_4$ development is clearly the same as that of nearby areas. However there is no obvious expression of D_5 structures seen in the Loch Lomond area (McArthur, 1971; Bowes, 1973, 1979; Mathavan, 1984). It is also consistent with the $D_1 - D_4$ deformational sequence found regionally (Harte *et al.*, 1984; Fig.1.2; see Chapter 1), in which the major structures are the D_1 Tay Nappe, (which caused inversion of the stratigraphy) and the D_4 open folds (e.g. Ben Lawers synform, etc.). The demonstration that the major fabric-forming and mineral-growth event is associated with D_2 (M_2) and that there was only limited post-D_2 dynamic mineral growth means that the products of the climactic metamorphism remain largely extant, (but with mimetic recrystallization, grain

growth etc.) and the gross disposition of the M_2 palaeoisotherms must remain. This is apparent from the regional pattern of isograds (Fig. 1.1). There is no evidence of the existence of structures away from the Highland Border Downbend that could result in major changes in their disposition, while the evidence of Richardson and Powell (1976) indicates the garnet isograd is essentially coincident with an isotherm.

The interpretation of Watkins (1984) that the isograd-isotherm pattern in the Balquhidder-Lochearnhead district is anomalous, when taken in the regional context of zonal patterns, and the proposal of an inverted thermal gradient is not closely integrated with textural studies demonstrating times of mineral growth and is based on a distribution of garnet which this study shows to be incorrect. Accordingly, additional discussion here of specific aspects of the model presented by Watkins (1984) is not considered to be relevant. The interpretation of a structural inversion of isograds proposed by Elles and Tilley (1930) is now known to be inconsistent with the regional structure (see also 5.1).

The evidence for increasing grade of metamorphism leading to climactic conditions during M_2 is consistent with crustal thickening due to tectonism (associated with nappe formation) using the model of England and Richardson (1977). Both the regional continuity of D_1 structures and the regional expression of the $D_1 - D_4$ structural sequence permits the time of the M_2 metamorphism at Balquhidder to be constrained as being pre-590Ma (Rogers *et al.* , 1989) and to be an expression of what these authors redefine as the Grampian Orogeny. The M_{2-4} ($?M_{2-3}$) static garnet growth and the M_3 dynamic mineral growth are interpreted as the result of heating associated with a separate crustal thickening event. Again on the basis of regional correlations, the D_3 event at Balquhidder is constrained to be *c.*500-490Ma (Rogers *et al.*, 1989, table 2). The crustal thickening would have been somewhat earlier "possibly around 520Ma" (Rogers *et al.*, 1989, p.796), with the increasing grade of metamorphism following the model of England and Richardson (1977). The existence in a flat-lying assemblage, with varying lithological types, including pelites and the very strong development of the S_2 (Sc) fabric, means that this crustal thickening could have taken place by movement essentially parallel to S_2 (Sc) and particularly in the less competent units. Such activity would account for the very patchy (presumed relict) distribution of the stretching lineation (L_2) and it is expected that there would have been mimetic recrystallization of M_2 phyllosilicates. The F_3 structures seen are interpreted as representing a late stage in this crustal thickening event in the more competent lithologies. Their patchy distribution and relatively small size are consistent with the dominance of slip

movement along pre-existing plane structures. On the basis that the thermal gradient during M_3 was similar to the thermal gradient during M_2, the features seen represent deformation and recrystallization in basement rocks at a depth of *c.* 15km.

Regionally D_4 is related to uplift and while it may have spanned a considerable time period it is well constrained to be *c.* 460Ma (Harte *et al.*, 1984). Upright F_4 axial planes and local S_4 would provide channelways for fluid movement which is interpreted to have been involved in the development of some S_4 minerals and continued during the post-M_4 retrogression. Neither the time nor the genetic relationships of the retrograde post-M_4 activity to the prograde post-M_4 activity is known. However the latter has the features of static growth consistent with thermal metamorphism but the present study is unable to assess either the nature of the heat source or whether there was any associated hydrothermal activity. The possibility of the existence of a late Caledonian igneous mass (es) as the heat source must be borne in mind.

The metamorphic history determined for the Balquhidder district would appear to be similar to, and possibly representative of, a considerable area of Dalradian rocks in the SW Highlands. It clearly differs from the metamorphic history in NE Scotland where the peak of metamorphism is generally D_3, thermal gradients can be higher (Buchan-type) and there were large masses of basic magma emplaced about D_3 time. Whether the NE Scotland presents a major D_3 thermal overprint of a Balquhidder-SW Scotland-type terrane where the climactic conditions are D_2 is a matter for further investigation.

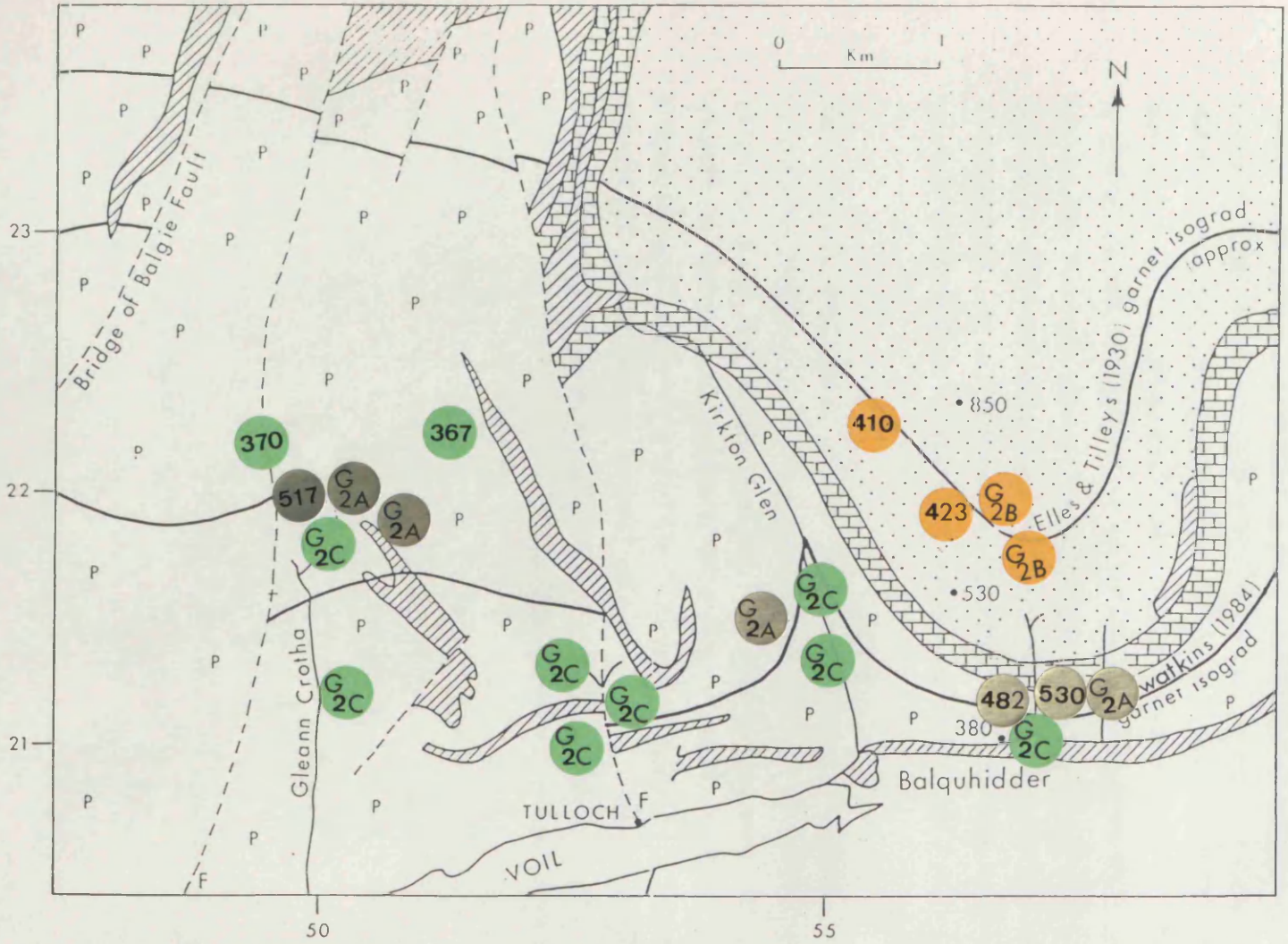

FIG. 5.1a Geological map of the Balquhidder area showing temperatures in °C derived from garnet-biotite and garnet-hornblende geothermometry for rocks containing G_{2A}, G_{2B} and G_{2C} garnet phase (*cf.* Fig. 1.4 for sample numbers)

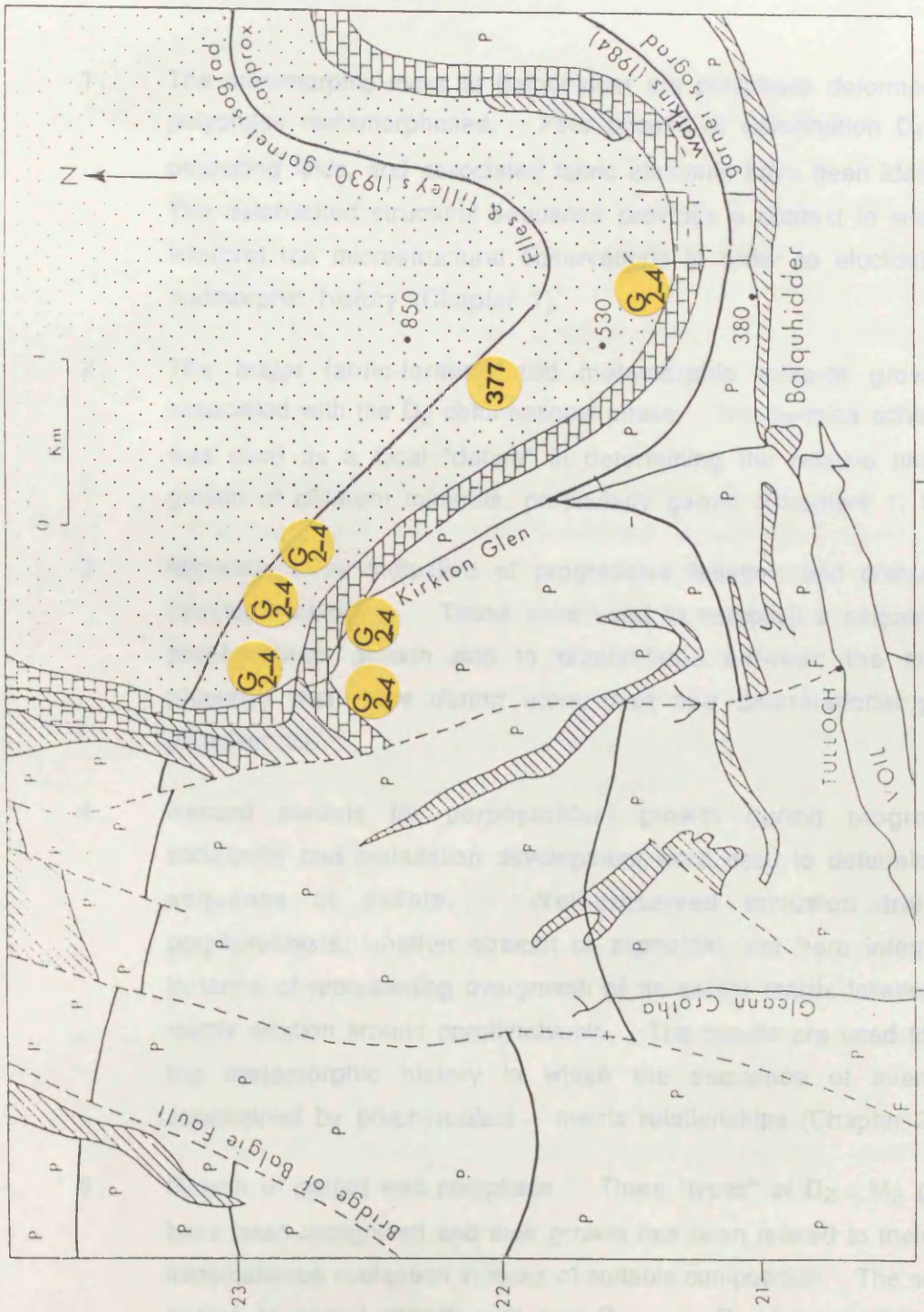

FIG. 5.1B Geological map of the Balquhidder area showing temperatures in °C derived from garnet-biotite geothermometry for rocks containing the $G_{2\text{-}4}$ garnet phase (*cf.* Fig. 1.4 for sample numbers)

CHAPTER 6

CONCLUSIONS

The following are the major conclusions from this study.

1. The metamorphic rocks at Balquhidder are polyphase deformed and polyphase metamorphosed. Four phases of deformation $D_1 - D_4$ producing folds, and associated fabric elements have been identified. The established structural sequence provides a context in which to interpret the microstructural observations in order to elucidate the metmorphic history (Chapter 1).

2. The major fabric-forming and metamorphic mineral growth is associated with the D_2 deformational phase. The S_2-mica schistosity was used as a local "datum" in determining the relative times of growth of different minerals, particularly garnet (Chapters 1, 2).

3. Microstructures indicative of progressive foliation and crenulation development occur. These were used to establish a sequence of porphyroblast growth and to discriminate between the mineral phase(s) that grew during more than one deformational phase (Chapter 2).

4. Recent models for porphyroblast growth during progressive schistosity and crenulation development were used to determine the sequence of events. Well-preserved inclusion trails in porphyroblasts, whether straight or sigmoidal, are here interpreted in terms of representing overgrowth of an earlier matrix foliation and matrix rotation around porphyroblasts. The results are used to infer the metamorphic history in which the sequence of events is constrained by porphyroblast – matrix relationships (Chapter 2).

5. Growth of garnet was polyphase. Three "types" of $D_2 - M_2$ garnet have been recognized and their growth has been related to their non-instantaneous nucleation in rocks of suitable composition. The second period of garnet growth was post-D_2 – pre-D_4, but possibly post-D_2 – pre-D_3 (Chapter 2).

6. All garnets exhibit growth zoning patterns indicative of prograde conditions during both M_2 and M_{2-4}. The garnets are characterized by decreasing amounts of Mn and Ca, shown by bell-shaped growth zoning curves, while Fe, Mg and the Mg/Fe ratio increase from core towards the rim due to reaction partitioning.

7. No single dominant reaction was responsible for producing garnets (chapter 3.5.5).

8. The type of garnet-producing reaction depended primarily on bulk rock composition which influenced the chemistry of the reactant phases. This controlled both the type of garnet developed and whether garnet is developed or not, and is used to explain (1) the nearby occurrence of garnetiferous schists and non-garnetiferous schists and (2) the presence of different types of garnet in the Pitlochry Schist (G_{2A}, G_{2C}) and in the Ben Lui Schist (G_{2B}, G_{2-4}) lithologies (Chapter 3).

9. The compositions of garnet rims and matrix biotite are used in the Ferry and Spear (1978) geothermometer to estimate temperature of M_2 and M_{2-4} garnet growths, while the composition of garnet rims and hornblende are used by Graham and Powell (1984) to estimate temperature of M_2 garnet growths in the hornblende schists. Temperature estimates for M_2 garnets are 530 – 482°C for type G_{2A}-almandine, 423 – 410°C for type G_{2B}-almandine and 370°C for type G_{2C}- spessartine-rich (Chapter 4).

10. It was not possible to predict unequivocally the order of growth of G_{2A} *vs.* G_{2B} *vs.* G_{2C}, but the growth zoning curves represent typical prograde growth conditions. The 530°C is considered to represent peak temperature during M_2. The temperature obtained for the G_{2-4} phase is 377°C and is considered to approximate to peak conditions during M_{2-4} (Chapter 4).

11. A single determination of pressure based on biotite – muscovite – chlorite – quartz geobarometer of Powell and Evans (1983) is 7Kb for a sample that contains the G_{2A} garnet phase.

12. On the basis of a peak temperature of 530°C and a pressure of 7Kb a Barrovian type geothermal gradient of *c.* 27°C/Km is deduced (Chapter 5).

13. Garnets are found throughout the whole Balquhidder area so that interpretations of inverted zonation, based on their occurrence only in lithologies at higher topographic levels, cannot be sustained (Chapter 5).

14. The garnet isograd is at least *c.*2Km above the present topography and the area studied is entirely within the M_2 almandine zone. It is possible that the initiation of staurolite growth could have taken place had there been rocks of suitable composition, but there is no garnet-biotite boundary present (Chapter 5).

15. On the basis of regional structural correlations, D_1 (M_1) _ D_2 (M_2) took place before 590Ma and are assigned to the Grampian Orogeny as redefined by Rogers *et al.* (1989). The M_{2-4} garnet growth, and D_3 are *c.* 75-100Ma younger and represent metamorphic-tectonic activity in basement crystalline rocks. D_4 is related to the major uplift period *c.* 460Ma ago (Chapter 5). There was subsequent prograde and retrograde mineral growth but this was not related to Barrovian zone formation.

16. The deformational and metamorphic history within Balquhidder area generally corresponds to, and may be representative of, Caledonian activity in at least considerable parts of the SW Highlands

REFERENCES

ALBEE, A.L. 1965b. Distribution of Fe, Mg and Mn between garnet and biotite in natural mineral assemblages. **J. Geol. 73**, 155-164.

AMBROSE, J.W. 1936. Progressive kinetic metamorphism in the Missi series near Flinflon, Manitoba. **Am. J. Sci. 32**, 257-286.

ANDERSON, D.E. & BUCKLEY, B.R. 1973. Zoning in garnets-diffusion models. **Contrib. Mineral. Petrol. 40**, 87-104.

ATHERTON, M.P. 1964. The garnet isograd in pelitic rocks and its relation to metamorphic facies. **Am. Mineral. 49**, 1331-1349

ATHERTON, M.P. 1968. The variation in garnet, biotite and chlorite composition in medium grade pelitic rocks from the Dalradian, Scotland, with particular reference to the zonation in garnet. **Contrib. Mineral. Petrol. 18**, 347-371.

ATHERTON, M.P. 1977. The metamorphism of the Dalradian rocks of Scotland. **Scott. J. Geol. 13**, 331-370.

ATHERTON, M.P. & BROTHERTON, M.S. 1982. Major element composition of the pelites of the Scottish Dalradian. **Geol. J. 17**, 185-221.

ATHERTON, M.P. & EDMUNDS, W.M. 1966. An electron microprobe study of some zoned garnet from metamorphic rocks. **Earth Planet.Sci. Lett. 1**, 185-193.

BALL, T.K. 1965. Element distribution in two epidiorite sills from the central Grampian Highlands of Scotland. **Geol. Mag. 102**, 91-105.

BALTATZIS, B. 1979. Distribution of Fe and Mg between garnet and biotite in Scottish Barrovian metamorphic zones. **Mineral. Mag. 43**, 155-157.

BANNO, S. 1964. Petrologic studies on Sanbagawa crystalline schists in the Bassi-Ino district, central Sikoku, Japan. **J. Fac. Sci. Univ. Tokyo 15**, 203-319.

BANNO, S. & KURATA, H. 1972. Distribution of Ca in zoned garnet of low-grade pelitic schists. **J. Geol. Soc. Japan 78**, 9, 507-512.

BARROW, G. 1893. On an intrusion of muscovite-biotite gneiss in the south-eastern Highlands of Scotland, and its accompanying metamorphism. **Q.J. geol. Soc. London 49**, 330-58.

BARROW, G. 1912. The geology of Lower Deeside and the Southern Highland Border. **Proc. Geol.Assoc. 23**, 268-90.

BELL, T.H. 1981. Foliation development: the contribution, geometry and significance of progressive, bulk inhomogeneous shortening. **Tectonophysics 75**, 273-296.

BELL, T.H. *et al.* 1986. Porphyroblast nucleation, growth and dissolution in regional metamorphic rocks as a function of deformation partitioning during foliation development. **J. met. Geol. 4**, 37-67.

BELL, T.H. & CUFF, C. 1989. Dissolution, solution transfer, diffusion versus fluid flow and volume loss during deformation/metamorphism. **J. met. Geol. 7**, 425-447.

BELL, T.H. & JOHNSON, S.E. 1989. Porphyroblast inclusion trails: the key to orogenesis. **J. met. Geol. 7**, 279-310.

BELL, T.H. & RUBENACH, M.J. 1983. Sequential porphyroblast growth and crenulation cleavage development during progressive deformation. **Tectonophysics 92**, 171-194.

BÉTHUNE, P. de,*et al.* 1968. Grenats zonés de la zone du Mont Rose (Valle Anzasca, Prov. de Novara, Italie). **Bull. suisse Minéral. Pétrog. 48**, 437-454.

BÉTHUNE, P. de, *et al.* 1975, Diffusion processes in resorbed garnets. **Contrib. Mineral Petrol 50**, 197-204.

BHATTACHARYY, D.S. & DAS, K.K. 1983. Inversion of metamorphic zones in the lower Himalayas at Gantok, Sikkim, India. **J. Geol. 91**, 98-102.

BLACK, P.M. 1975. Mineralogy of New Caledonian metamorphic rocks. IV. Sheet silicates from the Ouégoa District. **Contrib. Mineral. Petrol. 49**, 269-284.

BOWES, D.R. 1973. *In:* Geology of the Glasgow District. Bluck, B.J. (ed.), 81-87.

BOWES, D.R. 1979. Structural patterns in polyphase deformed schists as illustrated by Dalradian rocks, Scotland. **Krystalinikum 14** 145-154.

BOWES, D.R. & CONVERY, H.J.E. 1966. The composition of some Ben Ledi grits and its bearing on the origin of albite schists in the South-West Highlands. **Scott. J. Geol. 2,** 67-75.

BOYLE, A.P. 1987. A model for stratigraphic and metamorphic inversions at Sulitjelma, Central Scandes. **Geol. Mag. 124,** 451-466.

BROWN, E.H. 1967. The greenschist facies in part of Easter Otago, New Zealand. **Contrib. Mineral. Petrol,14,** 249-92.

BROWN, E.H. 1968. The Si^{+4} content of natural phengites: A discussion. **Ibid.** 78-81.

BROWN, E.H. 1969. Some zoned garnets from the greenschist facies. **Am. Mineral. 54,** 1662-1677.

BUTLER, B.C.M. 1967. Chemical study of minerals from the Moine Schists of the Ardnamurchan area, Argyllshire, Scotland. **J. Petrol. 8,** 233-67.

BUTLER, P. Jr. 1969. Mineral compositions and equilibria in the metamorphosed iron formation of the Gagnon Region, Quebec, Canada. **J. Petrol. 10,** 56-101.

CARMICHAEL, D.M. 1969. On the mechanism of prograde metamorphic reactions in quartz-bearing pelitic rocks. **Contrib. Mineral. Petrol. 20,** 244-267.

CHAMBERLAIN, C.P. & LYONS, J.B. 1983. Pressure, temperature and metamorphic zonation studies of pelitic schists in the Merrimack Synclinorium, south-central New Hampshire. **Am. Mineral.68, 530-540.**

CHINNER, G.A. 1960. Pelitic gneisses with varying ferrous/ferric ratios from Glen Clova, Angus, Scotland. **J. Petrol. 1,** 178-217.

CHINNER, G.A. 1962. Almandine in thermal aureoles. **J. Petrol. 3,** 316-340.

CHINNER, G.A. 1966. The distribution of pressure and temperature during Dalradian Metamorphism. **Q.J. geol.Soc. London 122,** 159-186.

CHRISTENSEN, J.N. *et al.* 1989. Rates of tectonometamorphic processes from rubdidium and strontium isotopes in garnet. **Science 244**, 1465-1469.

CIPRIANI, C. *et al.* 1971. Metamorphic white micas: definition of paragenetic fields. **Schweiz. Mineral. petrogr. Mitt. 51**, 259-302.

CLOUGH, C.T. 1897. (Gunn, W., Clough, C.T., and Hill, J.B.) The geology of Colval. **Mem. Geol. Surv.**

COX, F.C. 1969. Inclusions in garnet: discussion and suggested mechanism of growth for syntectonic garnets. **Geol. Mag. 106**, 57-62.

CRAWFORD, M,.L. 1974. Calcium zoning in almandine: a model based on plagioclase equilibria. *In:* The Feldspars. Manchester University Press, 629-644.

CRAWFORD, M.L. 1977. Calcium zoning in Almandine Garnet, Wissahickon Formation, Philadelphia, Pennsylvania. **Can. Mineral. 15**, 243-249.

DALLMAYER, R.D. 1974. The role of crystal structure in controlling the partitioning of Mg and Fe^{2+} between coexisting garnet and biotite. **Am. Mineral. 59**, 201-203.

DE WITT, M.J. 1976. Metamorphic textures and deformation: a new mechanism for the development of syntectonic porphyroblasts and its implication for interpreting timing relationships in metamorphic rocks. **Geol. J. 11**, 71-100.

DEER, W.A. *et al.* 1962. Rock Forming Minerals **3**, Sheet Silicates. New York: John Wiley.

DENNIS, J.G. 1972. Structural Geology: The Ronald Press Co., New York.

DEMPSTER, T.J. 1985. Uplift patterns and orogenic evolution in the Scottish Dalradian. **J. geol. Soc. London 142**, 111-128.

DEMPSTER, T.J. 1985b. Garnet zoning and metamorphism of the Barrovian type area, Scotland. **Contrib.Mineral. Petrol 89**, 30-38.

DEMPSTER, T.J. & HARTE, B. 1986. Polymetamorphism in the Dalradian of the Central Scottish Highlands. **Geol. Mag. 123**, 95-104.

DIETVORST, E.J.L. 1982. Retrograde garnet zoning at low water pressure in metapelitic rocks from Kemiö, SW Finland. **Conntrib.Mineral. Petrol. 79**, 37-45.

ELLES, G.L. & TILLEY, C.E. 1930. Metamorphism in relation to structure in the Scottish Highlands. **Trans. R. Soc. Edinburgh 56**, 621-46.

ELLIOTT, D. 1972. Deformation paths in structural geology. **Geol. Soc. Am. Bull. 83**, 2621-2638,

ELLIS, D.J. & GREEN, D.H. 1979. An experimental study of the effect of Ca upon garnet-clinopyroxene Fe-Mg exchange equilibria. **Contrib.Mineral Petrol. 71**, 13-22.

ENGLAND, P.C. & RICHARDSON, S.W. 1977. The influence of erosion upon the mineral facies of rocks from different metamorphic environments. **J. Geol. Soc. London 134**, 301-313.

ERNST, W.G. 1963. Significance of phengitic micas from low-grade schists. **Am. Mineral. 48**, 1357-1373.

ERNST, W.G. 1964. Petrochemical study of coexisting minerals from low grade schists, Eastern Shikoku, Japan. **Geochim. Cosmochim. Acta 28**, 1631-1668.

ERNST, W.G. 1983. Mineral parageneses in metamorphic rocks exposed along Tailuko Gorge, Central Mountain Range, Taiwan. **J. met. Geol. 1**, 305-329.

ESSENE, E.J. 1982. Geologic thermometry and barometry. *In:* Characterization of metamorphism through mineral equilibria (ed. Ferry, J.M.), Reviews in Mineralogy, **Min. Soc. Am. 10**, 153-206.

EVANS, B.W. & GUIDOTTI, C.V. 1966. The sillimanite-potash feldspar isograd in western Maine, U.S.A. **Contrib.Mineral. Petrol. 12**, 25-62.

FAWCETT, J.J. 1964. The muscovite-chlorite-quartz assemblage. **Carnegie Inst. Washington Year Book 63**, 137-141.

FERGUSON, C.C. *et al.* 1980. On the mechanical interaction between a growing porphyroblast and its surrounding matrix. **Contrib.Mineral. Petrol. 75**, 339-352.

FERGUSON, C.C. & HARTE, B. 1975. Textural patterns at porphyroblast margins and their use in determining the time relations of deformation and crystallization. **Geol. Mag. 112**, 467-480.

FERGUSON, C.C. & HARVEY, P.K. 1972. Thermally overprinted Dalradian rocks near Cleggan, Connemara, western Ireland. **Proc. geol. Assoc. 90**, 43-50.

FERRY, J.M. & SPEAR, F.S. 1978. Experimental calibration of the partitioning of Fe and Mg between biotite and garnet. **Contrib. Mineral. Petrol. 66**, 113-117.

FINLAY, C.A. 1976. Growth of garnet in some rocks from northern Sutherland, Scotland. Unpubl. Thesis Q.U.B.

FINLAY, C.A. & KERR, A. 1979. Garnet growth in a metapelite from the Moinian rocks of northern Sutherland, Scotland. **Contrib. Mineral. Petrol., 71**, 185-191.

FLETCHER, C.J.N. & GREENWOOD, H.J. 1979. Metamorphism and structure of Penfold Creek area, near Quesnel Lake, British Columbia. **J. Petrol. 20**, 743-794.

FOSTER, M.D. 1956. Correlation of dioctahedral potassium micas on the basis of their change relations. **U.S. Geol. Surv. Bull. 1036D**, 67-77.

FOSTER, M.D. 1960. Interpretation of the composition of trioctahedral micas. **U.S. Geol. Surv. Prof. Pap. 354B**, 11-46.

FOSTER, M.D. 1962. Interpretation of the composition and a classifiction of the chlorite. **U.S. Geol. Surv. Prof. Pap. 414A**, 1-33.

FRANCESCHELLI, M. *et al.* 1982. Ca distribution between almandine-rich garnet and plagioclase in pelitic and psammitic schists from the metamorphic basement of north-eastern Sardinia. **Contrib.Mineral. Petrol. 80**, 285-295.

FRANCESCHELLI, M. *et al.* 1986. Fine-scale chlorite-muscovite association in low-grade metapelites from Nurra (NW Sardinia), and the possible misidentification of metamorphic vermiculite. **Contrib.Mineral. Petrol. 93**, 137-143.

FROST, M.Y. 1962. Metamorphic grade and iron-magnesium distribution between coexisting garnet-biotite and garnet-hornblende. **Geol. Mag. 99**,5.

GALWEY, A.K. & JONES, K.A. 1962. Inclusion in garnets. **Nature 193**, 471-472.

GALWEY, A.K. & JONES, K.A. 1963. An attempt to determine the mechanism of a natural mineral-forming reaction from examination of the products. **J. Chem. Soc. 5861-5686.**

GANGULY, J. 1979. Garnet and clinopyroxene solid solutions, and geothermometry based on Fe-Mg distribution coefficient. **Geochim. Cosmochim. Acta 43**, 101-129.

GHENT, E.D. *et al.* 1979. Geothermometry, geobarometry and fluid compositions of metamorphosed calc-silicates and pelites, Mica Creek, British Columbia. **Am. Mineral. 64**, 874-885.

GHENT, E.D. *et al.* 1982. Geothermometry and geobarometry of pelitic rocks, upper kyanite and sillimanite zones, Mica Creek area, British Columbia. **Can. Mineral. 20**, 295-305.

GHENT, E.D. & STOUT, M.Z. 1981. Geobarometry and geothermometry of plagioclase-biotite-garnet-muscovite assemblages. **Contrib.Mineral. Petrol. 76**, 92-97.

GOLDMAN, D.S. & ALBEE, A.L. 1977. Correlation of Mg/Fe partitioning between garnet and biotite with $^{18}0/^{16}0$ partitioning between quartz and magnetite. **Am. J. Sci. 277**, 750-761.

GOLDSMITH, J.R. 1982. Review of the behavior of plagioclase under metamorphic conditions. **Am. Mineral. 67**, 643-652.

GRAHAM, C.M. *et al.* 1983. Genesis and mobility of the H_20-Co_2 fluid phase during regional greenschist and amphibolite facies metamorphism. A petrological and stable isotope study in the Scottish Dalradian.. **J.Geol. Soc. London 140** 577-599.

GRAHAM, C.M. & POWELL, R. 1984. A garnet-hornblende geothermometer: Calibrarion, testing, and application to the Pelona Schist, southern California.. **J. met. Geol. 2**, 13-31.

GRANT, J.A. & WEIBLEN, P.W. 1971. Retrograde zoning in garnet near the second sillimanite isograd. **Am. J. Sci. 270,** 281-296.

GRAPES, R. & OTSUKI, M. 1983. Peristerite compositions in quartzofeldspathic schists, Franz Josef Fox Glacier Area, New Zealand. **J. met. Geol. 1,** 47-61.

GREENWOOD, H.J.. 1967. The N-dimensional tie-line problem. **Geochim. Cosmochim. Acta 31,** 465-490.

GREENWOOD, H.J. *et al.* 1964. A discussion: Phase equilibria in the metamorphic rocks of St Paul Island and Cape North, Nova Scotia. **J. Petrol. 5,** 189-194.

GUIDOTTI, C.V. 1978. Compositional variation of muscovite in medium- to high-grade metapelites of northwestern Maine. **Am. Mineral. 63,** 878-884.

GUIDOTTI, C.V. & SASSI, F.P. 1976. Muscovite as a petrogenetic indicator mineral in pelitic schists. **N. Jahrb. Mineral. Abh. 127,** 92-142.

HARKER, A. 1939. Metamorphism. Methuen, London.

HARTE, B., *et al.* 1984. Aspects of the post-depositional evolution of Dalradian and Highland Border Complex rocks in the southern Highlands of Scotland. **Trans. R. Soc. Edinburgh; Earth Sci. 75,** 151-163.

HARTE, B. & HENLEY, K.J. 1966. Occurrence of compositionally zoned garnets in regionally metamorphosed rocks. **Nature 210,** 689-692.

HARTE, B. & HUDSON, N.F.C. 1979. Pelite facies series and the temperatures and pressures of Dalradian metamorphism in E Scotland. In: Harris, A.L., Holland, C.H., Leak, B.E., (eds), The Caledonides of the British Isles - reviewed. Geol. soc. London, Scottish Academic Press., 323-338.

HARTE, B. & JOHNSON, M.R.W. 1969. Metamorphic history of Dalradian rocks in Glens Clova, Esk and Lethnot, Angus, Scotland. **Scott. J. Geol. 5,** 54-80.

HESS, D.C. 1971. Prograde and retrograde equilibria in garnet-cordierite gneisses in south-central Massachusetts. **Contrib. Mineral. Petrol. 30,** 177-195.

HEY, M.H. 1954. A new review of the chlorites. **Mineral. Mag. 30,** 277-292.

HODGES, K.V. & CROWLEY, P.D. 1985. Error estimation and empirical geothermobarometry for pelitic systems. **Am. Mineral. 70,** 702-709.

HODGES, K.V. & McKENNA, L.W. 1987. Realistic propagation of uncertainties in geologic thermometry. **Am. Mineral. 72,** 671-680.

HODGES, K.V. & SPEAR, F.S. 1982. Geothermometry, geobarometry and the Al_2Si0_5 triple point at Mt. Moosilauke, New Hampshire. **Am. Mineral. 67,** 1118-1134.

HOLDAWAY, M.J. & LEE, S.M. 1977. Fe-Mg cordierite stability in high-grade pelitic rocks based on experimental, theoretical and natural observations. **Contrib. Mineral. Petrol. 63,** 175-198.

HOLLISTER, L.S. 1966. Garnet zoning: an interpretation based on the Rayleigh fractionation model. **Science 154,** 1647-1651.

HOLLISTER, L.S. 1969. Contact metamorphism in the Kwoick area of British Columbia: an end-member of the metamorphic process. **Bull. geol. Soc. Am. 80,** 2465-2494.

HSU, L.G. 1968. Selected phase relationships in the system Al-Mn-Fe-Si-0-H: A model for garnet equilibria. **J.Petrol. 9,** 40-83.

HYNES. A. & FORSET, R.C. 1988. Empirical garnet-muscovite geothermometry in low-grade metapelites, Selwyn Range, (Canadian Rockies). **J. met. Geol. 6,** 297-309.

INDARES, A. & MARTIGNOLE, J. 1985. Biotite-garnet geothermometry in the granulite facies: the influence of Ti and Al in biotite. **Am. Mineral. 70,** 272-278.

JAMIESON, R.A. & VERNON, R.H. 1987. Timing of porphyroblast growth in the Fleur de Lys Supergroup, Newfoundland. **J. met. Geol. 5,** 273-288.

JOHNSON, M.R.W. 1962. Relations of movement and metamorphism in the Dalradian of Banffshire. **Trans.geol. Soc. Edinburgh. 19,** 29-64.

JOHNSON, M.R.W. 1963. Some time relations of movement and metamorphism in the Scottish Highlands. **Geol. Mijnb. 42,** 121-142.

JONES, K.A. 1961. Origin of albite porphyroblasts in rocks of the Ben More-Am Binnein area, western Perthshire, Scotland. **Geol. Mag. XCVIII,** 1.

JONES K.A. 1964. Metamorphism of the Ben More-Am Binnein area, western Perthshire, Scotland. **Q.J. geol. Soc. London 120**, 51-76.

JONES, K.A. *et al.* 1972. The significance of the size distribution function of crystals formed in metamorphic reactions. **Chem. Geol. 9**, 137-143.

JONES, K.A. & GALWEY, A.K. 1964. A study of possible factors concerning garnet formation in rocks from Ardara, Co. Donegal, Ireland. **Geol. Mag. 101**, 76-93.

JONES, K.A. & GALWEY, A.K. 1966. Size distribution, composition and growth kinetics of garnet crystals in some metamorphic rocks from the west of Ireland. **Q.J. geol. Soc. London 122**, 29-44.

KENNAN, P.S. 1971. Porphyroblast rotation and the kinematic analysis of a small fold. **Geol. Mag. 108**, 221-228.

KRAUSKOPF, K.B. 1983. Introduction to Geochemistry (3rd edn). McGraw-Hill, New York.

KRETZ, R. 1959. Chemical study of garnet, biotite and hornblende from gneisses of southwestern Quebec, with emphasis on the distribution of elements in coexisting minerals. **J. Geol. 67**, 371-402.

KRETZ, R. 1961. Some applications of thermodynamics to coexisting minerals of variable composition. Examples: orthopyroxene-clinopyroxene and orthopyroxene-garnet. **J. Geol. 69**, 361-387.

KRETZ, R. 1963. Distribution of magnesium and iron between orthopyroxene and calcic pyroxene in natural mineral assemblages. **J.Geol. 71,** 773-785.

KRETZ, R. 1966. Grain-size distributions for certain metamorphic minerals in relation to nucleation and growth. **J. Geol. 74**, 147-173.

KRETZ, R. 1973. Kinetics of the crystrallization of garnet at two localities near Yellowknife. **Can. Mineral. 12**, 1-20.

LIOU, J.G. *et al.* 1981. Geology and petrology of some poly-metamorphosed amphibolites and associated rocks in northeastern Taiwan. **Bull.geol. Soc. Am. 92,** PART I, 219-224, PART II, 609-748..

LISTER, G.S. & SNOKE, A.W. 1984. S-C Mylonites. **J. struct.Geol. 6,** 617-638.

LOOMIS, T.P. 1975. Reaction of Zoning of Garnet. **Contrib.Mineral. Petrol. 52,** 285-305.

LOOMIS, T.P. 1986. Metamorphism of metapelites: calculations of equilibrium assemblages and numerical simulation of the crystallization of garnet. **J.met. Geol. 4,** 201-209.

LOOMIS, T.P. & NIMICK, F.B. 1982. Equilibrium in Mn-Fe-Mg aluminous pelitic compositions and the equilibrium growth of garnet. **Can. Mineral., 20,** 393-410.

LYONA, J.B. & MORSE, S.A. 1970. Mg/Fe partitioning in garnet and biotite from some granitic, pelitic and calcic rocks. **Am. Mineral. 55,** 231-245.

McARTHUR, A.C. 1971. Structural control of Caledonian igneous masses in the south-west Highlands of Scotland. Ph.D. Thesis (unpubl). Univ. of Glasgow.

McATEER, C. 1976. Formation of garnet in rock from Mallaig. **Contrib. Mineral. Petrol. 55,** 293-301.

McNAMARA, M.J. 1965. The lower greenschist facies in the Scottish Highlands. **Geol. Fören. i Stockholm Förh. 87,** 347-389.

MARESCH, W.V. *et al.* 1985. Ordered and disordered chlorite/biotite interstratifications as alteration products of chlorite. **Neues Jb. Mineral. Abh. 152,** 79-100.

MASON, R. 1984. Inverted isograds at Sulitjelma, Norway: the result of shear-zone deformation. **J. met. Geol. 2,** 77-82.

MATHAVAN, V. 1984. A textural and chemical study of some Dalradian Albite schists. (Unpubl. Ph.D. thesis, Queen's Univ. Belfast).

MATHER, J.D. 1970. The biotite isograd and the lower greenschist facies in the Dalradian rocks of Scotland. **J. Petrol. 11,** 253-275.

MENDUM, J.R. & FETTES, D.J. 1985. The Tay nappe and associated folding in the Ben Ledi-Loch Lomond area. **Scott. J. Geol. 21**, 41-56.

MISCH, P. 1968. Plagioclase compositions and non-anatectic origin of migmatitic gneisses in northern Cascada Mountains of Washington State. **Contrib. Mineral. Petrol. 17**, 1-70.

MISCH, P. 1969. Paracrystalline microboudinage of zoned grains and other criteria for synkinematic growth of metamorphic minerals. **Am. J. Sci. 267**, 43-63.

MISCH, P. 1971. Porphyroblasts and Crystallization Force: Some Textural Criteria. **Geol. Soc. Am. Bull. 82**, 245-252.

MISCH, P. 1972. Porphyroblasts and "Crystallization Force": Some Textural Criteria: Reply.. **Geol. Soc. Am. Bull. 83**, 1203-1204.

MIYASHIRO, A. 1973. Metamorphism and Metamorphic Belts. George Allen & Unwin, London.

MOHR, D.W. *et al.* 1986. Chemical processes and migration of elements during retrogression of a staurolite-zone assemblage in western North Carolina. **Contrib.Mineral. Petrol. 92**, 400-411.

MÜLLER, G. & SCHNEIDER, A. 1971. Chemistgry and genesis of garnets in metamorphic rocks. **Contrib. Mineral. Petrol. 31,** 178-200.

OLESEN, N.O. 1978. Distinguishing between inter-kinematic and syn-kinematic porphyroblastesis. **Geol. Rundsch. 67**, 278-287.

OLESEN, N.O. 1982. Heterogeneous strain of a phyllite as revealed by porphyroblast-matrix relationships. **J. struct. Geol. 4**, 481-490.

OLIVES, J. & AMOURIC, M. 1984. Biotite chloritization by interlayer brucitization as seen by HRTEM. **Am. Mineral. 69**, 869-871.

OSBERG, P.H. 1971. An equilibrium model for Buchan-type metamorphic rocks, south-central Maine. **Am. Mineral. 56**, 570-586.

OXBURGH, E.R. & TURCOTT, D.L. 1974. Thermal gradients and regional metamorphism in overthrust terrains with special reference to the Eastern Alps. **Schweiz. Mineral. Petrograph. Mitt. 54**, 641-651.

PEACOCK, S.M. 1986. Inverted metamorphic gradients in the westernmost Cordillera. **Geol. Soc. Am. Abstr. Prog. 18**, 170.

PERCHUK, L.L. 1970. Equilibrium of biotite with garnet in metamorphic rocks. **Geochem. Internatl 157-179.**

PHILLIPS, F.C. 1930. Some mineralogical and chemical changes induced by progressive metamorphism in the greenbed group of the Scottish Dalradian. **Mineral. Mag. XXII**, 239-256.

PHINNEY, W.C. 1963. Phase equilibria in the metamorphic rocks of St Paul Island and Cape North, Nova Scotia. **J. Petrol. 4.**

PIGAGE, L.C. & GREENWOOD, H.J. 1982. Internally consistent estimates of pressure and temperature: The staurolite problem. **Am. J. Sci. 282**, 943-969.

POWELL, D. & MACQUEEN, J.A. 1976. Relationships between garnet shape, rotational inclusion fabrics and strain in some Moine metamorphic rocks of Skye, Scotland. **Tectonophysics 35**, 391-402.

POWELL, D. & TREAGUS, J.E. 1970. Rotational fabrics in metamorphic minerals. **Min. Mag. 37**, 801-814.

POWELL, R. 1985. Geothermometry and geobarometry: a discussion. **J. geol. Soc. London 142**, 29-38.

POWELL, R. & EVANS, J. 1983. A new geobarometer for the assemblage biotite-muscovite-chlorite-quartz. **J. met. Geol. 1**, 331-336.

PRIOR, D.J. 1987. Syntectonic porphyroblast growth in phyllites: textures and processes. **J. met. Geol. 5**, 27-39.

RAMSAY, C.R. 1973a. The origin of biotite in Archaean meta-sediments near Yellowknife, N.W.T., Canada. **Contrib. Mineral. Petrol. 42**, 43-54.

RAMSAY, C.R. 1973b. Controls of biotite zone mineral chemistry in Archaean meta-sediments near Yellowknife, Northwest Territories, Canada. **J. Petrol. 14**, 467-488.

RAMSAY, J.G. 1962. The geometry and mechanisms of formation of "similar" type folds. **J. Geol. 70**, 309-327.

RAMSAY, J.G. & HUBER, M. 1987. The techniques of modern structural geology. Vol. 2: Folds and Fractures. Academic Press Inc. (London).

RAO, T.R. 1977. Distribution of elements between coexisting phengite and chlorite from the greenschist facies of the Tennant Creek area, central Australia. **Lithos 10**, 103-112.

RAST, N. 1958. Metamorphic history of the Schiehallion Complex. **Trans. R. Soc. Edinburgh 63**, 413-431.

RAST, N. 1958. The tectonics of the Schiehallion Complex. **Q.J. geol. Soc. London CXIV**, 25-46.

RAST, N. 1965. Nucleation and growth of metamorphic minerals. *In:* Pitcher, W.S. & Flinn, G.W. (eds). Controls of Metamorphism. Edinburgh: Oliver & Boyd, 73-102.

REYMER, A.P.S. & OERTEL, G. 1985. Horizontal cleavage in southeastern Sinai: the case for a coaxial strain history. **J. struct. Geol. 7,** 623-636.

RICE, A.H.N. & ROBERTS, D. 1988. Multi-textured garnets from a single growth event: an example from northern Norway. **J. Met. Geol. 6**, 159-172.

RICHARDSON, S.W. & POWELL, R. 1976. Thermal causes of the Dalradian metamorphism in the central Highlands of Scotland. **Scott. J. Geol. 12**, (3), 237-268.

RIDLEY, J. 1986. Modelling of the relations between reaction enthalpy and the buffering of reaction progress in metamorphism. **Mineral. Mag. 50,** 375-384.

ROGERS, G. *et al.* 1989. A high precision U-Pb age for the Ben Vuirich granite: implications for the evolution of the Scottish Dalradian. **J. Geol. Soc. London 146,** 789-798.

ROSENFELD, J.L. 1968. Garnet rotations due to the major Paleozoic deformations in southeast Vermont. *In:* W.S. White, E. Zen, J.B. Hadley, J.B. Tompson (eds), Studies of Appalachian geology: northern and maritime. Wiley-Interscience Publishers, New York, 185-202.

ROSENFELD, J.L. 1970. Rotated garnets in metamorphic rocks. **Geol. Soc. Am. Spec. Pap. 129,** 105pp.

SAXENA, S.K. 1968b. Distribution of elements among coexisting minerals and the nature of solid solution in garnet. **Am. Mineral. 53**, 994-1014.

SAXENA, S.K. 1969. Distribution of elements in coexisting minerals and the problem of chemical disequilibrium in metamorphosed basic rocks. **Contrib. Mineral. Petrol. 20,** 177-197.

SAXENA, S.K. 1969. Distribution of Fe and Mg between coexisting garnet and biotite. **Contrib. Mineral. Petrol. 22**, 259-267.

SAXENA, S.K. 1973. Thermodynamics of rock-forming crystalline solutions. Springer, New York. 188pp.

SCHOLZ, C.H. 1980. Shear heating and the state of stress on faults. **J. Geophys. Res.** 85, 6174-6184.

SCHONEVELD, C. 1977. A study of typical inclusion pattern in strongly paracrystalline-rotated garnets. **Tectonophysics 39**, 371-477.

SHELLEY, D. 1972. Porphyroblasts and 'Crystallization Force": Some textural criteria: Discussion. **Geol. Soc. Am. Bull. 83**, 919-920.

SEN, S.K. & CHAKRABORTY, K.R. 1968. Magnesium-iron exchange equilibrium in garnet-biotite and metamorphic grade. **Neues Jahrb. Mineral. Abh. 108**, 181-207.

SIVAPRAKASH, C. 1979. Studies in chemical petrology: Part I. Some Dalradian metapelites and metabasites. Ph.D. thesis (unpubl.) Univ. Cambridge.

SIVAPRAKASH, C. 1981. Zoned garnets in some Scottish Dalradian pelites. **Mineral. Mag. 44**, 301-307.

SIVAPRAKASH, C. 1982. Geothermometry and geobarometry of Dalradian metapelites and metabasites from the central Scottish Highlands. **Scott. J. Geol. 18**, 109-124.

SPEAR, F.S. & CHENEY, J.T. 1989. A petrogenetic grid for pelitic schists in the system SiO_2-Al_2O_3-FeO-MgO-K_2-H_2O. **Contrib. Mineral. Petrol. 101**, 149-164.

SPEAR, F.S. & SILVERSTONE, J. 1983. Quantitative P-T paths from zoned minerals: Theory and tectonic applications. **Contrib. Mineral. Petrol. 83**, 348-357.

SPRY, A. 1962. The chronological analysis of crystallization and deformation of some Tasmanian Precambrian rocks. **J. geol. Soc. Australia 10**, 193-208.

SPRY, A. 1963. Origin and significance of snowball structures in garnet. **J. Petrol. 4**, 211-222.

SPRY, A. 1969. Metamorphic textures. Pergamon Press (London).

SPRY, A. 1972. Porphyroblasts and "Crystallization Force": Some textural criteria: Discussion. **Geol. Soc. Am. Bull. 83**, 1201-1202.

ST-ONG, M.R. 1981. "Normal" and "inverted" metamorphic isograds and their relation to syntectonic Proterozoic batholiths in the Wopmay Orogen, Northwest Territories, Canada. **Tectonophysics 76**, 295-316.

STURT, B.A. & HARRIS, A.L. 1961. The metamorphic history of the Loch Tummel area, central Perthshire, Scotland. **Lpool. Manchr. geol. J. 2**, 689-711.

TEWHEY, J.D. & HESS, P.C. 1976. Reverse manganese-zoning in garnet as a result of high F_{O2} conditions during metamorphism. **Geol. Soc. Am. Abstr. Prog. 8**, 1135.

TILLEY, C.E. 1925. A preliminary survey of metamorphic zones in the southern Highlands of Scotland. **Q.J. geol. Soc. London 81**, 100-112.

THOMPSON, A.B. 1976. Mineral reactions in pelitic rocks: II. Calculation of some P-T-X (Fe-Mg) phase relations. **Am. J. Sci. 276**, 425-454.

THOMPSON A.B. *et al.* 1977. Prograde reaction histories deduced from compositional zonation and mineral inclusions in garnet from the Gassetts Schist, Vermont.. **Am. J. Sci. 277**, 1152-1167.

TORIUMI, M. 1979. A mechanism of shape-transformation of quartz inclusions in albite of regional metamorphic rocks. **Lithos 12**, 325-333.

TRACY, R.J. *et al.* 1976. Garnet composition and zoning in the determination of temperature and pressure of metamorphism. Central Massachusetts. **Am. Mineral. 61**, 762-775.

TRACY, R.J. 1982. Compositional zoning and inclusions in metamorphic minerals. *In:* Ferry, J.M. (ed.). Characterisation of metamorphism through mineral equilibria. **Reviews in Mineralogy 10,** Mineral Soc. Am. 355-397.

TRENDALL, A. 1953. The origin of albite gneisses. Ph.D. Thesis, (unpubl.) Univ. Liverpool.

TRZCIENSKI, W.E. JR., 1977. Garnet zoning - product of a continous reaction. **Can. Mineral. 15**, 250-256.

TUREKIAN, K.K. & WEDEPOHL, K.H. 1961. Distribution of the elements in some major units of the Earth's crust. **Geol. Soc. Am. Bull. 72**, D5-A2.

TURNER, F.J. 1968. Metamorphic Petrology, Mineralogical and Field Aspects. McGraw-Hill (N.Y.), 403pp.

TURNER, F.J. & VERHOOGEN, J. 1960. Igneous and metamorphic petrology. New York: McGraw-Hill.

VAN DE KAMP, P.C. 1970. The green beds of the Scottish Dalradian series: geochemistry, origin and metamorphism of mafic sediments. **J. Geol. Chicago 78**, 281-303.

VELDE, B. 1965. Phengite micas: synthesis, stability and natural occurrence. **Am. J. Sci. 263**, 886-913.

VELDE, B. 1978. High temperature or metamorphic vermiculites. **Contrib. Mineral. Petrol. 66**, 319-323.

VELDE, B. 1980. Cell dimensions, polymorph type and IR spectra of synthetic white micas: the importance of ordering. **Am. Mineral. 65**, 1277-1282.

VERNON, R.H. 1977. Relationships between microstructures and metamorphic assemblages. **Tectonophysics 39**, 439-452.

VERNON, R.H. 1978. Porphyroblast-matrix microstructural relationships in deformed metamorphic rocks. **Geol. Rundsch. 67**, 288-305.

VERNON, R.H. 1979. Formation of late sillimanite by hydrogen metasomatism (base-leaching) in some high-grade gneisses. **Lithos 12**, 143-152.

VERNON, R.H. 1987. A microstructural indicator of shear sense in volcanic rocks and its relationship to porphyroblast rotation in metamorphic rocks. **J. Geol. 95**, 127-133.

VERNON, R.H. 1988. Sequential growth of cordierite and andalusite porphyroblast, Cooma Complex, Australia: microstructural evidence of a prograde reaction. **J. met. Geol. 6**, 255-269.

VERNON, R.H. 1988. Microstructural evidence of rotation and non-rotation of mica porphyroblasts. **J. met. Geol. 6**, 595-601.

VERNON, R.H. & POWELL, C. MCA. 1976. Porphyroblastesis and displacement: some new textural criteria from pelitic hornfelses - a comment. **Mineral. Mag. 315**, 787-788.

VOLL,, G. 1960. New work on petrofabrics. **Lpool. Manch. geol. J. 2**, 503.

WATKINS, K.P. 1984. The structure of the Balquhidder-Crianlarich region of the Scottish Dalradian and its relation to the Barrovian garnet isograd surface. **Scott. J. Geol. 20**, 53-64.

WATKINS, K.P. 1985. Geothermometry and geobarometry of inverted metamorphic zones in the W central Scottish Dalradian. **J. geol. Soc. London 142**, 157-165.

WILLIAMS, P.F. & SCHONEVELD, CHR. 1981. Garnet rotation and the development of axial plane crenulation cleavage. **Tectonophysics 78**, 307-334.

WISEMAN, J.D.H. 1934. The central and southwest Highland epidiorites: a study in progressive metamorphism. **Q.J. geol. Soc. London 90**, 354-417.

WOODLAND, B.G. 1985. Relationship of concretions and chlorite-muscovite porphyroblasts to the development of domainal cleavage in low-grade metamorphic deformed rocks from north-central Wales, Great Britain. **J. struct. Geol. 7**, 205-215.

WOODSWORTH, G.H. 1977. Homogenization of zoned garnets from pelitic schists. **Can. Mineral. 15**, 230-242.

YARDLEY, B.W.D. 1977. An empirical study of diffusion in garnet. **Am. Mineral. 62**, 793-800.

ZEN, E. 1963. Components, phases, and criteria of chemical equilibrium in rocks. **Am. J. Sci., 261**, 929-942.

ZEN, E-AN. 1973. Thermochemical parameters of minerals from oxygen-buffered hydrothermal equilibrium data: method, applications to annite and almandine. **Contrib. Mineral. Petrol. 39**, 65-80.

ZEN, E-AN & ALBEE, A.L. 1964. Co-existent muscovite and paragonite in pelitic schists. **Am. Mineral. 49**, 904-925.

ZWART, H.J. 1960. Relations between folding and metamorphism in the Pyrenees and their chronological succession. **Geol. Mijnbouw. 39**, 163-180.

ZWART, H.J. 1962. On the determination of polymetamorphic mineral associations, and its application to the Bosost area (central Pyrenees). **Geol. Rundsch. 52**, 38-65.

ZWART, H.J. 1963. Some examples of the relation between deformation and metamorphism from central Pyrenees. **Geol. Mijnbouw. 42**, 143-154.